Synthesis of Novel Chloroquine Derivatives and Insights into the Interactions of a Resistance Protein.

By

Benita Mujinga Kapuku

A thesis submitted to McGill University in partial fulfillment of the requirements of the degree of

Doctor of Philosophy

Department of Chemistry

McGill University, Montreal

November 2020

To my mother, Espérance Kavira Kakule Kapuku, and father, Jean-Pierre Kapuku, for showing me unconditional love.

Abstract

The human toll caused by malaria remains devastating. In 2018 alone, there were 228 million cases, which resulted in 405,000 deaths. Malaria is caused by the *Plasmodium* parasite transmitted by the *Anopheles* mosquito. There are five species: *P. malariae*, *P.falciparum*, *P. vivax*, *P. ovale* and *P. knowlesi*, in which *P. falciparum* is the most common and most deadly. An antimalarial drug called chloroquine (CQ) was first introduced in the 1940s and is considered the gold-standard antimalarial drug due to its high efficacy, low-cost, and low-toxicity. It is listed under the World Health Organization (WHO) essential medicines and showed great promise in their endeavor to eradicate malaria.

Unfortunately, after two decades of use resistance began to arise, which led to its gradual withdrawal for *P. falciparum* cases. The WHO has reported an increase in the number of malaria cases over the last six years (214, 216, 228 million cases in 2014, 2016 and 2018, respectively), this is alarming as it greatly hampers the effects of eradication. Therefore, it remains crucial to invest in the research and development of new antimalarial drug candidates. Recent studies have reported the re-sensitization of chloroquine in countries where it was once completely banned, such as Malawi, Zambia and certain regions of The Ivory Coast. This indicates that resistance is reversible because it requires a fitness deficit. When drug pressure is removed, the frequency of resistance alleles is reduced but not eliminated. Therefore, the reintroduction of drug pressure will cause a rapid reemergence of resistance. As CQ was the ideal drug, many derivatives with varying sidechains and aryl substituents such as amodiaquine and piperaquine have emerged as commercial drugs. Aminoquinolines (AQs) continue to be prepared and tested, and two AQs were

recently undergoing phase II clinical trials, demonstrating the robustness of the AQ core and their future potential.

My research centres around the repurposing of chloroquine via modification at the 3-position of the quinoline ring. In chapter 2 I describe the synthesis and optimization of 3-aminochloroquine (3-NH_2CQ). The synthesis of this derivative allows for expansion at the 3-position for the synthesis of a diverse library of antimalarial candidates.

In chapter 3, I describe the synthesis of novel substituted chloroquine analogs. The structure-activity relationship (SAR) was determined as I synthesized a library of compounds with varying steric and electronic effects. It was determined that electron-withdrawing substituents at the para-position gave the best antimalarial activity. Although the synthesized compounds were not as effective as CQ, they may be candidates for combination therapy with chloroquine.

In chapter 4, I describe the synthesis of a CQ photoaffinity label with minor modifications. An aryl azide is installed at the 3rd-position on the quinoline ring, making it the first AQ photoaffinity label in the literature with the least number of modifications whilst retaining all features of the parent compound, to our knowledge. Labelling studies were then carried out to determine the lability of the photoaffinity label.

Lastly, the protein responsible for CQ resistance, *Plasmodium falciparum* chloroquine resistance transporter (PfCRT), has been isolated for the first time. In chapter 5, I describe binding studies carried out with PfCRT. In collaboration with Prof. Fidock's group at Columbia University,

fluorescence and UV-Vis binding studies were carried out to determine binding affinities of heme and CQ with PfCRT.

Résumé

Le bilan humain causé par le paludisme reste dévastateur. Rien qu'en 2018, il y a eu 228 millions de cas, entraînant 405000 décès. Le paludisme est causé par le parasite Plasmodium transmis par le moustique Anopheles. Il existe 5 espèces: P. malariae, P. falciparum, P. vivax, P. ovale et P. knowlesi, dans lesquelles P. falciparum est le plus commun et le plus mortel. Un médicament antipaludique appelé chloroquine (CQ) a été introduit pour la première fois dans les années 1940 et est considéré comme le médicament antipaludique de référence en raison de sa haute efficacité, son faible coût et sa faible toxicité. Il est répertorié dans la liste des médicaments essentiels de l'Organisation Mondiale de la Santé (OMS) et s'est montré très prometteur dans leurs efforts pour éradiquer le paludisme.

Malheureusement, après deux décennies d'utilisation, une résistance a commencé à apparaître et cela a conduit à son retrait progressif pour les cas de P. falciparum. L'OMS a signalé une augmentation du nombre de cas de paludisme au cours des 6 dernières années (214, 216, 228 millions de cas en 2014, 2016 et 2018 respectivement), ce qui est alarmant car cela entrave considérablement les effets de l'éradication. Par conséquent, il reste crucial d'investir dans la recherche et le développement de nouveaux médicaments antipaludiques. Des études récentes ont fait état d'un regain de l'efficacité de la chloroquine dans des pays où elle était autrefois complètement interdite, comme le Malawi, la Zambie et certaines régions de Côte d'Ivoire. Cela indique que la résistance est réversible car elle nécessite un déficit de forme physique. Lorsque la pression médicamenteuse est supprimée, la fréquence des allèles de résistance est réduite mais pas éliminée. Par conséquent, la réintroduction de la pression médicamenteuse provoquera une réémergence rapide de la résistance. Comme la CQ était le médicament idéal, de nombreux dérivés

avec des chaînes latérales et des substituants aryle variables tels que l'amodiaquine et la pipéraquine ont émergé en tant que médicaments commerciaux. Les aminoquinoléines (AQ) continuent d'être préparées et testées sous forme de deux AQ actuellement en phase II d'essais cliniques: AQ-13 et ferroquine. Démontrer la robustesse du noyau d'AQ et leur potentiel futur.

Mes recherches sont centrées sur la réutilisation de la chloroquine via une modification en position 3. Dans le chapitre 2 je détaille la synthèse et l'optimisation de la 3-aminochloroquine. La synthèse de ce dérivé permet une dérivatisation supplémentaire en position 3 pour la synthèse d'une bibliothèque diversifiée d'antipaludiques.

Au chapitre 3, je décris la synthèse de nouveaux analogues de chloroquine substitués. La relation structure-activité a été déterminée lorsque j'ai synthétisé une bibliothèque de composés avec divers effets stériques et électroniques. Il a été déterminé que les substituants attracteurs d'électrons en position para donnaient la meilleure activité antipaludique. Bien que les composés synthétisés ne soient pas aussi efficaces que la CQ, ils peuvent être des candidats pour une thérapie combinée avec la chloroquine.

Dans le chapitre 4, je décris la synthèse d'un marqueur de photoaffinité CQ avec des modifications mineures. Un aryl azide est installé en position 3, 3-azidochloroquine, ce qui en fait le premier marqueur de photoaffinité AQ de la littérature avec le moins de modifications tout en conservant à notre connaissance toutes les caractéristiques du composé parent. Des études de marquage ont ensuite été menées pour déterminer la labilité du marqueur de photoaffinité.

Enfin, la protéine responsable de la résistance à la CQ Plasmodium falciparum chloroquine résistance transporter (PfCRT) a été isolée pour la première fois. Dans le chapitre 5, je décris les études de liaison réalisées avec PfCRT. En collaboration avec le groupe Prof. Fidock de l'Université de Columbia, des études de fluorescence et de liaison UV-Vis ont été réalisées pour déterminer les affinités de liaison de l'hème et de la CQ avec PfCRT.

Acknowledgement

I am very thankful to my supervisor, Prof. Scott Bohle, who has taught me so much about the beauty of chemistry through his love for science. Thank you for challenging me, for all the imparted wisdom and interesting facts throughout the years.

I want to thank my research committee members Dr. Elias Georges, Prof. Karine Auclair, Prof. Hanadi Sleiman and Prof. Gonzalo Cosa, for their interest in my research and input over the years.

I would also like to thank Dr. Robin Stein and Dr. Tara Sprules for their help with NMR spectroscopy and Dr. Nadim K. Saadeh and Dr. Alex Wahba for carrying out High-Resolution Mass Spectroscopy.

I thank all the group members along the way: Cassidy VanderSchee, Dr. Danae Guerra, Dr. David Kuter, Harrison Cassidy, Dr. Ivor Wharf, Dr. Kristopher Rosadiuk, Dr. Munendra Yadav and Quentin Gaydon for the interesting conversations, solicited distractions, and valuable input. I'd also like to thank my friends Allie Domínguez, Jane Eiyegbenin, Ifenna Mbaezue, and Martin Sichinga for their support and laughs along the way. Working alongside such a talented group of individuals further enriched my experience at McGill.

The decision to pursue a doctorate and to see it through is not an easy one. It requires self-motivation, determination, mental strength, and plenty of support. The love and joy received from my support system helped make my journey more worthwhile.

I thank the Kapuku clan for being the best family members I could have ever wished for. Thank you for a lifetime of unforgettable moments and for helping shape the person that I am today. My success is our success, and this thesis is for all the Kapuku's.

I thank my sisters Nadine and Gloria for being there to listen. Thank you for the words of encouragement and for always keeping me smiling. Thank you for being my ride-or-die sisters and for being such great role models.

I thank my brothers Jeremie, Sam and Medi, for being my hype men. Thank you for the energy and joy that you bring into my life. I can always rely on you guys for a fun time and the most interesting conversations.

I thank my partner Hubert for being my cheerleader. Thank you for listening to all the rants and sitting through all the practice presentations. Thank you for the motivational speeches and your infectious smile. Thank you for keeping me grounded and for being the sugar in my ice-cream.

Finally, none of this would have been possible without my amazing parents' undying love and support. I thank my mother, Espérance, and father, Jean-Pierre, for teaching me the values of hard work and perseverance. Thank you for the endless prayers, words of wisdom and for being my rocks. Thank you for all the sacrifices made so that I could live my best life. Thank you for believing in me even when I did not believe in myself. I am so grateful to have been loved and to be loved by you.

Contribution of Authors

The author carried out all experimental design, compound synthesis, structural analysis, binding studies and all the work detailed in the thesis under the supervision of Prof. Scott Bohle.

Chapter 3: Antiplasmodial assays were carried out by our collaborators Dr. Fadi Baakdah, under the supervision of Dr. Elias Georges at McGill University Institute of Parasitology.

Chapter 5: PfCRT isoform 7G8, GtrB and empty nanodisc were gifted from Jonathan Kim, under the supervision of Prof. David Fidock at Columbia University.

.

Table of Contents

List of Figures

List of Schemes

List of Tables

List of Abbreviations

[*Q*]	Quencher concentration
3-BrCQ	3-bromochloroquine
3-ClCQ	3-chlorochloroquine
3-ICQ	3-iodochoroquine
3-N_3MeCQ	3-azidomethylchloroquine
3-NH_2CQ	3-aminochloroquine
3-NH_2MeCQ	3-aminomethylchloroquine
3-NO_2CQ	3-nitro chloroquine
3-NO_2DCQ	4,7-dichloro-3-nitroquinoline
3,6-BrCQ	3,6-dibromo chloroquine
Å	Angstrom
AcOH	Acetic acid
ACTs	Artemisinin combination therapies
ADQ	Amodiaquine
ADQQI	Amodiaquine quinone-imine
APCI	Atomospheric pressure chemical-ionization
AQ	Aminoquinoline
ASA-MQ	N-[4-[I-hydroxy-2-(dibutylamino) ethyl] quinolin-8-yl]-4-azido-2-hydroxybenzamide
ASA-Q	N-(l-(l-diethylamino-l-methylbutylamino)quinolin-6-yl)-4-azido-2-hydroxybenzamide
AzBCQ	Perfluorophenylazido biotinylated chloroquine
BHIA	b-Hematin inhibition assays
BQ	Bulaquine
cm^{-1}	Wavenumber
COSY	Correlation spectroscopy
CQ	Chloroquine
CQR	Chloroquine resistant
CQS	Chloroquine sensitive
Cu_2SO_4	Copper (I) sulfate
DADQ	N-desethylamodiaquine
DBU	1,8-diazabicyclo[5.4.0]undec-7-ene
DCM	Dichloromethane
DCQ	Dichloroquinoline
DIPEA	N,N-diisopropylethylamine
DMA	Dimethylacetamide
DMEDA	Dimethylethylenediamine

DMF	Dimethylformamide
DMSO	Dimethyl sulfoxide
DV	Digestive vacuole
equiv.	Equivalent
ESI	Electrospray ionization
EtOAc	Ethyl acetate
EtOH	Ethanol
FAQ	4-fluoroamodiaquine
Fe(III)PPIX	Iron protoporphyrin IX
FQ	Ferroquine
g	Gram(s)
G6PD	Glucose-6-phosphate dehydrogenase
Gtr	glycosyltransferase
H_2O	Water
Hb	Hemoglobin
HCQ	Hydroxychloroquine
Hex	Hexanes
HMBC	Heteronuclear multiple bond correlation spectroscopy
HRMS	High-resolution mass spectroscopy
HSQC	Heteronuclear single quantum coherence spectroscopy
Hz	Hertz
HZ	Hemozoin
IC_{50}	Half maximal inhibitory concentration
J	Coupling constant
K_2CO_3	Potassium carbonate
K_{SV}	Stern-Volmer quenching constant
L	Litre
$LiAlH_4$	Lithium aluminium hydride
M	Molar
MeCN	Acetonitrile
MeCQ	Methyl chloroquine
MeOH	Methanol
mg	Milligram(s)
$MgSO_4$	Magnesium sulfate
MHz	Megahertz
mL	Millilitre
mL	Microliter
MP	Mepacrine
MPLME	Membrane proteins and lipid membrane ensemble
MQ	Mefloquine

MW	Microwave
N_2	Nitrogen gas
Na_2CO_3	Sodium carbonate
$NaHCO_3$	Sodium bicarbonate
NaN_3	Sodium azide
NaOH	Sodium hydroxide
NBD	Nucleotide-binding domain
NBS	N-bromosuccinimide
NBu_4N_3	Tetrabutylammoniumazide
NEt_3	Triethylamine
NH_4OH	Ammonium hydroxide
nM	Nanomolar
nm	Nanometer
NMR	Nuclear magnetic resonance
NOSEY	Nuclear overhauser effect spectroscopy
PAL	Photoaffinity label
PfCRT	Plasmodium falciparum chloroquine resistant transporter
pfmdr1	Plasmodium falciparum multidrug resistance protein 1
PN	Pyronaridine
ppm	Parts per million
PPQ	Piperaquine
PQ	Primaquine
QD	Quinidine
QN	Quinine
RT	Room temperature
SAR	Structure-activity relationship
SET	Single-electron transfer
S_NAR	Nucleophilic aromatic substitution
SQ	Sontoquine
$S_{RN}1$	Unimolecular radical nucleophilic substitution
tBuOK	Potassium tert-butoxide
TCNE	Tetracyanoethylene
TEMPO	(2,2,6,6-Tetramethylpiperidin-1-yl)oxyl
TFQ	Tafenoquine
THF	Tetrahydrofuran
TLC	Thin-layer chromatography
TM	Transmembrane
$TMSN_3$	Azidotrimethyl silane
Trp	Tryptophan
UV-Vis	Ultraviolet-visible spectroscopy

VP	Verapamil
WHO	World health organization

Chapter 1

Development of Antimalarial Drugs

1.1 Introduction

1.2 Malaria

Malaria is a devastating disease in which over 3 billion people are at risk of contracting the disease. The most recent report by the World Health Organization (WHO) reported 228 million cases in 2018. Of those, there were 405,000 deaths. Africa bears 93% of all cases, followed by South-East Asia and the Eastern Mediterranean. Children under the age of 5 are the most vulnerable, accounting for 67% of deaths globally.[1] Pregnant women are also at high risk. Despite the WHO's sustained efforts, the number of malaria cases has increased year-over-year from 2015-2019 from 212 million to 228 million cases per year.[1,2]

Malaria is a vector-borne disease carried by the female *Anopheles* spp. mosquito. It transmits parasites of the *Plasmodium* genus. Five Plasmodium species are known to infect humans: *P. falciparum, P. vivax, P. ovale, P. malariae* and *P. knowlesi*. *Plasmodium falciparum* is the most deadly, followed by *P. vivax*.[3]

1.3 Parasite life cycle

The parasitic life cycle begins during a blood meal of an infected female *Anopheles* mosquito, **Figure 1.1**. The mosquito transmits parasites in their sporozoite stage from its saliva into the hosts' bloodstream while feeding. The sporozoites travel to and enter the liver within 60 minutes of entering the host to evade the hosts' immune system. The liver-stage is asymptomatic and can last between 5-16 days. Within the liver, sporozoites develop into a tissue schizont containing several thousand merozoites.[4] The asexual erythrocytic cycle begins when mature tissue schizonts rupture,

resulting in thousands of merozoites released into the bloodstream. These merozoites then enter red blood cells (RBCs), where they develop into blood schizonts. Once matured, the blood schizont ruptures, releasing up to 32 merozoites that can re-enter RBCs to continue the cycle.[5] This constant invasion and rupture of RBCs cause clinical symptoms to appear, such as fever, fatigue, and chills. These symptoms usually appear within one week after the commencement of the asexual cycle. The cycle ends at the intervention of the immune system, administration of prophylactic medication, or the host's death. The differentiation of merozoites into hypnozoites occurs only in *P. viva*x and *P. ovale*. Hypnozoites are parasites that can remain dormant in the host hepatocytes for months or years and are the cause of recrudescence of malaria in cured patients.[5]

Once in the bloodstream, some merozoites within infected erythrocytes differentiate into male and female gametocytes, which marks the beginning of the sexual cycle. These gametocytes travel to skin capillaries where they can be taken up during another blood meal. They remain in the bloodstream but are non-pathogenic; however, it is unclear how they evade the immune system. The beginning of sexual reproduction occurs within the mosquito's midgut, where gametes form a zygote, which develops into an ookinete and eventually forms an oocyst outside the midgut. Within the oocyst, sporozoites are formed, and once mature, the oocyst ruptures, releasing sporozoites, which concentrate in the mosquito salivary glands, ready to restart the life cycle. The sexual cycle within the mosquito takes 7-10 days.[4,6]

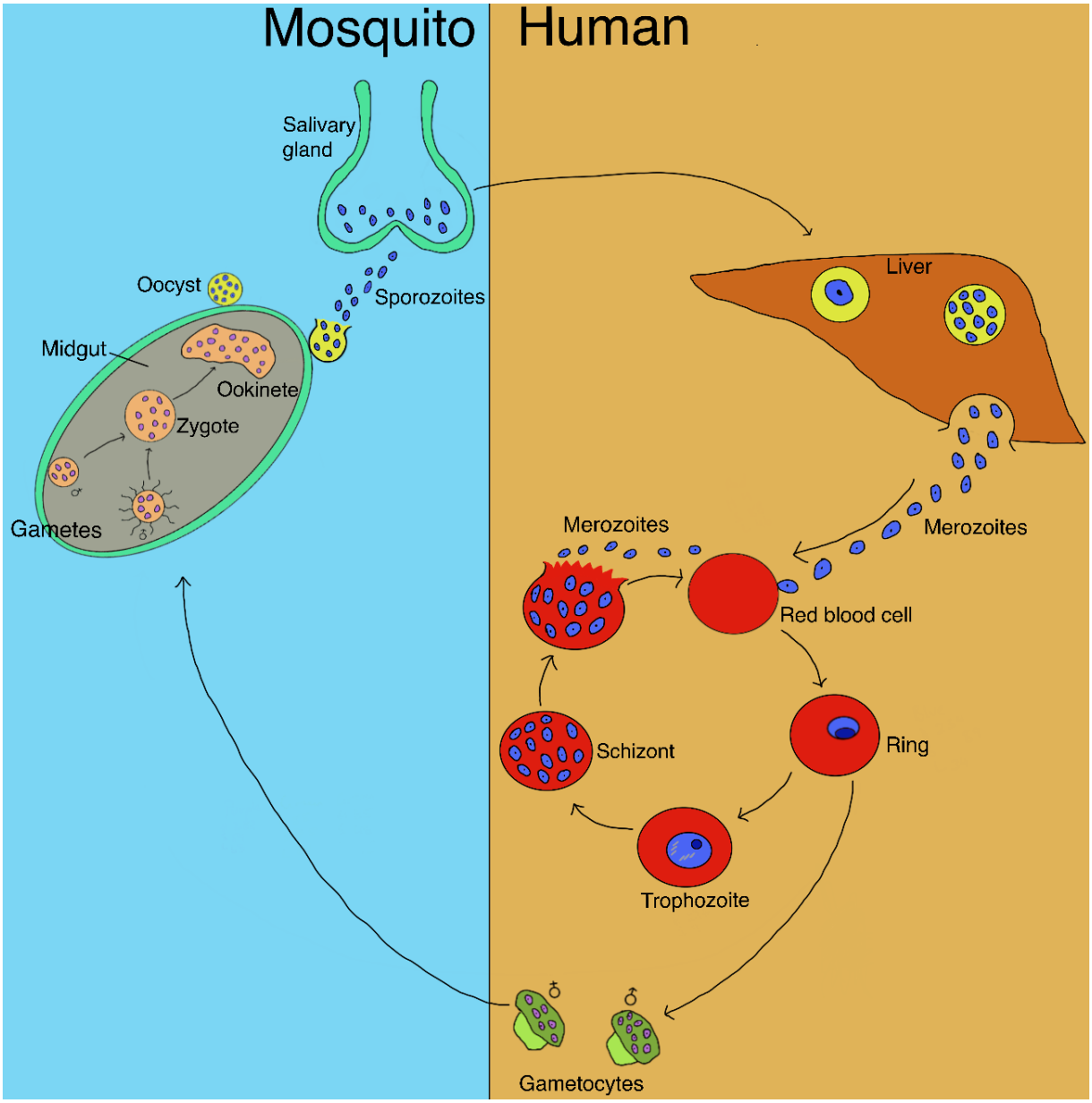

Figure 1.1. *Plasmodium* life cycle. Illustration adapted from Wirth.[7]

1.4 Hemozoin formation

1.4.1 Digestive Vacuole

During the trophozoite stage of the asexual cycle, the parasite degrades RBCs as it requires room to grow and to obtain nutrients via the catabolism of hemoglobin (Hb). Hb has a cytosolic

concentration of 5 mM, and it accounts for 95% of parasitic cytosolic proteins.[8] Hb is transported into the acidic digestive vacuole (DV), which has a pH of 5.0 – 5.6, where it is catabolized.[9–11] Hb catabolism releases Fe^{2+} and globin. Globin is hydrolyzed into amino acids as it is the primary source of amino acids for the parasite. The parasite incorporates Hb amino acids with its proteins as a source of nutrients and for *de novo* synthesis of proteins required for replication. However, the parasite does not solely rely on Hb amino acids as Hb is deficient in isoleucine, methionine, glutamic acid, and glutamine.[8] Therefore, it is a dual requirement to have host amino acids and the ability to synthesize amino acids as needed. Studies have shown that when Hb proteolysis is blocked, parasite development is interrupted.[12]

1.4.2 Hemoglobin Degradation

Hb proteolysis occurs in the DV. It is during the early trophozoite stage where hemozoin (HZ) formation becomes microscopically visible; however, HZ is present in most of the parasite life cycle.[13] Plasmepsins and falcipains are the main proteases involved in Hb degradation. More specifically, cysteine and aspartic proteases are the primary enzymes involved in Hb proteolysis as they account for 20-40% and 60-80% of globin degrading activity, respectively.[8]

Hb is denatured before heme is released from the peptide.[14] Two aspartic proteases, plasmepsin I and II, initiate Hb hydrolysis, **Figure 1.2**. Plasmepsin I and II initiate Hb cleavage by cleaving the hinges that hold the tetramer together when oxygen is bound. Once the tertiary structure falls apart, the plasmepsins further cleave Hb.[15] Plasmepsin I is primarily synthesized in the early ring stage but also synthesized in the trophozoite stage. Plasmepsin II is synthesized primarily in the trophozoite stage. Therefore, plasmepsin I is more involved in Hb degradation than plasmepsin II.

Studies show that blocking plasmepsin I leads to parasite death.[8] Plasmepsin II is predominantly active in the hydrolysis of the disassembled Hb units.[16] The cysteine protease involved in globin hydrolysis is the 28 kDa protein falcipain, synthesized in the trophozoite stage. Plasmepsins hydrolysis Hb into large fragments of globin. Falcipain catabolizes globin into smaller peptide fragments. Assays in which cysteine protease inhibitors were incubated with trophozoite stage parasite shows a considerable reduction in parasite development, highlighting the importance of falcipains in parasite survival.[14] There are two primary cysteine proteases that the parasite utilizes falcipain-2 and falcipain-3. Falcipain-2 exerts 90% of falcipain activity and is predominant in the early trophozoite stage. Falcipain-3 is only present in the late trophozoite stage, and both cleave native Hb and denatured globin.[17] Amino acids generated from globin hydrolysis are incorporated into the parasite's proteins.

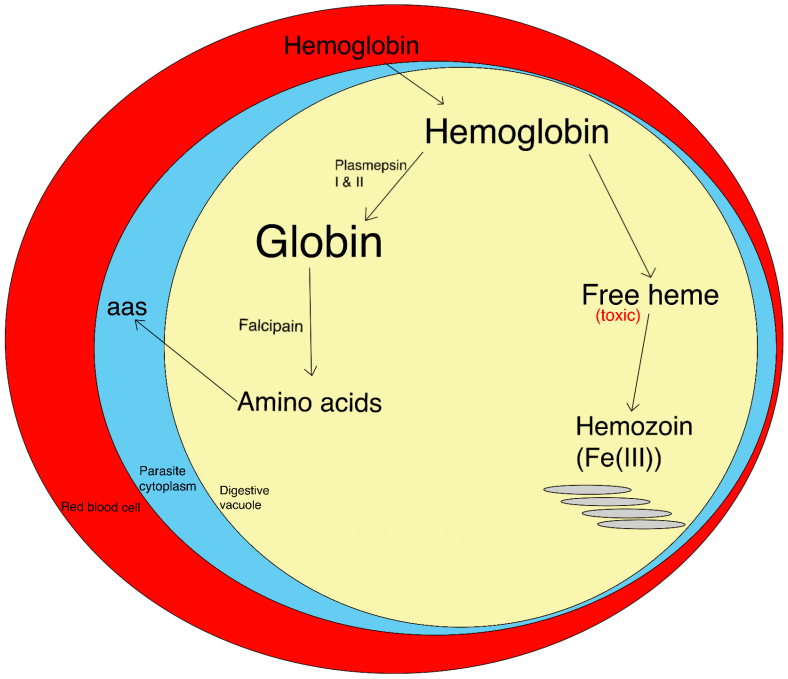

Figure 1.2. Catabolism of Hb and heme detoxification mechanism. Illustration adapted from Rosenthal and Meshnick.[14]

1.4.3 Heme Detoxification

Once Hb has been disassembled by the aspartic and cysteine proteases, heme is released into the cytosol of the DV. The released free heme is very reactive and toxic to the parasite. Free heme can cause the release of reactive oxygen species, which leads to oxidative stress, membrane rupture, and eventual death of the parasite. To circumvent this damage, the parasite transforms free heme into HZ. Studies have shown that 95% of released heme is converted to HZ.[18] Pagola *et al*. have shown that HZ is an insoluble biomineral that is identical to synthetic β-hematin. X-ray structures show that HZ is dimerized Fe(III)PPIX where a propionate group of each molecule coordinates with the adjacent central Fe(III), and the dimers are linked via hydrogen bonding with the uncoordinated propionate,[19] **Figure 1.3**.

It has been reported that HZ is completely encapsulated with a neutral lipid body upon its formation, which is comprised of mono-, di- and tri-acylglycerols. Specifically, neutral lipids monopalmitoyl- and monostearoyl glycerol promote HZ formation.[20] It is believed that these lipid bodies originate from the inner membrane of endocytotic transport vesicles that transport Hb to the DV.[18] Histidine-rich proteins have also been associated with HZ formation.

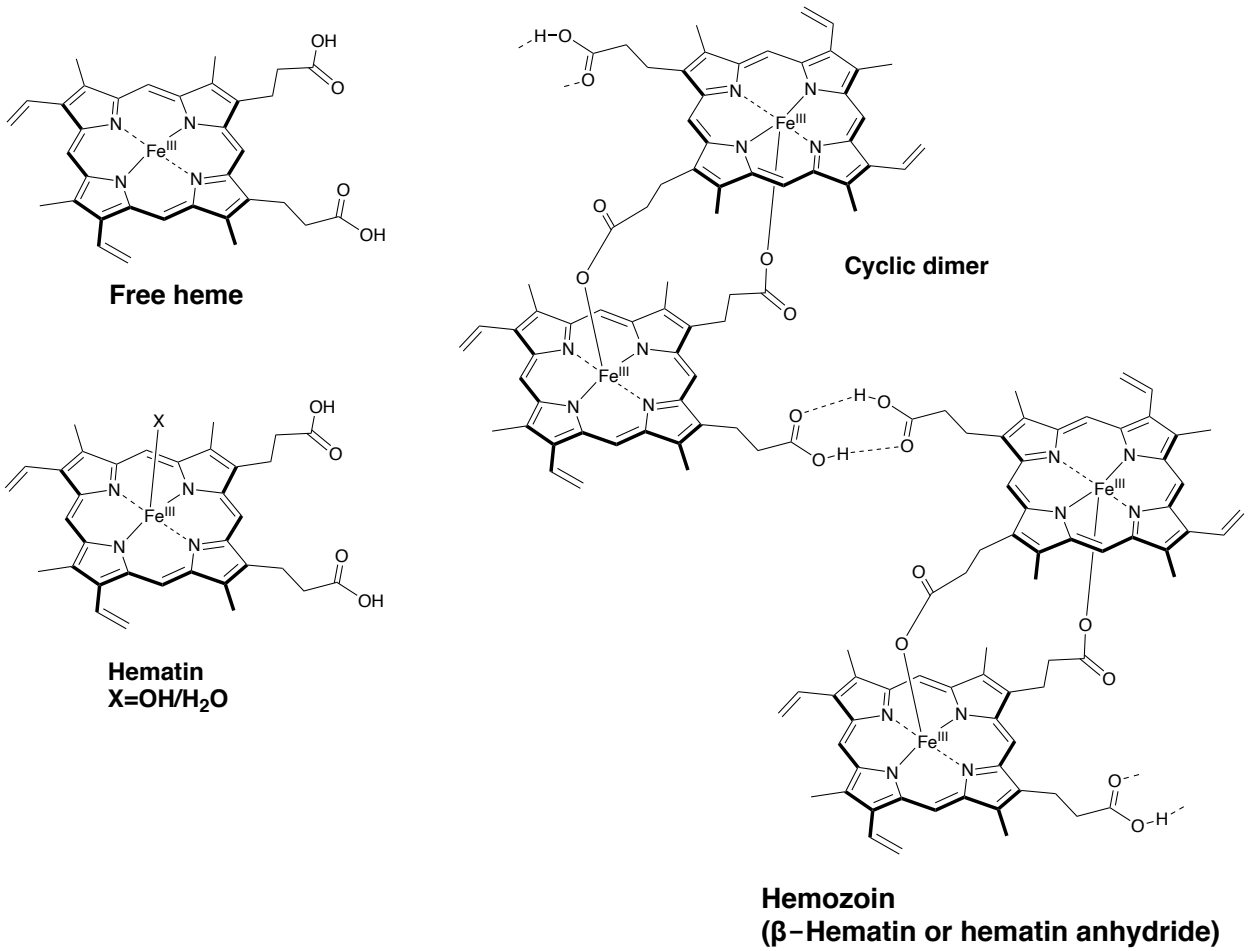

Figure 1.3. Structure of Fe(III)PPIX. Figure adapted from Egan.[18]

1.5 Antimalarial Drugs

Powdered cinchona tree bark has been used to treat malaria chills for centuries in South America. It was later discovered that the *cinchona* sp. contains several alkaloids, and the active ingredient for treating malaria was quinine (QN) and quinidine (QD), **Figure 1.*13***, first discovered in 1820 and 1833, respectively. QN was first isolated in 1820, and its first total synthesis was reported in 1944; however, its total synthesis is more laborious than its extraction. Depending on the species, a cinchona bark contains 6 - 10 % alkaloids, of which 2-8 % is QN, and 0.2 % is QD. The tree also contains smaller quantities of over 30 other alkaloids.[21,22] Despite its effectiveness, there are many

concerns about QNs toxicity profile; therefore, its use has been limited for treating severe malaria in combination with doxycycline when other front-line medications are not available.[23]

The discovery of QN led to the synthesis of different classes of antimalarial drugs, mostly still in use today. In an attempt to synthesize QN in 1856, William Henry Perkins accidentally synthesized the first synthetic dye methylene blue. In 1891 Paul Ehrlich cured malaria patients with the dye after noticing the dye was selectively taken up by the parasite. Methylene blue inhibits glutathione reductase, disturbing redox homeostasis of the parasite.[24] Modification of methylene blue led to the synthesis of 3 classes of antimalarial drug families: 8-aminoquinolines (8-AQs), acridines, and 4-AQs.[5]

1.5.1 8-Aminoquinolines

Modification of methylene blue led to the synthesis 8-AQs, which are used as a radical cure against malaria. The first 8-AQ, Pamaquine was synthesized in 1925 by the German pharmaceutical company Bayer but displayed many side effects; therefore, it was not widely used.[5] Modification via the removal of the diethylamino sidechain of pamaquine for an unsubstituted amine gave primaquine (PQ), **Figure 1.4**.

1.5.1.1 Primaquine

PQ, synthesized in 1946, has a much-improved safety profile compared to pamaquine and is currently used in clinics.[25] It is effective against hypnozoites in *P. vivax* and *P. ovale* and the liver stage of *P. falciparum*. Therefore, it is administered as a radical cure against malaria. Until recently, PQ was the only approved drug for the treatment of liver-stage parasites. It has a short

elimination half-life of 4-6 hours and is administered over 14 days at 15 mg/day.[26] PQ is contraindicated in patients deficient in glucose-6-phosphate dehydrogenase (G6PD) as it causes hemolysis and methemoglobinemia. This deficiency is present in 15 - 20% of the population in malaria-endemic regions.[27,28] 5-hydroxyprimaquine and 6-methoxy-8-AQ, **Figure 1.4**, are PQ metabolites that are directly responsible for its toxicity (quinone toxicity is discussed in section 1.5.3.4.1). PQ is not safe for pregnant women or children under the age of 4.[26] Due to its weak blood schizonticidal activity, monotherapy is highly discouraged. It is usually given as a co-therapy with an anti-schizonticide antimalarial to prevent relapse.

1.5.1.2 Tafenoquine

Tafenoquine (TFQ), developed by GlaxoSmithKline and Medicines for Malaria Venture, is a more lipophilic derivative of PQ that has a longer elimination half-life of 2 weeks. It was first developed in 1978 by the Walter Reed Army Institute of Research. In 2018 TFQ was approved by the USA's Food and Drug Administration as a prophylactic treatment of *P. vivax.*[29] Due to its long elimination half-life TFQ is administered orally at 200 mg once a day for three days and then 200 mg once a week for eight weeks.[30] TFQ is effective against liver-stage, asexual stage and sexual stage parasite in *P. vivax* and *P. falciparum*. Like PQ, TFQ is highly effective against hypnozoites. Although it is better tolerated, TFQ cannot be given to patients with a G6PD deficiency or pregnant women. TFQ is more potent than PQ against blood-stage parasites, but its activity is low; therefore, it is given in combination with other blood schizonticidal agents.[28,31]

1.5.1.3 Bulaquine

Bulaquine (BQ) is a PQ prodrug approved outside of North America. It was developed by the Central Drug Research Institute in India for the treatment of *P. vivax*,[32] and it is given in combination with chloroquine (CQ). BQ prevents relapse in *P. vivax* cases and has gametocytocidal activity. BQ can be used as a safe alternative to PQ. It is currently under Phase II clinical trial with a recommended dose of 25 mg/day for five days.[25]

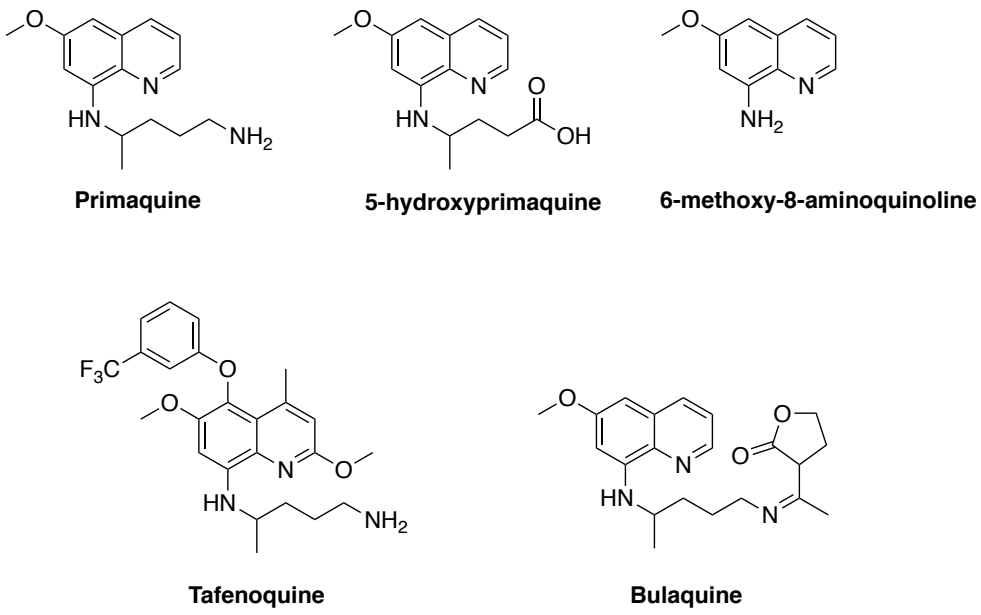

Figure 1.4. 8-Aminoquinolines.

1.5.2 Acridines

Another class of antimalarial drugs that arose from methylene blue modifications is acridines, **Figure 1.5**. Acridines were first synthesized in the 1930s, and their primary mode of action is on blood-stage parasites.[5] However, their use was short-lived because shortly after their introduction, CQ was synthesized. As CQ was a significantly better drug, due to its low toxicity and high

potency, acridine use was reduced. When CQ resistance became more widespread in the 1960s, the focus returned to acridines to produce non-resistant antimalarial drugs.

1.5.2.1 Mepacrine

Mepacrine (MP) was first synthesized in 1930; however, its use has not been widespread due to its many side effects. It accumulates in the liver, kidney, and spleen and has a long elimination half-life of up to 14 days. MP (also known as Quinacrine) has also been shown to accumulate in lysosomes and bind to nucleic acids. It is an effective inhibitor of parasitic nucleic acid synthesis, and it has been shown that low concentrations of MP inhibited the incorporation of 80% of P^{32} into erythrocytic DNA and RNA of rat *P. berghei.*[33] Another study showed MP inhibits the incorporation of ^{3}H adenosine triphosphate in *P. berghei.*[34] Despite this antimalarial activity, MP causes skin and tissue discolouration, dermatitis, diarrhea, and vertigo, to name a few. For these reasons, MP is no longer in use.

1.5.2.2 Pyronaridine

Pyronaridine (PN) was synthesized in China in 1970 by the Institute of Parasite Diseases. Similar to MP, PN contains an aza-acridine core; however, dissimilarly, it contains an aminophenol with two Mannich base side chains. Its mechanism of action remains unknown, but it is speculated that it interferes with HZ formation. It is highly effective against CQ resistant (CQR) and CQ sensitive (CQS) parasite strains. There is a possibility of cross-resistance / susceptibility between PN, and CQ.[35] PN is well tolerated; however, it can be metabolized to the quinone imine, a compound toxic to neutrophils, **Figure 1.5**. It is currently administered as combination therapy with the artemisinin artesunate to treat uncomplicated malaria for *P. falciparum* and *P. vivax.*[5,25]

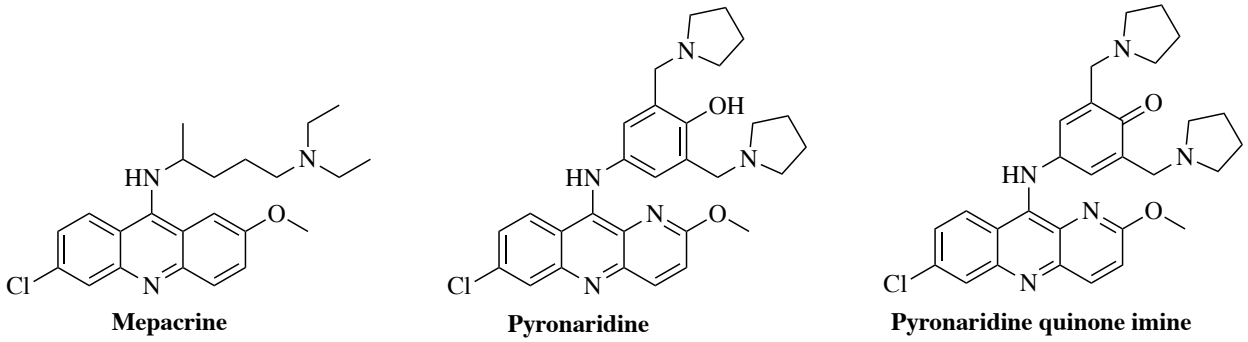

Figure 1.5. Acridines.

1.5.3 4-Aminoquinolines

The most important class of compounds to arise from methylene blue modifications are the 4-AQs, **Figure 1.6**. There have been countless derivatives and reviews on this group of compounds, which gave rise to the most crucial antimalarial ever synthesized, CQ, considered the gold standard of antimalarials due to its low cost and high efficacy.

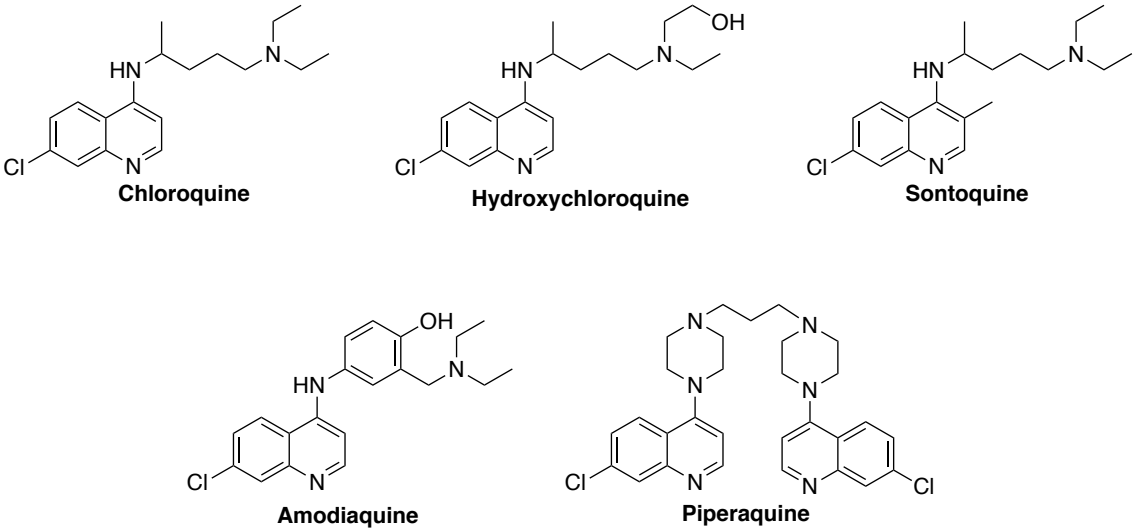

Figure 1.6. 4-aminoquinolines.

1.5.3.1 Chloroquine

CQ was first synthesized in 1934 by Bayer Pharmaceuticals. However, its first safety profile determined that it was too toxic. Interest in CQ was reignited in 1945 when its development was handed over to the USA.[36] 15 years after its introduction, there was a high occurrence of CQR parasite strains, and in 2001 the molecular biomarker of CQ resistance was discovered. It is a highly effective blood schizonticide in sensitive parasites with an elimination half-life of 1 - 2 months.[37]

1.5.3.1.1 Mode of action

CQ is a lipophilic, weak diprotic base, with pK_as of the quinoline nitrogen and the dialkylamino side chain of 8.1 and 10.2, respectively. CQ accumulates in the DV, where it is primarily active. Unprotonated CQ is membrane permeable and easily enters the DV down its pH gradient. The DV has a pH of ~ 5.2. Once CQ is within the vacuole, it becomes diprotonated and membrane-impermeable, thus trapped within its target organelle.[38] Once within the DV, it has been reported that CQ interferes with the parasite's detoxification mechanism of HZ formation, **Figure 1.7**. CQ forms a complex with Fe(III)PPIX, thus preventing the propagation of HZ.[39] This leads to the buildup of free heme and the eventual death of the parasite.

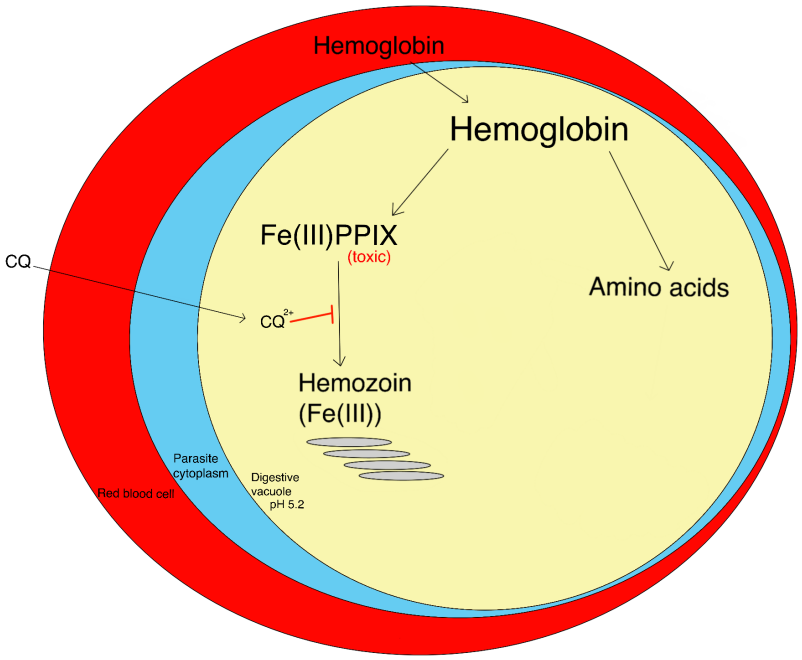

Figure 1.7. CQ mechanism of action.

1.5.3.1.2 Complex formation

CQ inhibits β-hematin formation by forming a complex with Fe(III)PPIX. This complex may inhibit crystal nucleation, block the fastest growing face of the HZ crystal,[19] or essentially bind to any stage of HZ formation to block propagation of growth.[40] It has been suggested that this complex is driven by coordination to the Fe(III) centre, H-bonding, and π – π interactions between the porphyrin and the quinoline ring. The association constant between the porphyrin and quinoline ring is dependent on the quinoline ring substituents. Lipophilic, electron-withdrawing groups form a stronger association than electron-donating groups. A stronger association is directly correlated with greater β-hematin inhibition.[41]

There has not yet been a universal consensus reached on the structure of the Fe(III)PPIX - CQ complex formed. With the use of a gallium protoporphyrin IX (Ga(III)PPIX) model, Dodd and Bohle were able to mimic the potential complex formed both in solution and in the solid-state,[42]

Figure 1.8. They show that CQ forms a distinct, well-defined complex with $[Ga(III)PPIX]_2$ and highlights the significance of alkoxide coordination and H-bonding as a stabilizing feature. Other publications focus on μ-oxo dimer formation and the reliance on $\pi - \pi$ stacking interactions to explain complex formation.[12,43,44] However, there is no evidence of the presence of μ-oxo dimer formation *in vivo*, though it is expected to form under slightly acidic conditions pH 5.5 – 6.0. Lower pH's promote the aggregation of the dimer and may accelerate HZ formation.[12,44]

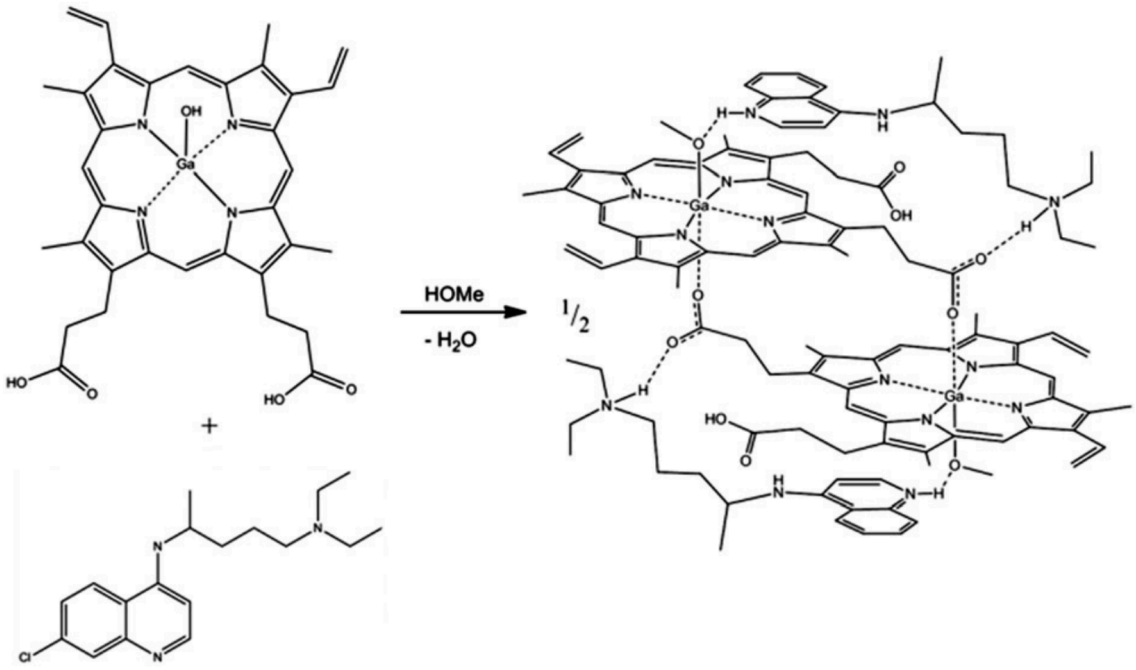

Figure 1.8. Ga(III)PPIX and CQ complex formed in the presence of methanol.[42]

1.5.3.1.3 CQ structure-activity relationship

CQ activity is highly dependent on each component of its structure, **Figure 1.9**. Structure-Activity Relationship (SAR) analyses have been carried out to determine the role of each structural component. As mentioned, CQ accumulates within the DV via the protonation of the two basic amines. The removal of the quinolinium amine reduces the accumulation of the compound 100 –

fold compared to compounds containing a basic side chain.[45] As accumulation within the active site is reduced, so is the antiplasmodial activity. Vippagunta *et al*. synthesized a CQ analogue in which the only modification was the absence of the tertiary alkylamine and found that it is 4 – fold less potent than CQ in CQS strain NF54.[46] Egan *et al*. were able to demonstrate that CQ analogs lacking a basic side chain retained their ability to inhibit β-hematin formation (discussed in chapter 2); however, they displayed poor antiplasmodial activity, with IC_{50} values between 3.8 – 5 μM.[45]

It has been shown that the length of the side chain has a significant impact on the antiplasmodial activity of the compound. Shortening the chain appears to increase potency, whereas increasing the length has a negative effect on activity. This is evident in the antimalarial drug candidate currently undergoing clinical trials, which contains a shortened chain, AQ13, **Figure 1.*11***. Furthermore, the length of the side chain has an impact on the stability of the quinoline-Fe(III)PPIX complex formed. Increasing the length by more than three carbons may force the chain outside the Fe(III)PPIX rim. A chain too short may lower van der Waals contributions, **Figure 1.*8***.[47]

A key feature of CQ's activity is its ability to accumulate within the DV and inhibit β-hematin formation. The nature of the substituent at the 7-position determines the compound's ability to inhibit β-hematin. This is because substituents on the quinoline ring will affect the compound's lipophilicity and the pK_a of the quinoline nitrogen, which determines the association constant with Fe(III)PPIX and its ability to accumulate with the DV. Studies have shown that the 7-chloro substituent is essential for inhibition of β-hematin formation.[48] The use of electron-withdrawing lipophilic groups such as Cl, CF_3, and NO_2 lowers the pK_a of the quinolinium nitrogen and

increases the compound's lipophilicity its association constant. Thus, the Cl moiety shows the highest inhibition of β-hematin formation.[48] The use of electron-donating groups such as NH_2 and OCH_3 raises the quinolinium pK_a, decreases the lipophilicity of the compound and its association constant relative to CQ. Substituents on the quinoline ring also affect the pK_a of the tertiary alkylamine; however, the effects on the side chain vary with varying side chain lengths. Hawley *et al*. reported the correlation between drug accumulation and β-hematin inhibition,[49] and Egan *et al*. have reported a linear correlation between β-hematin inhibition and antiplasmodial activity. Therefore, CQ activity is dependent on its accumulation within the DV and its ability to inhibit β-hematin formation, which are both influenced by the nature of the substituent at the 7-position.

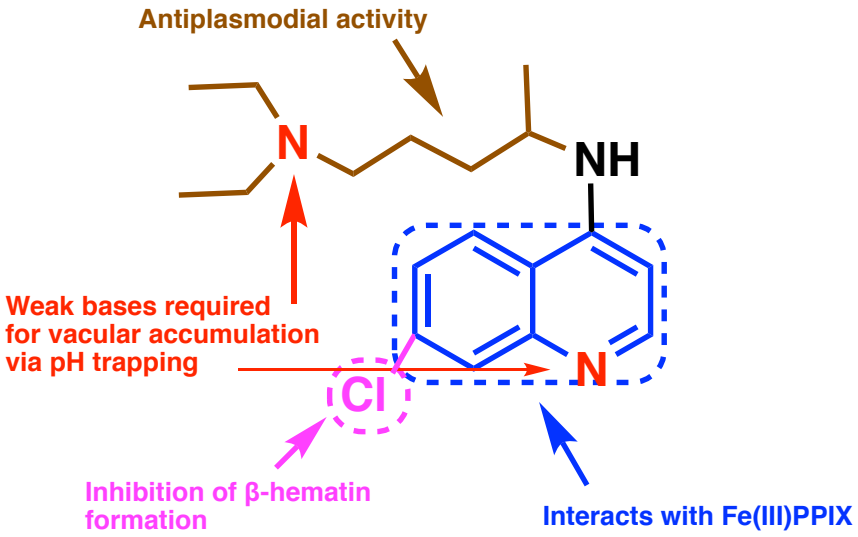

Figure 1.9. CQ Structure-Activity Relationship.

1.5.3.1.4 Metabolism

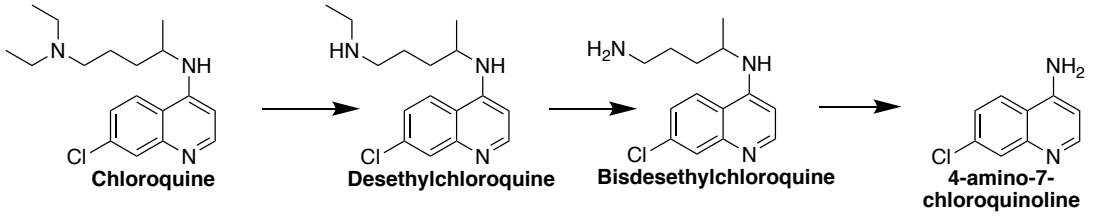

Scheme 1.1. CQ metabolism.

Following oral administration, CQ is metabolized into desethylCQ, bisdesethylCQ and to a lesser extent 4-amino-7-CQ by the kidney and liver, as shown in **Scheme 1.1**. DesethylCQ is the major metabolite that is found in high concentrations in the blood and plasma.[50] DesethylCQ is as active against CQS strains as CQ but is less active than CQ in CQR strains.[47,51] Furthermore, CQ is primarily excreted through urine and to a lesser extent in feces.[52]

1.5.3.1.5 Side effects

CQ is well tolerated; it is safe for use in children and pregnant women. However, it does have some side effects, which include nausea, dizziness, and headaches. CQ can cross the blood-retina wall and deposit into melanin-rich tissue. Long-term use of over five years can cause retinopathy, leading to blurred vision to complete vision impairment.[53,54] Retinopathy is irreversible, but early detection can prevent disease progression. An important contraindication of CQ is cardiotoxicity. The K^+ ion channel encoded by the human ether-a-go-go related gene (hERG), which regulates cardiac action potential, is inhibited by CQ. Inhibition of this channel can cause prolonged QTc intervals, arrhythmia and, in some cases, heart failure.[41,55] Therefore, it is crucial to identify patients with a history of retinopathy and arrhythmia to avoid adverse effects.

1.5.3.2 Hydroxychloroquine

Hydroxychloroquine (HCQ) was first synthesized in 1946. It is a more polar derivative with a hydroxy group on the alkyl side chain. The pK_a of the quinolinium nitrogen is similar to that of CQ; however, tertiary amine salt has a lowered pK_a of 9.7.[56] HCQ is less lipophilic therefore does not easily diffuse across cell membranes, resulting in less accumulation in the DV. HCQ is 1.6 – fold less potent than CQ in CQS strains and 8.8 - fold less potent than CQ in CQR strains.[56] For these reasons, HCQ is not commonly used as an antimalarial drug.

HCQ is the safer alternative to CQ as it does not readily cross the blood-retina barrier; therefore, it deposits less onto melanin-rich tissue. Thus, retinopathy is only observed after continuous long-term usage of HCQ. HCQ can also cross the placental as levels in maternal cells are equivalent to that of the fetus. Interestingly, to date, there has been no evidence of toxicity to the fetus, no congenital abnormalities, and no harm to newborns via breastfeeding. Therefore, HCQ is safe for pregnant and breastfeeding women.[57] The presence of the hydroxy group facilitates phase II conjugation allowing for bile excretion.[52] HCQ causes immunomodulatory effects such as inhibition of phagocytosis and proteolysis, interference with lysosomal acidification, and toll-like receptor signalling inhibition. In the USA, HCQ is commonly used to treat systemic lupus erythematosus and rheumatoid arthritis.[57]

1.5.3.3 Sontoquine

The 3-methyl CQ analogue sontoquine (SQ) was synthesized in 1936 by Bayer Pharmaceuticals. Its synthesis was fueled by the initial incorrect classification of CQ as too toxic for use. SQ is slightly less potent than CQ in CQS and CQR strains and was relatively safe. Initial human trials began in 1937 in Cameroon to treat *P. vivax* and *P. falciparum*. This led to further trials in 1942

in Tunisia by German and French scientists for the development of SQ. In 1943 research data was handed over to the USA for analysis, which led to the resynthesis of CQ.[36] The rediscovery of CQ showed that it was non-toxic and more potent antimalarial. SQ development was discontinued in favour of CQ development.

1.5.3.4 Amodiaquine

Amodiaquine (ADQ), first synthesized in 1948, is a Mannich base 4-AQ with a 4-aminophenol. It is a more potent and more lipophilic derivative of CQ. ADQ is a weaker base than CQ with pK_as of 7.1 and 8.1 for the quinolinium nitrogen and alkyl nitrogen, respectively. That being said, AQ accumulation is 2- to 3- fold greater than CQ in CQS strain (HB3). Indicating that its accumulation is energy and pH-dependent, as only 15% of ADQ accumulation can be attributed to its weak base properties.[58] Due to the hydroxy and diethylamino moieties' proximity, ADQ can form intramolecular hydrogen bonds at physiological pH. This potentially plays a role in its increased potency in CQR parasites. ADQ analogues with hydrogen bonding groups display greater in vitro activity than those unable to H-bond.

1.5.3.4.1 Metabolism

ADQ is quickly metabolized in the liver and has an elimination half-life of 5.2 hours, **Scheme 1.2**. Its metabolic products are slowly excreted from the body and have an elimination half-life >4 days. N-desethylamodiaquine (DADQ) is the primary ADQ metabolite mediated by cytochrome P_{450}2C8. AQ is 3 - fold more potent than DADQ, but due to its high concentration, DADQ contributed to the observed antiplasmodial activity.[59]

The presence of the 4-hydroxyanilino group is a cause of toxicity to the compound. The toxic metabolite ADQ quinone-imine (ADQQI) is formed in the presence of cytochrome P_{450}. This metabolite is then susceptible to nucleophilic attack by glutathione to give ADQ-GS, which is non-toxic. However, long-term use or high dosage of ADQ leads to the depletion of glutathione levels,[60] leading to liver toxicity due to the increased concentration of ADQQI. ADQQI is also susceptible to nucleophilic attack by thiol-containing enzymes that can cause hepatotoxicity. They are also highly immunogenic and lead to agranulocytosis. Hepatoxicity is observed within three weeks to 10 months of continuous use, and agranulocytosis is observed after five to 14 weeks of continuous use.[5] Thus, prophylactic use of ADQ is not recommended. The WHO lists ADQ use only for combination therapy with the artemisinin artesunate.[23]

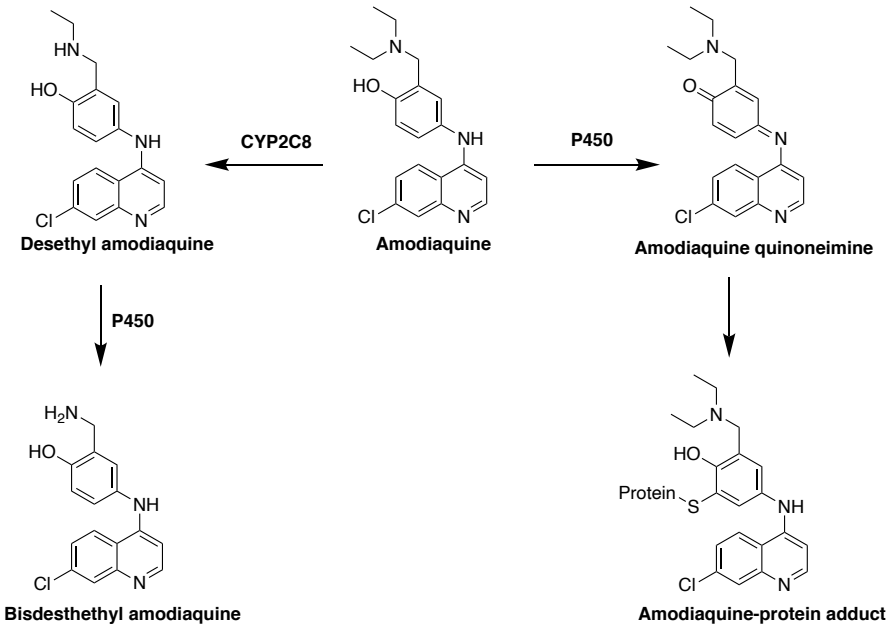

Scheme 1.2. ADQ metabolism.

1.5.3.4.2 Detoxification

Although ADQ is effective in CQR strains, its side effects are a significant deterrent. In an attempt to reduce its toxicity, several analogs with good antimalarial profiles have been synthesized. Incorporating a fluorine group can lead to increased lipophilicity, increased oxidation potential, stronger H-bonding, and changes in pK_as. O'Neill *et al.* substituted the 4-hydroxy group for a 4-fluoro group, **Figure 1.10**, to improve the stability of the aryl ring to oxidation, thus blocking bioactivation to the quinone imine. The 4-fluoroamodiaquine (FAQ) analog shows retention of antiplasmodial activity with no bioactivation.[61]

The exchange of the methylene N-diethyl with the hydroxy group gives rise to isoquine. This exchange completely inhibits the formation of ADQQI, and it is more potent than ADQ in both CQS and CQR *P. falciparum* strains. However, the desethyl metabolic product displays hepatotoxicity.[50] To combat the formation of ADQQI and dealkylation of FAQ4, tert-butylisoquine was synthesized. Tert-butylisoquine contains an N-tert-butyl group, which cannot be dealkylated due to steric hindrance, and bioactivation is inhibited due to the positioning of the hydroxy group. This compound also retains its antiplasmodial activity and is less toxic than ADQ. It is currently in clinical trials at GlaxoSmithKline. FAQ4 contains the N-tert-butyl moiety, and the 4-hydroxy is replaced with fluorine. Dealkylation is blocked due to steric hindrance, and there is no observed quinone-imine formed because of the 4-fluoro group. FAQ4 is active in CQS and CQR strains in *P. falciparum*. This compound is also currently under clinical trials with Medicines for Malaria Venture.[47]

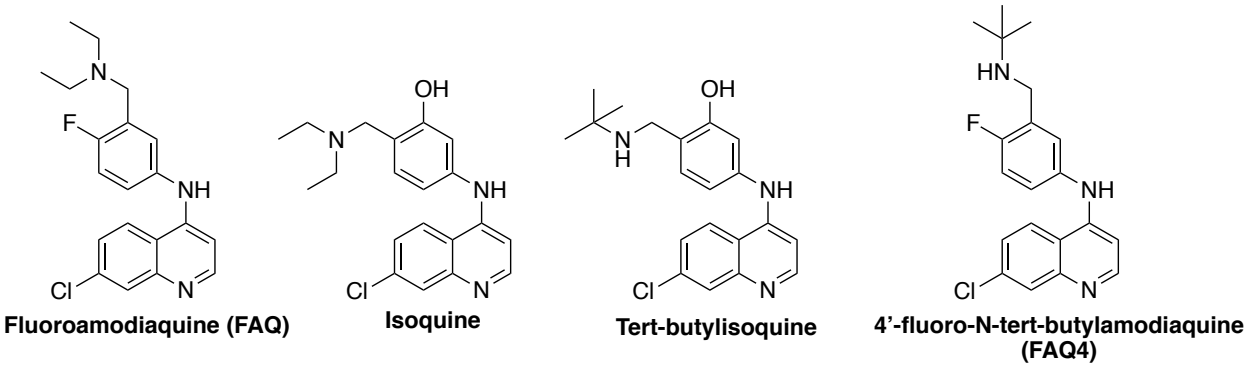

Figure 1.10. ADQ analogs.

1.5.3.5 Piperaquine

Piperaquine (PPQ) was first synthesized in the 1960s by a group in China and France independently. It is a bis-4-AQ linked by an alkyl chain. It was synthesized as a replacement for CQ after the rise of resistance and used exclusively in China. It was phased out in the late 1980s due to resistance. PPQ is a less toxic CQ analog that is equipotent to CQ in CQS strains and is 6 - fold more active in CQR strains than CQ. It has a quinolinium pK_a of 8.9, and it is highly lipid-soluble. It has a similar elimination half-life to that of CQ of 1-2 months. PPQ is believed to exert its activity similarly to CQ; however, there is insufficient research on its mode of action. PPQ contains more protonation sites than CQ, which may allow for greater accumulation in CQR strains. Molecular modelling shows that both quinoline nuclei are capable of forming a complex with β-hematin.[62]

PPQ is relatively safe and well-tolerated with minor side effects such as dizziness, vomiting and mild headache. A rare significant side effect is the increase in blood pressure. PPQ is not recommended for pregnant women or children under the age of two, as there is insufficient evidence of safety for these at-risk groups.[63] PPQ has been reintroduced in the Chinese market as

a combination therapy with the artemisinin derivative dihydroartemisinin. It is worth noting that PPQ resistance has not been observed in high transmission areas such as Sub-Saharan Africa as it is not widely used.

1.5.4 AQs in clinical trials

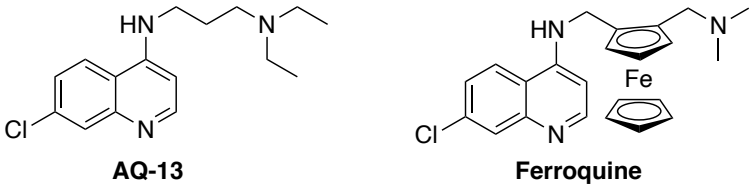

Figure 1.11. Antimalarial drug candidates in clinical trials.

1.5.4.1 Ferroquine

Ferroquine (FQ) is a 4-amino-organometalo-quinoline. It was first designed in 1993, and its first published synthesis was in 1997.[64] FQ is the first organometallic antimalarial, with an elimination half-life of 16 days, see **Figure 1.11**. It completed Phase II clinical trials in 2011 by Sanofi-Aventis and has not entered Phase III trials (ClinicalTrials.gov Identifier: NCT00988507). The presence of 1,2-unsymmetrically substituted ferrocene gives the molecule planar chirality. Experiments have shown no significant difference in activity between the enantiomerically pure S (-)-FQ and R (+)-FQ; therefore, it is prepared and administered as a racemate. FQ is highly effective against CQS and CQR strains of *P. falciparum*, and there is little chance of cross-resistance with CQ. FQ is a weaker base than CQ with pK_as of 7.0 and 8.5 for the quinolinium nitrogen and tertiary nitrogen. Furthermore, FQ is 100 - times more lipophilic than CQ at cytosolic pH and is more lipophilic than CQ at vacuolar pH. FQ accumulates 50 times more than CQ at pH 5[65] despite being a weaker base.

Unlike CQ, neutral FQ can easily form a strong intramolecular H-bond, as shown in **Figure 1.12**. A 2.17 Å bond is formed between the anilino (N11) and tertiary amino (N24), resulting in a folded conformation. In contrast, diprotonated FQ adopts an open conformation to allow H-bonding with the solvent. The folded conformation results in the increase of hydrophobicity and the protrusion of the ferrocenyl moiety towards the outside. It is believed that the hydrophobic ferrocenyl moiety interacts with lipid structures in the membrane, and the quinoline stacks with Fe(III)PPIX. This reversible open/folded conformation allows for the transport of FQ between membranes and is believed to facilitate FQs ability to accumulate in the DV and to evade resistance transport system.[65,66]

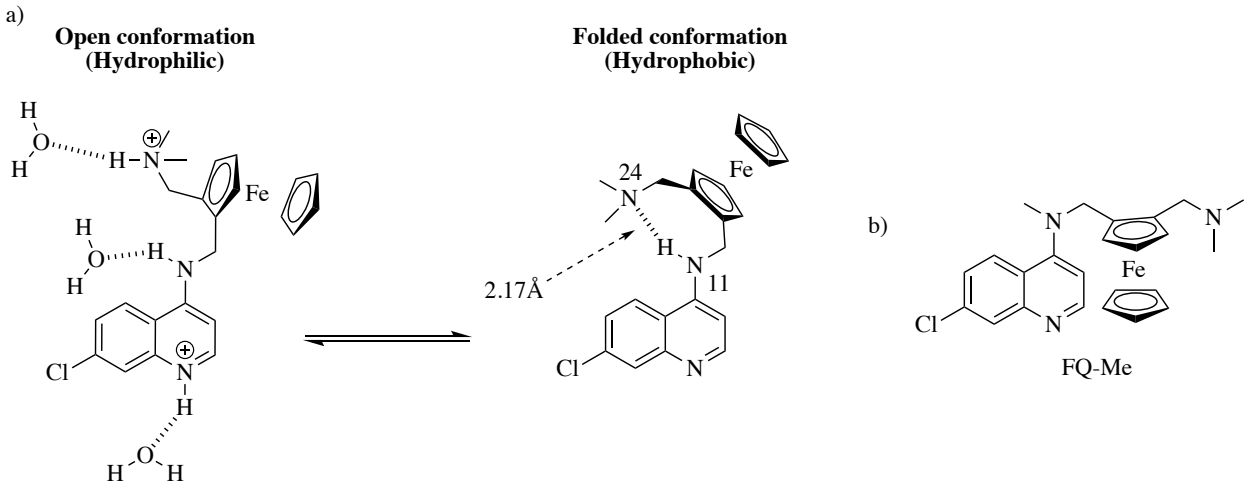

Figure 1.12. a) Hydrogen-bonding in FQ and b) the structure of methyl FQ.

To determine the importance of H-bonding in FQ, a 4-methyl analog was synthesized with a methyl group on the anilino nitrogen. FQ-Me is a more lipophilic and slightly more basic analog with pK_as of 7.1 and 8.8 for quinolinium and tertiary nitrogen, respectively. FQ-Me can inhibit β-hematin formation; however, its antiplasmodial activity is considerably reduced in CQS and CQR strains.[67] Thus, the H-bond characteristic is required for effective antiplasmodial activity.

FQ is considered to be relatively non-toxic, with no significant side effects reported. Experiments to induce resistance under drug pressure shows a low chance of cross-resistance of FQ with CQ and other antimalarials and a low possibility of the emergence of resistance. Due to its high antimalarial potency and low change of resistance, FQ could be administered as monotherapy. However, Phase II clinical trials for combination therapy with artefenomel were recently terminated due to a lack of efficacy.

1.5.4.2 AQ-13

AQ-13 synthesis was first published in 1948;[68] however, its development in clinical trials was not pursued until 1996.[69] It is a CQ analog in which the isopentyl chain is replaced with a propyl chain, **Figure 1.11**. AQ-13 was found to be effective against *P. vivax* and CQS and CQR strains of *P. falciparum*. It has similar antiplasmodial activity to CQ in CQS strains and is more potent than CQ in CQR strains. Like CQ, it is safe for human use with a low toxicity profile. AQ-13 is less bioavailable than CQ and has a shorter elimination half-life of 13 days. The N-diethyl moieties are susceptible to oxidative dealkylation. The metabolic products that result in mono- and di-dealkylation are active in CQS strains but not on CQR *P. falciparum*.[70]

Side effects are similar to that of CQ: headache, nausea and diarrhea, and major side effect such as QTc interval prolongation was observed only in high dosage patients.[70] These effects are avoided when drug concentration is reduced. AQ-13 is currently under phase II clinical trials sponsored by Tulane University Health Sciences Centre.

1.5.5 Aryl aminoalcohols

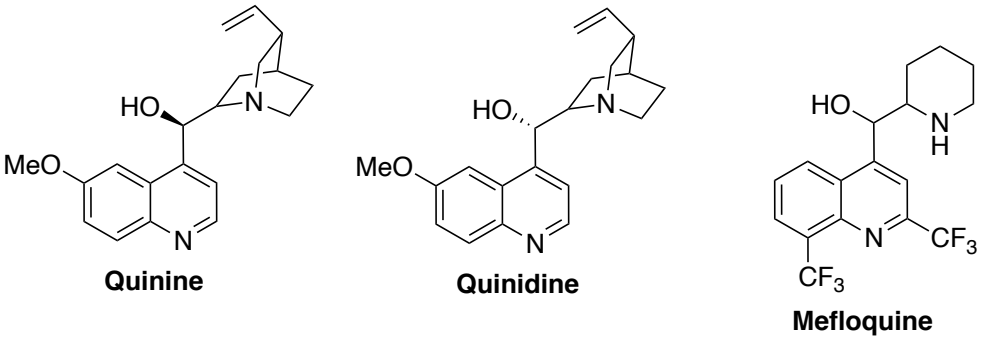

Figure 1.13. Aryl aminoalcohols

1.5.5.1 Quinine

QN is extracted from cinchona bark and was the first antimalarial discovered. It was first isolated in 1820 by Pettetier and Caventon,[71] and its first total synthesis was carried out in 1944 by Woodward and Doering, **Figure 1.13**.[72] As it currently stands, it is more economical to extract QN than to synthesize it. QN was the front-line antimalarial used until the discovery and synthesis of more potent AQ antimalarials. QN is a weaker base than CQ with the quinolinium pK_a of 5.1[73] versus 8.2 for CQ. Therefore, QN accumulates in the DV in its monoprotonated form. QN is a fast-acting schizonticide effective in *P. falciparum* and *P. vivax.* Moreover, it is also active against gametocytes of *P. vivax* and *P. malariae*. It has an elimination half-life of 11-18 hours and is used to treat severe malaria.

Most patients undergoing QN treatment experience a condition called cinchonism. Cinchonism symptoms include tinnitus, nausea, headaches and slight hearing loss, which is reversible when drug dosage is reduced. More severe symptoms include vertigo, diarrhea, vision and hearing loss.[71] The WHO currently recommends that QN only be used for cases of severe malaria and in combination with doxycycline.[23]

1.5.5.2 Mefloquine

Mefloquine (MQ) contains a single piperidine ring and two trifluoromethyl groups at the 2- and 8-position, **Figure 1.13**. MQ was first synthesized during World War II and used as a CQ replacement in the 1980s. Like CQ, it is a weak diprotic base, and at physiological pH, it can form an intramolecular H-bond between the hydroxyl group and protonated tertiary amino group.[24] MQ is a blood schizonticide that is active against *P. falciparum* and *P. vivax*. Its mechanism of action is unknown; however, it is believed to act similarly to CQ and QN. MQ can cause severe side effects, particularly related to the central nervous system, such as neuropsychiatric effects. It is contraindicated in patients with hypersensitivity to QN-related compounds, and it is not recommended for pregnant women and children weighing less than 15 kg.[74]

1.5.6 Non-quinoline antimalarials

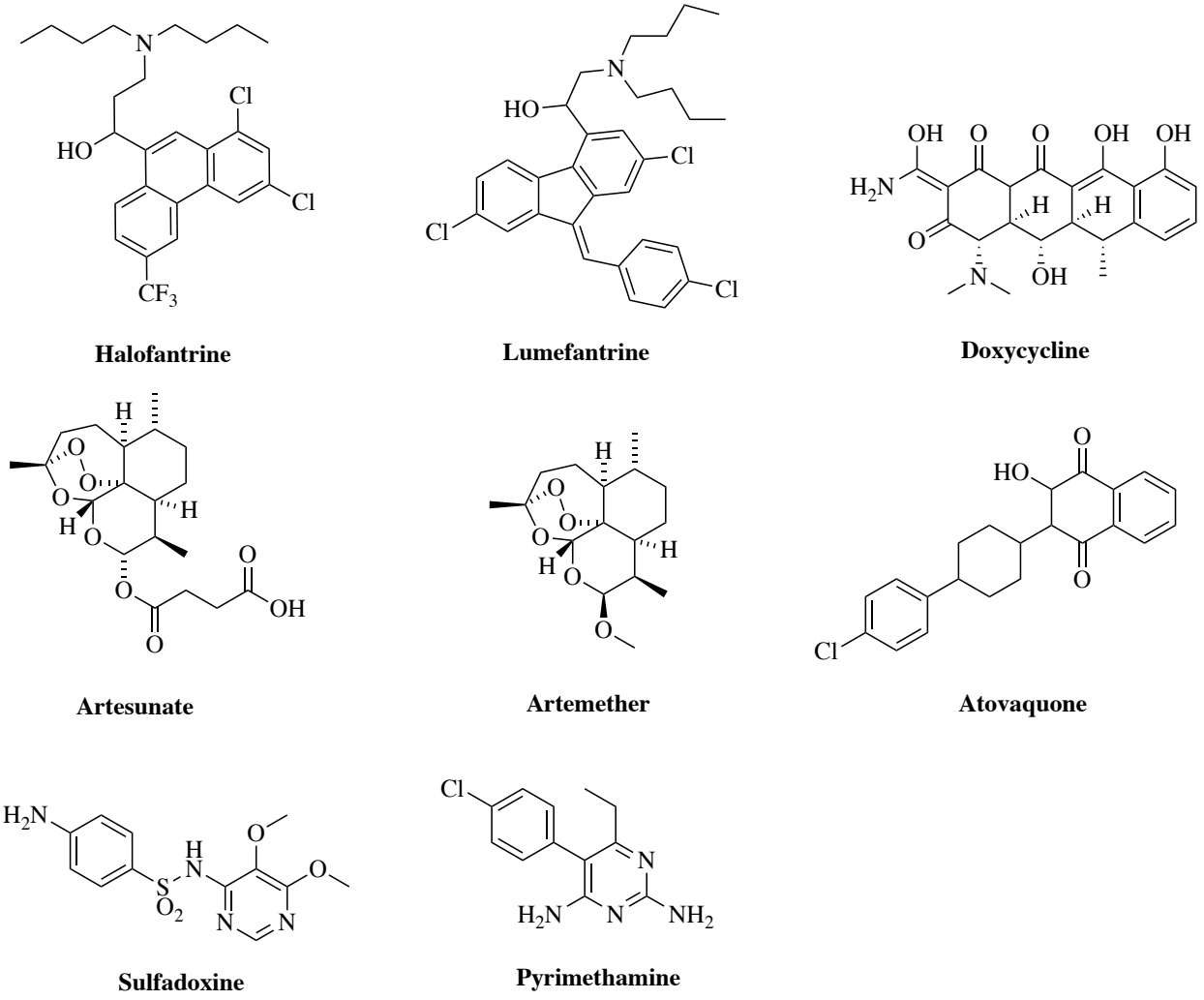

Figure 1.14. Non-quinoline antimalarial drugs.

We have discussed various quinoline-based antimalarial drugs as they are the most extensively studied classes. Other classes of antimalarial drugs and their modes of action are listed in **Table 1.1**. These antimalarials are often used in combination with schizonticides to ensure the clearance of the parasite and to reduce the occurrence of resistance.

Table 1.1. Mode of action of non-quinoline based antimalarial drugs.

Drug	Class	Mode of action
Halofantrine	Aryl aminoalcohol	Inhibit hemozoin formation.[75]
Lumefantrine	Aryl aminoalcohol	Inhibit hemozoin formation.[76]
Doxycycline	Antibiotic	Inhibition of apicoplast.[77]
Artesunate	Sesquiterpene lactone	Membrane disruption via free radical production.[78]
Artemether	Sesquiterpene lactone	Membrane disruption via free radical production.[78]
Atovaquone	Naphthoquinone	Parasitic mitochondrial membrane disruption via inhibition of electron transport chain.[5]
Sulfadoxine	Sulfonamide	Antifolate: inhibition of dihydropteroate synthase.[79]
Pyrimethamine	Diaminopyrimidine	Antifolate: inhibition of dihydrofolate reductase.[79]

1.6 Antimalarial Resistance

CQ resistance first appeared in the late ’50s and early ’60s in Southeast Asia and South America. Resistance is a result of sustained drug pressure in a geographical region. Resistance may also arise due to monotherapy, incorrect dosage, self-medication, and the administration of cheap counterfeit drugs.

1.6.1 *Plasmodium falciparum* Chloroquine Resistance Transporter (PfCRT)

In the year 2000, the primary determinant for CQ resistance was identified.[80,81] PfCRT is a 48 kDa protein located on the membrane of the DV. It is a member of the drug – metabolite transporter (DMT) superfamily, **Figure 1.15**.[80,82] It is a monomeric transmembrane (TM) protein that consists of 10 TM helices and two juxtamembrane helices: one is located parallel to the parasite cytosol and the other parallel to the membrane in the DV.

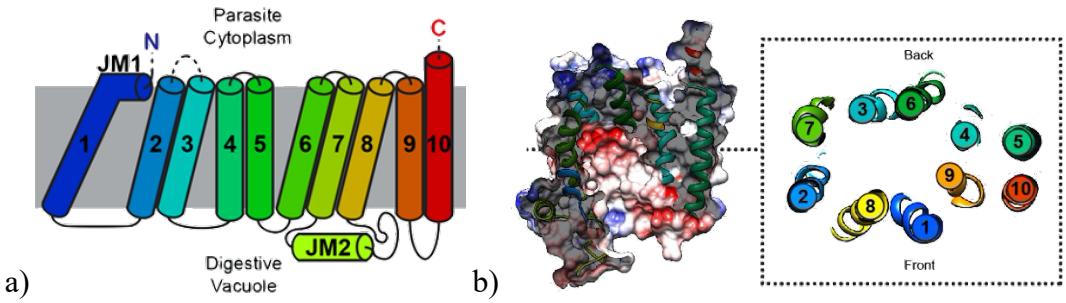

Figure 1.15. Structure of PfCRT 7G8 isoform. A) Topology showing inverted antiparallel TM helices. B) Surface representation of the central cavity's electrostatic potential with red and blue, indicating negative and positive residues, respectively. Figures are taken from Kim *et al.*[83]

The TM domains form 5 helical pairs, and TM1-4 and 6-9 form a central cavity of around 3,300 Å^3. The point mutation K76T has become a molecular marker for resistance. This mutation replaces the positively charged lysine with a neutral threonine at the 76 position in the transmembrane domain.[80] The presence of a neutral residue removes the cation – cation repulsion between protonated CQ and the lysine residue, speculated to prevent CQ efflux from the DV, **Figure 1.16**. Consequently, the mutation allows CQ to diffuse out of the DV down its concentration gradient and reduces CQ accumulation in its active site.[84] The cavity has a net negative charge influenced by three aspartate residues, suggesting possible substrates for the transporter could be positively charged, **Figure 1.15**.[83]

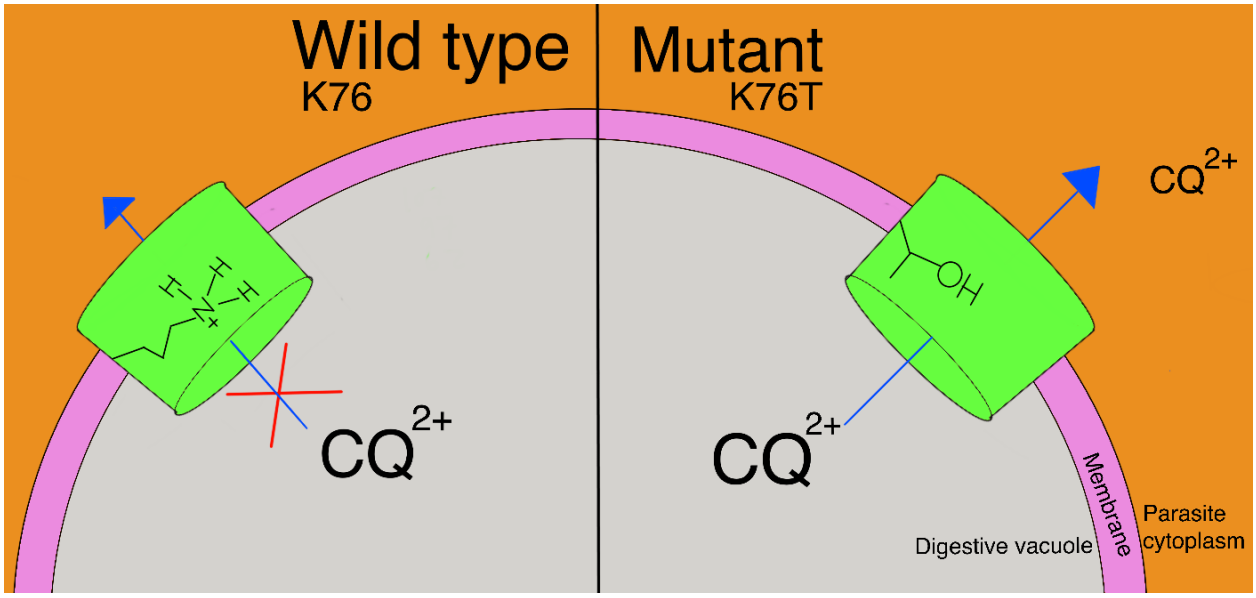

Figure 1.16. K76T mutation removes a positive charge, which allows CQ^{2+} efflux from its active site.

It has been proposed that PfCRT functions as a channel or transporter that mediates the efflux of CQ out of the DV. In the channel model, PfCRT allows protonated CQ to passively diffuse out the DV down its concentration gradient, **Figure 1.16**. However, in the transporter model, PfCRT functions as an energy coupled transporter that actively effluxes CQ out of the DV.[85,86] It is believed that at low external concentrations of CQ, CQR parasites accumulate up to 10 – fold less CQ than CQS parasites. This is achieved through the enhanced efflux capacity of the resistance parasite resulting in higher survival rates.[85,87]

1.6.2 *Plasmodium falciparum* multidrug resistance protein 1 (*pfmdr1*)

Another protein supposedly involved in CQ resistance is *Plasmodium falciparum* multidrug resistance protein (*pfmdr1*). *pfmdr1* is a 162 kDa protein that belongs to the ABC (ATP – binding cassette) superfamily. This protein is structurally similar to the mammalian multidrug resistance transporter P-glycoprotein. It comprises two homologous halves, which contain six TM domains

with one nucleotide-binding domain (NBD), **Figure 1.17**.[88] *pfmdr1* is localized to the DV membrane and is believed to behave like an energy - coupled transporter that regulates drug influx into the vacuole. [89,90]

It contains point mutations N86Y, Y184F, S1034C, N1042D, and D1246Y associated with resistance to AQs and aryl aminoalcohol antimalarial drugs. These mutations arose as a consequence of drug pressure, and their expression varies with geographical region. For instance, N84Y is mainly found in Southeast Asian isolates, and the remaining mutations are primarily found in South American isolates.[88] Although these mutations are associated with antimalarial resistance, it is not believed that they are the sole cause of resistance. It has been shown that the level of expression of *pfmdr1* is correlated to the degree of CQ resistance, which consequently results in decreased sensitivity to MQ and vice versa. Cross-resistance is also observed with halofantrine, lumefantrine and artemether. Therefore, the overexpression of *pfmdr1* and the presence of mutations results in decreased sensitivity of the parasite to certain antimalarial drugs.[84,91] Mutations may reduce *pfmdr1*s ability to transport drugs into the DV, resulting in the possible reduction of drug accumulation in their active site.

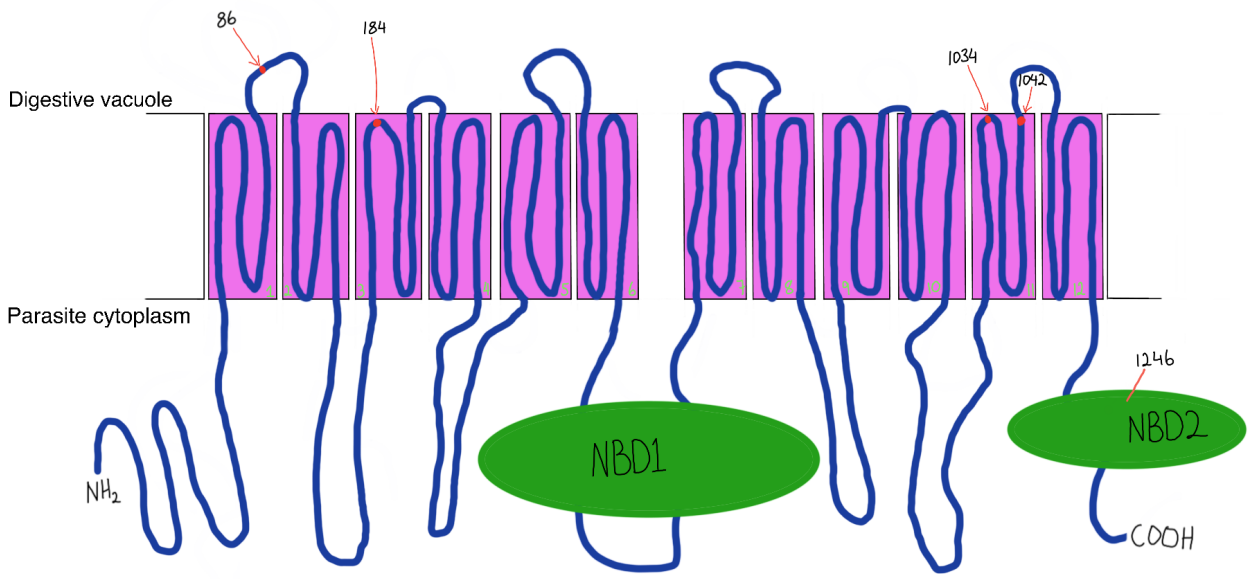

Figure 1.17 Structure of *pfmdr1* with highlighted mutations: N86Y, Y184F, S1034C, N1042D, D1246Y and two nucleotide-binding domains. Illustration adapted from Valderramos and Fidock.[91]

1.7 Vaccines

Malaria vaccine development is a long sorry saga of disappointment. Naturally acquired immunity from the disease arises after sustained repeated exposure to the parasite to maintain immunity.[92] Vaccine development has been complicated because the immune response to *P. falciparum* infection is not well understood. There are 5,300 parasitic antigens that elicit an immune response; however, it is unclear which antigens are responsible for a protective response.[92] Vaccine development is currently prioritizing administration to children under the age of five, as they represent 67% of all malaria related deaths.

1.7.1 RTS,S

In 1985 GlaxoSmithKline and the Walter Reed Army Institute of Research began testing and developing a pre-erythrocytic vaccine named RTS,S which protects against sporozoites. The DNA of a pre-erythrocytic antigen circumsporozoite protein is expressed in yeast and fused with hepatitis B surface antigen DNA to produce RTS. RTS binds hepatitis B surface antigens (S) to form RTS,S particles. Then a proprietary adjuvant system AS01 (a mixture of deacylated monophosphoryl lipid A and an emulsion QS21) is mixed with the particles to form a vaccine concoction that is given intramuscularly over several months.[93,94]

Clinical trials carried out in Mozambique, Kenya and Tanzania on children aged 5 – 17 months show that RTS,S/AS01 only provides partial immunity. Up to four doses reduced clinical cases by 56% and severe malaria cases by 47%.[95] However, vaccine efficacy decreases over time. In a trial involving children 6 – 12 weeks old, the vaccine has an initial efficacy of 33%.[4] Gambian adults given RTS,S with adjuvant AS02 over 15 weeks showed a 34% efficacy, but most importantly, efficacy is high at 71% in the first nine weeks, but it drops to 0% in the following six weeks.[92,93] It is believed that the vaccine's low and unsustainable efficacy is because it does not induce a memory T cell immune response for long-term protection.[94] Despite the lack of long-term immunity RTS,S is the first pre-erythrocytic vaccine that protects *P. falciparum*.

In 2019 the Malaria Vaccine Implementation Program launched in Ghana, Malawi, and Kenya. Children aged 6 – 24 months are given a dose at 6, 7, 9 and 24 months in Kenya and Ghana. In Malawi children aged 5 – 22 months are given a dose at 5, 6, 7 and 22 months.[96–98] In the following years we will discover the effectiveness of this implementation program.

Over the last century, there have been significant advances in the development of antimalarial drugs. However, the rise of resistance has hindered progress towards the eradication of the disease. More than ever, we require more tools for treating and preventing malaria as the number of cases and deaths increases year over year. We need to develop effective drugs that can circumvent resistance for known targets and develop drugs for new targets. Vaccine development has been challenging, however successful implementation of RTS,S along with ACT treatment can help drive down infection rates. The use of insecticide-treated mosquito nets has proven successful, therefore ensuring that a greater proportion of at-risk populations have access to these can help reduce the spread of the disease. The road to eradicating malaria has been long and strenuous; however, we must sustain research efforts if we are to meet this ambitious goal.

1.8 References

(1) World Health Organization. *World Malaria Report 2019*; 2019.

(2) World Health Organization. *World Malaria Report 2016*; 2016.

(3) Barnes, K. I. Antimalarial Drugs and the Control and Elimination of Malaria. In *Treatment and Prevention of Malaria*; Springer Basel: Basel, 2011; pp 1–17.

(4) Phillips, M. A.; Burrows, J. N.; Manyando, C.; van Huijsduijnen, R. H.; Van Voorhis, W. C.; Wells, T. N. C. Malaria. *Nat. Rev. Dis. Prim.* **2017**, *3*, 17050.

(5) Schlitzer, M. Malaria Chemotherapeutics Part I: History of Antimalarial Drug Development, Currently Used Therapeutics, and Drugs in Clinical Development. *ChemMedChem* **2007**, *2* (7), 944–986.

(6) Josling, G. A.; Llinás, M. Sexual Development in Plasmodium Parasites: Knowing When It's Time to Commit. *Nat. Rev. Microbiol.* **2015**, *13* (9), 573–587.

(7) Wirth, D. F. Biological Revelations. *Nature* **2002**, *419* (6906), 495–496.

(8) Francis, S. E.; Sullivan, D. J.; Goldberg, and D. E. Hemoglobin Metabolism In The Malaria Parasite Plasmodium Falciparum. *Annu. Rev. Microbiol.* **1997**, *51* (1), 97–123.

(9) Spiller, D. G.; Bray, P. G.; Hughes, R. H.; Ward, S. A.; White, M. R. . The PH of the Plasmodium Falciparum Digestive Vacuole: Holy Grail or Dead-End Trail? *Trends Parasitol.* **2002**, *18* (10), 441–444.

(10) Kuhn, Y.; Rohrbach, P.; Lanzer, M. Quantitative PH Measurements in Plasmodium Falciparum-Infected Erythrocytes Using PHluorin. *Cell. Microbiol.* **2007**, *9* (4), 1004–1013.

(11) Dzekunov, S. M.; Ursos, L. M. B.; Roepe, P. D. Digestive Vacuolar PH of Intact Intraerythrocytic P. Falciparum Either Sensitive or Resistant to Chloroquine. *Mol. Biochem.*

Parasitol. **2000**, *110* (1), 107–124.

(12) Gorka, A. P.; de Dios, A.; Roepe, P. D. Quinoline Drug–Heme Interactions and Implications for Antimalarial Cytostatic versus Cytocidal Activities. *J. Med. Chem.* **2013**, *56* (13), 5231–5246.

(13) Sullivan, D. J. Hemozoin: A Biocrystal Synthesized during the Degradation of Hemoglobin. In *Biopolymers Online*; Matsumura, S., Steinbüchel, A., Eds.; Wiley-VCH Verlag GmbH & Co. KGaA: Weinheim, Germany, 2005; pp 129–137.

(14) Rosenthal, P.; Meshnick, S. R. Hemoglobin Catabolism and Iron Utilization by Malaria Parasites. *Mol. Biochem. Parasitol.* **1996**, *83* (2), 131–139.

(15) Ursos, L. M. B.; Roepe, P. D. Chloroquine Resistance in the Malarial Parasite,Plasmodium Falciparum. *Med. Res. Rev.* **2002**, *22* (5), 465–491.

(16) Eggleson, K. K.; Duffin, K. L.; Goldberg, D. E. Identification and Characterization of Falcilysin, a Metallopeptidase Involved in Hemoglobin Catabolism within the Malaria Parasite Plasmodium Falciparum. *J. Biol. Chem.* **1999**, *274* (45), 32411–32417.

(17) Rosenthal, P. J. Falcipains and Other Cysteine Proteases of Malaria Parasites. *Adv. Exp. Med. Biol.* **2011**, *712*, 30–48.

(18) Egan, T. J. Haemozoin Formation. *Mol. Biochem. Parasitol.* **2008**, *157* (2), 127–136.

(19) Pagola, S.; Stephens, P. W.; Bohle, D. S.; Kosar, A. D.; Madsen, S. K. The Structure of Malaria Pigment β-Haematin. *Nature* **2000**, *404* (6775), 307–310.

(20) Casabianca, L. B.; Kallgren, J. B.; Natarajan, J. K.; Alumasa, J. N.; Roepe, P. D.; Wolf, C.; de Dios, A. C. Antimalarial Drugs and Heme in Detergent Micelles: An NMR Study. *J. Inorg. Biochem.* **2009**, *103* (5), 745–748.

(21) Nair, K. P. P. Cinchona (Cinchona Sp.). *Agron. Econ. Important Tree Crop. Dev. World*

2010, 111–129.

(22) Sullivan, D. J. Cinchona Alkaloids: Quinine and Quinidine. In *Treatment and Prevention of Malaria*; Springer Basel: Basel, 2011; pp 45–68.

(23) World Health Organization. World Health Organization Model List of Essential Medicines. *Ment. Holist. Heal. Some Int. Perspect.* **2019**, 119–134.

(24) Kaur, K.; Jain, M.; Reddy, R. P.; Jain, R. Quinolines and Structurally Related Heterocycles as Antimalarials. *Eur. J. Med. Chem.* **2010**, *45* (8), 3245–3264.

(25) Teixeira, C.; Vale, N.; Pérez, B.; Gomes, A.; Gomes, J. R. B.; Gomes, P. "Recycling" Classical Drugs for Malaria. *Chem. Rev.* **2014**, *114* (22), 11164–11220.

(26) Vale, N.; Moreira, R.; Gomes, P. Primaquine Revisited Six Decades after Its Discovery. *Eur. J. Med. Chem.* **2009**, *44* (3), 937–953.

(27) Staines, H. M.; Krishna, S. Treatment and Prevention of Malaria: Antimalarial Drug Chemistry, Action and Use. *Treat. Prev. Malar. Antimalar. Drug Chem. Action Use* **2012**, 1–315.

(28) Waters, N. C.; Edstein, M. D. 8-Aminoquinolines: Primaquine and Tafenoquine. In *Treatment and Prevention of Malaria*; Springer Basel: Basel, 2011; pp 69–94.

(29) Tafenoquine Approved for Malaria Prophylaxis and Treatment | Travelers' Health | CDC https://wwwnc.cdc.gov/travel/news-announcements/tafenoquine-malaria-prophylaxis-and-treatment.

(30) Kitchener, S.; Nasveld, P.; Edstein, M. D. Short Report: Tafenoquine for the Treatment of Recurrent Plasmodium Vivax Malaria. *Am. J. Trop. Med. Hyg.* **2007**, *76* (3), 494–496.

(31) Frampton, J. E. Tafenoquine: First Global Approval. *Drugs* **2018**, *78* (14), 1517–1523.

(32) Bulaquine https://drugs.ncats.io/drug/TSQ6U39Q3G.

(33) Agents, A. *Mechanism of Action of Antimicrobial and Antitumor Agents*; Corcoran, J. W., Hahn, F. E., Snell, J. F., Arora, K. L., Eds.; Springer Berlin Heidelberg: Berlin, Heidelberg, 1975.

(34) Van Dyke, K.; Lantz, C.; Szustkiewicz, C. Quinacrine: Mechanisms of Antimalarial Action. *Science (80-.).* **1970**, *169* (3944), 492–493.

(35) Elueze, E. I.; Croft, S. L.; Warhurst, D. C. Activity of Pyronaridine and Mepacrine against Twelve Strains of Plasmodium Falciparum in Vitro. *J. Antimicrob. Chemother.* **1996**, *37* (3), 511–518.

(36) Coatney, G. R. Pitfalls in a Discovery: The Chronicle of Chloroquine *. *Am. J. Trop. Med. Hyg.* **1963**, *12* (2), 121–128.

(37) Al-Bari, M. A. A. Chloroquine Analogues in Drug Discovery: New Directions of Uses, Mechanisms of Actions and Toxic Manifestations from Malaria to Multifarious Diseases. *J. Antimicrob. Chemother.* **2015**, *70* (6), 1608–1621.

(38) Egan, T. J. Structure-Function Relationships in Chloroquine and Related 4-Aminoquinoline Antimalarials. *Mini-Reviews Med. Chem.* **2001**, *1* (1), 113–123.

(39) Cohen, S. N.; Phifer, K. O.; Yielding, K. L. Complex Formation between Chloroquine and Ferrihæmic Acid in Vitro, and Its Effect on the Antimalarial Action of Chloroquine. *Nature* **1964**, *202* (4934), 805–806.

(40) Sullivan, D. J. Quinolines Block Every Step of Malaria Heme Crystal Growth. *Proc. Natl. Acad. Sci.* **2017**, *114* (29), 7483–7485.

(41) Nsumiwa, S.; Kuter, D.; Wittlin, S.; Chibale, K.; Egan, T. J. Structure–Activity Relationships for Ferriprotoporphyrin IX Association and β-Hematin Inhibition by 4-Aminoquinolines Using Experimental and Ab Initio Methods. *Bioorg. Med. Chem.* **2013**,

21 (13), 3738–3748.

(42) Dodd, E. L.; Bohle, D. S. Orienting the Heterocyclic Periphery: A Structural Model for Chloroquine's Antimalarial Activity. *Chem. Commun.* **2014**, *50* (89), 13765–13768.

(43) Gorka, A. P.; Sherlach, K. S.; De Dios, A. C.; Roepe, P. D. Relative to Quinine and Quinidine, Their 9-Epimers Exhibit Decreased Cytostatic Activity and Altered Heme Binding but Similar Cytocidal Activity versus Plasmodium Falciparum. *Antimicrob. Agents Chemother.* **2013**, *57* (1), 365–374.

(44) Alumasa, J. N.; Gorka, A. P.; Casabianca, L. B.; Comstock, E.; De Dios, A. C.; Roepe, P. D. The Hydroxyl Functionality and a Rigid Proximal N Are Required for Forming a Novel Non-Covalent Quinine-Heme Complex. *J. Inorg. Biochem.* **2011**, *105* (3), 467–475.

(45) Egan, T. J.; Hunter, R.; Kaschula, C. H.; Marques, H. M.; Misplon, A.; Walden, J. Structure−Function Relationships in Aminoquinolines: Effect of Amino and Chloro Groups on Quinoline−Hematin Complex Formation, Inhibition of β-Hematin Formation, and Antiplasmodial Activity. *J. Med. Chem.* **2000**, *43* (2), 283–291.

(46) Vippagunta, S. R.; Dorn, A.; Matile, H.; Bhattacharjee, A. K.; Karle, J. M.; Ellis, W. Y.; Ridley, R. G.; Vennerstrom, J. L. Structural Specificity of Chloroquine−Hematin Binding Related to Inhibition of Hematin Polymerization and Parasite Growth. *J. Med. Chem.* **1999**, *42* (22), 4630–4639.

(47) Bray, P. G.; Park, B.; Asadollaly, E.; Biagini, G.; Jeyadevan, J.; Berry, N.; Ward, S.; O' Neill, P. A Medicinal Chemistry Perspective on 4-Aminoquinoline Antimalarial Drugs. *Curr. Top. Med. Chem.* **2006**, *6* (5), 479–507.

(48) Kaschula, C. H.; Egan, T. J.; Hunter, R.; Basilico, N.; Parapini, S.; Taramelli, D.; Pasini, E.; Monti, D. Structure−Activity Relationships in 4-Aminoquinoline Antiplasmodials. The

Role of the Group at the 7-Position. *J. Med. Chem.* **2002**, *45* (16), 3531–3539.

(49) Hawley, S. R.; Bray, P. G.; Mungthin, M.; Atkinson, J. D.; O'Neill, P. M.; Ward, S. A. Relationship between Antimalarial Drug Activity, Accumulation, and Inhibition of Heme Polymerization in Plasmodium Falciparum In Vitro. *Antimicrob. Agents Chemother.* **1998**, *42* (3), 682–686.

(50) Parhizgar, A. R.; Tahghighi, A. Introducing New Antimalarial Analogues of Chloroquine and Amodiaquine: A Narrative Review. *Iran. J. Med. Sci.* **2017**, *42* (2), 115–128.

(51) Ducharme, J.; Farinotti, R. Clinical Pharmacokinetics and Metabolism of Chloroquine. Focus on Recent Advancements. *Clin. Pharmacokinet.* **1996**, *31* (4), 257–274.

(52) O'Neill, P. M.; Bray, P. G.; Hawley, S. R.; Ward, S. A.; Kevin Park, B. 4-Aminoquinolines - Past, Present, and Future: A Chemical Perspective. *Pharmacol. Ther.* **1998**, *77* (1), 29–58.

(53) Browning, D. J. *Hydroxychloroquine and Chloroquine Retinopathy*; 2014.

(54) Shinjo, S. K.; Maia Júnior, O. O.; Tizziani, V. A. P.; Morita, C.; Kochen, J. A. L.; Takahashi, W. Y.; Laurindo, I. M. M. Chloroquine-Induced Bull's Eye Maculopathy in Rheumatoid Arthritis: Related to Disease Duration? *Clin. Rheumatol.* **2007**, *26* (8), 1248–1253.

(55) Silva, J. A.; Silva, M. B.; Skare, T. L. Chloroquine and QTc Interval. *Clin. Exp. Rheumatol.* **2007**, *25* (5), 795.

(56) Warhurst, D. C. Hydroxychloroquine Is Much Less Active than Chloroquine against Chloroquine-Resistant Plasmodium Falciparum, in Agreement with Its Physicochemical Properties. *J. Antimicrob. Chemother.* **2003**, *52* (2), 188–193.

(57) Ben-Zvi, I.; Kivity, S.; Langevitz, P.; Shoenfeld, Y. Hydroxychloroquine: From Malaria to Autoimmunity. *Clin. Rev. Allergy Immunol.* **2012**, *42* (2), 145–153.

(58) Hawley, S. R.; Bray, P. G.; Park, B. K.; Ward, S. A. Amodiaquine Accumulation in

Plasmodium Falciparum as a Possible Explanation for Its Superior Antimalarial Activity over Chloroquine. *Mol. Biochem. Parasitol.* **1996**, *80* (1), 15–25.

(59) Parikh, S.; Ouedraogo, J. B.; Goldstein, J. A.; Rosenthal, P. J.; Kroetz, D. L. Amodiaquine Metabolism Is Impaired by Common Polymorphisms in CYP2C8: Implications for Malaria Treatment in Africa. *Clin. Pharmacol. Ther.* **2007**, *82* (2), 197–203.

(60) Shimizu, S.; Atsumi, R.; Itokawa, K.; Iwasaki, M.; Aoki, T.; Ono, C.; Izumi, T.; Sudo, K.; Okazaki, O. Metabolism-Dependent Hepatotoxicity of Amodiaquine in Glutathione-Depleted Mice. *Arch. Toxicol.* **2009**, *83* (7), 701–707.

(61) O′Neill, P. M.; Harrison, A. C.; Storr, R. C.; Hawley, S. R.; Ward, S. A.; Park, B. K. The Effect of Fluorine Substitution on the Metabolism and Antimalarial Activity of Amodiaquine. *J. Med. Chem.* **1994**, *37* (9), 1362–1370.

(62) Warhurst, D. C.; Craig, J. C.; Adagu, I. S.; Guy, R. K.; Madrid, P. B.; Fivelman, Q. L. Activity of Piperaquine and Other 4-Aminoquinoline Antiplasmodial Drugs against Chloroquine-Sensitive and Resistant Blood-Stages of Plasmodium Falciparum. *Biochem. Pharmacol.* **2007**, *73* (12), 1910–1926.

(63) Davis, T. M. E.; Hung, T.-Y.; Sim, I.-K.; Karunajeewa, H. A.; Ilett, K. F. Piperaquine. *Drugs* **2005**, *65* (1), 75–87.

(64) Biot, C.; Glorian, G.; Maciejewski, L. A.; Brocard, J. S.; Domarle, O.; Blampain, G.; Millet, P.; Georges, A. J.; Abessolo, H.; Dive, D.; Lebibi, J. Synthesis and Antimalarial Activity in Vitro and in Vivo of a New Ferrocene−Chloroquine Analogue. *J. Med. Chem.* **1997**, *40* (23), 3715–3718.

(65) Biot, C.; Chavain, N.; Dubar, F.; Pradines, B.; Trivelli, X.; Brocard, J.; Forfar, I.; Dive, D. Structure–Activity Relationships of 4-N-Substituted Ferroquine Analogues: Time to Re-

Evaluate the Mechanism of Action of Ferroquine. *J. Organomet. Chem.* **2009**, *694* (6), 845–854.

(66) Biot, C.; Taramelli, D.; Forfar-Bares, I.; Maciejewski, L. A.; Boyce, M.; Nowogrocki, G.; Brocard, J. S.; Basilico, N.; Olliaro, P.; Egan, T. J. Insights into the Mechanism of Action of Ferroquine. Relationship between Physicochemical Properties and Antiplasmodial Activity. *Mol. Pharm.* **2005**, *2* (3), 185–193.

(67) Biot, C.; Pradines, B.; Dive, D. Ferroquine: A Concealed Weapon. *Apicomplexan Parasites Mol. Approaches Towar. Target. Drug Dev.* **2011**, 397–411.

(68) Berliner, R. W.; Earle, D. P.; Taggart, J. V.; Zubrod, C. G.; Welch, W. J.; Conan, N. J.; Bauman, E.; Scudder, S. T.; Shannon, J. A. Studies On The Chemotherapy Of The Human Malarias. VI. The Physiological Disposition, Antimalarial Activity, And Toxicity Of Several Derivatives Of 4-Aminoquinoline. *J. Clin. Invest.* **1948**, *27* (3 Pt 2), 98–107.

(69) Cogswell, F. B.; Krogstad, D. J.; De, D.; Krogstad, F. M. Aminoquinolines That Circumvent Resistance in Plasmodium Falciparum in Vitro. *Am. J. Trop. Med. Hyg.* **1996**, *55* (6), 579–583.

(70) Mengue, J. B.; Held, J.; Kreidenweiss, A. AQ-13 - an Investigational Antimalarial Drug. *Expert Opin. Investig. Drugs* **2019**, *28* (3), 217–222.

(71) Achan, J.; Talisuna, A. O.; Erhart, A.; Yeka, A.; Tibenderana, J. K.; Baliraine, F. N.; Rosenthal, P. J.; D'Alessandro, U. Quinine, an Old Anti-Malarial Drug in a Modern World: Role in the Treatment of Malaria. *Malar. J.* **2011**, *10* (1), 144.

(72) Woodward, R. B.; Doering, W. E. The Total Synthesis Of Quinine. *J. Am. Chem. Soc.* **1944**, *66* (5), 849–849.

(73) Schlesinger, P. H.; Krogstad, D. J.; Herwaldt, B. L. Antimalarial Agents: Mechanisms of

Action. *Antimicrob. Agents Chemother.* **1988**, *32* (6), 793–798.

(74) Palmer, K. J.; Holliday, S. M.; Brogden, R. N. Mefloquine. *Drugs* **1993**, *45* (3), 430–475.

(75) Bryson, H. M.; Goa, K. L. Halofantrine. *Drugs* **1992**, *43* (2), 236–258.

(76) Nosten, F.; Phillips-Howard, P. A.; ter Kuile, F. O. Other 4-Methanolquinolines, Amyl Alcohols and Phentathrenes: Mefloquine, Lumefantrine and Halofantrine. In *Treatment and Prevention of Malaria*; Springer Basel: Basel, 2011; pp 95–111.

(77) Gaillard, T.; Madamet, M.; Pradines, B. Tetracyclines in Malaria. *Malar. J.* **2015**, *14* (1), 445.

(78) Meshnick, S. R. Artemisinin: Mechanisms of Action, Resistance and Toxicity. *Int. J. Parasitol.* **2002**, *32* (13), 1655–1660.

(79) Mungthin, M.; Rungsihirunrat, K.; Na-Bangchang, K.; Sibley, C. H.; Hawkins, V. N. Sensitivity To Antifolates And Genetic Analysis Of Plasmodium Vivax Isolates From Thailand. *Am. J. Trop. Med. Hyg.* **2007**, *76* (6), 1057–1065.

(80) David A. Fidock; Nomura, T.; Talley, A. K.; Cooper, R. A.; Dzekunov, S. M.; Ferdig, M. T.; Ursos, L. M. B.; Sidhu, A. bir S.; Naudé, B.; Deitsch, K. W.; Su, X.; Wootton, J. C.; Roepe, P. D.; Wellems, T. E. Mutations in the P. Falciparum Digestive Vacuole Transmembrane Protein PfCRT and Evidence for Their Role in Chloroquine Resistance. *Mol. Cell* **2000**, *6* (4), 861–871.

(81) Djimdé, A.; Doumbo, O. K.; Cortese, J. F.; Kayentao, K.; Doumbo, S.; Diourté, Y.; Coulibaly, D.; Dicko, A.; Su, X.; Nomura, T.; Fidock, D. A.; Wellems, T. E.; Plowe, C. V. A Molecular Marker for Chloroquine-Resistant Falciparum Malaria. *N. Engl. J. Med.* **2001**, *344* (4), 257–263.

(82) Cooper, R. A.; Hartwig, C. L.; Ferdig, M. T. Pfcrt Is More than the Plasmodium Falciparum

Chloroquine Resistance Gene: A Functional and Evolutionary Perspective. *Acta Trop.* **2005**, *94* (3), 170–180.

(83) Kim, J.; Tan, Y. Z.; Wicht, K. J.; Erramilli, S. K.; Dhingra, S. K.; Okombo, J.; Vendome, J.; Hagenah, L. M.; Giacometti, S. I.; Warren, A. L.; Nosol, K.; Roepe, P. D.; Potter, C. S.; Carragher, B.; Kossiakoff, A. A.; Quick, M.; Fidock, D. A.; Mancia, F. Structure and Drug Resistance of the Plasmodium Falciparum Transporter PfCRT. *Nature* **2019**, *576* (7786), 315–320.

(84) Ibraheem, Z. O.; Abd Majid, R.; Noor, S. M.; Sedik, H. M.; Basir, R. Role of Different Pfcrt and Pfmdr-1 Mutations in Conferring Resistance to Antimalaria Drugs in Plasmodium Falciparum. *Malar. Res. Treat.* **2014**, *2014*, 950424.

(85) Sanchez, C. P.; Stein, W. D.; Lanzer, M. Is PfCRT a Channel or a Carrier? Two Competing Models Explaining Chloroquine Resistance in Plasmodium Falciparum. *Trends Parasitol.* **2007**, *23* (7), 332–339.

(86) Sanchez, C. P.; Dave, A.; Stein, W. D.; Lanzer, M. Transporters as Mediators of Drug Resistance in Plasmodium Falciparum. *Int. J. Parasitol.* **2010**, *40* (10), 1109–1118.

(87) Roepe, P. D. PfCRT-Mediated Drug Transport in Malarial Parasites. *Biochemistry* **2011**, *50* (2), 163–171.

(88) Sidhu, A. B. S.; Valderramos, S. G.; Fidock, D. A. Pfmdr1 Mutations Contribute to Quinine Resistance and Enhance Mefloquine and Artemisinin Sensitivity in Plasmodium Falciparum. *Mol. Microbiol.* **2005**, *57* (4), 913–926.

(89) Duraisingh, M. T.; Cowman, A. F. Contribution of the Pfmdr1 Gene to Antimalarial Drug-Resistance. *Acta Trop.* **2005**, *94* (3), 181–190.

(90) Koenderink, J. B.; Kavishe, R. A.; Rijpma, S. R.; Russel, F. G. M. The ABCs of Multidrug

Resistance in Malaria. *Trends Parasitol.* **2010**, *26* (9), 440–446.

(91) Valderramos, S. G.; Fidock, D. A. Transporters Involved in Resistance to Antimalarial Drugs. *Trends Pharmacol. Sci.* **2006**, *27* (11), 594–601.

(92) Moorthy, V. S.; Good, M. F.; Hill, A. V. S. Malaria Vaccine Developments. *Lancet* **2004**, *363* (9403), 150–156.

(93) Casares, S.; Brumeanu, T.-D.; Richie, T. L. The RTS,S Malaria Vaccine. *Vaccine* **2010**, *28* (31), 4880–4894.

(94) Crompton, P. D.; Pierce, S. K.; Miller, L. H. Advances and Challenges in Malaria Vaccine Development. *J. Clin. Invest.* **2010**, *120* (12), 4168–4178.

(95) Mehta, S. R. et al. First Results of Phase 3 Trial of RTS,S/AS01 Malaria Vaccine in African Children. *N. Engl. J. Med.* **2011**, *365* (20), 1863–1875.

(96) Organization, W. H. First malaria vaccine: Kenya https://www.who.int/immunization/diseases/malaria/malaria_vaccine_implementation_programme/RTSS_Kenya_Web_FINAL_August_2019.pdf.

(97) Organization, W. H. First malaria vaccine: Malawi https://www.who.int/immunization/diseases/malaria/malaria_vaccine_implementation_programme/RTS_S_Malawi_04_19.pdf.

(98) Organization, W. H. First malaria vaccine: Ghana https://www.who.int/immunization/diseases/malaria/malaria_vaccine_implementation_programme/RTS_S_Ghana_4_19.pdf.

Chapter 2

Optimization of 3-Aminochloroquine synthesis for Chloroquine Derivatization.

2.1 Preamble

In this chapter, we explore the synthesis of CQ functionalized at the 3-position with an amine. There are only a few reports on the syntheses of 3-substituted CQ analogs in the literature for malaria treatment.[1–4] Most reported examples of 3-substituted CQ were for *Leishmania spp*. and ocular melanoma treatment.[5,6] The shortage of examples of such compounds might be due to their lack of synthetic access and preceding literature that reported a decrease in antimalarial activity due to quinoline substitution at the 3-position. However, we remained interested in functionalizing this position because previous work carried out in our lab showed promising results in the combination therapy between CQ and 3-ICQ.[7,8] Moreover, substitution at this position will also result in the synthesis of a new class of antimalarials drug candidates.

2.2 Introduction

The quinoline scaffold has been one of the most significant in antimalarial drug history.[9–12] Some of the most important antimalarial drugs are quinolines, such as CQ, PPQ and PQ. These AQs have two substituents on the quinoline ring: a secondary amine group and a chloro- or methoxy group. It was proposed that modifications to the quinoline ring, such as replacing the 7-chloro group (present in CQ and PPQ) for an electron-withdrawing or an electron-donating group impacts, its binding affinity to β-hematin.[13] The presence of an amine group at the 3-, 5-, 6- or 8-position decreased activity, and these simple AQs do not form a significant association with β-hematin, **Figure 2.1**. However, 2-aminoquinolines (AQs) form a complex with β-hematin but do not inhibit β-hematin formation[14], **Figure 2.2**.

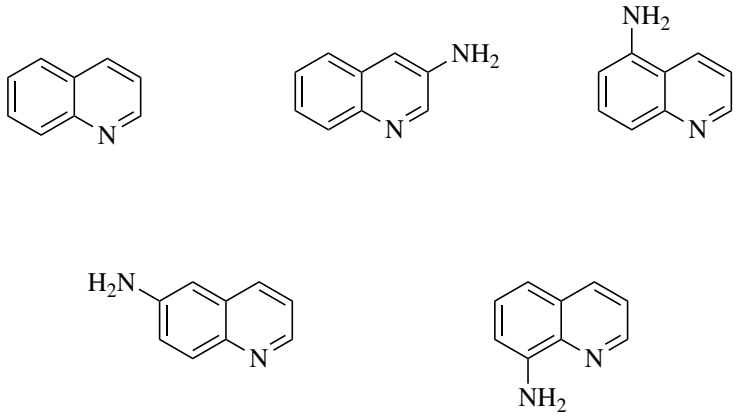

Figure 2.1. Simple AQs that do not inhibit hemozoin formation.

These findings deterred other research groups from synthesizing compounds with such modifications. It is important to note that the aforementioned AQs do not include the 4-amino and 7-chloro moieties required for antimalarial activity. Tim Egan's group has shown that the 7-chloro group is crucial for efficient β-hematin association and inhibition.[13] Furthermore, the secondary 4-amino group is essential for antiplasmodial activity as its tautomeric form contributes to the drug's activity.[15,16] One must also keep in mind that although modifications on the ring will impact the compound's association constant with β-hematin, research also shows no direct correlation between β-hematin inhibition and antiplasmodial activity.[15] Such compounds interact with β-hematin in varying conformations. Furthermore, it is highly probable that β-hematin is not the sole target of these drugs. As discussed in chapter 1, antiplasmodial activity is dependent on the compound's ability to accumulate in the DV and to inhibit β-hematin formation, which are both dependent on the nature of the substituents on the quinoline ring.

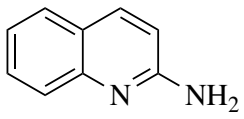

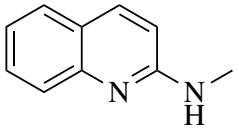

-Does strongly associate with Fe(III)PIX

-Does not inhibit hemazoin formation

Figure 2.2. AQs that do not inhibit hemozoin formation.

As will be discussed in the next chapter, 3-haloCQ derivatives have been synthesized previously in our group. These derivatives contain a halogen group at the 3-position of the quinoline ring. The 3-haloCQ derivatives are less potent than CQ in CQ-sensitive (CQS) and CQ-resistant (CQR) parasites, they inhibit β-hematin formation but to a lesser extent than CQ. Interestingly, it was found that of the 3-haloCQs synthesized, 3-ICQ was the most potent. When given as a combination treatment with CQ in CQR parasites, 3-ICQ resensitizes the parasite to CQ. Thus, combination treatment *in vitro* is more effective than monotherapy of CQ alone.[7]

For these reasons, we decided to explore further how functionality at the 3-position affects activity. In this chapter, I will discuss the installation of an amino-functional group, which allows for further derivatization to benzamides, sulfonamides and Schiff bases. To install the C_{sp2}-N bond at this position, we carried out Ullmann-type coupling reactions from a 3-BrCQ precursor.

2.3 Results and Discussion

2.3.1 Optimization of 3-BrCQ synthesis

Bromination of CQ has been previously reported in our lab using trifluoroacetic acid and *N*-bromosuccinimide (NBS) in acetonitrile.[8] The preparation involves activation of *N*-halosuccinimide with trifluoroacetic acid in acetonitrile at 80℃ for 30 minutes, followed by CQ addition. The reaction mixture is then stirred at 80℃ for 2 hours to yield 73-81% of 3-BrCQ following workup. However, the yield is greatly reduced when the reaction is scaled to gram scale where the yields are consistently below 30%. Thus, we optimized this reaction to achieve consistently high yields at the gram scale.

We carried the following reactions under microwave-assisted synthesis. Initially, we carried out a small-scale reaction in 0.5 mL acetic acid, and the reaction mixture is heated at 80℃ for 30 minutes (**Table 2.1**, entry 2). This results in an excellent yield of the desired product and the formation of 3,6-dibromochloroquine (3,6-BrCQ) with a regioselectivity ratio of 89:11 mono: di-brominated product. Moreover, when the reaction is then carried out on the gram scale in 4.5 mL acetic acid at 85℃ for 40 minutes, ^{1}H NMR analysis shows 32% consumption of starting material with 41:59 mono-: di- selectivity. An additional equiv. of NBS was added, and the reaction is heated at 80℃ for an additional 30 minutes. This results in 100% consumption of starting material with regioselectivity of 48:52 (mono-: di-) with an isolated yield of 21% of the mono-brominated product (entry 1). The poor yield and regioselectivity were unsatisfactory, which may be due to the acidic environment which favours the activation of the 6-position due to the 7-chloro group

with is an ortho-director. Therefore, we carried out the reaction in acetonitrile on a small scale with 0.5 mL solvent heated at 80°C for 30 minutes (entry 4).

Table 2.1. Optimization of 3-BrCQ synthesis using microwave-assisted synthesis.

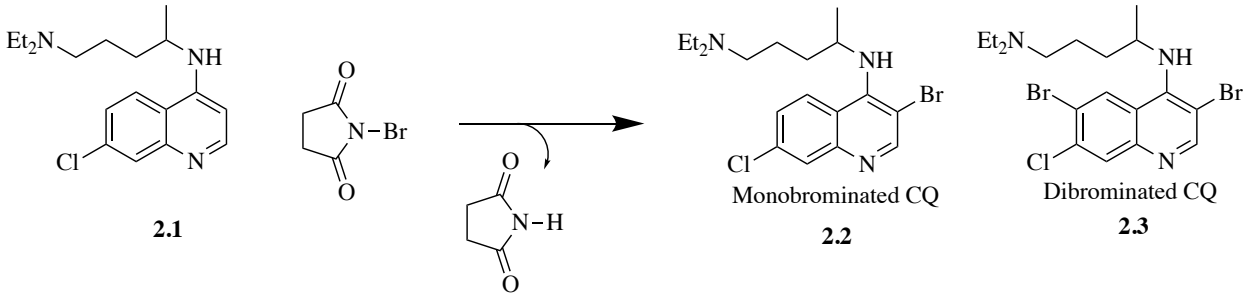

Entry	CQ (mg)	NBS equiv.	Solvent	Temperature (°C)	Time (minutes)	Mono:Di	Monobromo Yield (%)
1	1,000	2.5	AcOH	85	70[a]	48:52	21
2	100	1.5	AcOH	80	30	89:11	99
3	1,000	2.5	MeCN	80-100[b]	130[b]	100:0	40
4	100	1.5	MeCN	80	30	96:4	96
5	1,000[c]	1.5	MeCN	100	60	-[d]	64
6	1,000	2	MeCN	100-140[e]	100[e]	100:0	40

Conditions: Chloroquine, NBS (1.5 equiv.) and solvent placed in a microwave vial and heated for the stated amount of time. a) additional 1 equiv. of NBS added after 40 minutes. b) Additional 1 equiv. of NBS added and temperature increased to 100°C after 110 minutes. c) Chloroquine diphosphate salt used instead of the free base. d) Regioselectivity and conversion not measured before purification. e) Additional 0.5 equiv. of NBS added and the temperature increased to 140°C after 90 minutes.

^{1}H NMR analysis shows 64% conversion of starting material with a regioselectivity of 96:4 (mono- : di-), and we isolated 96% of the desired mono-brominated product. The reaction is then scaled up to 1 gram with 5 mL acetonitrile in a 5 mL microwave vial heated at 80°C for 1 hour. After 1 hour, the TLC shows that the starting material is still present; therefore, the vial is returned to the microwave and set at 85°C for 40 minutes. Thereafter, ^{1}H NMR shows 39% conversion of the

starting material with regioselectivity of 100:0 mono-: di-. An additional equiv. of NBS is added, and the reaction runs at 100℃ for an additional 30 minutes. The ^{1}H NMR analysis then shows 94% consumption of starting material to only the desired mono-BrCQ. However, we got an isolated yield of 40%. The lower than expected yield may be due to side product formation stemming from the high reaction temperature. As the yields were still low for the gram scale reactions, we decided to carry out a gram-scale reaction with CQ diphosphate rather than the free base (entry 5). The reaction with CQ salt is carried out at 100℃ for 1 hour to give an isolated yield of 64%. The ^{1}H NMR conversion and regioselectivity for this reaction were not measured before purification; however, only one product spot is observed on the TLC. It is important to note that the salt does not fully dissolve in acetonitrile at 100℃, and the starting material is visible in the vial after the reaction is removed from the microwave, reducing the potential yield. To determine the effect of temperature on the reaction, free base CQ is placed in a microwave vial with 1.5 equiv. NBS and 5 mL acetonitrile, set at 100℃ for 1 hour (entry 6). After the time elapsed, the starting material is still present as verified by TLC and 0.5 equiv. NBS is added, and the reaction is run at 100℃ for an additional 30 minutes. Finally, in an attempt to further push the reaction to completion, it is run at 140℃ for 10 minutes; thus, the reaction was carried out from 100-140℃ for a total of 100 minutes. ^{1}H NMR analysis of the crude mixture shows 36% conversion of the starting material with regioselectivity 100: 0 (mono-: di-), and we are able to isolate 40% of the product.

This bromination reaction works best on a small scale to form the 3-BrCQ as the major product with a minor formation of 3,6-BrCQ. Once the reaction is scaled up in acetic acid, we obtain greater formation of 3,6-BrCQ, with 3-BrCQ as the minor product. However, we get better regioselectivity

in acetonitrile. Similarly, small scale reactions in acetonitrile result in a high yield of our desired product. When $CQ{\cdot}2H_3PO_4$ is used, we are able to get good yields at gram scale with a yield of 64%. Finally, when higher temperatures are used for CQ free-base in acetonitrile, the reaction yield greatly suffers, and longer reaction times are required.

As we achieved good yields with gram scale bromination, we continued to the synthesis of 3-aminochloroquine (3-NH_2CQ). The formation of the heteroatom- C_{sp2} bond occurs under Ullmann-type coupling reaction conditions,[17,18] the mechanism for this cross-coupling is described later in this chapter.

2.3.2 Optimization of 3-NH_2CQ synthesis

3-NH2CQ can be synthesized using the linear route displayed in **Scheme 2.1**. We began with the nucleophilic aromatic substitution of 4,7-dichloroquinoline **2.4,** to make 7-chloroquinolin-4-ol, **2.5**. Then nitration at the 3-position with nitric acid to give **2.6,** followed by chlorination with phosphoryl chloride gives 4,7-dichloro-3-nitroquinoline, **2.7**.[19] Condensation of **2.7** with a diamine side chain **2.8** gives 3-NO_2CQ **2.9,** which is then reduced to 3-NH_2CQ **2.10** with stannous chloride.[19] This route involves 5 steps carried out over 5 days; thus, there was a need to create a faster synthetic route to 3-NH_2CQ. We achieved this by creating a 2-step synthesis carried out in 1 day, with the bromination of CQ followed by an amination via an Ullmann-type coupling reaction.

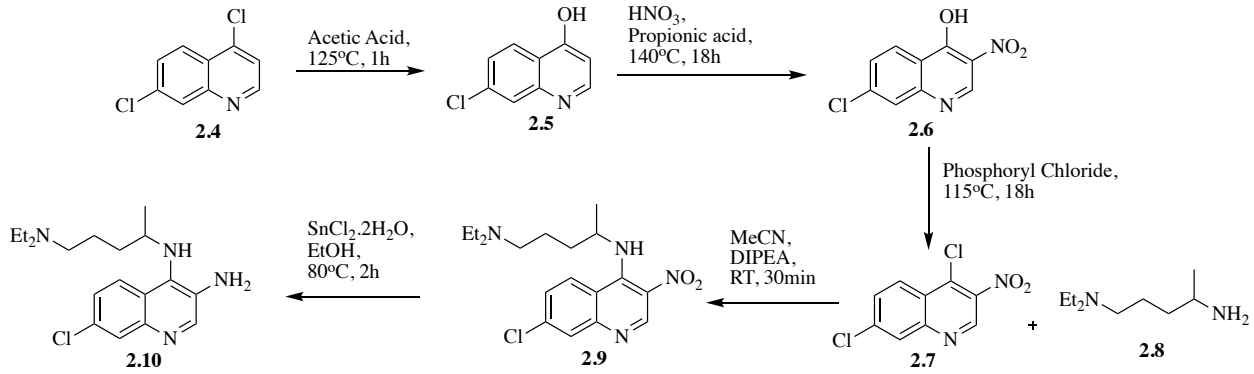

Scheme 2.1. Linear synthesis to 3-AminoCQ synthesis.

The Ullmann-type reaction is a coupling reaction that involves a copper catalyst and an aryl halide with various heteroatoms to form a heteroatom - C_{sp2} bond, with Cu(I) as the active species in this reaction. However, Cu(0) and Cu(II) salts are used with a base or reducing agent for *in situ* reduction/oxidation to generate the active Cu(I) species.[17] The use of a reducing agent such as sodium ascorbate was required to obtain higher yields of the amine. The omission of the reducing agent did not result in azide formation, It is desirable that we use easily accessible, cheap reagents for this coupling reaction because antimalarial drug candidates used for treatment in developing countries require cost-efficient production. We first began with ammonium hydroxide as the amine source under various conditions with/ without the presence of a ligand or base, **Table 2.2**.

2.3.2.1 Optimization using ammonium hydroxide as the nitrogen source

Table 2.2. 3-NH_2CQ formation with NH_4OH as NH_2 source.

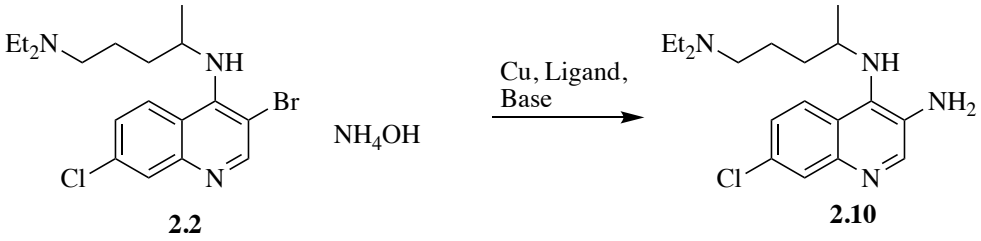

2.2 **2.10**

Entry	Catalyst [mol%]	Ligand [mol%]	Reducing agent/base [mol%]	Solvent	Temperature (°C)	Yield (%)
1	Cu [20]	-	-	EtOH	95	-
2	CuI [20]	DMEDA [200]	L-Ascorbic Acid [200]	2M NH_3 in EtOH	95	Trace[a]
3	Cu_2O [10]	Diethylenetriamine pentaacetic acid [20]	KOH [200]	H_2O	100	-
4	Cu_2O [100]	Trans +/- Diamino cyclohexane [20]	Sodium ascorbate [200]	7N NH_3 in MeOH	95	-

[a]: 4% conversion of starting material to CQ determined by ^{1}H NMR.

Copper-catalyzed amination reactions from aryl halides using ammonium hydroxide have been well reported in the literature, **Scheme 2.2**.[20–22] Lang *et al.* reported the amination of 2-bromopyridine without the need of a ligand or base.[21] They report that amination worked best in an aqueous or alcoholic solvent; however, they see the formation of a C-O byproduct due to competing hydroxide attack from the solvent. When polar, aprotic solvents were used, they had low product conversion, which was attributed to ammonia's poor solubility in such solvents. Similarly, Jiao *et al*. carried out the amination reaction on 3- and 4-bromopyridine and achieved near quantitative yields with copper powder, exposure to air and optional use of a Lewis base.[20] Yang *et al.* were able to successfully carry out amination of 2- and 3-bromopyridine using a ligand and inorganic base in H_2O.[22]

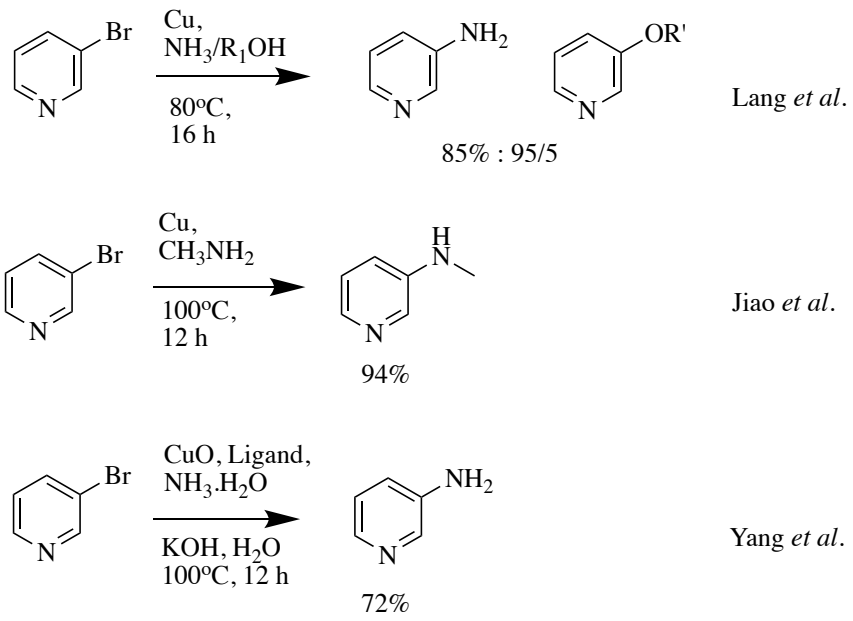

Scheme 2.2. Known examples of pyridine amination.

In our experimentation, the use of ammonia did not yield any desired product (**Table 2.2**, entries 2 and 4). The reaction is monitored by TLC for up to 24 hours, and if no product spots were detected by TLC, the reaction was deemed unsuccessful. The use of copper powder in degassed ethanol (EtOH) was unsuccessful, so was the use of copper(I) oxide with a base or reducing agent. Dimethylethylenediamine (DMEDA) as a ligand and excess L-ascorbic acid as the reducing agent for CuI results in trace amounts of the desired product (<2% conversion) and interestingly results in 4% conversion (determined by ^{1}H NMR) to reductive CQ product formation.

2.3.2.2 Optimization using azidotrimethyl silane as the nitrogen source

We then decided to use an organic azide, azidotrimethyl silane ($TMSN_3$), to improve the solubility of our amine source in organic solvents and increase the reaction yield. As expected, the control experiment of 3-BrCQ in 1.5 equiv. $TMSN_3$ (**Table 2.3**, entry 10), heated at 53°C overnight, did

not yield any product. We then used CuI with an excess of potassium carbonate (K_2CO_3) in 1,4-dioxane; however, no product spots were detected on TLC (entry 6). The absence of a ligand gives a low yield of 11% (entry 5), and the yield is not significantly improved when L-proline (entry 4) or trans +/- diamino cyclohexane (entry 7) are used as ligands. When a stoichiometric amount of copper powder is used with excess 2-aminoethanol as a ligand, and excess sodium ascorbate (entry 8) as the reducing agent in dimethylacetamide (DMA) are used, we observe a significant increase in yield.[23] The 2-aminoethanol ligand is essential for this reaction as there is no product formation in its absence after heating at 95℃ for 23 hours when used with stoichiometric amounts of copper powder (entry 8). We get similar results using catalytic amounts of copper powder with DMEDA and sodium ascorbate in anhydrous EtOH (entry 2). The use of excess ligand combined with copper iodide gave 1.7 - fold increase in yield (entry 1). A different organic azide, tetrabutylammonium azide (NBu_4N_3), was used as an amine source (entry 11); however, no product was formed from this reaction.

Table 2.3. 3-NH_2CQ formation with $TMSN_3$ as the nitrogen source.

Entry	Catalyst [mol%]	Ligand [mol%]	Reducing agent/base [mol%]	Solvent	Temperature (°C)	Yield (%)
1	CuI [20]	DMEDA [1200]	L-Ascorbic Acid [30]	EtOH	95	42
2	CuI [20]	DMEDA [50]	Sodium Ascorbate [20]	EtOH	85	20
3	Cu [20]	DMEDA [30]	L-Ascorbic Acid [30]	EtOH 95%	85	13
4	CuI [20]	L-Proline [30]	Sodium Ascorbate [30]	EtOH 95%	85	13
5	CuI [20]	-	Sodium Ascorbate [30]	EtOH 95%	85	11
6	CuI [20]	-	K_2CO_3 [200]	1,4-Dioxane	95	-
7	CuI [20]	Trans +/- Diamino cyclohexane [20]	Sodium Ascorbate [200]	EtOH	95	14
8	Cu [200]	2-Amino ethanol [250]	Sodium Ascorbate [200]	DMA	95	25
9	Cu [200]	-	Sodium Ascorbate [200]	DMA	95	-
10	-	-	-	-	53	-
11[a]	CuI [100]	DMEDA [20]	Sodium Ascorbate [200]	1,4-Dioxane	95	-

a) NBu_4N_3 was used as the nitrogen source.

2.3.2.3 Optimization using sodium azide as the nitrogen source

We then decided to carry out the amination reaction with sodium azide as the amine source. The control reaction does not proceed in dimethylformamide (DMF) (**Table 2.4**, entry 6).[24,25] The use of copper sulfate with sodium ascorbate did not yield any product (entry 4),[26,27] and Cu(I) iodide with excess potassium carbonate did not yield any product (entry 2).[28] When Cu(I) iodide was used with bidentate ligand DMEDA in a degassed solution of 70% EtOH, 30% H_2O at 95°C, we saw product formation and were able to isolate 29% of the desired product.[29–31] We repeated the experiment in anhydrous EtOH with the addition of sodium ascorbate and were able to isolate 55%

of our desired product.[27,32] Goriya and Ramana reported the direct amination of aryl halides with sodium azide under a Cu(II)-ascorbate redox system.[27] They reported that arylamine formation can occur without the presence of copper and that various concentrations of sodium ascorbate with copper(I) sulfate (Cu_2SO_4), sodium carbonate (Na_2CO_3) and L-proline greatly increases product formation rate and decreases reaction time. However, in our system, we have found that copper is required for this synthesis and the combination of DMEDA and sodium ascorbate produces the highest yield.

Table 2.4. 3-NH_2CQ formation with NaN_3 as the nitrogen source.

Entry	Catalyst [mol%]	Ligand [mol%]	Reducing agent/base [mol%]	Solvent	Temperature (ºC)	Yield (%)
1	CuI [20]	DMEDA [1200]	-	EtOH/H_2O (7:3)	95	29
2	CuI [20]	-	K_2CO_3 [200]	EtOH (95%)	95	-
3	CuI [50]	DMEDA [50]	Sodium Ascorbate [50]	EtOH/H_2O (7:3)	85	55
4	$CuSO_4.H_2O$ [20]	L-Proline [20]	Sodium Ascorbate [20]	DMF/H_2O (2:1)	85	-
5	$CuSO_4.H_2O$ [20]	DMEDA [30]	Sodium Ascorbate [30] + Na_2CO_3 [20]	DMF/H_2O (2:1)	85	-
6	-	-	-	DMF	100	-

Surprisingly, conditions in **Table 2.4** entry 3 results in the formation of the desired 3-aminoCQ product and the reduction of CQ as a product. We then carried out experiments in an attempt to minimize the reductive formation of CQ. Heating the reaction in an oil bath instead of microwave-irradiation resulted in 50% conversion of the 3-BrCQ into 3-NH2CQ and 50% to CQ at 85°C. We then ran the reaction at 75°C for 2 hours (**Table 2.5**, entry 4). However, there was little product or byproduct formation at this temperature. The temperature was then increased to 85°C, heated for a further 3 hours and we were able to isolate 44% of the desired product. CQ was also formed, but

it was not collected during the purification. A longer reaction time of 19 hours (entry 3) did not improve the selectivity nor the yield of the desired product. The reaction was carried out in the presence of 2 equiv. of (2,2,6,6-Tetramethylpiperidin-1-yl)oxyl (TEMPO) - a radical trapping agent. We got lower yields of both 3-NH_2CQ and CQ but also slightly greater selectivity for 3-NH_2CQ. When ten equiv. of TEMPO is used, we got no formation of CQ and trace amounts of 3-NH_2CQ. The greatest selectivity and yield are achieved with three equiv. NaN_3, 0.5 equiv. CuI, 0.5 equiv. DMEDA, and 0.5 equiv. sodium ascorbate at 85℃ in an oil bath for 3 hours.

Table 2.5. Reaction conditions to minimize byproduct formation.

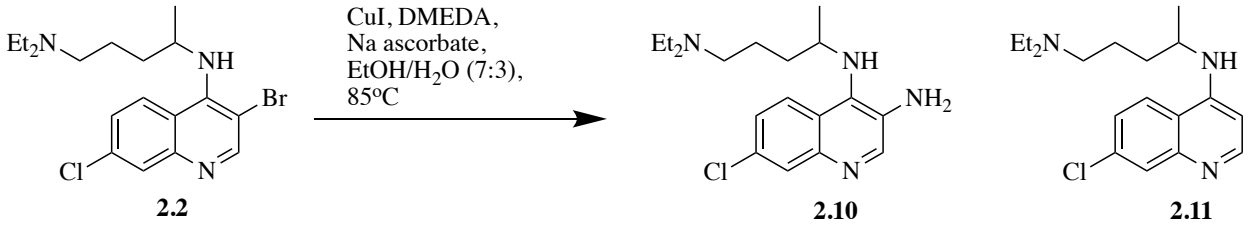

2.2 **2.10** **2.11**

Entry	Heating method	Reaction time (hours)	NaN_3	CuI	DMEDA	Sodium Ascorbate	Conversion (NH_2:CQ)	3-NH_2CQ Isolated Yield (%)
1	Oil	3	2	0.3	0.4	0.3	-	49
2	Oil	3	2	0.3	0.4	0.3	-	32[b]
3	Oil	19	2	0.3	0.4	0.3	-	50
4	Oil[c]	5	2	0.3	0.3	0.3	-	44
5	Oil	4	2	0.3	0.3	0.3	-	Trace[d]
6	Oil	3	3	0.5	0.5	0.5	-	55
7	MW[e]	0.7	3	3	3	2	91 (30:70)	16
8	MW[f]	0.5	3	3[g]	3	3	81 (37:63)	19
9	MW	1	3	0.5	0.5	0.5	69 (36:64)	26
10	MW	1	3	0.5	0.5	0.5	84 (51:49)	NA[h]

a) Reactions run at 85°C in EtOH /H_2O (7:3). b) Reaction included 2 equiv. TEMPO. c) Starting temperature of 75°C after 2 hours temperature increased to 85°C. d) Reaction included 10 equiv. TEMPO, starting temperature of 75°C, after 2 hours temperature increased to 85°C. e) Heated at 100°C for 30 minutes and then at 140°C for 10 minutes. f) Heated at 100°C for 30 minutes. g) 3 equiv. of copper powder used. h) Purification not carried out; product contained 5 equiv. of TEMPO.

We then carried out this coupling reaction via microwave-assisted synthesis (MW) with reduced reaction times. When we replicated our optimized reaction conditions in the microwave, we saw a 2-fold decrease in yield (entry 9). One might assume that it may be due to reduced reaction times, but we observe greater conversion to CQ in microwave-assisted synthesis. We then used

stoichiometric amounts of our reagents and increased the temperature from 85°C to 140°C. However, we obtain lower yields of 3-NH_2CQ and greater conversion of starting material to CQ (entry 7 and 8). We then carried out the reaction in the presence of 5 equiv. of TEMPO and surprisingly saw 84% conversion of the starting material with a significantly improved selectivity for 3-NH_2CQ. Hence microwave-assisted synthesis is not recommended for these Ullmann-type coupling reactions as we get lower yields and greater reductive CQ formation.

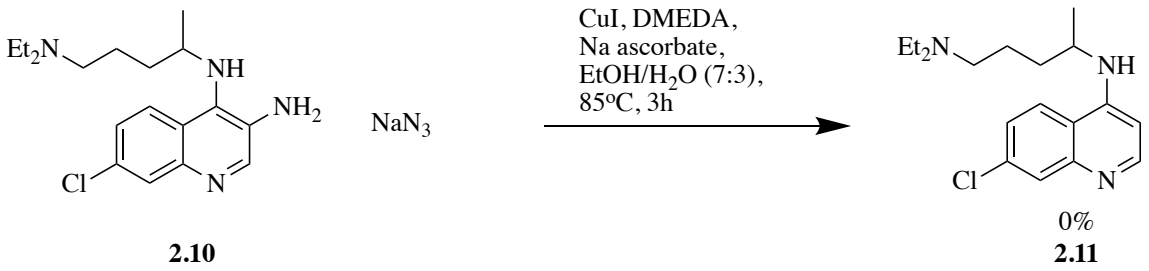

2.10 **2.11**

Scheme 2.3. Determination of 3-NH_2CQ stability.

We were then curious to determine the stability of the C_{sp2}-N bond. We replicated the reaction with 3-NH_2CQ as our starting material with CuI, DMEDA, sodium ascorbate and sodium azide in degassed EtOH /H_2O (7:3), which is heated at 85°C for 3 hours. A TLC is taken, and no CQ spots are detected, and only the 3-NH_2CQ starting material is present. This indicates that there is competition for the formation of CQ and our desired amine, **Scheme 2.3**.

2.3.3 Proposed Ullmann-type coupling mechanisms of product formation

The reductive formation of the CQ byproduct was unexpected and reduced the yield of the desired product. We reexamined the proposed catalytic cycle for Ullmann-type coupling reactions to determine the cause. As shown in **Figure 2.3** there are two proposed pathways for this coupling reaction, with the upper cycle being the most widely accepted.[17,33,34] Copper-catalyzed Ullmann-

type coupling is believed to occur via a Cu(I) / Cu(III) catalytic cycle, which is initiated by the coordination of the nucleophile onto the Cu(I) center. This is followed by oxidative addition of the aryl halide to form an NR_2 - Cu(III) - aryl species and the release of the halide anion. The activation of the aryl halide is believed to be the rate-limiting step. Reductive elimination then occurs to form the NR_2 - Ar coupling product and releases Cu(I) which can then reenter the cycle. The less probable route is the initial oxidative addition of the aryl halide to form a halide - Cu(III) - aryl intermediate, followed by coordination of the nucleophile via the release of the halide to form an NR_2 - Cu(III) - aryl species. Reductive elimination follows to release the product and Cu(I). We believe that both pathways contribute to the formation of our desired 3-NH_2CQ product and that the lower cycle might be the main contributor to the formation of the CQ byproduct. The formed ligand – Cu(III) – Ar species can undergo proton-coupled electron transfer causing the release of the reductive CQ product. It is possible that the amines present in the 3-BrCQ side-chain act as ligands on the Cu(I) center, and if oxidative addition occurs first, then all coordination sites could be occupied, preventing nucleophile coordination.

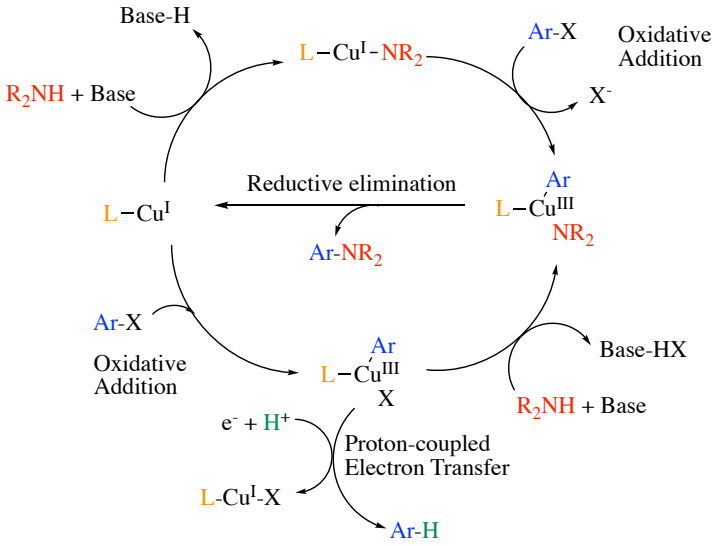

Figure 2.3. Proposed pathways for Cu(I)/ Cu(III) Ullmann-type amination catalytic cycle.

The 2-electron catalytic cycle is the most widely accepted mechanism as the reaction is not inhibited with radical trapping agents or radical initiators.[35] We tested this with the use of TEMPO in both traditional oil heating and with microwave-assisted synthesis. When using an oil bath with two equiv. of TEMPO we saw a slight reduction in product and byproduct formation. When ten equiv. of TEMPO were used, we see no formation of byproduct and little formation of the desired product. When five equiv. of TEMPO is used under microwave-assisted synthesis, we still observe 84% conversion to products. This suggests that the radical trap has little effect on the reaction process. It is only when a large excess is used that we see an impact on product formation.

The mentioned Cu(I) / Cu(III) cycle is not the only proposed Ullmann-type mechanism. Another proposed mechanism is a Cu(I) / Cu(II) Single Electron Transfer (SET) mechanism with aryl radicals that might lead to product formation.[36] Through experimentation with iodoarenes, Kim and Bunnett proposed 'outer sphere' electron transfer through a radical chain mechanism involving SET as the initiation step.[36] They performed experiments in the presence of tetraphenylhydrazine (a radical trapping agent) and proposed a unimolecular radical nucleophilic substitution ($S_{RN}1$), as shown in **Figure 2.4**.

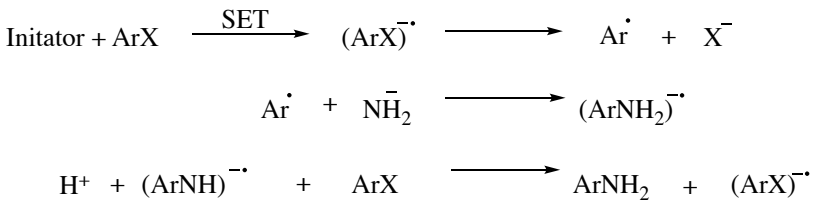

Figure 2.4. Proposed Cu(I)/ Cu(II) $S_{RN}1$ mechanism.

A proposed mechanism that does not involve a change in oxidation state is the π-complexation of Cu(I) with the aryl halide, **Figure 2.5**. This coordination of Cu(I) with the aromatic ring activates the C - X bond making it more susceptible to nucleophilic substitution.[37]

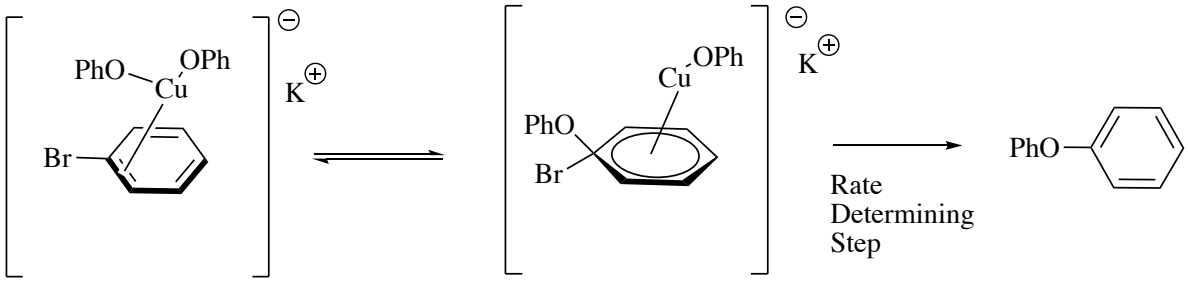

Figure 2.5. Proposed π-complexation Ullmann-type mechanism.

2.4 Conclusion

The 3-substituted quinolines are surprisingly poorly explored as antimalarial drug candidates. We have previously published papers on the synthesis of 3-haloCQs.[7,8] Thus, we sought to functionalize this position to explore the potential advantages and disadvantages of such a substitution. In this chapter, the reaction optimization of 3-BrCQ while using fewer reagents and decreasing reaction times was reported. We were able to scale up the reaction from 300 mg to 1 gram, and regioselectivity for the product was improved.

With 3-BrCQ in hand, we were able to synthesize 3-NH_2CQ via Ullmann-type coupling. We discovered that ammonium hydroxide is not a good amine source for this coupling reaction. We then tested azidotrimethyl silane as an amine source because of its increased solubility in organic solvents, and it proved to be a better candidate than NH_4·OH. We determined that a base is not

required for this reaction; however, the presence of the reducing agent as sodium ascorbate or L-ascorbic acid in combination with ligand DMEDA gave the best results, although the yields were still poor. Tetrabutylammonium azide was also tested with DMEDA and sodium ascorbate; however, no product was formed. Lastly, sodium azide was tested, and we were able to significantly increase product yield to 55%, although, we observed the formation of CQ as a byproduct. Therefore, we created a 2-step synthesis to form 3-NH_2CQ from CQ in 35% overall yield over 2 days.

We concluded that the formation of 3-NH_2CQ and CQ occurred mainly via two competing mechanisms. It is possible that amine formation occurs when nucleophile coordination precedes oxidative addition and vice versa for CQ. Currently, there is no exact proven mechanism for the Ullmann-type coupling in the literature. There may be several mechanisms through which our byproduct is formed. As we have synthesized 3-NH_2CQ, we can now derivatize the 3 position further to synthesize novel 3-substituted CQ antimalarial candidates.

2.5 Experimental

2.5.1 General Information

All amination reactions were carried out in the presence of N_2 gas by standard syringe and septa techniques. Glassware was taken directly from the oven (120°C) and allowed to cool in a desiccator before use. Bromination reactions were carried out in 2 mL and 5 mL Biotage Microwave Vials under air. All solvents and reagents were obtained commercially and used without further purification unless noted.

Microwave-assisted reactions were carried out in a Biotage Initiator Classic. High-Resolution Mass Spectroscopy (HRMS) was obtained by positive/negative ESI, or positive/negative APCI on a Bruker Maxis Impact QTOF, or a Thermo Scientific ExactivePlus Orbitrap, with results reported as mass/charge ratios (*m/z*). Thin-layer chromatography (TLC) plates were visualized using ultra-violet light, 254 nm. Flash column chromatography was carried out manually using 230 - 400 mesh silica gel (Silicycle) using reagent grade solvents or using Biotage Isolera One system with Biotage ZIP 30 g columns.

^{1}H and ^{13} C NMR spectra were recorded at ambient temperature on Bruker AVIIIHD 400 MHz (^{1}H 400 MHz, ^{13}C 100 MHz), Bruker AVIIIHD 500 MHz (^{1}H 500 MHz, ^{13}C 125 MHz) and Bruker AVIIIHD 800 MHz (^{1}H 800 MHz, ^{13}C 201 MHz) using tetramethylsilane as the internal standard. Chemical shifts are reported relative to the residual deuterated solvent peaks. Chemical shifts are expressed in parts per million (ppm = δ) values and coupling constants (J) in Hertz (Hz). The terms m, s, d, t, q and p represent multiplicities of ^{1}H NMR resonances: multiplet, singlet, doublet, triplet, quartet and pent, respectively. For previously unknown compounds, a combination of 2D

experiments (COSY, HSQC, HMBC) was often used to complete the assignment of ^{1}H and ^{13}C signals. ^{1}H NMR signals are described by chemical shift δ (multiplicity, J (Hz), integration). ^{13}C NMR signals are described by chemical shift δ and are singlets unless otherwise specified.

2.5.2 Experimental procedures

Chloroquine free-base preparation (2.1)

To chloroquine diphosphate (2 g) dissolved in deionized H_2O (300 mL) in a 750 mL Erlenmeyer flask is added sodium hydroxide (1.86 g, 0.16 M) to give a pH of 11/12. At this pH all the drug has precipitated. This mixture is then transferred into a 1 L separatory funnel, and dichloromethane (DCM) (200 mL) is added to extract the free base (repeated three times). The combined organic layers are washed with brine and then dried over anhydrous magnesium sulfate ($MgSO_4$). $MgSO_4$ is filtered off, and the solvent is removed under reduced pressure. To the flask containing the free-base, which appears as a colourless oil, is added 15 mL of diethyl ether and is swirled. The solvent is then removed under reduced pressure, and the flask is transferred into a vacuum oven and left to dry overnight. White solid, 1.05 g, 84%. The ^{1}H and ^{13}C NMR was consistent with the literature.[38]

***N*⁴-(3-bromo-7-chloroquinolin-4-yl)-*N*¹,*N*¹-diethylpentane-1,4-diamine**

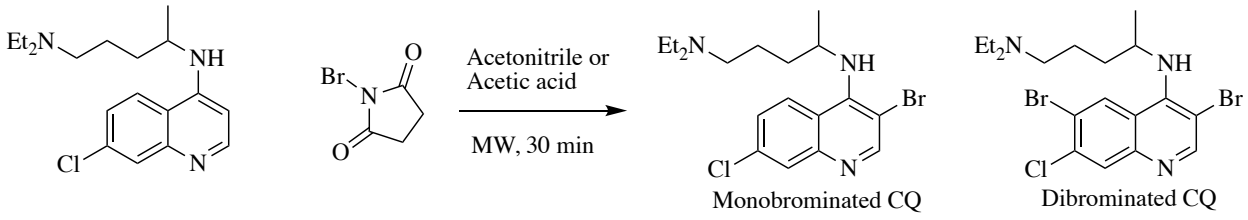

Chloroquine free-base (100 mg, 0.31 mmol), *N*-Bromosuccinimide (83.5 mg, 0.47 mmol) and 0.5 mL of acetonitrile or acetic acid are placed in a 2 mL Biotage microwave vial. The mixture is

subjected to microwave irradiation at 80°C for 30 minutes. When complete, the reaction is diluted in ethyl acetate (EtOAc) and basified with saturated sodium hydroxide and extracted with EtOAc (3 X 50 mL) and washed with brine. The combined organic extracts are then dried over anhydrous $MgSO_4$, and the solvent is removed under reduced pressure. The crude product is purified by flash chromatography with silica gel, solvent system: 70% hexanes (Hex), 25% EtOAc, 5% triethylamine (NEt_3) to reveal a brown oil.

N^4-(3-bromo-7-chloroquinolin-4-yl)-N^1,N^1-diethylpentane-1,4-diamine (2.2)

As reported in the literature.[7]

N^4-(3,6-dibromo-7-chloroquinolin-4-yl)-N^1,N^1-diethylpentane-1,4-diamine (2.3)

Yield: 119.4 mg, 8%. **^{1}H NMR** (400 MHz, Chloroform-*d*) δ 8.68 (s, 1H), 8.29 (s, 1H), 8.08 (s, 1H), 4.57 (d, J = 10.1 Hz, 1H), 4.00 (dq, J = 10.0, 6.2 Hz, 1H), 2.57 (q, J = 7.2 Hz, 4H), 2.47 (d, J = 7.0 Hz, 2H), 1.63 (dtd, J = 13.2, 6.9, 3.8 Hz, 4H), 1.29 (d, J = 6.3 Hz, 3H), 1.04 (t, J = 7.2 Hz, 6H). **^{13}C NMR** (201 MHz, Chloroform-*d*) δ 153.01, 148.61, 148.14, 135.46, 130.84, 128.19, 121.88, 119.74, 107.54, 55.05, 52.55, 46.92, 36.67, 23.40, 22.39, 11.26. **HRMS** (ESI) calcd. for $C_{18}H_{25}Br_2ClN_3$ [M+H]: 476.0098, found: 476.0097

General procedure for 7-chloro-N^4-(5-(diethylamino)pentan-2-yl)quinoline-3,4-diamine (2.4) synthesis:

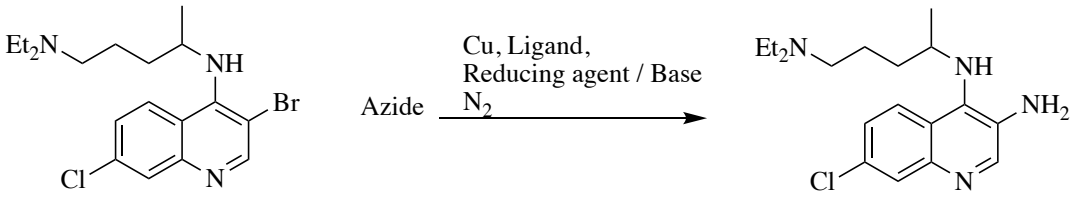

Azide (2 equiv.), copper (0.5 equiv.), ligand (0.5 equiv.) and reducing agent (0.5 equiv.) or base (2 equiv.) are placed in a 10 mL round bottom flask fitted with a septum. A needle connected to the vacuum/N_2 manifold was inserted, the flask is evacuated and backfilled with N_2 gas, this procedure is repeated three times. Then N^4-(3-bromo-7-chloroquinolin-4-yl)-N^1,N^1-diethylpentane-1,4-diamine (1 equiv.) dissolved in degassed EtOH/ H_2O (7:3 v/v) is added to the flask via syringe through the septum. The reaction mixture is refluxed at 85°C under N_2 for 3 hours while stirring vigorously. After the time elapses, the reaction mixture is left to cool down to room temperature (RT). The reaction mixture is then diluted in H_2O and basified with 1 M NaOH. It is then extracted three times with DCM or EtOAc, and the combined organic phases are washed with brine and dried over $MgSO_4$. The solvent is then removed by reduced pressure and purified by prep TLC 50% Hex, 40% EtOAc, 5% methanol (MeOH), 5% NEt_3 to give an orange oil 331 mg, 55%. The ^1H and ^{13}C NMR was consistent with the literature.[5]

2.6 References

(1) Surrey, A. R.; Cutler, R. A. The Preparation of 3-Halo-4-Dialkylaminoalkylaminoquinoline Derivatives. *J. Am. Chem. Soc.* **1946**, *68* (12), 2570–2574.

(2) Kinawi, A.; Dietz, M.; Schmidt, R.; Löwe, W. Kurzmitteilung. Bindung von Razemischen Chloroquin Sowie Einiger Derivate an Humanserumalbumin. *Arch. Pharm. (Weinheim).* **1995**, *328* (1), 93–94.

(3) Pou, S.; Winter, R. W.; Nilsen, A.; Kelly, J. X.; Li, Y.; Doggett, J. S.; Riscoe, E. W.; Wegmann, K. W.; Hinrichs, D. J.; Riscoe, M. K. Sontochin as a Guide to the Development of Drugs against Chloroquine-Resistant Malaria. *Antimicrob. Agents Chemother.* **2012**, *56* (7), 3475–3480.

(4) Bass, G. E.; Hudson, D. R.; Parker, J. E.; Purcell, W. P. Mechanism of Antimalarial Activity of Chloroquine Analogs from Quantitative Structure-Activity Studies. Free Energy Related Model. *J. Med. Chem.* **1971**, *14* (4), 275–283.

(5) Konstantinović, J.; Videnović, M.; Orsini, S.; Bogojević, K.; D'Alessandro, S.; Scaccabarozzi, D.; Terzić Jovanović, N.; Gradoni, L.; Basilico, N.; Šolaja, B. A. Novel Aminoquinoline Derivatives Significantly Reduce Parasite Load in Leishmania Infantum Infected Mice. *ACS Med. Chem. Lett.* **2018**, *9* (7), 629–634.

(6) van Langevelde, A.; Bakker, C. N. M.; Boer, H.; Ilmer, T. A. M.; Journée-de Korver, J. A.; Kaspersen, F. M.; Noach, E. L.; Oosterhuis, J. A.; Pauwels, E. K. J. Potential Radiopharmaceuticals for the Detection of Ocular Melanoma - Part II. Iodoquinoline Derivatives and 67Ga-Citrate. *Eur. J. Nucl. Med.* **1986**, *12* (2), 96–104.

(7) Edaye, S.; Tazoo, D.; Bohle, D. S.; Georges, E. 3-Iodo-4-Aminoquinoline Derivative Sensitises Resistant Strains of Plasmodium Falciparum to Chloroquine. *Int. J. Antimicrob.*

Agents **2016**, *47* (6), 482–485.

(8) Edaye, S.; Tazoo, D.; Bohle, D. S.; Georges, E. 3-Halo Chloroquine Derivatives Overcome Plasmodium Falciparum Chloroquine Resistance Transporter-Mediated Drug Resistance in P. Falciparum. *Antimicrob. Agents Chemother.* **2015**, *59* (12), 7891–7893.

(9) Kaur, K.; Jain, M.; Reddy, R. P.; Jain, R. Quinolines and Structurally Related Heterocycles as Antimalarials. *Eur. J. Med. Chem.* **2010**, *45* (8), 3245–3264.

(10) Coatney, G. R. Pitfalls in a Discovery: The Chronicle of Chloroquine *. *Am. J. Trop. Med. Hyg.* **1963**, *12* (2), 121–128.

(11) Okombo, J.; Chibale, K. Recent Updates in the Discovery and Development of Novel Antimalarial Drug Candidates. *Medchemcomm* **2018**, *9* (3), 437–453.

(12) Schlitzer, M. Malaria Chemotherapeutics Part I: History of Antimalarial Drug Development, Currently Used Therapeutics, and Drugs in Clinical Development. *ChemMedChem* **2007**, *2* (7), 944–986.

(13) Kaschula, C. H.; Egan, T. J.; Hunter, R.; Basilico, N.; Parapini, S.; Taramelli, D.; Pasini, E.; Monti, D. Structure−Activity Relationships in 4-Aminoquinoline Antiplasmodials. The Role of the Group at the 7-Position. *J. Med. Chem.* **2002**, *45* (16), 3531–3539.

(14) Egan, T. J. Structure-Function Relationships in Chloroquine and Related 4-Aminoquinoline Antimalarials. *Mini-Reviews Med. Chem.* **2001**, *1* (1), 113–123.

(15) Egan, T. J.; Hunter, R.; Kaschula, C. H.; Marques, H. M.; Misplon, A.; Walden, J. Structure−Function Relationships in Aminoquinolines: Effect of Amino and Chloro Groups on Quinoline−Hematin Complex Formation, Inhibition of β-Hematin Formation, and Antiplasmodial Activity. *J. Med. Chem.* **2000**, *43* (2), 283–291.

(16) Natarajan, J. K.; Alumasa, J. N.; Yearick, K.; Ekoue-Kovi, K. A.; Casabianca, L. B.; De

Dios, A. C.; Wolf, C.; Roepe, P. D. 4-N-, 4-S-, and 4-O-Chloroquine Analogues: Influence of Side Chain Length and Quinolyl Nitrogen PKa on Activity vs Chloroquine Resistant Malaria. *J. Med. Chem.* **2008**, *51* (12), 3466–3479.

(17) Ribas, X.; Güell, I. Cu(I)/Cu(III) Catalytic Cycle Involved in Ullmann-Type Cross-Coupling Reactions. *Pure Appl. Chem.* **2014**, *86* (3), 345–360.

(18) Sambiagio, C.; Marsden, S. P.; Blacker, A. J.; McGowan, P. C. Copper Catalysed Ullmann Type Chemistry: From Mechanistic Aspects to Modern Development. *Chem. Soc. Rev.* **2014**, *43* (10), 3525–3550.

(19) Terzić, N.; Konstantinović, J.; Tot, M.; Burojević, J.; Djurković-Djaković, O.; Srbljanović, J.; Štajner, T.; Verbić, T.; Zlatović, M.; Machado, M.; Albuquerque, I. S.; Prudêncio, M.; Sciotti, R. J.; Pecic, S.; D'Alessandro, S.; Taramelli, D.; Šolaja, B. A. Reinvestigating Old Pharmacophores: Are 4-Aminoquinolines and Tetraoxanes Potential Two-Stage Antimalarials? *J. Med. Chem.* **2016**, *59* (1), 264–281.

(20) Jiao, J.; Zhang, X. R.; Chang, N. H.; Wang, J.; Wei, J. F.; Shi, X. Y.; Chen, Z. G. A Facile and Practical Copper Powder-Catalyzed, Organic Solvent-and Ligand-Free Ullmann Amination of Aryl Halides. *J. Org. Chem.* **2011**, *76* (4), 1180–1183.

(21) Lang, F.; Zewge, D.; Houpis, I. N.; Volante, R. . Amination of Aryl Halides Using Copper Catalysis. *Tetrahedron Lett.* **2001**, *42* (19), 3251–3254.

(22) Yang, B.; Liao, L.; Zeng, Y.; Zhu, X.; Wan, Y. A Simple and Recyclable Copper/DTPA Catalyst System for Amination of Aryl Halides with Aqueous Ammonia in Water. *Catal. Commun.* **2014**, *45*, 100–103.

(23) Maejima, T.; Shimoda, Y.; Nozaki, K.; Mori, S.; Sawama, Y.; Monguchi, Y.; Sajiki, H. One-Pot Aromatic Amination Based on Carbon–Nitrogen Coupling Reaction between Aryl

Halides and Azido Compounds. *Tetrahedron* **2012**, *68* (6), 1712–1722.

(24) Dunn, A. D. A Facile Synthesis Of 3-Amino-1(2)H-Pyrazolo[3,4-C]Pyridine. *Org. Prep. Proced. Int.* **1997**, *29* (5), 577–579.

(25) Peterson, J. R.; Zjawiony, J. K.; Liu, S.; Hufford, C. D.; Clark, A. M.; Rogers, R. D. Copyrine Alkaloids: Synthesis, Spectroscopic Characterization, and Antimycotic/Antimycobacterial Activity of A- and B-Ring-Functionalized Sampangines. *J. Med. Chem.* **1992**, *35* (22), 4069–4077.

(26) Liu, Y.; Xiao, Q.; Liu, Y.; Li, Z.; Qiu, Y.; Zhou, G.-B.; Yao, Z.-J.; Jiang, S. Biological Evaluation of New Mimetics of Annonaceous Acetogenins: Alteration of Right Scaffold by Click Linkage with Aromatic Functionalities. *Eur. J. Med. Chem.* **2014**, *78*, 248–258.

(27) Goriya, Y.; Ramana, C. V. The [Cu]-Catalyzed SNAR Reactions: Direct Amination of Electron Deficient Aryl Halides with Sodium Azide and the Synthesis of Arylthioethers under Cu(II)–Ascorbate Redox System. *Tetrahedron* **2010**, *66* (38), 7642–7650.

(28) Altman, R. A.; Buchwald, S. L. Cu-Catalyzed Goldberg and Ullmann Reactions of Aryl Halides Using Chelating N- and O-Based Ligands. *Nat. Protoc.* **2007**, *2* (10), 2474–2479.

(29) Markiewicz, J. T.; Wiest, O.; Helquist, P. Synthesis of Primary Aryl Amines Through a Copper-Assisted Aromatic Substitution Reaction with Sodium Azide. *J. Org. Chem.* **2010**, *75* (14), 4887–4890.

(30) Lanke, S. R.; Bhanage, B. M. Copper Bis(2,2,6,6-Tetramethyl-3,5-Heptanedionate)–Catalyzed Coupling of Sodium Azide with Aryl Iodides/Boronic Acids to Aryl Azides or Aryl Amines. *Synth. Commun.* **2014**, *44* (3), 399–407.

(31) Sklorz, J. A. W.; Hoof, S.; Rades, N.; De Rycke, N.; Könczöl, L.; Szieberth, D.; Weber, M.; Wiecko, J.; Nyulászi, L.; Hissler, M.; Müller, C. Pyridyl-Functionalised 3 H -1,2,3,4-

Triazaphospholes: Synthesis, Coordination Chemistry and Photophysical Properties of Low-Coordinate Phosphorus Compounds. *Chem. - A Eur. J.* **2015**, *21* (31), 11096–11109.

(32) Messaoudi, S.; Brion, J.-D.; Alami, M. An Expeditious Copper-Catalyzed Access to 3-Aminoquinolinones, 3-Aminocoumarins and Anilines Using Sodium Azide. *Adv. Synth. Catal.* **2010**, *352* (10), 1677–1687.

(33) Sung, S.; Braddock, D. C.; Armstrong, A.; Brennan, C.; Sale, D.; White, A. J. P.; Davies, R. P. Synthesis, Characterisation and Reactivity of Copper(I) Amide Complexes and Studies on Their Role in the Modified Ullmann Amination Reaction. *Chem. - A Eur. J.* **2015**, *21* (19), 7179–7192.

(34) Sperotto, E.; Van Klink, G. P. M.; Van Koten, G.; De Vries, J. G. The Mechanism of the Modified Ullmann Reaction. *Dalt. Trans.* **2010**, *39* (43), 10338–10351.

(35) Cohen, T.; Cristea, I. Kinetics and Mechanism of the Copper(I)-Induced Homogeneous Ullmann Coupling of o-Bromonitrobenzene. *J. Am. Chem. Soc.* **1976**, *98* (3), 748–753.

(36) Kim, J. K.; Bunnett, J. F. Evidence for a Radical Mechanism of Aromatic "Nucleophilic" Substitution. *J. Am. Chem. Soc.* **1970**, *92* (25), 7463–7464.

(37) Weingarten, H. Mechanism of the Ullmann Condensation. *J. Org. Chem.* **1964**, *29* (12), 3624–3626.

(38) Sinha, M.; Dola, V. R.; Soni, A.; Agarwal, P.; Srivastava, K.; Haq, W.; Puri, S. K.; Katti, S. B. Synthesis of Chiral Chloroquine and Its Analogues as Antimalarial Agents. *Bioorg. Med. Chem.* **2014**, *22* (21), 5950–5960.

Chapter 3

Synthesis of Novel Substituted Chloroquine Derivatives

3.1 Preamble

Following the optimization of 3-NH_2CQ synthesis, we wanted to derivatize the 3-position further. The installed arylamine serves as a precursor for various derivatives such as secondary amines, benzamides, sulfonamides, triazoles, and Schiff-bases. We were interested in the synthesis of such derivatives as possible combination therapy partners for CQ. Additionally, β-hematin may not be their only target. 3-substituted CQs may target other stages of the parasite's life cycle. As we know, 8-AQs such as PQ are active against liver-stage hypnozoites. We discovered that 3-haloCQs when used in combination with CQ, resensitize resistance strains of the parasite to CQ. Furthermore, the potencies of 3-haloCQ are unaffected by VP, which suggests that they are not substrates for mutant PfCRT. This was an exciting discovery that inspired us to create a library of novel 3-substituted CQs. We are interested in their drug targets and their ability to resensitize resistant parasites to CQ. Artemisinin combination therapies (ACTs) are the recommended treatments for malaria, which are beginning to fail in Asian countries. Insights into new combination therapies, especially ones that utilize a cheap drug, would be very valuable.

3.2 Introduction

As illustrated in chapter 1, the 4-aminoquinolines are the most studied of all the classes of antimalarial drugs. Although the quinoline structure has been extensively modified, it still has great potential, as seen with antimalarial drug candidates FQ and AQ-13. Both antimalarial candidates were in phase II clinical trials but have not yet advanced to phase III.

Previous results from our group included the synthesis of 3-halo CQs: 3-ClCQ, 3-BrCQ and 3-ICQ.[1] Their preparation involves activation of *N*-halosuccinimide with trifluoroacetic acid in

acetonitrile at 80ºC for 30 minutes, followed by CQ addition. The reaction mixture is then stirred at 80ºC for 2 hours. Yields ranged between 73% - 81%. *In vitro* assays were carried out and it was determined that each derivative is equally potent against CQS and CQR *P. falciparum* strains; however, they were ~8.5 - fold less potent than CQ.[1] These results are in-line with previous structure-activity relationship (SAR) reports which showed that modifications to the quinoline ring resulted in decreased antiplasmodial activity.[2,3] In CQS strain 3D7, 3-haloCQ had a 19 - fold decrease in potency compared to CQ. The IC_{50} values range between 367 nM - 747 nM in CQS 3D7 strain and 623 nM – 1163 nM in CQR strain Dd2, **Scheme 3.1**. Of the three derivatives synthesized, 3-ICQ was the most potent with IC_{50} values of 367 nM and 623 nM in 3D7 and Dd2, respectively.[4]

a)

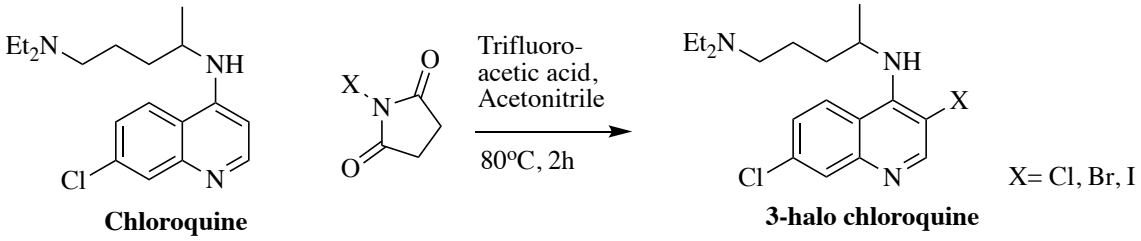

Chloroquine **3-halo chloroquine** X= Cl, Br, I

b)

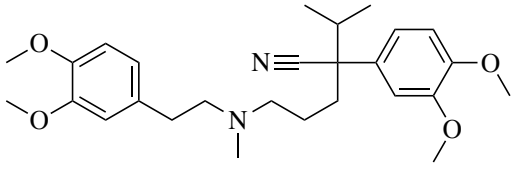

Verapamil

Scheme 3.1. a) Halochloroquine synthesis, b) structure of verapamil.

Furthermore, a β-hematin inhibition assay was carried out to determine 3-ICQ's ability to inhibit β-hematin formation, and it was found that 3-ICQ does inhibit β-hematin formation but to a lesser extent than CQ. This is possibly due to the presence of the electron-withdrawing iodine that lowers

the pK_a of the quinolinium nitrogen (**Table 3.3**) and may reduce the compound's affinity to Fe(III)PIX. These results are not surprising or unexpected as substituents on the quinoline ring affect the drug's ability to interact with heme.[5] A large, electron-withdrawing group such as iodine can reduce affinity for heme.

Verapamil (VP), **Scheme 3.1**, is a chemosensitizer that presumably inhibits PfCRT allowing CQ to remain in its active site and exert its potency. When resistant parasites are treated with 3-ICQ and VP, there was no improvement of activity, suggesting that 3-ICQ may not be a substrate for mutant PfCRT, as its activity is independent of the presence of VP. A surprising and significant finding of these results is that combination treatment of CQ and 3-ICQ was more potent than either drug alone against CQR parasites. This chemosensitization effect suggests that 3-ICQ may act like VP to resensitize the parasite to CQ.[4]

With these promising results in hand, we wanted to explore the functionality of the 3-position further. In this chapter, we describe the synthesis of CQ derivative, their antiplasmodial activity and their structure-activity relationships. We will also describe pK_a studies carried out to determine the effect of substituents on the quinolinium pK_a.

3.3 Results and Discussion

3.3.1 3-CQ derivatives

Previous work in our lab demonstrated the chemosensitization effect that 3-ICQ had on CQ.[4] It was evident that 3-ICQ sensitizes CQR parasites to CQ, suggesting it may not be a substrate for mutant PfCRT. The possibility of synthesizing drugs for combination therapy was attractive as that is the basis of ACT. We wanted to further explore modifications at the 3rd position of the quinoline to find other drug candidates that modulate CQ activity.

We began with the functionalization of the 3rd position of the quinoline, with the installation of an amine functional group (discussed in chapter 2), **Scheme 3.2**. With the amine installed, we were then able to carry out the final step of the synthesis. We explored three classes of derivatives: amides, sulfonamides and Schiff-bases. The formation of amides was straightforward as benzoyl chlorides are widely available and relatively inexpensive, **Figure 3.2**. Amides add rigidity to the molecule as well as the introduction of an H-bond acceptor. The resulting derivatives were then tested for their antiplasmodial activity *in vitro*.

While designing the new CQ-derivatives, we used Lipinski's rule of 5 as a guide to possibly make the compounds more drug-like for oral administration.[6,7] The rules state that a drug should: i) have a molar mass of less than 500 g/mol, ii) have a partition coefficient of less than 5, iii) have no more than 5 H-bond donors and iv) have no more than 10 H-bond acceptors. As a starting point, we began with the synthesis of benzamides and used the Craig Plot [8,9] as a guide to determine which substituents to place on the ring, **Figure 3.1**.

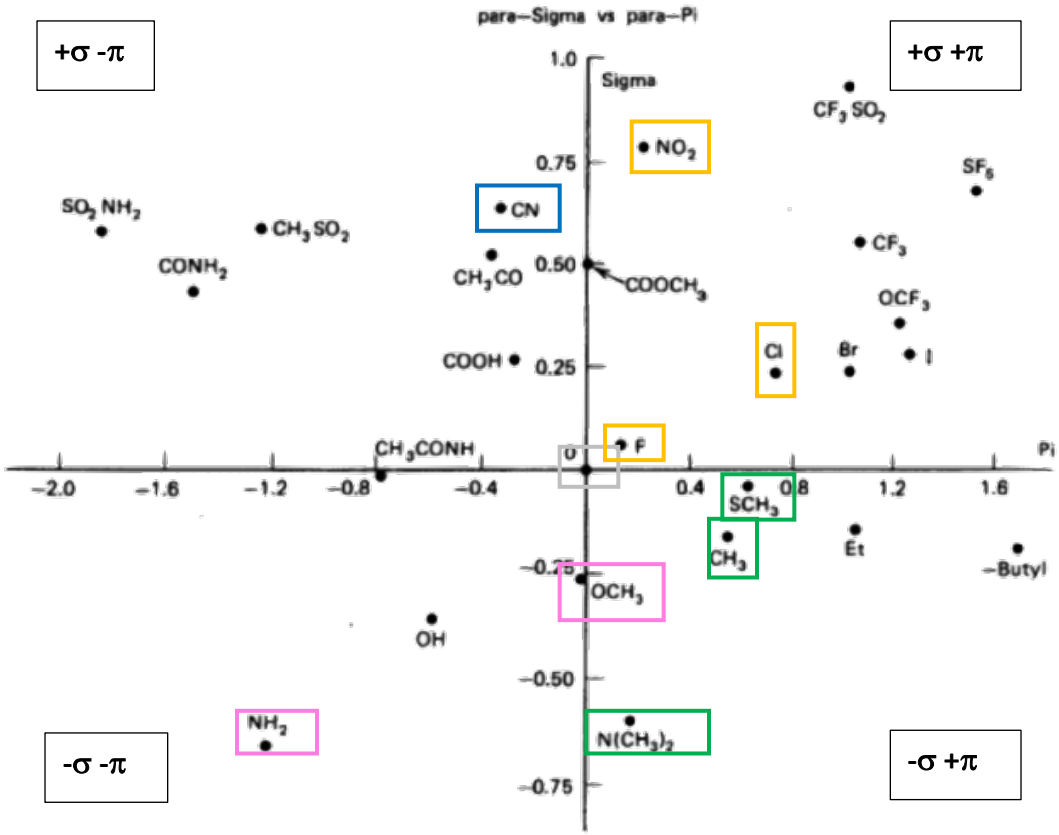

Figure 3.1. Craig Plot groups substituents with similar electronic and hydrophobic effects. Highlighted are synthesized compounds containing substituents at various locations on the phenyl ring.

The Craig Plot groups various substituents based on their electronic and hydrophobic properties using benzoic acid as the reference point, the center of the graph. This helps identify simple changes to make on a compound to possibly increase activity and/or lipophilicity. We then experimented with substitution patterns on the benzoyl ring to get a complete SAR profile.

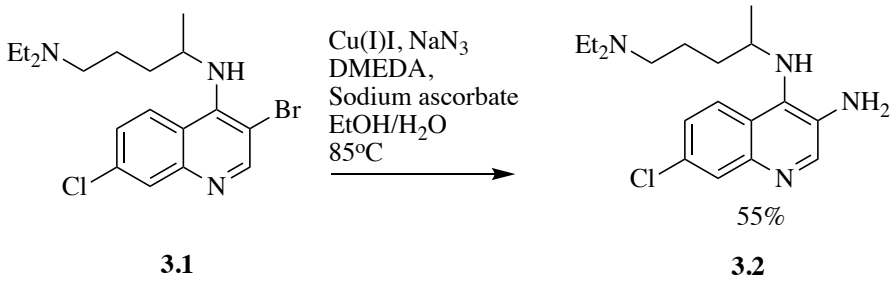

3.1 **3.2**

Scheme 3.2. Amination with 3-BromoCQ as a precursor.

Our collaborators, Dr. Fadi Baakdah, supervised by Dr. Elias Georges at the McGill University Institute of Parasitology, carried out *in vitro* antiplasmodial assays to identify which substituents showed the greatest potency, the results are displayed in **Table 3.1**.

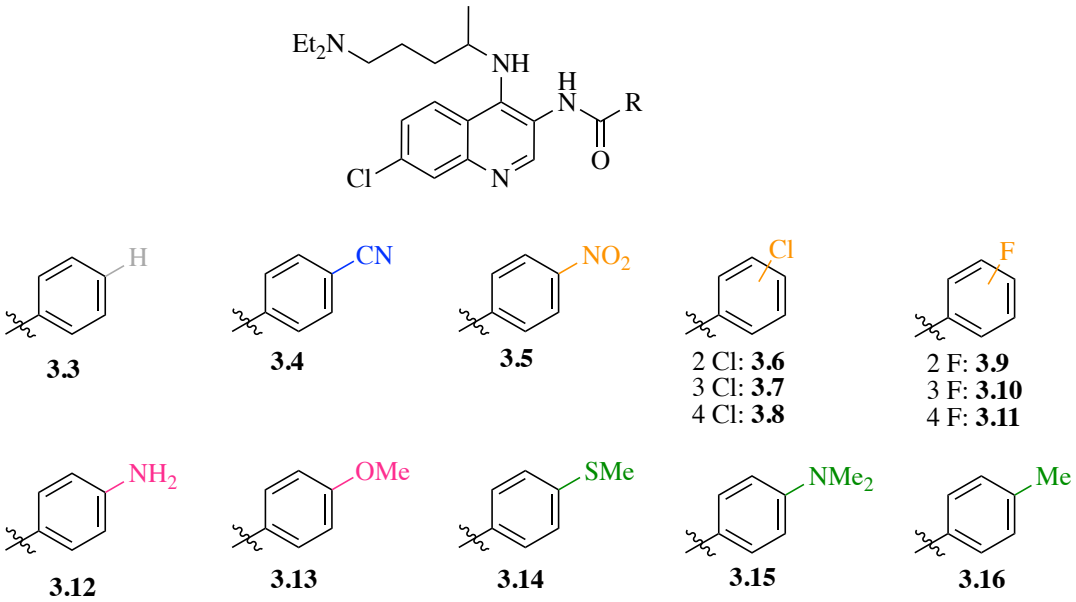

3.3 **3.4** **3.5** 2 Cl: **3.6** 3 Cl: **3.7** 4 Cl: **3.8** 2 F: **3.9** 3 F: **3.10** 4 F: **3.11**

3.12 **3.13** **3.14** **3.15** **3.16**

Figure 3.2. Synthesized compounds. Colours: grey: the reference compound, blue: electron-withdrawing and hydrophilic, orange: electron-withdrawing and hydrophobic, purple: electron-donating and hydrophilic, green: electron-donating and hydrophobic.

Table 3.1. Antiplasmodial activities of CQ derivatives in sensitive and resistant parasitic strains

Entry	R	% Yield	IC_{50} (nM) CQS 3D7	IC_{50} (nM) CQR Dd2
1	H	85	50.5 ± 2.3	1,192.0 ± 232.0
2	4-NH_2	41	10.4 ± 0.8	1,564.0 ± 53.0
3	4-Me	59	265.1 ± 10.1	564.4 ± 11.4
4	4-OMe	75	114.2 ± 18.6	963.0 ± 8.5
5	4-SMe	61	79.5 ± 9.1	205.5 ± 21.6
6	4-NMe_2	31	280.4 ± 25.4	619.9 ± 89.0
7	4-CN	66	391.3 ± 37.2	808.4 ± 85.0
8	4-NO_2	76	278.6 ± 6.0	870.9 ± 99.8
9	2-F	66	502.9 ± 19.9	1,010.0 ± 11.8
10	3-F	64	255.1 ± 2.0	733.9 ±79.0
11	4-F	60	8.7 ± 0.4	667.0 ± 60.4
12	2-Cl	59	69.8 ± 8.3	918.0 ± 3.0
13	3-Cl	61	84.0 ± 9.7	497.2 ± 36.7
14	4-Cl	51	7.0 ± 0.4	311.1 ± 63.5
15	[a]	11	266.2 ± 33.5	1,007.0 ± 457.0
16	[b]	17	105.8 ± 12.2	404.0 ± 42.7
3-NH_2CQ	-	-	297.0 ± 52.0	720.0 ± 107.0
3-ICQ	-	-	367.0 ± 24	623.5 ± 72.5
CQ	-	-	20.5 ± 4.5	169.9 ± 16.6

a) 4-Cl sulfone derivative b) 4-Cl Schiff-base derivative, **Figure 3.8**

The vast majority of the synthesized drug candidates show some antiplasmodial activity; however, most are less potent than CQ in CQS 3D7 strain and CQR Dd2 strain. The benzamido-analog, **3.3**, was 2.5 - fold less potent than CQ in CQS 3D7 strains, and was 7 - fold less potent than CQ in CQR Dd2 strains. We believe this decrease in activity is due to decreased affinity to heme, similar to 3-ICQ, which is correlated to antiplasmodial activity.[5] For the Dd2 strain, the mutations might

cause reduced accumulation of the benzamidoCQ in the DV, it was reported that accumulation is correlated to antiplasmodial activity.[10]

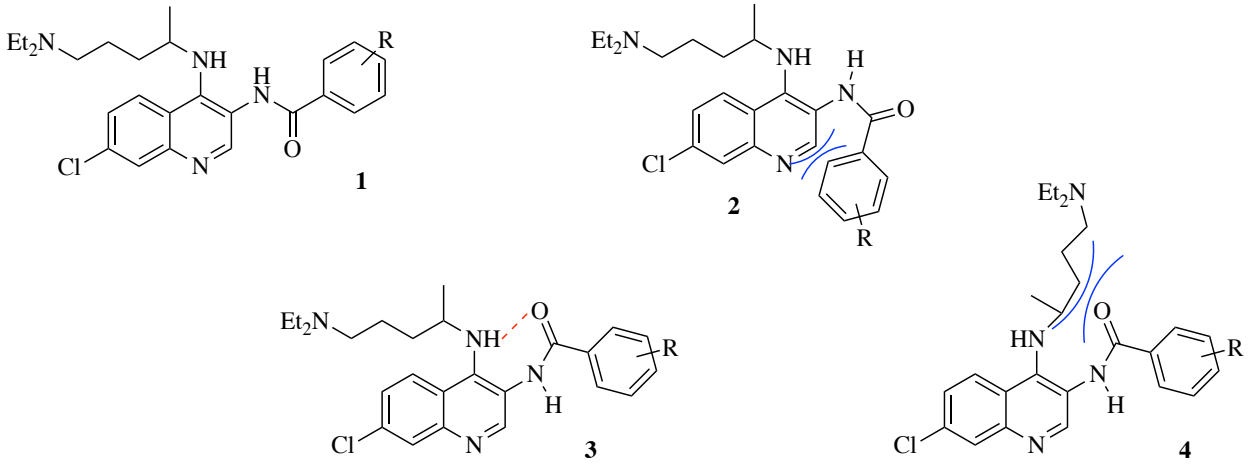

Figure 3.3. Possible benzamidoCQ conformations.

Halogen substituents such as fluoride and chloride had varying activity depending on their position on the benzoyl ring. We discovered that the para-position gave the best activity for both halogens, **3.8** and **3.11**. They were more potent than the benzamidoCQ compound; 7.2 and 5.8 - fold better in CQS strain than benzamidoCQ for chloro- and fluoro-respectively. The activity at the meta-position, **3.7** and **3.10**, was in between that of the ortho- and para- positions. The ortho-position gave the worst activity for both substituents, **3.6** and **3.9**, with the chloro- being more potent in CQS strain. They were more potent than benzamidoCQ in CQR strains but not as effective on CQS strains. Overall, the para-chloro-substituent, **3.8**, was the most potent.

Electron-withdrawing, hydrophobic nitro-substituent, **3.5**, was 5.5 - fold less potent than the reference compound in CQS strain and was 1.4 – fold more potent than the reference compound

in CQR strain. The decrease in activity in CQS strain is likely due to an increase in the size of the moiety. Furthermore, the rigidity of this substituent might play a role in its reduced activity.

The addition of an electron-withdrawing, hydrophilic cyano group, **3.4**, was 7.7 - fold weaker in CQS strain and 1.5 - fold better in CQR than the benzamidoCQ. The decrease in activity in 3D7 strains might be due to the addition of an H-bond acceptor. The lack of flexibility at the 4th position might reduce the compound's ability to enter the target / active site. In Dd2 strains, the activity is essentially the same; thus, the reduced activity compared to CQ might be due to decreased accumulation.

The electron-donating, hydrophilic amino group, **3.12**, was 5 - fold more potent than benzamidoCQ in CQS but 1.3 – fold weaker in the CQR parasite. In contrast, the methoxy, **3.13**, was 2 - fold weaker in CQS and 1.2 – fold stronger in the CQR parasite than the benzamidoCQ. The addition of an H-bond donor NH_2 group significantly improves the antiplasmodial activity in CQS strains. This increase in activity might be due to a slight increase in accumulation as a small percentage of the amine will be protonated at lysosomal pH. Furthermore, the ability to form strong hydrogen bonds might further stabilize the compound.[11] In contrast, the methoxy derivative's reduced potency might result from reduced H-bonding ability and increased size of the methoxy in CQS strains. In resistant strains, however, the H-bonding ability of the amino group is a disadvantage, this is a trend in all our compounds. Therefore, we observe that the methoxy group, which does not H-bond as strongly as the amine, in CQR strains, is 1.6 - fold more potent than the amine counterpart.

We found that electron-donating, hydrophobic methyl, **3.16**, and dimethylamino-substituents, **3.15**, have similar activity in CQS and CQR strains. They were 5 - fold less potent than benzamidoCQ, **3.3**, in CQS parasites but ~2.3 - fold more potent in resistant parasites. However, the methylthio-substituent, **3.14**, was 1.6 – fold less potent than benzamidoCQ in CQS strains but was 5.8 - fold more potent in CQR strains. Although these substituents belong within the same quadrant, it is important to note that there is a difference in electronegativity and steric bulk. The methylthio-substituent is 3.4 - fold more potent than the methyl and dimethylamino-substituent in CQS strains. The methylthio-derivative is also 3 - fold more potent than these derivatives in CQR strains. This might be due to the favorable electronics and size of the methylthio over the simple methyl and H-bond accepting dimethylamino-substituents.

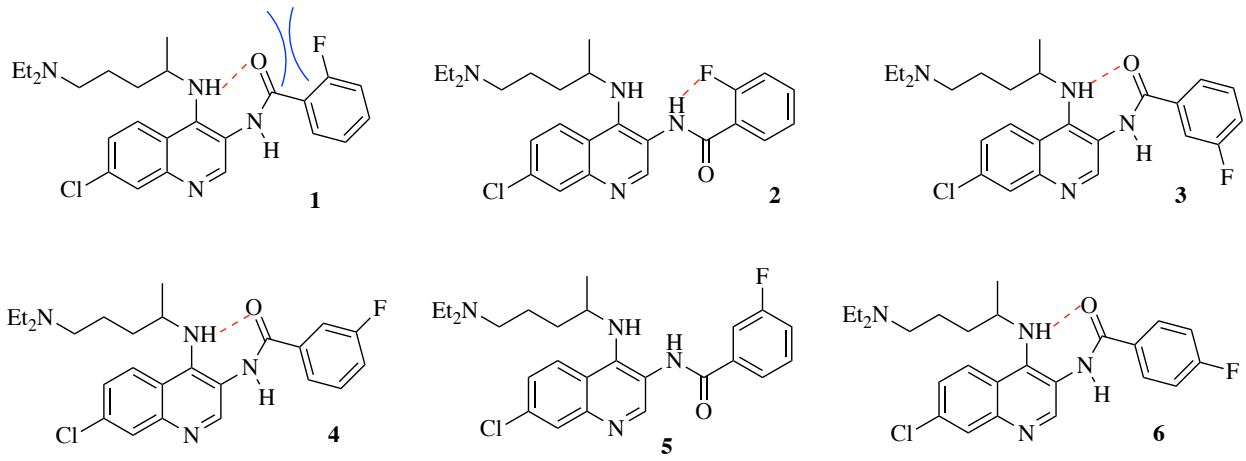

Figure 3.4. Possible fluorobenzamidoCQ conformations.

When looking at the possible configurations to explain differences in activity, one can see how electronic effects and steric hindrance may impact activity (see **Figure 3.3** to **Figure 3.5**). The ortho-position which showed the worst antiplasmodial activity exhibits lone pair / lone pair repulsion with the carbonyl oxygen. These forces may be unfavourable for activity. However,

these conformers also possibly exhibit intramolecular H-bonding, which could constrain the steric effects. However, the repulsion might be stronger than H-bonding stabilization. The meta-position contains conformers that possibly exhibit intramolecular H-bonding. This reduced repulsion might contribute to an increase of antiplasmodial activity in both CQS and CQR strains. The para-fluoro-substituent exhibits the least steric effects with the possible H-bond of the carbonyl and secondary amine, further stabilizing the compound and contributing to increased activity in CQS strains. However, it was clear that these factors do not enhance activity in CQR strains. As mentioned above, H-bonding ability is disadvantageous in resistant strains.

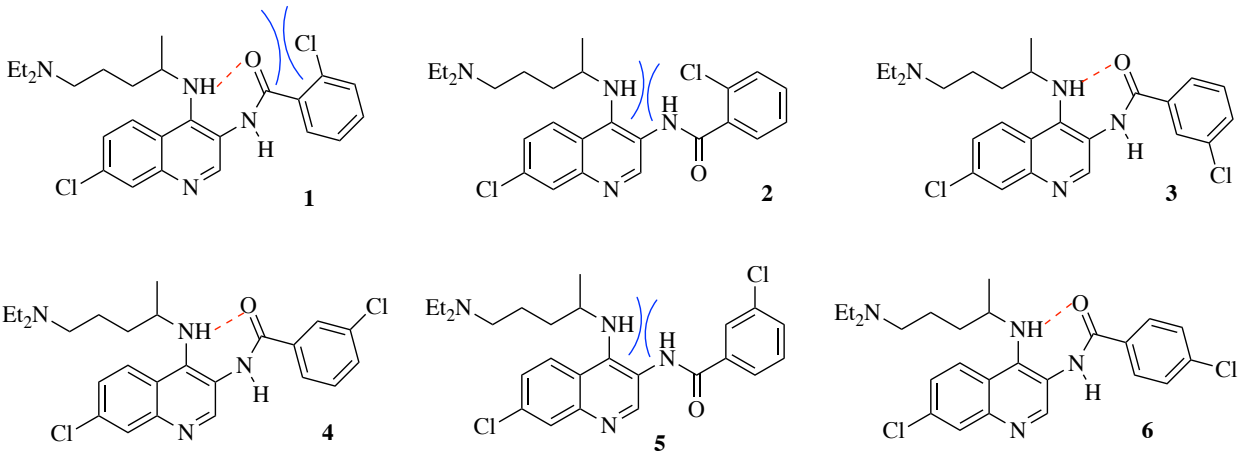

Figure 3.5. Possible chlorobenzamidoCQ conformations.

In contrast, the chloro-substituent shows better antiplasmodial activity across the board in CQS strains. A likely explanation is the reduced electronegativity of the chloride and longer C - X bond, which minimizes the π - delocalization. Furthermore, the chloride is unable to H – bond, explaining its better antiplasmodial activity in CQR strains.

To summarize, in 3D7 strains, the best substituents are chloro, **3.8**, fluoro, **3.11**, methylthio, **3.14**, and amino **3.12**. These are relatively compact or can form strong hydrogen bonds. In the case of

Dd2 strains, H-bonding substituents are disfavoured. The best substituents are chloro, **3.8**, and methylthio-substituent **3.14**. These are relatively small or flexible and do not form H-bonds. The optimal substituent positioning is the para-position. This position is void of possible steric effects, which are favourable for activity.

3.3.2 3-chlorobenzamidoCQ not a substrate for PfCRT

To determine whether the synthesized derivatives were substrates for PfCRT*, in vitro* assays were carried out in CQS and CQR strains in the presence of VP. VP is believed to act as a chemosensitizer that works on resistant strains by inhibiting mutant PfCRT's ability to transport drugs out of the DV. Assays of CQ with VP in Dd2 show a significant increase in activity as mutant PfCRT is inhibited. When 3-ICQ is assayed with VP in 3D7 and Dd2, no significant increase in activity is observed. This suggests that 3-ICQ is not a possible substrate for wild-type or mutant PfCRT.[4] Similarly, VP does not modulate **3.16** activity in Dd2 strains. Our next objective would be to determine whether 3-chlorobenzamidoCQ displays synergistic or antagonistic effects when used in combination with CQ. Interestingly, VP increases the IC_{50} value of wild-type PfCRT, **Table 3.2**. There is currently no evidence of VP interacting with wild-type PfCRT; furthermore, there are only a few reports on the speculated normal function(s) of wild-type PfCRT.

Table 3.2. Effect of verapamil on compound activity.

Compound	1 μM verapamil	IC_{50} CQS (nM) 3D7	IC_{50} CQR (nM) Dd2
CQ	-	20.5 ± 4.5	169.9 ± 16.6
	+	16.2 ± 0.6	21.0 ± 4.5
3-ICQ	-	367.0 ± 24.0	623.5 ± 72.5
	+	335.4 ± 46.1	621.2 ± 23.3
3-chloro benzamidoCQ	-	7.0 ± 0.4	311.1 ± 63.5
	+	146.3 ± 21.5	282.1 ± 50.0

3.3.3 Isomerization

The synthesized derivatives can adapt two main isomeric forms: the cis or trans-isomers, **Figure 3.6**. These isomers can be easily distinguished in an NMR spectrum as major or minor contributors. However, we found that all of the compounds were isolated as one isomer at RT, according to the ^{1}H NMR. As the rotational barrier of rotamers is high, it was assumed that they were isolated as one rotamer. The expected major isomer is the trans-amide because it exhibits the least steric effects. This is confirmed as the NOESY NMR does not show evidence of there being the E isomer. We do not observe the expected 2 - H / phenyl interaction associated with the E isomer.

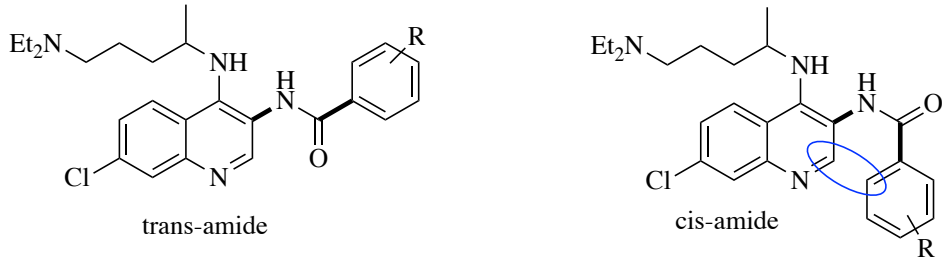

Figure 3.6. Trans and Cis benzamidoCQ isomers.

3.3.4 Fluoride coupling in ^{1}H NMR

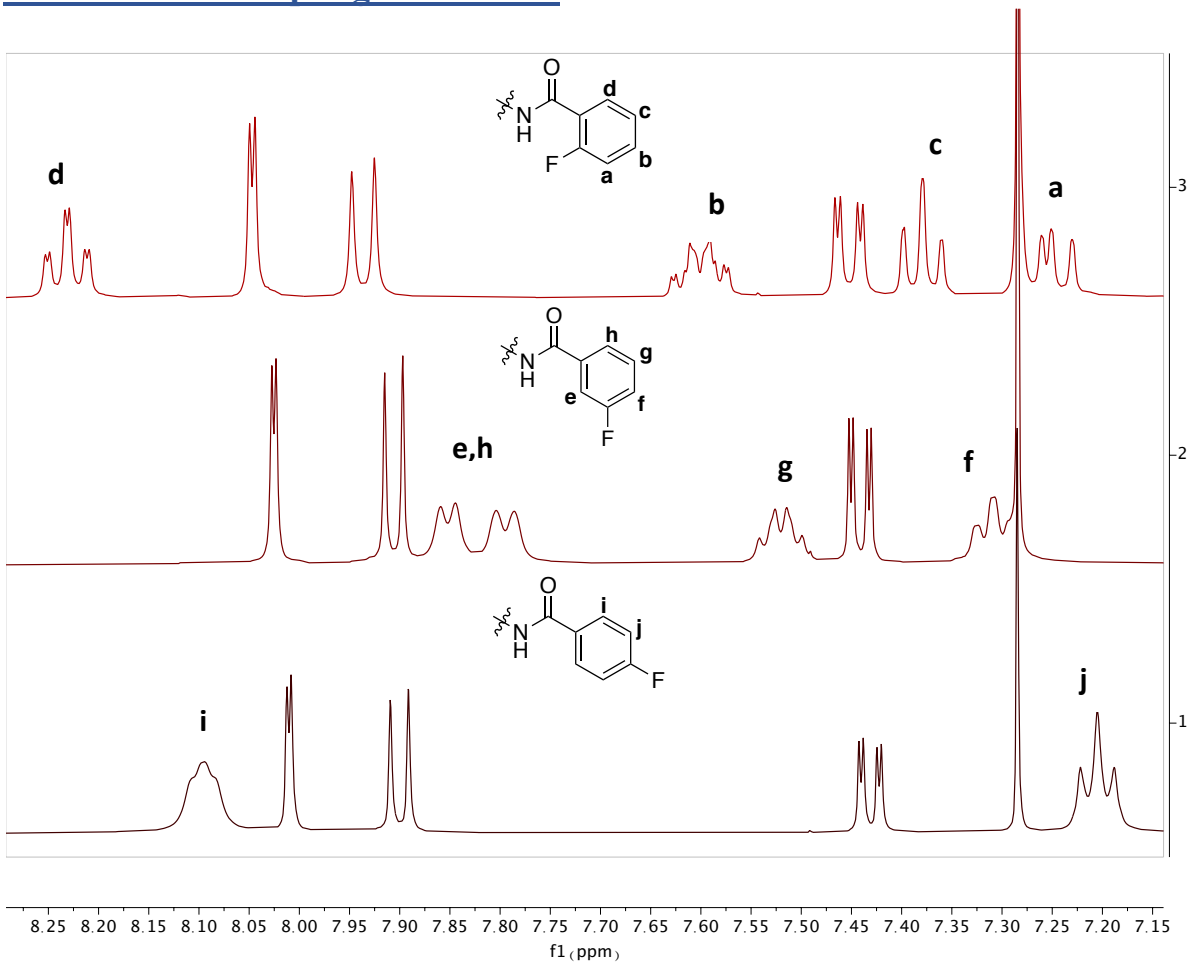

Figure 3.7. Fluorine and hydrogen coupling.

For the fluoride-containing derivatives, ^{1}H NMR analysis was carried out with H-F coupled mode. Evident in the spectra, **Figure 3.7**, is the extend of fluoride coupling on the benzoyl ring. We observe up to ^{4}J coupling in all derivatives, as evidenced by the splitting patterns. The coupling constant for proton **i,** a triplet is 6.5 Hz, while the coupling constant for proton **j,** a triplet is 8.4 Hz. Similarly, it is evident the extent of proton-fluorine coupling in proton **b,** which is a triplet of double of doublets (tdd) where J = 1.9, 5.3 and 7.2 Hz and proton **d,** which is a triplet of doublets (td) where J = 5.6 and 8 Hz. The multiplicity of proton **a,** is a double of double of doublets (ddd) pattern with J = 1.1, 3.9 and 8.3 Hz.

3.3.5 Synthesis of Sulfonamides and Schiff-base derivatives

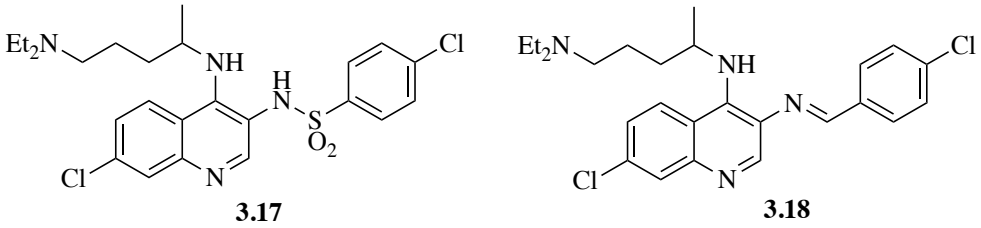

Figure 3.8. Structure of sulfonamide and Schiff-base derivatives

Once we discovered that the 4-chlorobenzamidoCQ, **3.8**, was the most potent compound, we synthesized sulfonyl, **3.17**, and Schiff-base, **3.18**, equivalents to determine the effect of the carbonyl group on activity, as shown in **Figure 3.8**. We found that the addition of the sulfone has a negative impact on the activity of the compound. This might be due to the increased mass by 36 g/mol, which breaks the Lipinski rule that states a drug should have a molar mass less than 500 g/mol and the introduction of an additional H-bond acceptor, **Figure 3.9**. This further reinforces the notion that H-bonding groups are disfavoured in resistant strains. Furthermore, the sulfone group might sterically hinder localization in the active site. The Schiff-base was 15 - fold less potent in the 3D7 strain and 1.3 - fold less potent in the Dd2 strain than the 4-chlorobenzamide. The decrease in activity in the sensitive strain might indicate the need for some electron density in the active site. Therefore, the electronegativity of the carbonyl is beneficial to activity. In Dd2, the activity is similar, further reinforcing that H-bonding is not beneficial in mutant parasites.

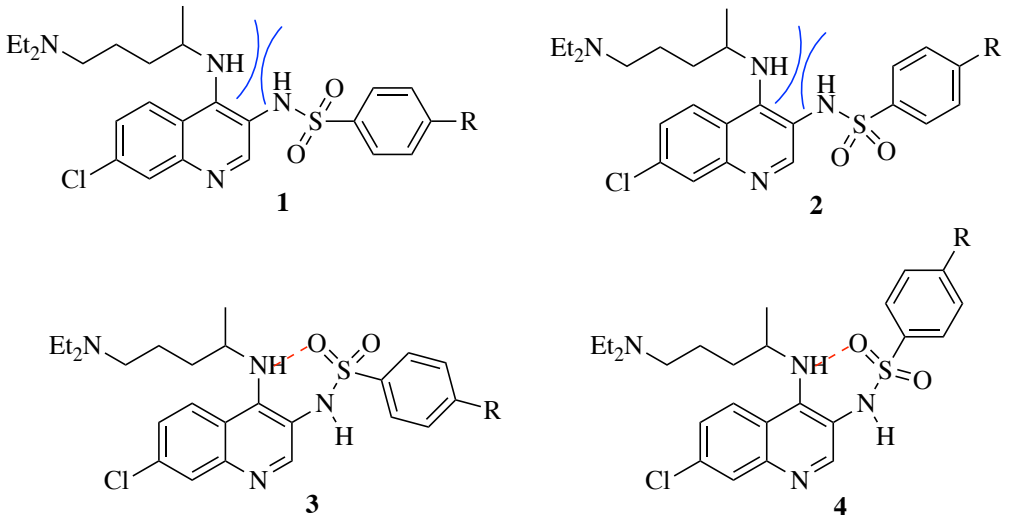

Figure 3.9. Possible sulfonamide conformations.

Due to the size of these compounds and the positioning of the modifications, β-hematin inhibition assays (BHIA) were not carried out. It is known that modification on the quinoline ring reduces the affinity of heme - CQ complex formation. These compounds are not expected to be able to prevent β-hematin formation to any significant extent. For this reason, BHIA was not performed.

Furthermore, although the current widely accepted mechanism of action for 4-aminoquinolines is β-hematin inhibition, it may not be the only way these compounds exert their activity.[12–16] Although these derivatives may not be as potent as CQ, their activity may be linked to a different mechanism. For this reason, the next step of this project would be to carry out assays in which parasites are given both CQ and our derivatives to determine if they behave as 3-ICQ in a synergistic manner.

3.3.6 pK_a studies

CQ is a weak base that can accumulate within its target site via the protonation of its tertiary alkyl nitrogen and quinoline nitrogen.[17] At pH 7.4, CQ is 17% mono-protonated and still lipid-soluble and can cross cell membranes. At lysosomal pH of 5.2, it is entirely diprotonated and no longer membrane permeable.[15] Thus, the pK_as of the molecule plays a crucial role in its localization, **Table 3.3**.

Table 3.3. Antiplasmodial activity and pKa of quinolinium nitrogen.

Drug	IC_{50} (3D7) nM	IC_{50} (Dd2) nM	Quinolinium pK_a
CQ	20.5 ± 4.5	169.9 ± 16.6	8.2
3-ChloroCQ	747.2 ± 65.0	1163.3 ± 46.0	5.3
3-BromoCQ	712.4 ± 89.6	987.8 ± 48.5	5.4
3-IodoCQ	367.0 ± 24	623.5 ± 72.5	5.5
NH_2-CQ	297.0 ± 52.0	720.0 ± 107.0	6.3

The presence of the electron-withdrawing halogens at the 3-position has a significant effect on the quinolinium pK_a. 3-halo CQs are 2 - 3 log units lower than CQ; therefore, they are not expected to be extensively diprotonated at physiological or lysosomal pH. Halogen substitution increases the overall lipophilicity of the molecule, which may promote membrane permeability; however, due to the decreased pK_a, it is not expected to become acid trapped within the DV as seen with CQ. This lack of accumulation in the target site may contribute to the observed decreased antiplasmodial activity. Furthermore, acid trapping is not believed to be the only method used for accumulation within the DV.[2] Unsurprisingly, the presence of an electron-donating amine

substituent does not lower the quinolinium pK_a as much as the halogens. This log unit difference in pK_a means a greater portion of 3-NH_2CQ will be protonated at physiological and lysosomal pH. Interestingly, although the pK_a is higher for 3-NH_2-CQ, the IC_{50} values are similar to 3-ICQ in CQS and CQR strains; this might suggest a similar mode of action for 3-substituted CQ's.

3.4 Conclusion

CQ has not been extensively modified at the 3-position in prior studies. A possible reason for this is the reduced antiplasmodial activity resulting from the lowered pK_a of the quinolinium nitrogen as a result of such a modification. However, we have observed a resensitization effect of the parasite to CQ when 3-substituted CQs derivatives are used in combination with CQ. We were able to further derivatize 3-substituted CQs via the installation of an amine. A library of derivatives was successfully synthesized represented across in the Craig Plot. Derivatives contain varying electronic and hydrophobic properties, which allow us to compare the effectiveness of substituents and the significance of regioselectivity. We determined that the hydrophilic and electron-withdrawing chloro-substituent was the most effective; furthermore, the para-position gives the best activity. Although the derivatives were active towards the parasite, they were on average 8 – fold less effective than CQ in sensitive strains and 6 – fold less effective than CQ in resistant strains. A sulfone and Schiff-base derivative were also synthesized; however, they were less potent than 4-chlorobenzamidCQ.

3.5 Experimental

3.5.1 General information

Glassware was taken directly from the oven (120ºC) and let cool in a desiccator before use. All reactions were carried out under N_2 pressure. Anhydrous DCM was obtained from MBraun MB-SPS solvent purification system into an oven-dried flask on the day of use. All solvents and reagents were obtained commercially and used without further purification unless noted.

High-Resolution Mass Spectroscopy (HRMS) was obtained by positive/negative ESI, or positive/negative APCI on a Bruker Maxis Impact QTOF, or a Thermo Scientific ExactivePlus Orbitrap, with results reported as mass/charge ratios (*m/z*). Thin-layer chromatography plates were visualized using ultra-violet light, 254nm. Flash column chromatography was carried out manually using 230 - 400 mesh silica gel (Silicycle) using reagent grade solvents or using Biotage Isolera One system with Biotage ZIP 30 g columns. Cole Parmer Microcomputer pH-Vision Model 05669-20 pH Meter used with Sigma-Aldrich micro pH combination electrode, glass body. The UV-Vis spectra were measured on Agilent 8453.

^{1}H and ^{13} C NMR spectra were recorded at ambient temperature on Bruker AVIIIHD 400 MHz (^{1}H 400 MHz, ^{13}C 100 MHz) and Bruker AVIIIHD 500 MHz (^{1}H 500 MHz, ^{13}C 125 MHz) using tetramethylsilane as the internal standard. Chemical shifts are reported relative to the residual deuterated solvent peaks. Chemical shifts are expressed in parts per million (ppm = δ) values and coupling constants (J) in Hertz (Hz). The terms m, s, d, t and q represent multiplicities of ^{1}H NMR resonances: multiplet, singlet, doublet, triplet and quartet, respectively. For previously unknown compounds, a combination of 2D experiments (COSY, HSQC, HMBC) was often used to

complete the assignment of ^{1}H and ^{13}C signals. ^{1}H NMR signals are described by chemical shift δ (multiplicity, J (Hz), integration). ^{13}C NMR signals are described by chemical shift δ and are singlets unless otherwise specified.

3.5.2 pKa Determination

A 0.01M stock solution of XH_3PO_4.haloCQ was made in a 1 mL volumetric flask. In a 4 mL cuvette, 1,990 µL of deionized H_2O was added, and into this cuvette was added 10 µL of the 0.01 M stock solution to make a final concentration of 50 µM XH_3PO_4.haloCQ and a total volume in the cuvette of 2,000 µL. The pH of the solution was measured on a calibrated pH meter. The pH should be acidic. Base (NaOH) will be added to the cuvette to increase the pH. Solutions of 10mM and 1mM NaOH and HCl were made. 5-20 µL of NaOH was added to increase the pH by 0.2 units. If the pH increases were too large, HCl was added to lower the pH. After each addition of NaOH, the solution was well mixed, the pH probe was fully submerged into the cuvette, and the pH was measured. The pH, incremental volume increase and absorbance at the λ_{max} were recorded. NaOH was added until a pH > 11/12 was reached or until the Absorbance versus pH graph plateaus. The graph was adjusted for dilution with the formula:

$$Dilution\ Correction_{pHx} = \frac{Initial\ volume + Total\ volume_{pHx}}{Initial\ volume}$$

The measured absorbance was then adjusted for dilution at *pHx* with the following formula:

$$Corrected\ Absorbance = Measured\ absorbance \times Dilution\ Correction$$

The pH and corrected absorbances were plotted on a non-linear curve fit graph on Origin Pro or GraphPad Prism 7. The equation used to fit absorbance values to produce a pKa value is as follows:

$$A = \left(1 - \frac{1}{1 + 10^{pH-pKa}}\right) A_{CQ} + \left(\frac{1}{1 + 10^{pH-pKa}}\right) A_{CQ^+}$$

Where A_{CQ} is the absorbance of neutral CQ, A_{CQ}^{+} is the absorbance of protonated CQ. Where $pKa = 7.35 \pm 0.1$.

3.5.3 Parasite cytotoxicity assays and IC_{50} estimation

Parasite proliferation assays using CQ or CQ-derivatives were tested on CQS 3D7 and CQR Dd2 *Plasmodium falciparum* lab strains. Briefly, 0.5% ring-stage parasites were incubated in a 0.2% hematocrit in 96 black well clear bottom plates in triplicates (Corning Inc.; ref: 3603) for 72hrs in an incubator maintaining 37°C and atmospheric conditions of 3% O_2, 5% CO_2 and 92% N_2. Later, the plates were frozen at -80°C and thawed at RT. Then they were treated with a lysis-developing solution (Tris; 20 mM pH 7.5, 5 mM EDTA; 0.008% w/v saponin, 0.08% v/v Triton X-100, 0.2 µL /ml of 10,000x SYBR® Green I Nucleic Acid gel stain dye) and kept away from light for 1 hour. Fluorescence was measured using Synergy H4 plate reader with Ex 485 nm / Em 535 nm. The resulting data were analyzed using GraphPad Prism version 8.4.0 (671) to obtain the 50% inhibitory concentration (IC_{50}).

3.5.4 Synthesis of 3-substituted CQ Derivatives

To a stirring solution of 3-NH_2CQ (1 equiv.) in anhydrous DCM at 0ºC is added benzoyl chloride (1.5 equiv.) under nitrogen followed by NEt_3 (3 equiv.). The solution is stirred and allowed to warm to RT. The reaction progress is monitored by TLC. When complete, the reaction is poured into saturated $NaHCO_3$ solution and extracted with DCM (3 X 20 mL) and washed with brine. The combined organic extracts are then dried over anhydrous $MgSO_4$, and the solvent is removed under reduced pressure. The crude product is purified by prep-TLC with silica gel, solvent system: 90%

EtOAc, 5% MeOH, 5% NEt_3 or with C18 prep-TLC in 50% H_2O, 50% acetonitrile, 1% trifluoroacetic acid (unless otherwise stated) to give an off-white powder.

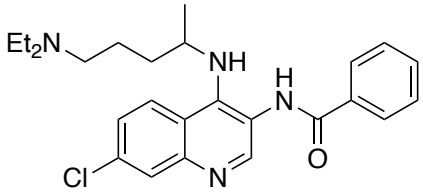

***N*-(7-chloro-4-((5-(diethylamino)pentan-2-yl)amino)quinolin-3-yl)benzamide (3.3)**

Yield: 53.3 mg, 85%. **^{1}H NMR** (800 MHz, Methanol-d_4) δ 8.56 (d, J = 9.2 Hz, 2H), 8.07 (dt, J = 7.1, 1.3 Hz, 2H), 7.94 (d, J = 2.1 Hz, 1H), 7.76 (dd, J = 9.1, 2.1 Hz, 1H), 7.69 (td, J = 7.3, 1.3 Hz, 1H), 7.61 (t, J = 7.8 Hz, 2H), 4.57 (dt, J = 12.4, 7.0 Hz, 1H), 3.10 (tq, J = 12.5, 5.8, 5.1 Hz, 4H), 3.07 – 3.02 (m, 1H), 3.00 – 2.94 (m, 1H), 1.82 (dq, J = 12.1, 7.6, 6.7 Hz, 1H), 1.70 – 1.62 (m, 3H), 1.43 (d, J = 6.5 Hz, 3H), 1.20 (q, J = 6.9 Hz, 6H). **^{13}C NMR** (201 MHz, Methanol-d_4) δ 169.09, 153.47, 151.04, 145.62, 139.46, 138.61, 132.71, 132.69, 128.77, 127.55, 125.29, 119.60, 117.39, 111.52, 51.57, 51.02, 33.27, 20.79, 20.20, 7.70, 7.64. **HRMS** (ESI) calcd. for $C_{25}H_{31}ClN_4O$ [M+H]: 439.2259, found: 439.2247.

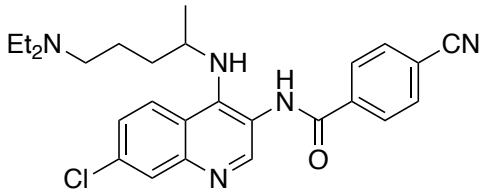

***N*-(7-chloro-4-((5-(diethylamino)pentan-2-yl)amino)quinolin-3-yl)-4-cyanobenzamide (3.4)**

Yield: 45.6 mg, 66%, mixture of isomers. **^{1}H NMR** (500 MHz, Chloroform-*d*) δ 8.85 (s, 1H), 8.20 (d, *J* = 7.9 Hz, 2H), 7.99 (dd, *J* = 3.8, 2.1 Hz, 1H), 7.88 (dd, *J* = 9.2, 7.5 Hz, 2H), 7.80 (d, *J* = 8.0 Hz, 2H), 7.42 (ddd, *J* = 8.5, 6.1, 2.2 Hz, 1H), 4.32 (s, 1H), 3.72 (s, 1H), 2.52 (q, *J* = 7.1 Hz, 4H),

2.39-2.35 (m, 2H), 1.60 – 1.40 (m, 4H), 1.24 (d, *J* = 9.0 Hz, 3H), 0.99 (t, *J* = 7.2 Hz, 6H). **^{13}C NMR** (126 MHz, Chloroform-*d*) δ 164.96, 150.39, 150.26, 148.53, 148.15, 145.96, 145.17, 143.09, 137.64, 135.05, 134.73, 132.72, 130.94, 129.70, 129.08, 129.05, 128.57, 127.59, 126.51, 126.47, 124.07, 123.76, 121.50, 121.26, 119.82, 119.01, 118.07, 115.85, 53.62, 53.51, 52.72, 52.60, 46.82, 46.73, 36.71, 23.78, 23.40, 22.40, 22.26, 21.69, 11.19, 10.57. **HRMS** (ESI) calcd. for $C_{26}H_{31}ClN_5O$ [M+H]: 464.2212, found: 464.2206.

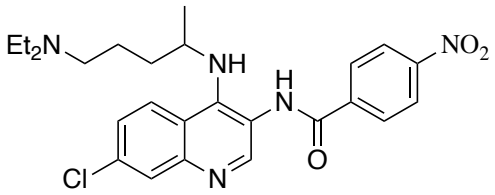

***N*-(7-chloro-4-((5-(diethylamino)pentan-2-yl)amino)quinolin-3-yl)-4-nitrobenzamide (3.5)**

Yield: 109.5 mg, 76%. **^{1}H NMR** (500 MHz, Methanol-*d*$_4$) δ 8.60 (s, 1H), 8.58 (d, *J* = 9.3 Hz, 1H), 8.44 (d, *J* = 8.5 Hz, 2H), 8.29 (d, *J* = 8.7 Hz, 2H), 7.95 (d, *J* = 2.1 Hz, 1H), 7.76 (dd, *J* = 9.2, 1.9 Hz, 1H), 4.65 – 4.53 (m, 1H), 3.14 (q, *J* = 7.3 Hz, 4H), 3.10 – 3.03 (m, 2H), 1.90 – 1.81 (m, 1H), 1.77 – 1.66 (m, 3H), 1.43 (d, *J* = 6.5 Hz, 3H), 1.23 (t, *J* = 7.3 Hz, 6H). **^{13}C NMR** (126 MHz, Methanol-*d*$_4$) δ 167.24, 153.71, 150.34, 145.10, 139.63, 138.53, 138.33, 129.02, 127.57, 125.62, 123.60, 119.42, 117.04, 111.31, 51.94, 51.09, 46.94, 33.30, 20.81, 20.25, 7.62. **HRMS** (ESI) calcd. for $C_{25}H_{30}ClN_5O_3$ [M+H]: 484.2110, found: 484.2105.

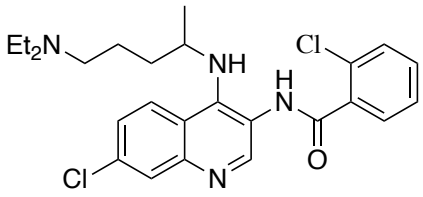

2-chloro-*N*-(7-chloro-4-((5-(diethylamino)pentan-2-yl)amino)quinolin-3-yl)benzamide (3.6)

Yield: 42 mg, 59%. **^{1}H NMR** (500 MHz, Methanol-*d*$_4$) δ 8.60 (s, 1H), 8.55 (d, *J* = 9.2 Hz, 1H), 7.95 (s, 1H), 7.79 – 7.70 (m, 2H), 7.63 – 7.48 (m, 3H), 4.73 (q, *J* = 6.7, 5.9 Hz, 1H), 3.14 (q, *J* = 7.3 Hz, 4H), 3.10 – 3.02 (m, 2H), 1.93 – 1.84 (m, 1H), 1.77 (dq, *J* = 12.1, 7.6, 6.0 Hz, 3H), 1.45 (d, *J* = 6.4 Hz, 3H), 1.22 (q, *J* = 7.0 Hz, 6H). **^{13}C NMR** (126 MHz, Methanol-*d*$_4$) δ 170.67, 154.26, 147.24, 140.60, 136.11, 133.34, 132.14, 131.59, 130.39, 128.90, 128.66, 126.75, 121.75, 119.26, 52.65, 52.58, 34.84, 22.16, 21.95, 9.08, 8.99. **HRMS** (ESI) calcd. for $C_{25}H_{31}Cl_2N_4O$ [M+H]: 473.1869, found: 473.1869.

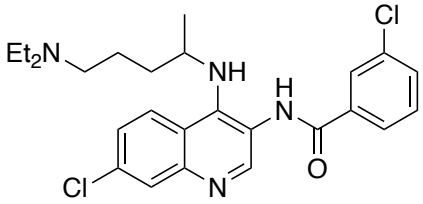

3-chloro-*N*-(7-chloro-4-((5-(diethylamino)pentan-2-yl)amino)quinolin-3-yl)benzamide (3.7)

Yield: 43.3 mg, 61%. **^{1}H NMR** (500 MHz, Chloroform-*d*) δ 8.87 (s, 1H), 8.10 (s, 1H), 8.01 (d, *J* = 8.7 Hz, 1H), 7.91 (d, *J* = 9.0 Hz, 1H), 7.56 (d, *J* = 8.1 Hz, 1H), 7.47 (t, *J* = 7.8 Hz, 1H), 7.42 (d, *J* = 9.6 Hz, 1H), 4.31 (d, *J* = 11.2 Hz, 1H), 3.73 (d, *J* = 13.1 Hz, 2H), 2.57 (t, *J* = 7.5 Hz, 5H), 2.42 (d, *J* = 6.7 Hz, 2H), 1.52 (dt, *J* = 10.6, 6.8 Hz, 1H), 1.26 (d, *J* = 7.3 Hz, 7H), 1.02 (t, *J* = 7.2 Hz, 7H). **^{13}C NMR** (126 MHz, Chloroform-*d*) δ 165.40, 150.70, 148.64, 145.89, 135.46, 135.18, 134.86, 132.37, 130.24, 129.15, 128.37, 126.37, 126.02, 124.30, 121.36, 119.41, 53.58, 52.48,

46.72, 36.69, 22.84, 22.52, 10.09. **HRMS** (ESI) calcd. for $C_{25}H_{31}Cl_2N_4O$ [M+H]: 473.1869, found: 473.1874.

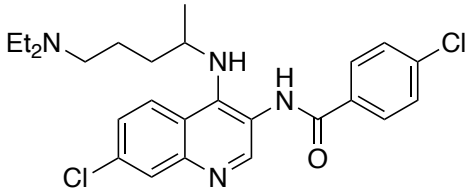

4-chloro-*N*-(7-chloro-4-((5-(diethylamino)pentan-2-yl)amino)quinolin-3-yl)benzamide (3.8)

Yield: 36.4 mg, 51%. **^{1}H NMR** (400 MHz, Chloroform-*d*) δ 9.35 (s, 1H), 8.83 (s, 1H), 8.11 (d, *J* = 8.2 Hz, 2H), 8.04 – 7.97 (m, 1H), 7.90 (d, *J* = 9.0 Hz, 1H), 7.48 (dd, *J* = 8.4, 2.1 Hz, 2H), 7.41 (dd, *J* = 9.0, 2.0 Hz, 1H), 4.35 (s, 1H), 3.76 (s, 1H), 2.63 (q, *J* = 7.2 Hz, 4H), 2.47 (t, *J* = 7.4 Hz, 2H), 1.62 (d, *J* = 9.3 Hz, 1H), 1.58 – 1.44 (m, 3H), 1.27 (d, *J* = 6.4 Hz, 3H), 1.05 (t, *J* = 7.2 Hz, 6H). **^{13}C NMR** (126 MHz, Chloroform-*d*) δ 165.91, 151.05, 148.71, 146.63, 138.64, 134.81, 131.99, 129.66, 129.09, 129.04, 126.22, 124.53, 121.23, 119.38, 53.49, 52.30, 46.58, 36.58, 22.61, 22.30, 9.54. **HRMS** (ESI) calcd. for $C_{25}H_{31}Cl_2N_4O$ [M+H]: 473.1869, found: 473.1872.

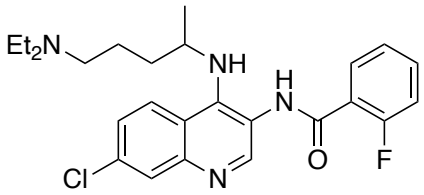

***N*-(7-chloro-4-((5-(diethylamino)pentan-2-yl)amino)quinolin-3-yl)-2-fluorobenzamide (3.9)**

Yield: 45.1 mg, 66%. **^{1}H NMR** (500 MHz, Methanol-*d*$_4$) δ 8.58 (d, J = 9.2 Hz, 1H), 8.56 (s, 1H), 7.99 – 7.91 (m, 2H), 7.73 (dd, J = 9.2, 1.7 Hz, 1H), 7.68 (tdd, J = 7.4, 5.1, 1.8 Hz, 1H), 7.41 (t, J = 7.6 Hz, 1H), 7.36 (dd, J = 11.3, 8.4 Hz, 1H), 4.71 (h, J = 6.9, 6.0 Hz, 1H), 3.13 (q, J = 7.3 Hz, 4H), 3.09 – 3.00 (m, 2H), 1.87 (dt, J = 13.5, 8.2 Hz, 1H), 1.73 (dq, J = 12.4, 7.8, 6.1 Hz, 3H), 1.43

(d, J = 6.5 Hz, 3H), 1.22 (t, J = 7.3 Hz, 6H). **^{13}C NMR** (126 MHz, Methanol-*d*$_4$) δ 167.59, 154.51, 147.18, 140.74, 140.26, 135.60, 135.53, 132.13, 128.89, 126.77, 126.23, 126.20, 122.98, 122.88, 121.20, 52.71, 52.52, 48.34, 34.71, 22.19, 21.73, 9.02. **^{19}F NMR** (377 MHz, Methanol-*d*$_4$) δ -115.14. **HRMS** (ESI) calcd. for $C_{25}H_{30}ClFN_4O$ [M+H]: 457.2165, found: 457.2162.

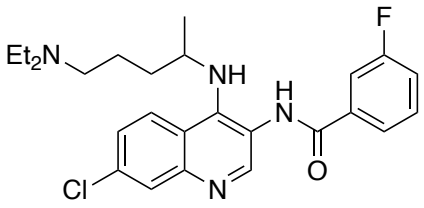

***N*-(7-chloro-4-((5-(diethylamino)pentan-2-yl)amino)quinolin-3-yl)-3-fluorobenzamide (3.10)**

Yield: 43.7 mg, 64%. **^{1}H NMR** (500 MHz, Chloroform-*d*) δ 8.89 (s, 1H), 8.75 (s, 1H), 8.00 (d, *J* = 2.2 Hz, 1H), 7.88 (d, *J* = 9.0 Hz, 1H), 7.80 (dd, *J* = 28.6, 8.5 Hz, 2H), 7.50 (td, *J* = 8.0, 5.6 Hz, 1H), 7.42 (dd, *J* = 9.0, 2.1 Hz, 1H), 7.29 (dd, *J* = 8.0, 2.3 Hz, 1H), 4.28 (d, *J* = 9.5 Hz, 1H), 3.72 (s, 1H), 2.50 (q, *J* = 7.1 Hz, 4H), 2.40 – 2.32 (m, 2H), 1.59 – 1.42 (m, 4H), 1.22 (d, *J* = 6.4 Hz, 3H), 0.97 (t, *J* = 7.2 Hz, 6H). **^{13}C NMR** (126 MHz, Chloroform-*d*) δ 165.24, 164.04, 162.07, 150.30, 148.37, 145.43, 136.10, 136.04, 134.86, 130.72, 130.66, 129.14, 126.50, 123.87, 123.15, 121.43, 119.51, 119.46, 119.34, 115.25, 115.06, 53.55, 52.62, 46.77, 36.69, 23.51, 22.33, 10.82. **^{19}F NMR** (377 MHz, Chloroform-*d*) δ -111.57. **HRMS** (ESI) calcd. for $C_{25}H_{31}ClFN_4O$ [M+H]: 457.2165, found: 457.2160.

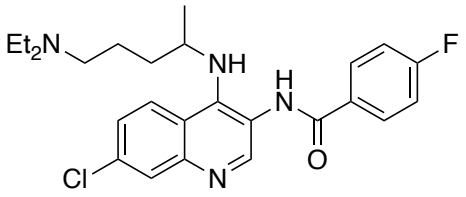

***N*-(7-chloro-4-((5-(diethylamino)pentan-2-yl)amino)quinolin-3-yl)-4-fluorobenzamide (3.11)**

Yield: 41 mg, 60%. **^{1}H NMR** (500 MHz, Chloroform-*d*) δ 8.86 (s, 1H), 8.74 (s, 1H), 8.07 (t, *J* = 6.7 Hz, 2H), 7.99 (d, *J* = 2.1 Hz, 1H), 7.88 (d, *J* = 9.0 Hz, 1H), 7.41 (dd, *J* = 9.0, 2.2 Hz, 1H), 7.18 (t, *J* = 8.4 Hz, 2H), 4.28 (d, *J* = 9.4 Hz, 1H), 3.71 (s, 1H), 2.49 (q, *J* = 7.2 Hz, 4H), 2.40 – 2.30 (m, 1H), 1.59 – 1.37 (m, 2H), 1.21 (d, *J* = 6.4 Hz, 3H), 0.97 (t, *J* = 7.2 Hz, 6H). **^{13}C NMR** (126 MHz, Chloroform-*d*) δ 166.20, 165.35, 164.18, 150.25, 148.20, 145.37, 134.64, 130.09, 130.02, 129.78, 129.76, 128.95, 126.28, 123.79, 121.27, 119.52, 115.98, 115.81, 53.40, 52.45, 46.61, 36.50, 23.27, 22.19, 10.57. **^{19}F NMR** (377 MHz, Chloroform-*d*) δ -107.08. **HRMS** (ESI) calcd. for $C_{25}H_{31}ClFN_4O$ [M+H]: 457.2165, found: 457.21.

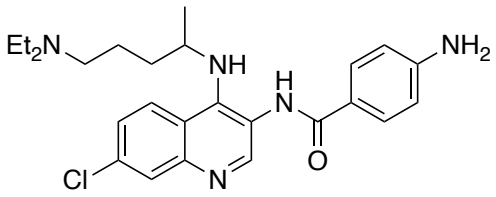

4-amino-*N*-(7-chloro-4-((5-(diethylamino)pentan-2-yl)amino)quinolin-3-yl)benzamide (3.12)

Yield: 53.8 mg, 41%. **^{1}H NMR** (400 MHz, Methanol-d_4) δ 8.31 (s, 1H), 8.26 (d, *J* = 9.1 Hz, 1H), 7.84 (d, *J* = 2.2 Hz, 1H), 7.83 – 7.78 (m, 2H), 7.48 (dd, *J* = 9.1, 2.2 Hz, 1H), 6.76 – 6.70 (m, 2H), 2.48 (q, *J* = 7.1 Hz, 4H), 2.39 (d, *J* = 8.0 Hz, 2H), 1.64 (d, *J* = 7.2 Hz, 1H), 1.52 – 1.38 (m, 3H), 1.26 (d, *J* = 6.4 Hz, 3H), 0.96 (t, *J* = 7.2 Hz, 6H). **^{13}C NMR** (126 MHz, Methanol-d_4) δ 169.78, 154.45, 154.12, 148.95, 148.71, 136.26, 130.65, 127.88, 126.72, 125.18, 121.94, 121.23, 115.33,

114.70, 53.36, 52.16, 47.64, 36.67, 23.79, 21.90, 10.92. **HRMS** (ESI) calcd. for $C_{25}H_{33}ClN_5$ [M+H]: 454.2368, found: 454.2369.

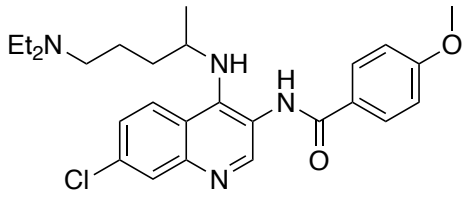

***N*-(7-chloro-4-((5-(diethylamino)pentan-2-yl)amino)quinolin-3-yl)-4-methoxybenzamide (3.13)**

Yield: 52.2 mg, 75%. **^{1}H NMR** (500 MHz, Chloroform-*d*) δ 8.92 (s, 1H), 8.34 (s, 1H), 7.99 (d, *J* = 2.2 Hz, 1H), 7.97 (d, *J* = 8.6 Hz, 2H), 7.87 (d, *J* = 9.0 Hz, 1H), 7.40 (dd, *J* = 9.0, 2.2 Hz, 1H), 6.99 (d, *J* = 8.8 Hz, 2H), 4.25 (d, *J* = 9.7 Hz, 1H), 3.88 (s, 3H), 3.73-3.67 (m, 1H), 2.46 (q, *J* = 7.1 Hz, 4H), 2.33 (t, *J* = 6.7 Hz, 2H), 1.62 – 1.40 (m, 4H), 1.18 (d, *J* = 6.3 Hz, 3H), 0.95 (t, *J* = 7.2 Hz, 6H). **^{13}C NMR** (126 MHz, Chloroform-*d*) δ 165.98, 162.96, 150.28, 148.13, 145.14, 134.61, 129.52, 129.05, 126.40, 125.98, 123.80, 121.55, 120.07, 114.20, 55.64, 53.55, 52.73, 46.81, 36.71, 23.80, 22.25, 11.22. **HRMS** (ESI) calcd. for $C_{26}H_{34}ClN_4O_2$ [M+H]: 469.2365, found: 469.2369.

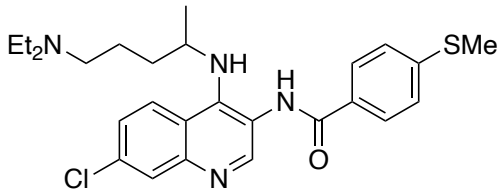

***N*-(7-chloro-4-((5-(diethylamino)pentan-2-yl)amino)quinolin-3-yl)-4(methylthio)benzamide (3.14)**

Yield: 47 mg, 61%. **^{1}H NMR** (500 MHz, Chloroform-*d*) δ 8.80 (s, 1H), 8.17 (d, *J* = 8.0 Hz, 2H), 8.01 (d, *J* = 2.2 Hz, 1H), 7.95 (d, *J* = 9.0 Hz, 1H), 7.41 (dd, *J* = 9.0, 2.2 Hz, 1H), 7.34 (d, *J* = 8.6 Hz, 2H), 4.41 (d, *J* = 10.2 Hz, 1H), 3.80 (s, 1H), 2.77 – 2.67 (m, 4H), 2.58-2.45 (m, 5H), 1.74-1.65

(m, 1H), 1.57 – 1.44 (m, 3H), 1.33 (d, *J* = 6.4 Hz, 3H), 1.11 (t, *J* = 7.3 Hz, 6H). **^{13}C NMR** (126 MHz, Chloroform-*d*) δ 166.45, 151.45, 148.80, 144.30, 137.55, 134.50, 129.25, 128.81, 128.73, 125.80, 125.29, 124.96, 121.01, 119.38, 53.31, 51.95, 46.32, 36.39, 22.70, 21.15, 14.95, 8.37. **HRMS** (ESI) calcd. for $C_{26}H_{34}ClN_4OS$ [M+H]: 485.2136, found: 485.2146.

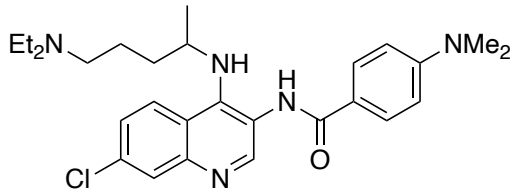

***N*-(7-chloro-4-((5-(diethylamino)pentan-2-yl)amino)quinolin-3-yl)-4-(dimethylamino)benzamide (3.15)**

Yield: 22.3 mg, 31%. **^{1}H NMR** (800 MHz, Dimethyl sulfoxide-d_6) δ 9.71 (s, 1H), 8.40 (d, *J* = 9.1 Hz, 1H), 8.29 (s, 1H), 7.91 (d, *J* = 8.9 Hz, 2H), 7.84 (d, *J* = 2.3 Hz, 1H), 7.50 (dd, *J* = 8.9, 2.3 Hz, 1H), 6.78 – 6.74 (m, 2H), 5.97 (d, *J* = 9.1 Hz, 1H), 3.98 (dq, *J* = 8.8, 6.4 Hz, 1H), 3.00 (s, 9H), 2.38 (s, 4H), 2.28 (s, 2H), 1.60 – 1.54 (m, 1H), 1.36 (ddt, *J* = 12.6, 9.8, 6.1 Hz, 1H), 1.29 (t, *J* = 7.9 Hz, 2H), 1.12 (d, *J* = 6.4 Hz, 3H), 0.85 (t, *J* = 7.1 Hz, 6H). **^{13}C NMR** (201 MHz, Dimethyl sulfoxide-d_6) δ 165.98, 154.20, 152.42, 147.67, 146.07, 133.05, 129.05, 127.50, 124.85, 124.61, 120.32, 119.96, 114.71, 110.84, 51.99, 50.41, 46.06, 39.99, 34.97, 22.61, 21.51, 7.16. **HRMS** (ESI) calcd. for $C_{27}H_{36}ClN_5O$ [M+H]: 482.2681, found: 482.2675.

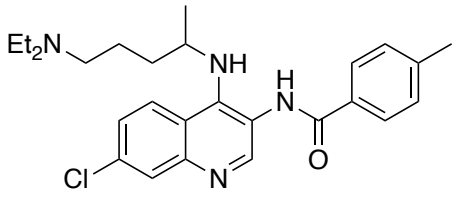

***N*-(7-chloro-4-((5-(diethylamino)pentan-2-yl)amino)quinolin-3-yl)-4-methylbenzamide (3.16)**

Yield: 38.1 mg, 59%. **^{1}H NMR** (500 MHz, Chloroform-*d*) δ 8.95 (s, 1H), 8.34 (s, 1H), 8.01 (d, *J* = 2.2 Hz, 1H), 7.89 (dd, *J* = 11.0, 8.2 Hz, 3H), 7.41 (dd, *J* = 8.9, 2.2 Hz, 1H), 7.31 (d, *J* = 7.7 Hz, 2H), 4.25 (d, *J* = 9.8 Hz, 1H), 3.75 – 3.64 (m, 1H), 2.51 – 2.40 (m, 7H), 2.33 (t, *J* = 6.6 Hz, 2H), 1.61 – 1.41 (m, 4H), 1.19 (d, *J* = 6.4 Hz, 3H), 0.96 (t, *J* = 7.2 Hz, 6H). **^{13}C NMR** (126 MHz, Chloroform-*d*) δ 166.42, 150.35, 148.23, 145.26, 143.02, 134.66, 130.93, 129.67, 129.09, 127.66, 126.40, 123.88, 121.54, 119.95, 53.53, 52.68, 46.80, 36.67, 23.57, 22.30, 21.69, 10.99. **HRMS** (ESI) calcd. for $C_{26}H_{34}ClN_4O$ [M+H]: 453.2416, found: 453.2417.

To a stirring solution of 3-NH_2CQ (1 equiv.) in anhydrous EtOH at 0^{o}C is added 4-chlorobenzenesulfonyl chloride (1 equiv.) under nitrogen followed by NEt_3 (1 equiv.). The solution is stirred and allowed to warm to RT. The reaction progress is monitored by TLC. After 24 hours the solvent is removed under reduced pressure. The residue is then diluted with DCM, and the solution is poured into a flask containing saturated $NaHCO_3$ solution and is extracted with DCM (3 X 20 mL) and washed with brine. The combined organic extracts are then dried over anhydrous $MgSO_4$ and the solvent removed under reduced pressure. The crude product is purified by prep-TLC with silica gel, solvent system: 70% Hex, 20% EtOAc, 5% MeOH, 5% NEt_3 to give a bright yellow powder. Due to the low-yielding nature of the reaction, we were unable to obtain full NMR characterization, but preliminary data is consistent with the expected product.

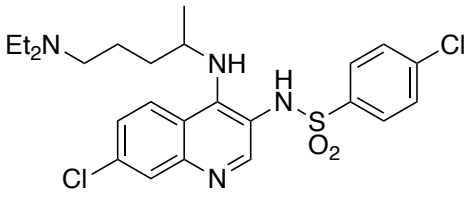

4-chloro-*N*-(7-chloro-4-((5-(diethylamino)pentan-2-yl)amino)quinolin-3-yl)benzenesulfonamide (3.17)

HRMS (ESI) calcd. for $C_{24}H_{30}Cl_2N_4O_2S$ [M+H]: 509.1539, found: 509.1520.

To a stirring solution of 3-NH_2CQ (1 equiv.) in anhydrous EtOH at 0°C is added 4-chlorobenzaldehyde (1.5 equiv.) under nitrogen followed by NEt_3 (3 equiv.). The solution is stirred and allowed to warm to RT. The reaction progress is monitored by TLC. After 24 hours the solvent is removed under reduced pressure. The residue is then diluted with DCM, and the solution is poured into a flask containing saturated $NaHCO_3$ solution and is extracted with DCM (3 X 20 mL) and washed with brine. The combined organic extracts are then dried over anhydrous $MgSO_4$ and the solvent removed under reduced pressure. The crude product is purified by prep-TLC with silica gel, solvent system: 70% Hex, 20% EtOAc, 5% MeOH, 5% NEt_3 to give a bright yellow powder.

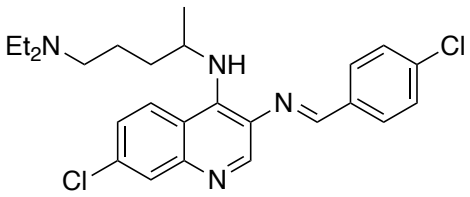

(E)-N^4-(7-chloro-3-((4-chlorobenzylidene)amino)quinolin-4-yl)-N^1,N^1-diethylpentane-1,4-diamine (3.18)

HRMS (ESI) calcd. for $C_{25}H_{30}Cl_2N_4$ [M+H]: 457.1920, found: 457.1921.

3.6 References

(1) Edaye, S.; Tazoo, D.; Bohle, D. S.; Georges, E. 3-Halo Chloroquine Derivatives Overcome Plasmodium Falciparum Chloroquine Resistance Transporter-Mediated Drug Resistance in P. Falciparum. *Antimicrob. Agents Chemother.* **2015**, *59* (12), 7891–7893.

(2) Egan, T. J. Structure-Function Relationships in Chloroquine and Related 4-Aminoquinoline Antimalarials. *Mini-Reviews Med. Chem.* **2001**, *1* (1), 113–123.

(3) Bass, G. E.; Hudson, D. R.; Parker, J. E.; Purcell, W. P. Mechanism of Antimalarial Activity of Chloroquine Analogs from Quantitative Structure-Activity Studies. Free Energy Related Model. *J. Med. Chem.* **1971**, *14* (4), 275–283.

(4) Edaye, S.; Tazoo, D.; Bohle, D. S.; Georges, E. 3-Iodo-4-Aminoquinoline Derivative Sensitises Resistant Strains of Plasmodium Falciparum to Chloroquine. *Int. J. Antimicrob. Agents* **2016**, *47* (6), 482–485.

(5) Kaschula, C. H.; Egan, T. J.; Hunter, R.; Basilico, N.; Parapini, S.; Taramelli, D.; Pasini, E.; Monti, D. Structure−Activity Relationships in 4-Aminoquinoline Antiplasmodials. The Role of the Group at the 7-Position. *J. Med. Chem.* **2002**, *45* (16), 3531–3539.

(6) Lipinski, C. A. Lead- and Drug-like Compounds: The Rule-of-Five Revolution. *Drug Discov. Today Technol.* **2004**, *1* (4), 337–341.

(7) Lipinski, C. A.; Lombardo, F.; Dominy, B. W.; Feeney, P. J. Experimental and Computational Approaches to Estimate Solubility and Permeability in Drug Discovery and Development Settings. *Adv. Drug Deliv. Rev.* **1997**, *23* (1–3), 3–25.

(8) Craig, P. N. Interdependence between Physical Parametess and Selection of Substituent Groups for Correlation Studies. *J. Med. Chem.* **1971**, *14* (8), 680–684.

(9) Ertl, P. Craig Plot 2.0: An Interactive Navigation in the Substituent Bioisosteric Space. *J.*

Cheminform. **2020**, *12* (1), 10–15.

(10) Hawley, S. R.; Bray, P. G.; Mungthin, M.; Atkinson, J. D.; O'Neill, P. M.; Ward, S. A. Relationship between Antimalarial Drug Activity, Accumulation, and Inhibition of Heme Polymerization in Plasmodium Falciparum In Vitro. *Antimicrob. Agents Chemother.* **1998**, *42* (3), 682–686.

(11) Madrid, P. B.; Liou, A. P.; DeRisi, J. L.; Guy, R. K. Incorporation of an Intramolecular Hydrogen-Bonding Motif in the Side Chain of 4-Aminoquinolines Enhances Activity against Drug-Resistant P. Falciparum (Journal of Medical Chemistry (2006) 49 (4540)). *J. Med. Chem.* **2008**, *51* (3), 699.

(12) Egan, T. J.; Marques, H. M. The Role of Haem in the Activity of Chloroquine and Related Antimalarial Drugs. *Coord. Chem. Rev.* **1999**, *190–192*, 493–517.

(13) Nsumiwa, S.; Kuter, D.; Wittlin, S.; Chibale, K.; Egan, T. J. Structure–Activity Relationships for Ferriprotoporphyrin IX Association and β-Hematin Inhibition by 4-Aminoquinolines Using Experimental and Ab Initio Methods. *Bioorg. Med. Chem.* **2013**, *21* (13), 3738–3748.

(14) Thomé, R.; Lopes, S. C. P.; Costa, F. T. M.; Verinaud, L. Chloroquine: Modes of Action of an Undervalued Drug. *Immunol. Lett.* **2013**, *153* (1–2), 50–57.

(15) Al-Bari, M. A. A. Chloroquine Analogues in Drug Discovery: New Directions of Uses, Mechanisms of Actions and Toxic Manifestations from Malaria to Multifarious Diseases. *J. Antimicrob. Chemother.* **2015**, *70* (6), 1608–1621.

(16) Hänscheid, T.; Egan, T. J.; Grobusch, M. P. Haemozoin: From Melatonin Pigment to Drug Target, Diagnostic Tool, and Immune Modulator. *Lancet Infect. Dis.* **2007**, *7* (10), 675–685.

(17) Schlesinger, P. H.; Krogstad, D. J.; Herwaldt, B. L. Antimalarial Agents: Mechanisms of

Action. *Antimicrob. Agents Chemother.* **1988**, *32* (6), 793–798.

Chapter 4

Synthesis and Reactivity of a Compact Chloroquine Photoaffinity label.

4.1 Preamble

In drug discovery protein:compound interactions can be detected by covalently linking the drug to the potential active site of the protein of interest. This technique is known as photoaffinity labelling and facilitates the determination of a compound's mechanism of action. The formation of a label generally involves installing a photoreactive aryl azide or an aryl/ alkyl diazirine onto the compound. Cross-linking between the compound and protein of interest occurs following the irradiation of the photoreactive azide or diazirine. Historically, installation of the photoreactive moiety is generally accompanied with the installation of large functional groups that may impact the activity of the parent compound and interact with surrounding proteins. Photoaffinity labels (PAL) can mimic the biological mechanism of the parent compound, but one cannot ignore the influence of any additional functional group. With this in mind, we wanted to synthesize a PAL for CQ that required the least amount of modifications to the CQ structure. With our 3-NH_2CQ precursor, we decided that it was the ideal location to install an azide PAL. We discovered that the secondary amine at the 4-position is labile and subject to cyclization to form a triazole product during the installation of the azide. We were able to prevent cyclization via the placement of a methyl group to give a tertiary amine at the 4-position. All modifications resulted in the addition of 2 small functional groups, a methyl and azide, where the methyl is unreactive. The resulting PAL is easily activated under UV irradiation. The successful installation of a PAL with minimal structural modifications will allow for a more precise mechanistic determination of the substrate-binding site. The PAL is currently being used for labelling studies at the Fidock group at Columbia University.

4.2 Introduction

Quinoline-based antimalarials have been in use for centuries. Despite the long tenure of AQs on the commercial market, their mechanism of action is still a matter of debate.[1–5] There is a consensus that blood-stage AQs interact with heme to inhibit the parasite's proliferation; however, it is not believed to be their sole function. The mechanism of quinoline accumulation into its active site and its targets are still being investigated. Thus, to determine the site and identity of the proteins with which the antimalarial drugs interact, several PALs have been previously synthesized, **Figure 4.1**. These labels are useful because they form strong covalent bonds with the surrounding proteins and allow for the isolation and identification of the ligated product.

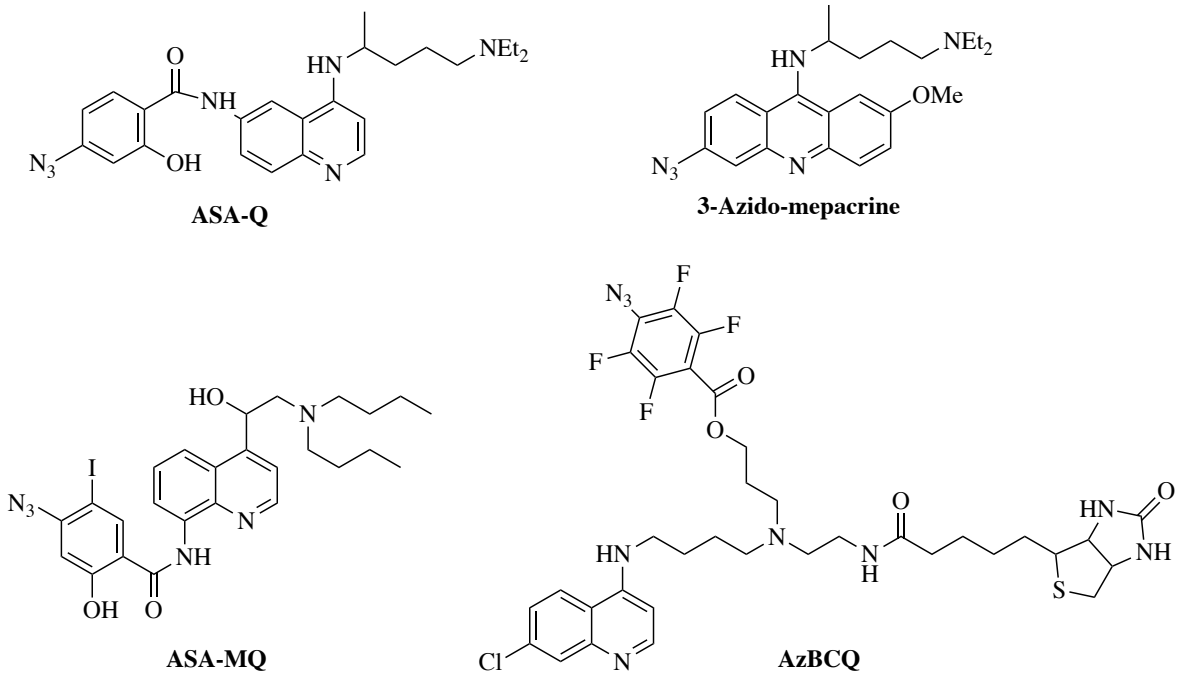

Figure 4.1. Known photoaffinity labels.

When designing a PAL, one wants to mimic the biochemical binding sites of the parent compound as closely as possible. This means that one must minimize the interactions of the label with

surrounding residues to avoid unnecessary interaction. Therefore, it is best to avoid adding reactive functional groups to PALs. Known PALs of AQs and MP are shown in **Figure 4.1** and include: N-(l-(l-diethylamino-l-methylbutylamino)quinolin-6-yl)-4-azido-2-hydroxybenzamide (ASA-Q),[6] 3-azido-9-[[4-(diethylamino)-1-methylbutyl]amino]-7-methoxyacridine (3-azido-mepacrine),[7] N-[4-[I-hydroxy-2-(dibutylamino) ethyl] quinolin-8-yl]-4-azido-2-hydroxybenzamide (ASA-MQ),[8] and perfluorophenylazido biotinylated CQ (AzBCQ).[9] Although the PALs mentioned above can cross-link to proteins of interest, their design omits certain core functionalities of the parent compound. ASA-Q completely removes the 7-chloro group found in CQ, which is essential for inhibiting hemozoin formation. It introduces an amide, hydroxy and phenyl group, which can hydrogen bond and form additional π-stacking interactions. These are unfavourable modifications as they can interact with the surrounding environment. 3-Azido-mepacrine replaces the 7-chloro group found in MP for the photoreactive aryl azide, this is unfavourable because, as mentioned above, the chloro group is required for hemozoin inhibition. ASA-MQ, an MQ PAL, does a poor job of retaining the parent compound's core functions. Desneves *et al*. claim that ASA-MQ is 10-fold more potent than mefloquine and that ASA-MQ is inactive in the CQR Kl Mef2 strain which is selected *in vitro* for resistance to MQ. AzBCQ is a CQ PAL that contains a biotin tag and a perfluorophenylazido group, and the quinoline ring remains unmodified. However, there is the addition of large groups on the side chain.

In this chapter, I describe the synthesis of the first PAL, which contains the least modifications, where all the essential features for CQ activity remain unmodified, **Figure 4.2**. Photolysis studies were carried out with the PAL to determine the optimal wavelength for its activation. Examples of labelling partners will also be described.

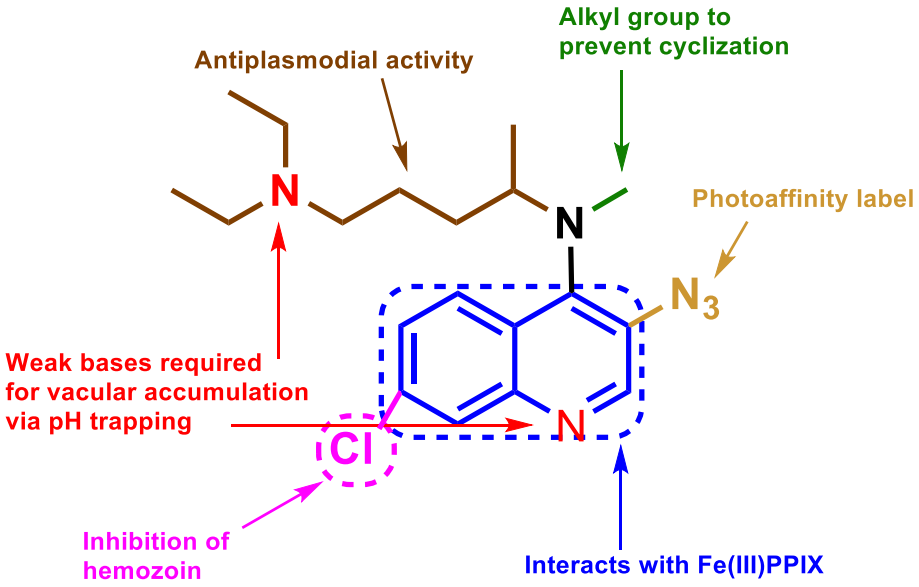

Figure 4.2. Structure of novel 3-Azidomethylchloroquine in which all important CQ features are present.

4.3 Results and Discussion

We have synthesized a CQ PAL derivative with minimal modification of the quinoline structure. The aryl azide is placed at the 3-position, a position that our group has previously utilized.[10,11] Installation of the aryl azide can occur via Ullman coupling to form the C_{sp2} - N bond.[12] This is generally carried out in the presence of air, with a copper catalyst and ligand in a polar solvent, with or without the presence of a base.[13–15] In our experimentation, the azidation reaction from an aryl bromide did not yield any trace of aryl azide. Rather an arylamine was the only product observed. A further search of the literature shows that direct amination of aryl bromide with sodium azide as an amine source is a common observation.[16–18] Initially, Thatcher *et al.* suggest this to be a result of thermal decomposition.[19] Then Alami *et al*. proposed a mechanism of amine formation via a nitrene intermediate, **Scheme 4.1**.[17] However, they were unable to gather experimental evidence of azide formation, but believe that the aryl azide is first formed and through Cu(I) catalyzed thermo-initiation, N_2 is liberated to form a nitrene, which abstracts protons and electrons from the solvent.

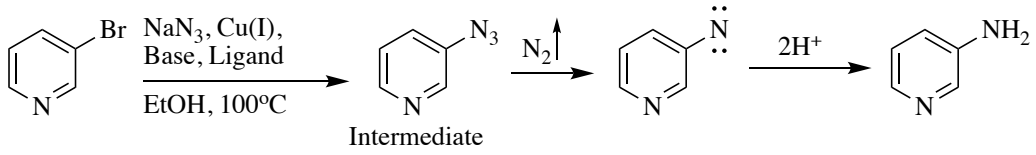

Scheme 4.1. Proposed mechanism for arylamine formation.

However, Helquist *et al.* later disproved the notion of amine formation due to azide thermal decomposition by heating an aryl azide in DMSO for 72 hrs and found that the azide remained intact.[16] They then heated an aryl bromide in the presence of a copper catalyst and DMEDA and only recovered an azo compound. They determined that amine formation from an azide precursor

is dependent on the presence of a copper catalyst and excess sodium azide (see **Table 2.2** – **2.4**). We did not isolate the desired azido product in our experiments, nor did we isolate any azo product; only aryl amine was detected and isolated, **Scheme 4.2**. As shown in Chapter 2, regardless of the reaction conditions the arylamine is the only isolated product.

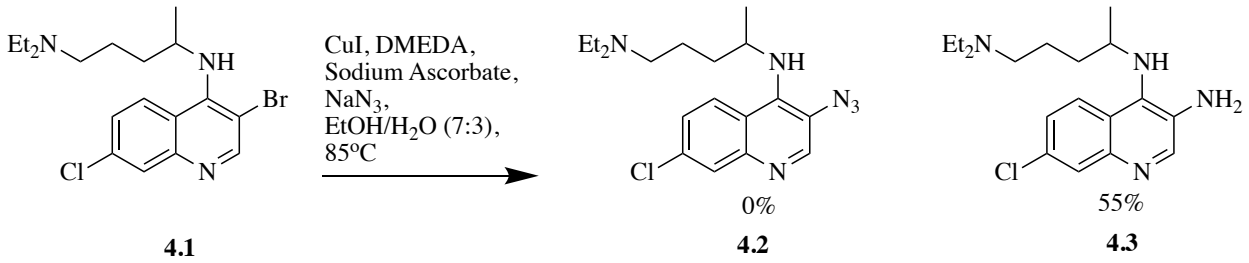

4.1 **4.2** **4.3**

Scheme 4.2. Ullman amination of aryl bromide in 30% aqueous solution in the presence of a ligand and reducing agent.

With the arylamine in-hand, we continued to form the aryl azide via a route that first involves forming a diazonium salt with sodium nitrite in the presence of sulfuric acid. Following the diazonium's formation, sodium azide is added to the reaction mixture to form the aryl azide. However, the aryl azide was not isolated; rather, a cyclized triazole compound was isolated, as depicted in **Scheme 4.3**. NMR and HRMS confirmed this structure. Formation of the triazole indicates reactivity of the secondary amine at the 4-position. The reactive amine had to be permanently blocked to prevent cyclization because if we were to temporarily protect the secondary amine and then deprotect after azide installation, there remains a high probability of cyclization still occurring.

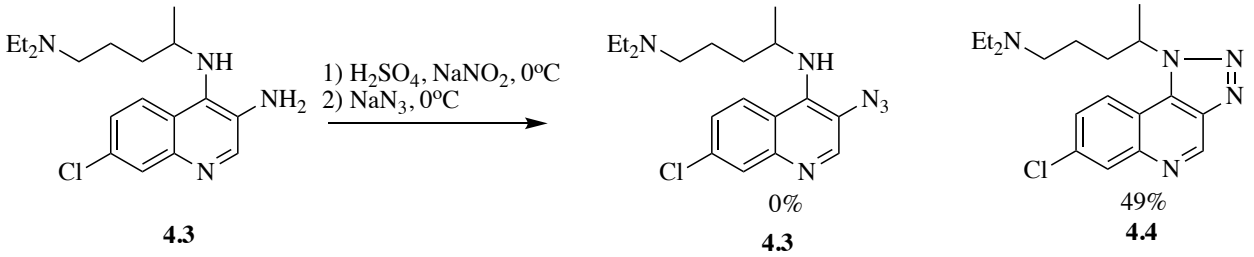

Scheme 4.3. Azidation of arylamine leads to the formation of a triazole CQ product.

Initially, the goal of this project was to synthesize a PAL with the least possible modifications of the parent compound. To remain true to the objective, we opted to methylate the secondary amine. Methylation allows for the addition of an unreactive functional group. The first attempt of methylation involves the use of methyl iodide for direct methylation of CQ, **Table 4.1**.[20,21] However, this method was low yielding and in some instances resulted in a dimethylated product. Dimethylation occurs at the tertiary amine and the secondary amine.

Table 4.1. Methylation of CQ with methyl iodide.

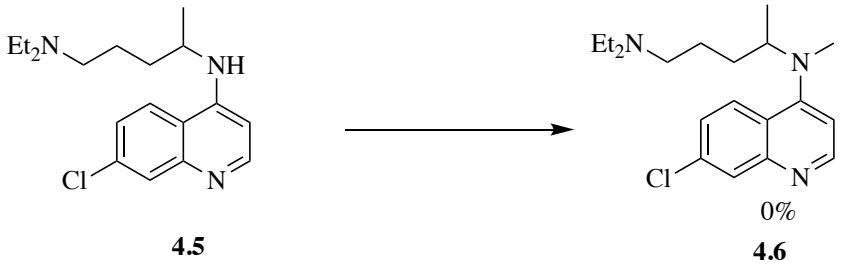

Base	Solvent	Methylating agent	Temperature (ºC)	Yield (%)
NaH	DMF	MeI	-20 to 0	23
NaH	DMF	MeI	Room temp.	15
NaH	DMF	MeI	-20	9
NaH	DMF	MeI	-20	N.D.
NaH	MeCN	MeI	-20	-

Varying reaction conditions did not improve product yield or selectivity, and the HRMS continuously shows the formation of mono and dimethylated CQ. We then attempted methylating the secondary amine via the formation of a formamide, followed by a reduction of the formamide to produce the desired methyl CQ (MeCQ), **Table 4.2**.

Table 4.2. Methylation of CQ.

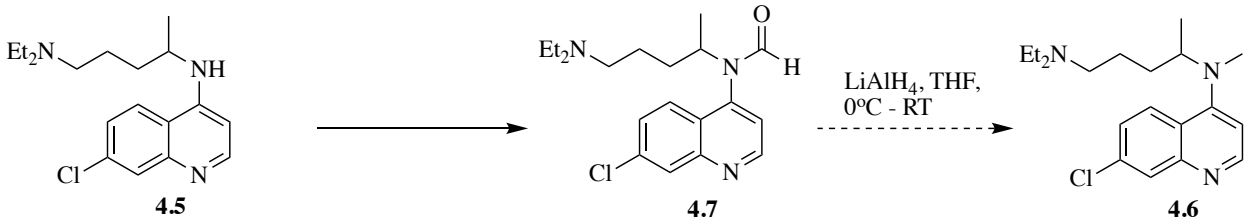

Formulating agent	Solvent	Temperature (°C)	Catalyst	4.7 Yield (%)
Formic acid	-	70-84	-	-
Formic acid	-	70	I_2	-
Sodium Ethoxide	$CHCl_3$	55	-	-

Rahman *et al*. reported the 60% yield of *N*-formamide formation from diphenylamine with formic acid in the absence of solvent.[22] Kim and Jang reported 82% formation of *N*-formamide from *N*-methylaniline from formic acid with I_2 as a catalyst,[23] and Shastri *et al*. report the formation of *N*-formamide with the use of sodium ethoxide in chloroform via the Riemer– Teimann reaction.[24] However, in our experiments only starting material was present. Following these attempts, we deduced that the formylation of the aniline was not viable.

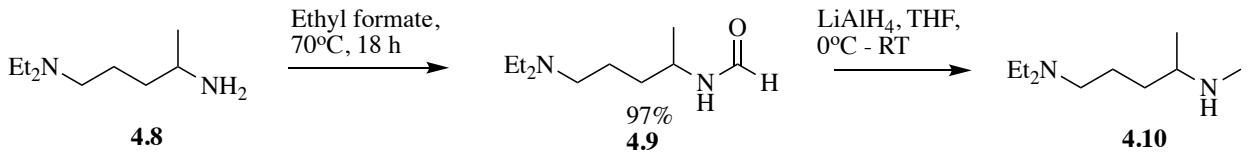

4.8 **4.9** **4.10**

Scheme 4.4. Methylation of 2-Amino-5-diethylaminopentane with ethyl formate.

It was decided that methylation of the side chain followed by a nucleophilic aromatic substitution (S_NAr) reaction would be the most efficient method for the synthesis of MeCQ, **Scheme 4.4**. Formylation of the primary amine with formic acid and acetic anhydride proved to be unsuccessful. This is likely due to the insufficient formation of acetic formic anhydride before the addition of primary amine. However, the reaction with a primary amine and formic acid produced the desired formamide in a 57% yield.[22] Reactivity is improved using ethyl formate to give 97% of a product and easy recovery with a simple acid and base workup.[25] When ethyl formate, is used the side chain does not get protonated; as is the case with formic acid, the primary amine is more nucleophilic resulting in our higher yield. Once the formamide is formed, the final step in the formation of **4.10** is a reduction with lithium aluminum hydride,[26] which results in a 65% yield.

Lastly, to form our desired MeCQ, we performed a condensation reaction between 4,7-dichloroquinoline (DCQ), **4.11** and **4.10**, **Table 4.3.** Generally, this type of condensation reaction occurs under basic conditions. As the alkyl side chain contains a basic secondary amine, we opted to carry out the reaction with the amine acting as the base and/or solvent.

Table 4.3. Condensation reaction between DCQ and methylated side chain under basic conditions.

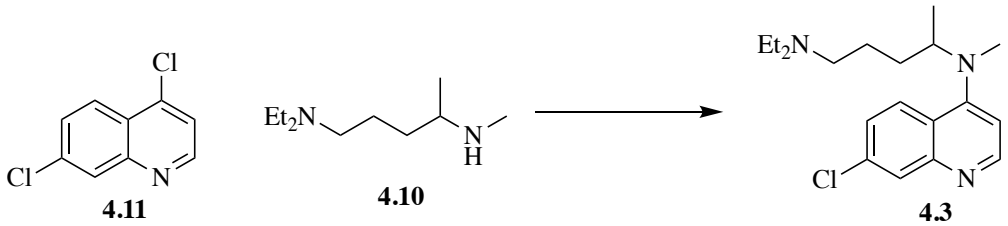

4.11 **4.10** **4.3**

Base	Solvent	Temperature (°C)	Yield (%) Side product	% Yield of 4.3
-	-	85		-
-	-	120-125		6
-	-	120[a]		-
-	Ethylene glycol	120[a]		6
NEt_3	-	125		-
NEt_3	-	85[a]		-
NEt_3	EtOH	0-40		-
DBU	-	80[a]		10
DBU	-	125	82[b]	-
DIPEA	DMSO	80		-
DIPEA	DMSO	120		-
DIPEA	MeCN	85		-
^{t}BuOK	DMSO	80-120		Decomp.
^{t}BuOK	THF	RT-80°C		-
[c]	1,4-dioxane	85		8

a) Microwave-assisted reaction, b) 1-(3-((7-chloroquinolin-4-yl)amino)propyl)azepan-2-one formed, see **Scheme 4.4** b, c) $Pd(OAc)_2$, DPEPhos, K_3PO_4.

There are numerous examples of thermal activation for this type of condensation reaction with primary amines that give moderate to excellent yields.[27–29] However, in our experiments, diamine used as a base results in low yields of our product, even at elevated temperatures. The use of a polar solvent such as ethylene glycol did not improve the yield. Therefore, it became clear that the diamine was not nucleophilic enough to initiate the S_NAr reaction; thus, we used stronger bases

such as triethylamine (NEt_3), 1,8-Diazabicyclo[5.4.0]undec-7-ene (DBU), *N*,*N*-Diisopropylethylamine (DIPEA) and potassium tert-butoxide (^tBuOK). NEt_3 did not result in product formation, nor did DIPEA with various polar solvents. DBU gave 10% product yield at 80°C; however, when the temperature was increased to 125°C, we get 82% formation of a ring-opened DBU adduct, as illustrated in **Scheme 4.5**. Such adducts of ring-opened amidine bases have been observed in the literature, formed in the presence of an inorganic base.[30,31] A recent publication from Merck scientists details their discovery of a ring-opened DBU adduct during the development of a hepatitis C drug. Hyde *et al.* hypothesized that the hydrolysis of DBU occurs in trace amounts of H_2O and high temperatures or during an aqueous workup.[32] When examining the reactivity of electrophilic reactions in the presence of DBU they proposed two pathways to the observed ring-opened DBU adduct. In the first pathway, the amidine base is hydrolyzed generating a primary amine, which reacts with an electrophile. In the second pathway, a cationic intermediate is formed via a reversible interaction of an amidine and an electrophile. This then reacts with trace amounts of H_2O or an aqueous workup that results in the ring-opened product. In our experiments, while monitoring the reaction with TLC, the product is formed before quenching the reaction; thus, trace amounts of H_2O are responsible for the hydrolysis of DBU.

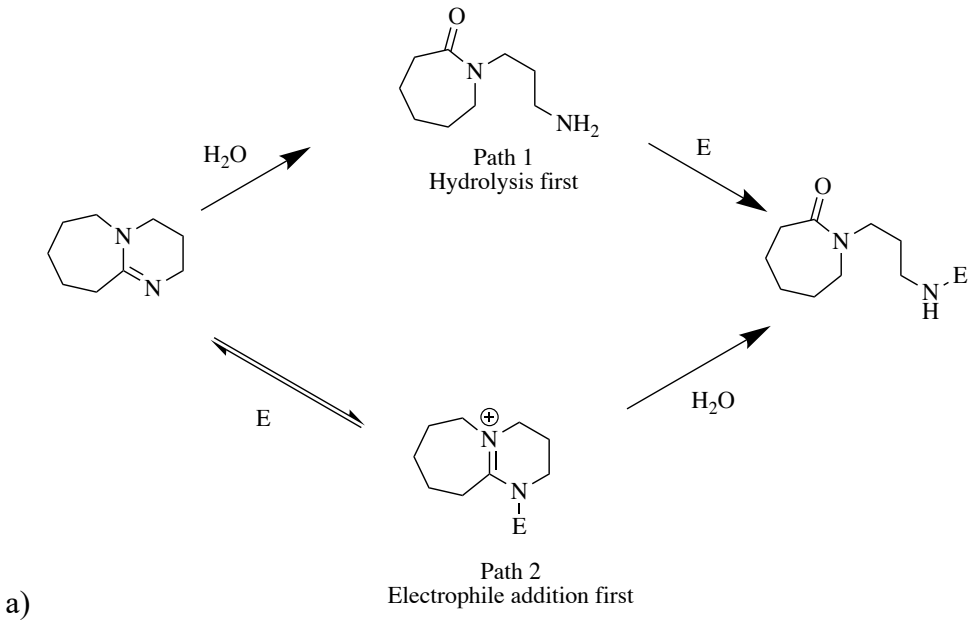

a)

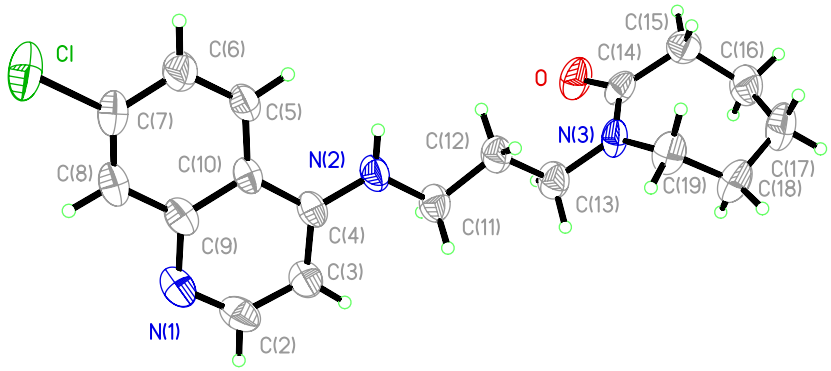

b)

Scheme 4.5. A) Potential pathways for DBU reaction with an electrophile. B) Crystal structure of obtained open DBU adduct.

When potassium tert-butoxide is used, it leads to the decomposition of the reaction mixture and palladium acetate catalyzed condensation was unsuccessful, **Table 4.3**.

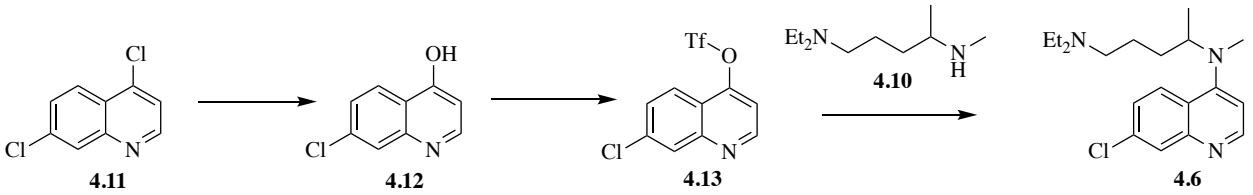

Scheme 4.6. Increasing the electrophilicity of C-4 with the installation of a triflate.

We then concluded that the C-4 was not electrophilic enough; therefore, we opted for a better leaving group than the chloride, **Scheme 4.6**. Triflic acid has a pK_a value of -14, whereas hydrochloric acid has a pK_a of -8; therefore, we opted for the weaker conjugate base being the triflate. Installation of the triflate involves nucleophilic substitution with acetic acid to give 7-chloroquinolin-4-ol, **4.12**. With the hydroxy in hand, we then carried out an electrophilic carbonyl reaction to afford the triflate quinoline, **4.13**.[33] The final step to obtaining our desired MeCQ, **4.6**, was the condensation reaction with the methylated side chain, **4.10, Table 4.4**.

Table 4.4. Condensation reaction conditions for 7-chloroquinolin-4-yl trifluoromethanesulfonate **4.13** and the methylated side chain **4.10**.

Base	Solvent	Temperature (°C)	% Yield of 4.6
-	-	80-125	24
DIPEA	DMSO	80-125	trace
DIPEA	Acetonitrile	RT-40	15
DIPEA	-	125	26
NEt_3	-	80-125	22
NEt_3	EtOH	0-40	-

Initially, the reactions were placed in an 80°C oil bath, and the reaction was monitored for one hour. When monitoring the reaction, if no product formed after one hour, the flask was then transferred into a 125°C oil bath and heated for a further hour before quenching. It is evident from

the results that using a weaker base as a leaving group more than doubled the product yield, thus proving the hypothesis for a need to make C-4 more electrophilic. However, although yields were improved, they were still low.

We then decided to carry out the reaction under acidic conditions. There are examples in the literature of this reaction being carried out in weakly acidic conditions with the use of phenol and examples in strongly acidic conditions such as hydrochloric acid.[34–37] The acid protonates the secondary amine, which forms a quaternary ammonium cation, which would be slightly less basic than NEt_3, **Table 4.5**.

Table 4.5. Condensation reaction between DCQ **4.11**, and methylated side chain **4.10** under acidic conditions.

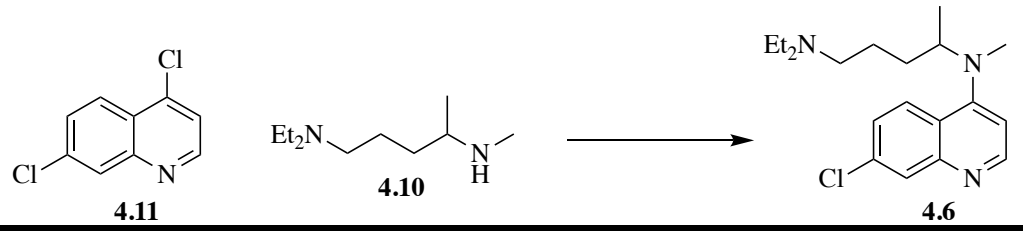

4.11 **4.10** **4.6**

Acid	Solvent	Temperature (°C)	Yield (%) Side product	Yield (%)
Phenol[a]	-	125	36[b]	14
Phenol	-	125[c]		16
p-toluenesulfonic acid	DMSO	125		-
p-toluenesulfonic acid	-	120[c]		63

a) Reaction mixture includes 1.2 eq NEt_3. b) 36% of 7-chloro-4-phenoxyquinoline formed. c) microwave-assisted reaction.

Phenol is a weak acid with a pK_a value of 10. It did not improve the reaction yield compared to the use of strong bases. We observed a 7-chloro-4-phenoxyquinoline side product formation in the reaction mixture containing phenol and NEt_3. This side product has been reported by other research

groups, formed in the absence of NEt_3.[38] As phenol did not optimize the reaction, we decided to use a stronger organic acid p-toluenesulfonic acid with a pKa of -3, **Table 4.5**. The reaction containing DMSO did not yield any product, which might be due to hydrogen bonding between the sulfonic acid and the sulfoxide when prevented the protonation of the amine. Pan *et al.* reported similar reaction conditions between primary and secondary amines with 4-chloro-2-methylquinoline.[39] Under traditional thermal conditions, a reaction mixture containing acid, a cyclic secondary amine, quinoline, DMF and high temperatures give yields ranging 25 – 52%. However, they demonstrated that they could produce good to excellent yields, 55 – 75%, under microwave-assisted conditions and yields were improved to 81% when the solvent was removed from the reaction.[39] In our experiments, a microwave-assisted system without the use of solvent improved the yield of the reaction to 63%. With this improved result we were satisfied with the yield and proceeded to the final stage of the synthesis to form 3-azidomethylchloroquine (3-N_3MeCQ), **4.17**.

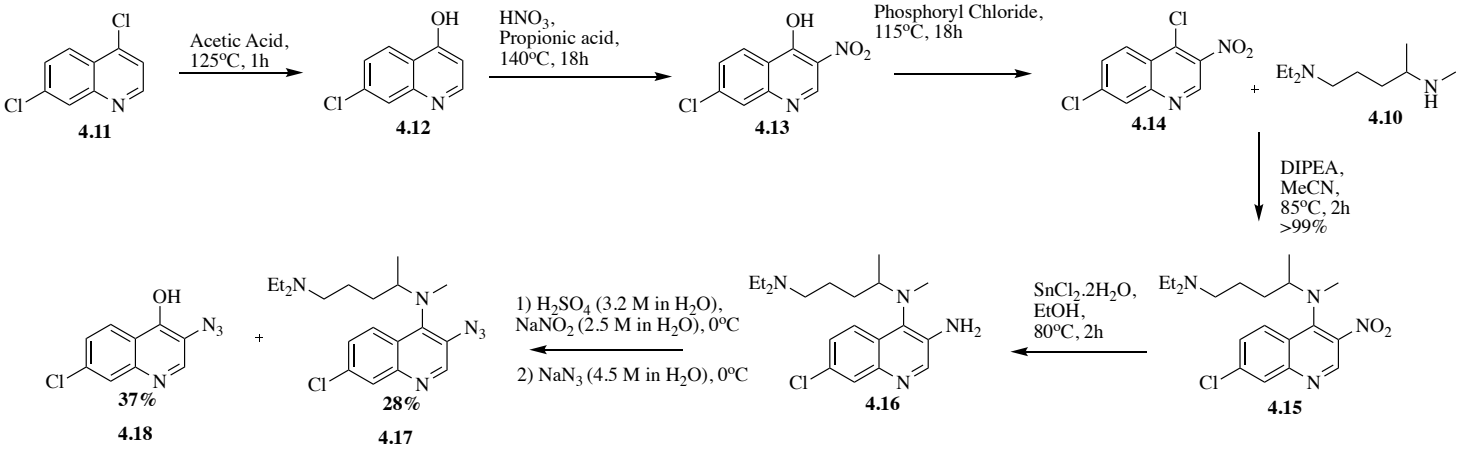

Scheme 4.7. Linear synthesis of 3-azidomethylchloroquine.

Once 4,7-dichloro-3-nitroquinoline, **4.14**, is synthesized, we carried out the condensation reaction to form the 3-NO_2MeCQ, **4.15**, see **Scheme 4.7**. Remarkably, in the case of **4.14,** the optimal

reaction conditions are with the use of DIPEA in acetonitrile. This reaction occurs very quickly and gives quantitative yields. An explanation for this observation is the proximity of the electron-withdrawing nitro group, which greatly increases the electrophilicity of the C-4 position. The nitro group is then reduced with stannous chloride to afford 3-aminomethylchloroquine (3-NH_2MeCQ), **4.16**. The final step is converting the amine to azide via a diazonium salt with sodium nitrite and sulfuric acid. The diazotization reaction occurs immediately following the addition of sodium nitrite. However, a 3-azido-7-chloroquinolin-4-ol, **4.18** side product begins to form just as rapidly; thus, the addition of sodium azide followed by quenching the reaction with sodium carbonate must be done within 10 minutes of starting the reaction. A proposed pathway for side product formation is shown below, **Scheme 4.8**. Once the diazonium ion forms, it can form an iminium salt that results in an electrophilic C-4. This is then subject to nucleophilic attack by H_2O. The methylated side chain is then expulsed to give **4.22**. The formation of **4.18** occurs after the addition of sodium azide. The side product is insoluble in the acidic media and is filtered out of the solution to allow the collection of the desired **4.17** product.

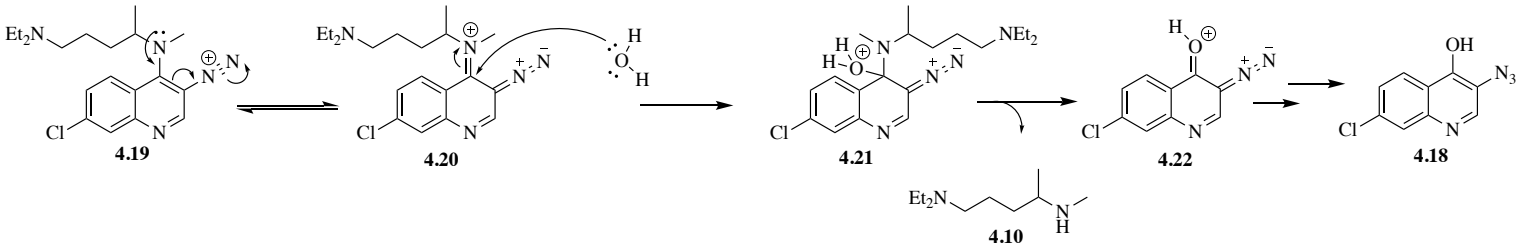

Scheme 4.8. Proposed mechanism for 3-azido-7-chloroquinolin-4-ol formation.

To reduce side product formation, we carried out the reaction in an organic solvent to minimize H_2O concentration. All reagents used have a degree of solubility in MeOH which was the chosen solvent. The strong organic acid p-toluenesulfonic acid was chosen, and this reaction was carried

out at 0°C to RT and stirred for 18 hours. TLC showed minimal product conversion. When the time elapsed and purification was performed only 1.4% of the product was isolated with no side product formation. Factors affecting product formation for the new method included partial solubility of sodium nitrite and sodium azide, therefore a lower rate of formation of the diazonium intermediate. Another factor affecting the formation of the product is the pH of the solution. For the nitrosonium ion to form an acidic environment is needed, which is not the case with p-toluenesulfuric acid in MeOH.

4.3.1 Photoaffinity Properties

With the desired 3-N_3MeCQ in hand, we have synthesized the first known quinoline-based PAL with the least modifications to the parent compound. In doing so, we are able to retain all the necessary functionality for antimalarial activity.

We first determined the UV-Vis spectroscopic difference between CQ, 3-NH_2MeCQ and 3-N_3MeCQ. The spectroscopic profile for CQ diphosphate salt was prepared in H_2O and measured at pH 7.3. The samples for 3-NH_2MeCQ and 3-N_3MeCQ were prepared in MeOH. As expected, CQ has a very different profile to its derivatives, whereas there are several similarities between 3-NH_2MeCQ and 3-N_3MeCQ. As shown in **Figure 4.3**, there is a 6 nm bathochromic shift in the λ_{max} of the amine compared to the azide from 237 nm to 243 nm. Both compounds have weak $\pi \rightarrow \pi^*$ bands at 278 nm and 282 nm for the amine and azide, respectively, and weaker $n \rightarrow \pi^*$ bands at 357 nm and 358 nm for the amine and azide, respectively. CQ diphosphate is a colourless salt and this is proven in the spectra where the absorbances are in the ultraviolet region. 3-NH_2MeCQ and 3-N_3MeCQ have a yellow tint, this is due to the tailed absorbance at 400 nm.

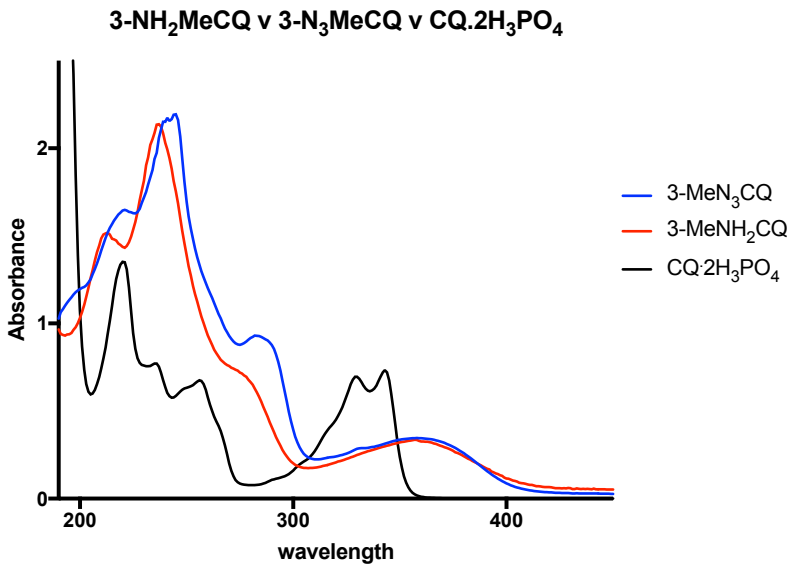

Figure 4.3. Overlaying spectra of 3-NH_2MeCQ, 3-N_3MeCQ and CQ.$2H_3PO_4$ for comparison.

We then determined the excitation wavelength for the photolabile moiety. It has been reported that aryl azides can be irradiated at 254 nm without causing damage to the compound; therefore, we decided to test its stability at that excitation wavelength, **Figure 4.4**.[40,41] The azide was first exposed to 254 nm using a UV mercury penlight in the dark, exposure lasted 1 hour, and the spectra were taken at different time intervals. As shown in the spectra, photoexcitation/ decomposition is rapid as the $\pi \rightarrow \pi^*$ band disappears within one minute. However, photodecomposition begins to occur within 30 minutes, with the compound having little UV-Vis signature after one hour.

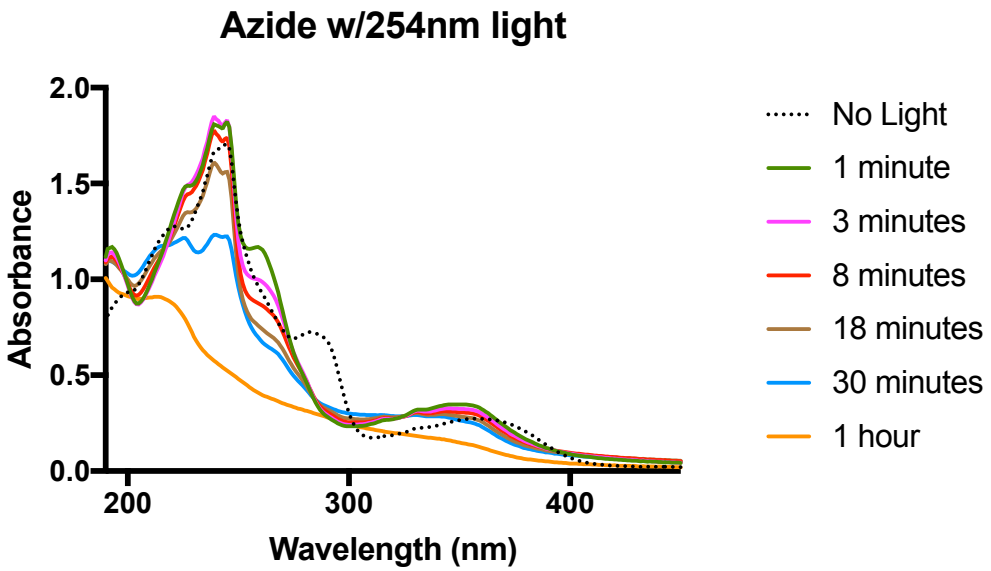

Figure 4.4. Photolysis of 3-N_3MeCQ at 254 nm excitation.

With this observation, we decided that photolysis at 254 nm was too energetic and tried photoexcitation at 365 nm. There are also many examples of azide irradiation above 300 nm which result in insertion reactions.[6,42,43] We carried out stability tests in H_2O and MeOH, and the aryl azide remains intact after longer than 18 hours with exposure to 365 nm of light, **Figure 4.5**.

Due to the high reactivity of the nitrene, the below spectra are the results of product formation from the nitrene reacting with the polar solvent, **Figure 4.5**. These results show that the aryl azide is indeed photolabile; however, it is also a cause of concern that the reaction with the solvent will occur faster than insertion with a chosen compound, making detection of azide-compound insertion difficult with UV-Vis spectroscopy. Furthermore, binding regioselectivity is important as the photo label should ideally insert at the binding site.

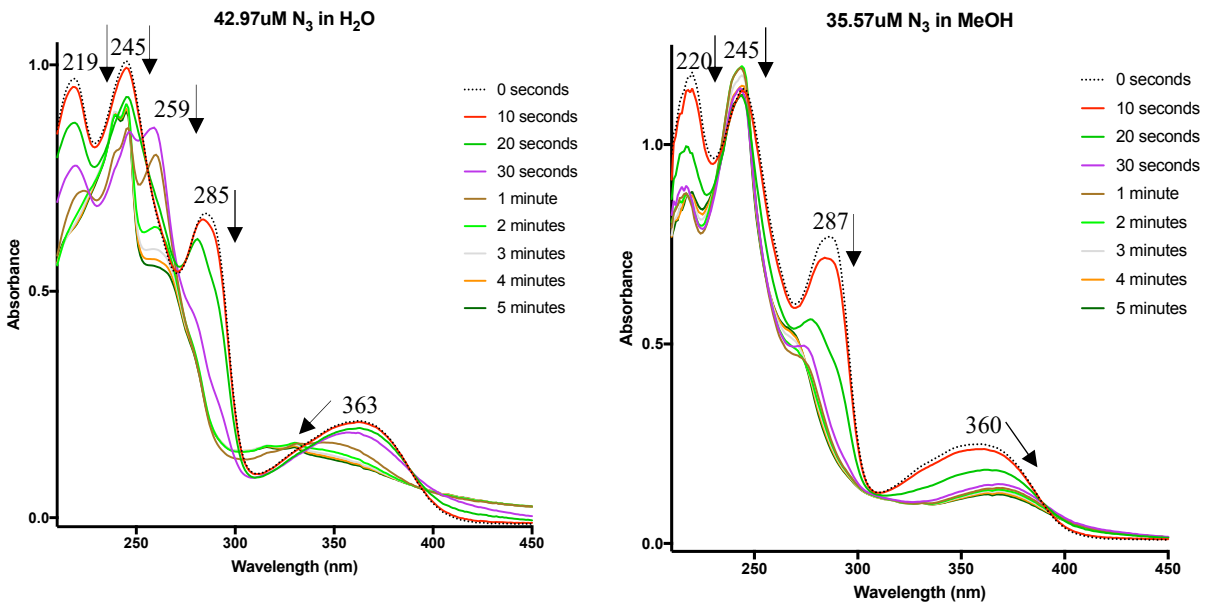

Figure 4.5. Photolysis of 42.97 μM N_3 in H_2O and 35.57 μM N_3 in MeOH at 365 nm.

We then carried out the same reaction in an NMR tube with a 365 nm penlight in the dark in deuterated MeOH.

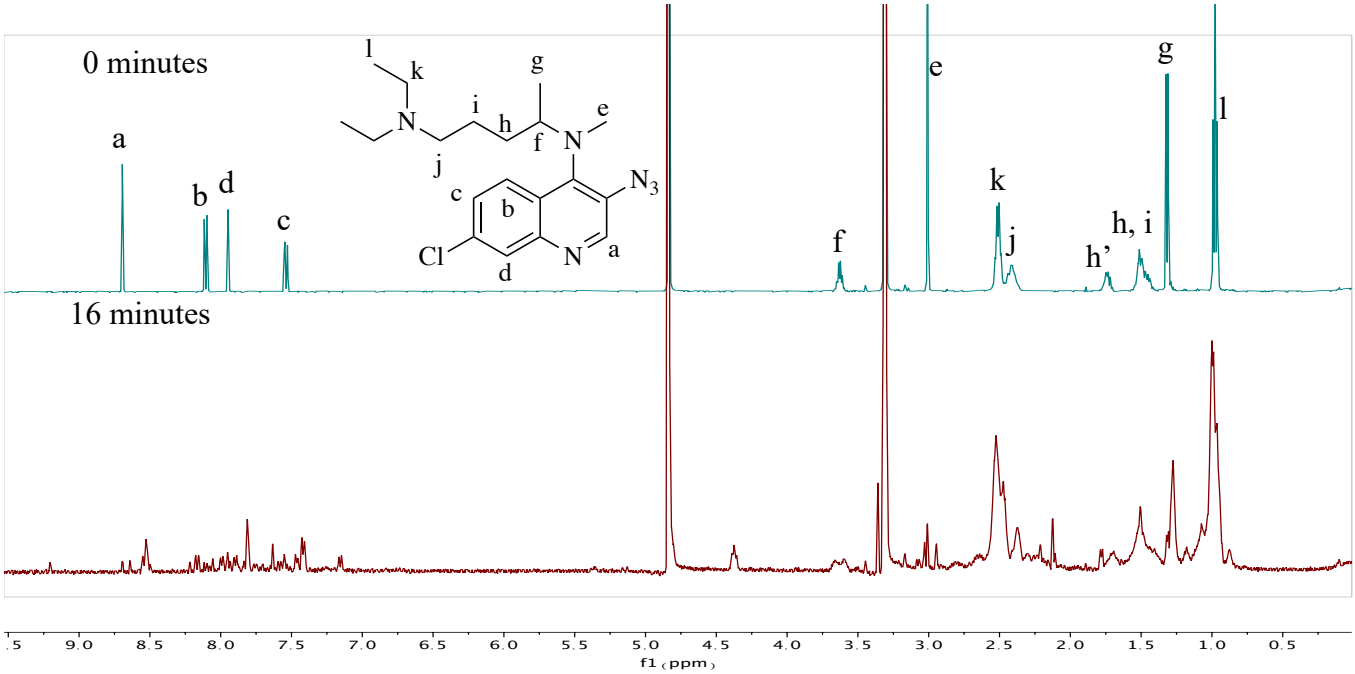

Figure 4.6. Photolysis of 3-N_3MeCQ at 0 and 16 minutes in MeOD-d_4.

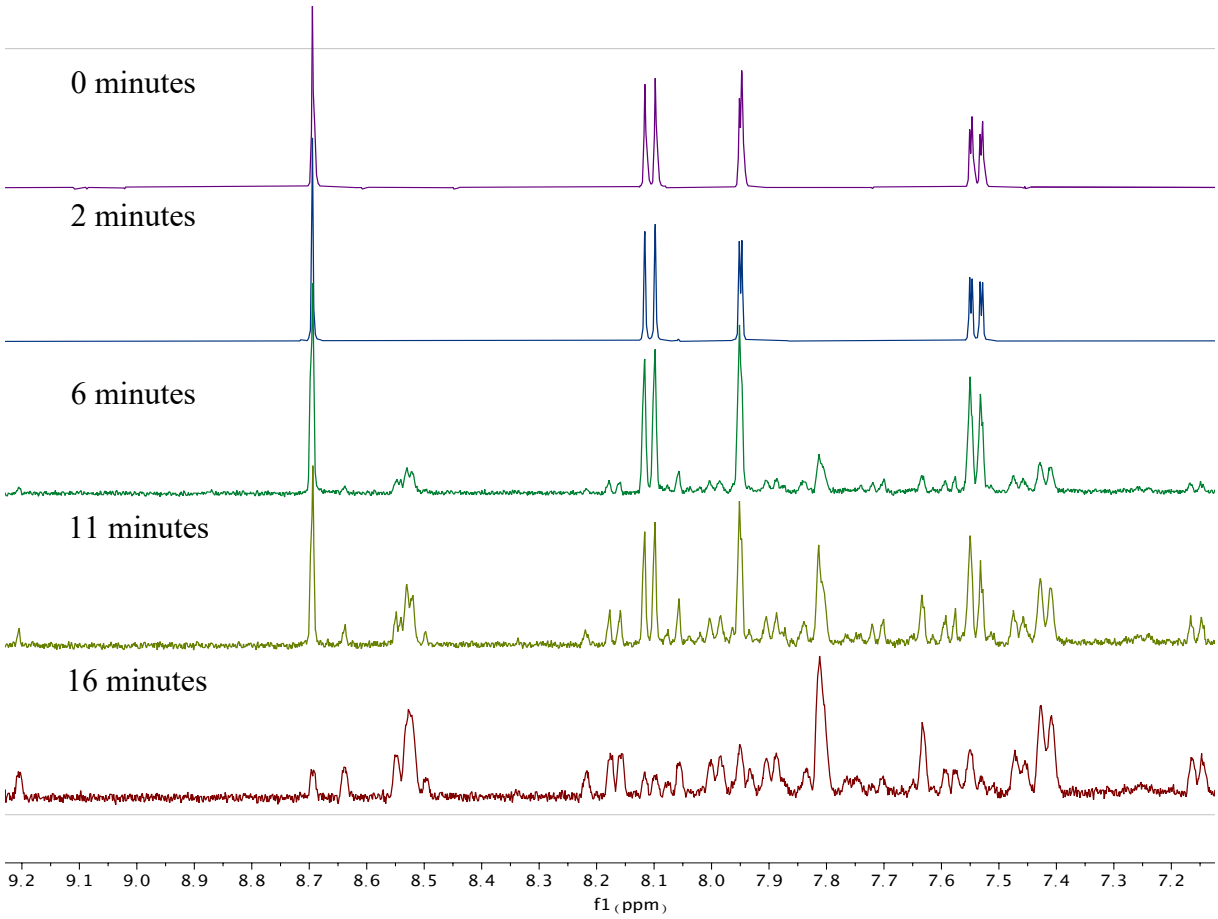

Figure 4.7. Photolysis of 3-N_3MeCQ in MeOD-d_4 over 16 minutes.

Irradiation of the aryl azide with 365 nm shows an apparent change in the structure, **Figure 4.6**. Changes become evident after 2 minutes of exposure. As seen in the UV spectra, the $\pi \rightarrow \pi^*$ band disappears, in the NMR spectra we can see the aromatic protons decrease in intensity as additional peaks arise. Additional photodecomposition occurs with longer exposure times, **Figure 4.7**, the aromatic region is more affected than the aliphatic regions as one would expect. Therefore, when carrying out photolysis experiments exposure times did not exceed 10 minutes. High-Resolution Mass Spectroscopy was carried out for the azide samples in H_2O and MeOH. We discovered the formation of 3 consistent molecular ions with their possible structures shown below, **Figure 4.8**.

The formation of nitroso-methylCQ occurs in the presence of H_2O and MeOH when irradiated at 365 nm for 5 minutes, this might be a result of hydroxyl insertion. Interestingly, only in the presence of H_2O do we get the formation of a nitroso-chloroquine derivative that has lost a methyl group. The formation of this product may also result from H_2O insertion and the HRMS data leads us to believe the shown structure is the most probable product. Not-so surprisingly, we have the formation of an intramolecular insertion product; however, it only formed in the presence of MeOH. Formations of such azirines are well documented for phenyl azide, which exists in resonance with the corresponding ketenimine.[44–46]

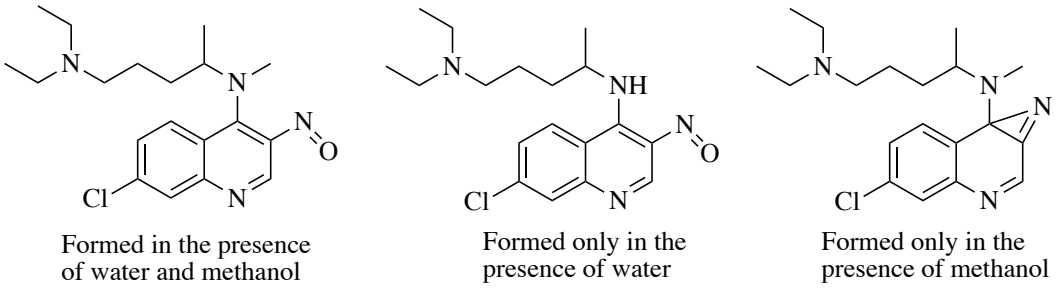

Figure 4.8. Possible irradiated 3-N_3MeCQ products formed.

4.3.2 Nitrene insertion

We carried out experiments to determine if the expected singlet nitrene intermediate that forms inserts into C-H, C-N or C=C bonds. To achieve this, we first used a simple tripeptide GlyGlyGly. A UV-Vis spectrum of the azide and GlyGlyGly was taken at different stoichiometries, **Figure 4.9**, and the change in the UV-Vis signature is evident at the different concentrations. From the UV-Vis spectra it is clear that there is a change in the aromatic system of the aryl azide when mixed with the peptide. To confirm that insertion occurred with the peptide

we carried out HRMS for the resulting product. However, there were no peaks related to an insertion product detected by HRMS.

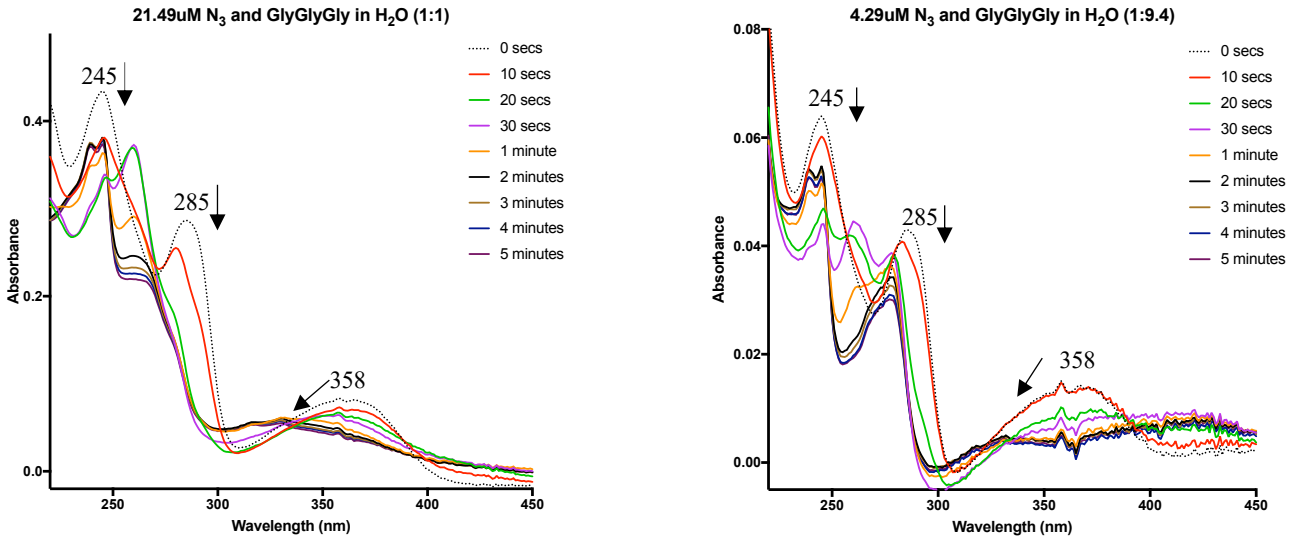

Figure 4.9. Photolysis of 21.49 μM 3-N_3MeCQ with 22.32 μM GlyGlyGly and 4.29 μM 3-N_3MeCQ with 40.18 μM GlyGlyGly at 365 nm excitation over five minutes.

We then decided to carry out UV-Vis and NMR studies to trap the nitrene with strong electron acceptors. First, we used *N*-phenylmaleimide with 3-N_3MeCQ in the dark exposed to 365 nm of light, **Figure 4.10**. At higher concentrations, the absorbance associated with *N*-Phenylmaleimide begin to obscure that of the quinoline; however, it seems to follow a similar pattern to that of the control experiment. The HRMS did not detect any molecular ions associated with a possible insertion product.

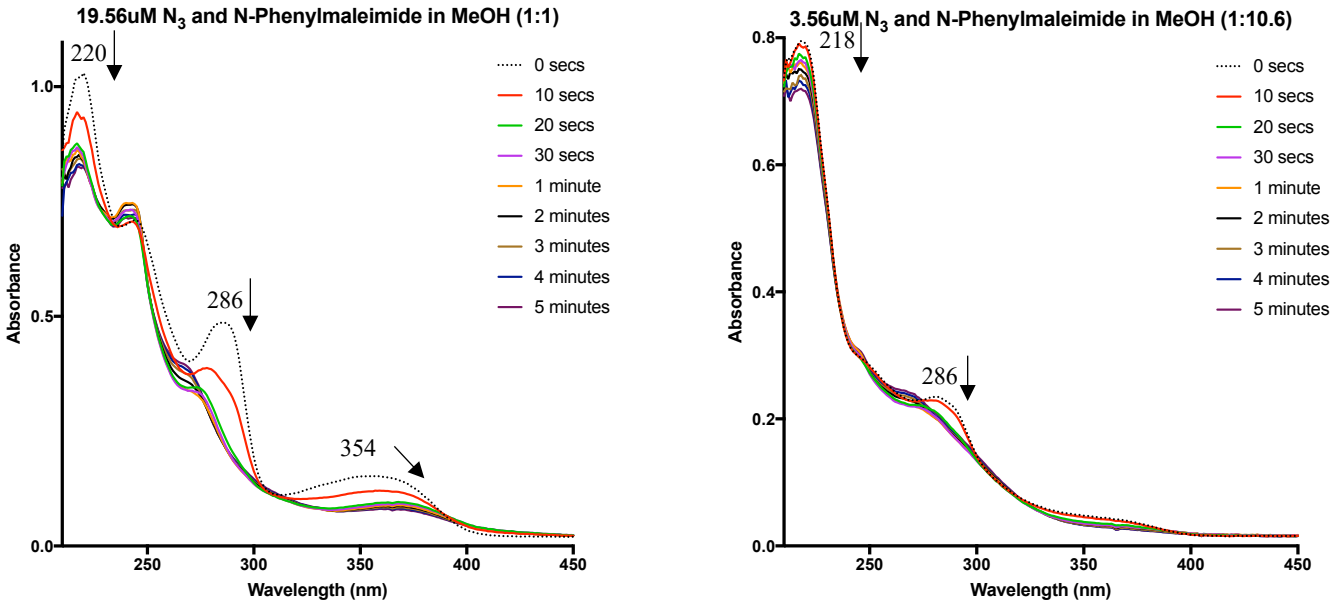

Figure 4.10. Photolysis of 19.56 µM 3-N_3MeCQ with 18.77 µM maleimide, 7.11 µM 3-N_3MeCQ with 33.37 µM maleimide and 3.56 µM 3-N_3MeCQ and 37.54 µM maleimide at 365 nm excitation over 5 minutes.

We then carried out the same experiment in an NMR tube to detect product formation at higher concentrations of both reagents. As shown in **Figure 4.11,** doublets appear at 6.53 ppm and 6.29 ppm. To further investigate *N*-phenylmaleimide, was irradiated alone in MeOH for a total of nine minutes, and we saw the appearance of the vinyl protons indicating independent activation of the maleimide, **Figure 4.12**.

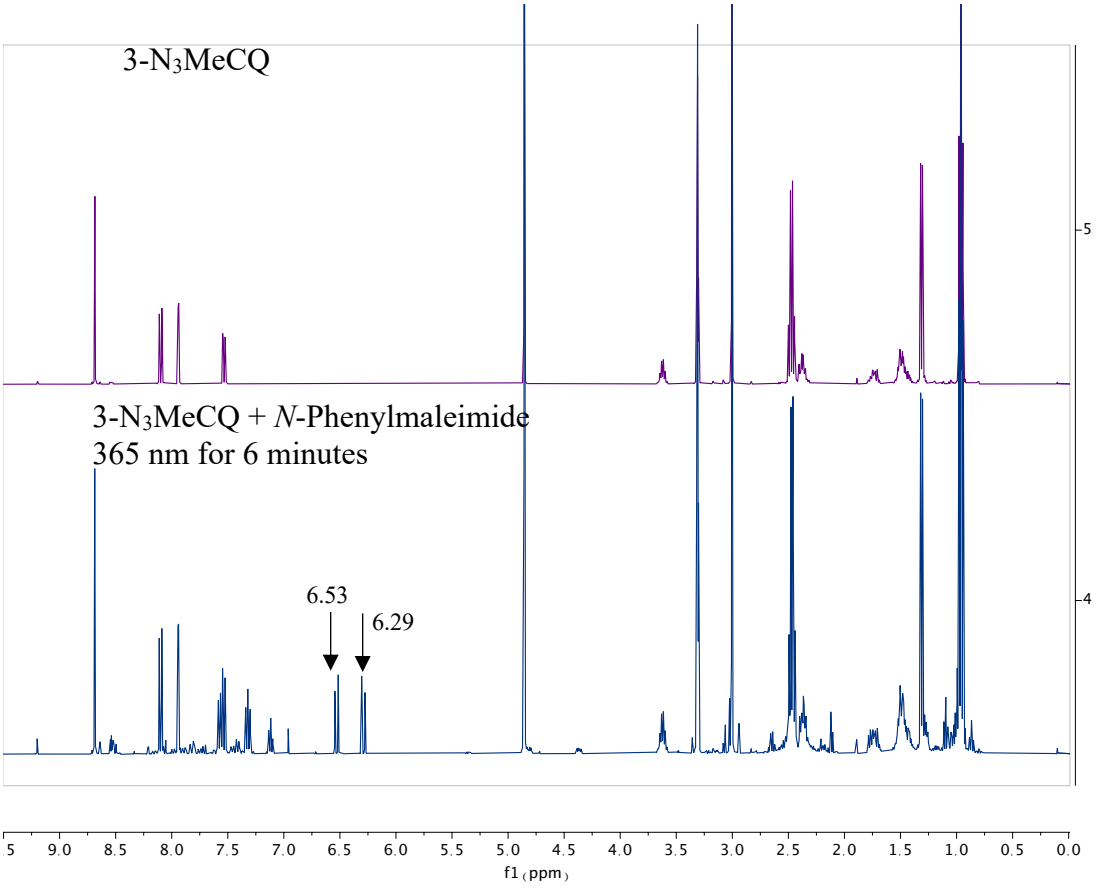

Figure 4.11. Photolysis of 26.7mM 3-N_3MeCQ and 26.6mM maleimide at 365 nm in d_4-MeOD.

Hott and Heusinger (1977) investigated the photolysis of maleimides in polar solutions using electron spin resonance.[47] They note the detection of radical anions of maleimides in alcohol solutions. They determined that radical anions are the primary ion species. Kiselev *et al.* have reported the slow hydrolysis of *N*-phenylmaleimide to the acid in the presence of H_2O.[48] It is possible that the radical anion formation speeds up the hydrolysis of the maleimide, resulting in the ring-opened carboxylic acid.

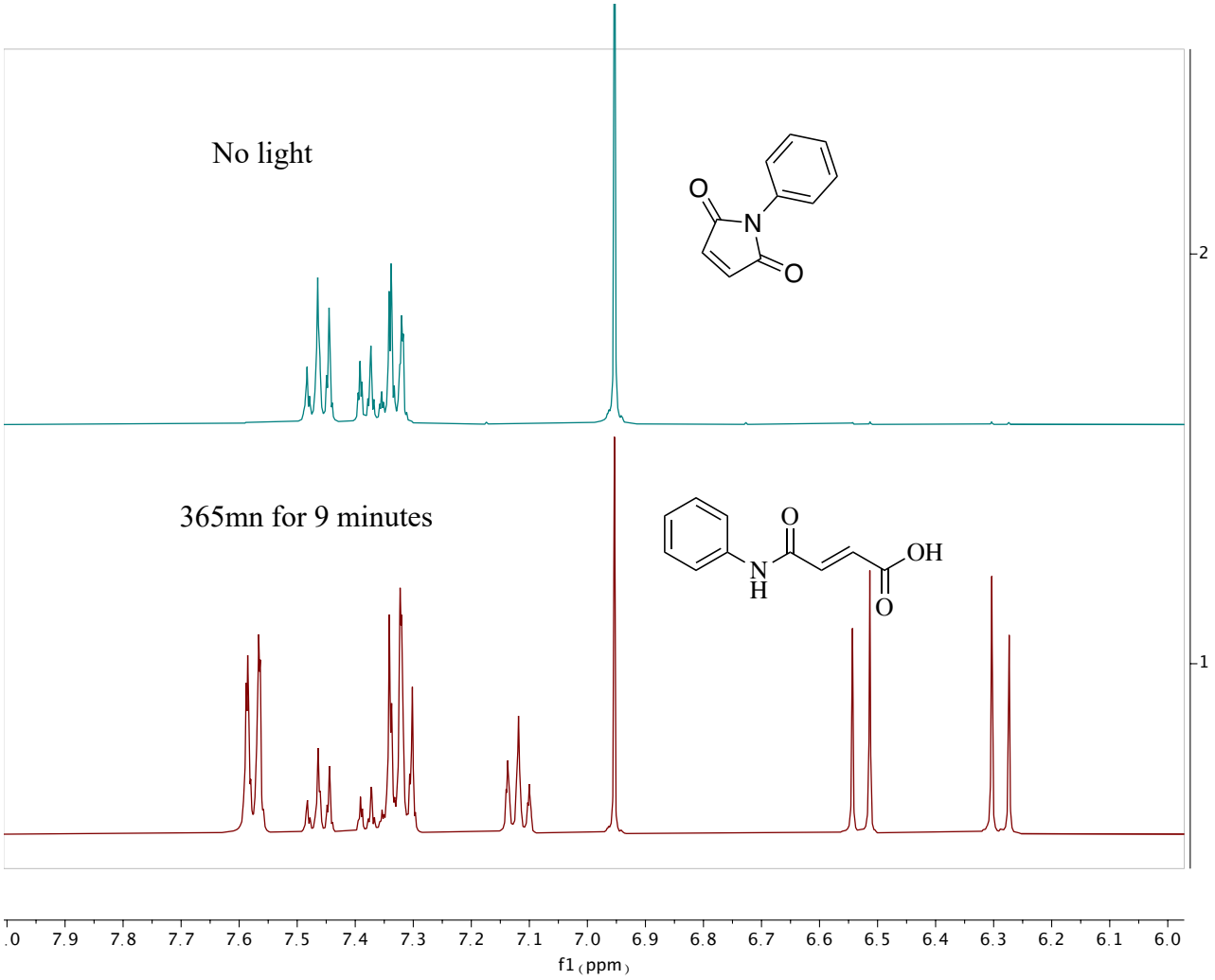

Figure 4.12. Comparison between activated and unactivated *N*-phenylmaleimide.

We then decided to use the stronger electron acceptor tetracyanoethylene (TCNE). Murata *et al.* reported the photochemical reaction of mesityl azide with TCNE with 360 nm ± 15 nm light produced two adducts formed via singlet nitrene trapping.[49] Irradiation of our aryl azide and TCNE for 9 minutes shows the formation of a minor product (23% conversion); however, the HRMS of the mixture did not detect the formation of the expected photolysis product but rather corresponds to a formal HCN insertion product.

a)

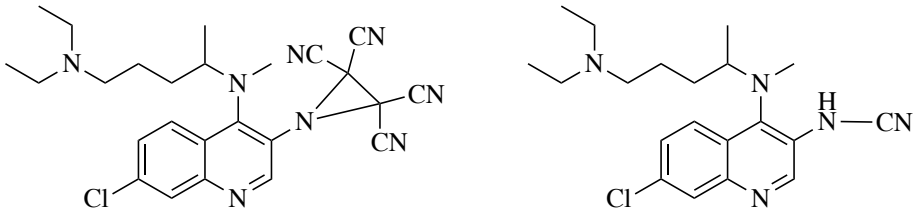

Expected product

Possible product
23% conversion

b)

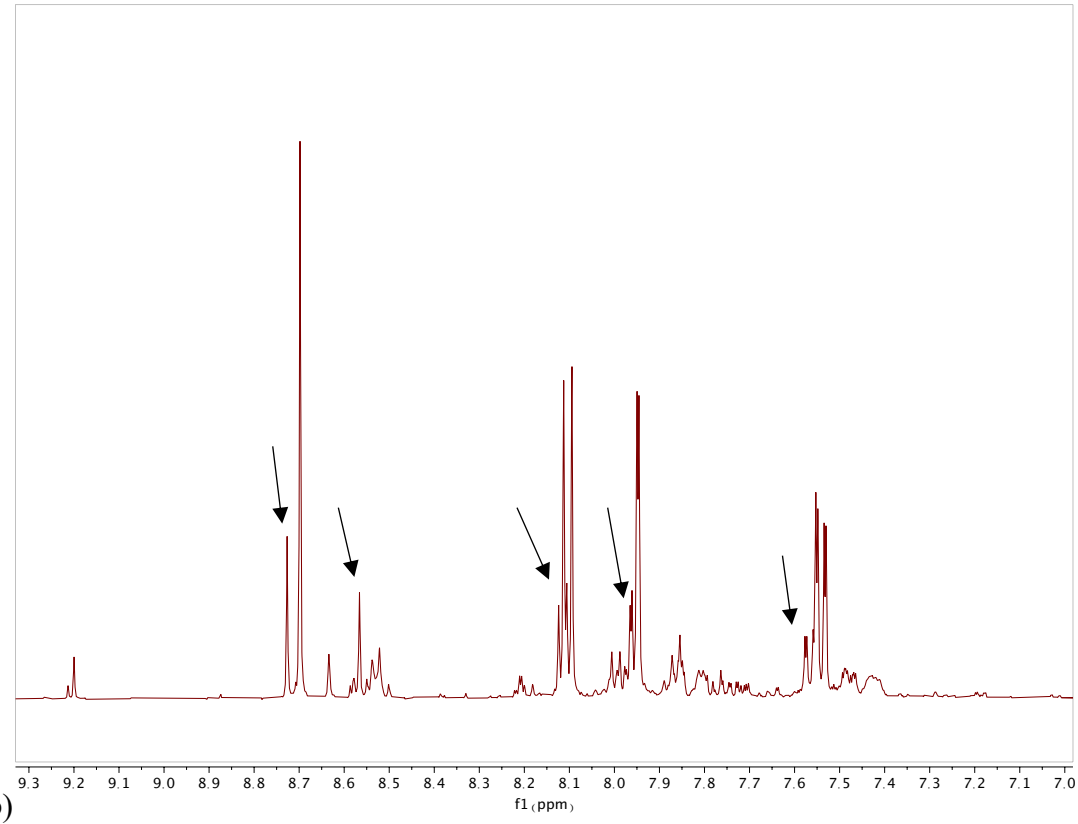

Figure 4.13. a) Desired product v possible observed photolysis product, b) NMR of photolysis product formation.

The exact mass and chemical formula obtained from HRMS ([M+H$^+$] m/z: 374.21) led us to the proposed structure, **Figure 4.13**. This product was not isolated and longer excitation times leads to the decomposition of the spectroscopically detected intermediate.

4.4 Conclusion

We have synthesized the first photolabile CQ derivative with minimal modifications of the parent compound. The modification involved installing a methyl group on the 4-AQ to prevent cyclization to a triazole derivative. In order to install the amine we first methylated the side chain and then carried out a condensation reaction with 4,7-dichloro-3-nitroquinoline. Once the desired azide was obtained we carried out UV-Vis stability tests to determine the best-suited photoexcitation energy. We found that irradiation at 254 nm was too energetic and led to the decomposition of the aromatic system and 365 nm of light was the most suitable as it activated the azide, causing a release of nitrogen gas to form a new compound. The reactive nitrene intermediate species forms an adduct with the surrounding solvent which was detected by HRMS. We then carried out photolysis studies with a GlyGlyGly, *N*-phenylmaleimide and tetracyanoethylene and discovered that the electron acceptor and the solvent determine the conditions for insertion. We could not detect the expected insertion product with TCNE in which the nitrene intermediate is inserted into the C-N triple bond; however, we detected a possible HCN insertion product. The PAL is currently being used for photoaffinity labelling on PfCRT with the Fidock group at Columbia University.

4.5 Experimental

4.5.1 General information

Glassware was taken directly from the oven (120ºC) and let cool in a desiccator before use. NMR experiments were carried out in New Era NMR routine grade tubes 5 mm X 8". All solvents and reagents were obtained commercially and used without further purification unless noted.

UV irradiation was carried out using Analytik Jena UVP Pen-Ray UV mercury lamp 254 nm and 365 nm. High-Resolution Mass Spectroscopy (HRMS) was obtained by positive/negative ESI, or positive/negative APCI on a Bruker Maxis Impact QTOF, or a Thermo Scientific ExactivePlus Orbitrap, with results reported as mass/charge ratios (*m/z*). Thin-layer chromatography plates were visualized using ultra-violet light, 254nm. Flash column chromatography was carried out manually using 230 - 400 mesh silica gel (Silicycle) using reagent grade solvents or using Biotage Isolera One system with Biotage ZIP 30 g columns. Cole Parmer Microcomputer pH-Vision Model 05669-20 pH Meter used with Sigma-Aldrich micro pH combination electrode and glass body. The UV-Vis spectra were measured on Agilent 8453.

^{1}H and ^{13} C NMR spectra were recorded at ambient temperature on Bruker AVIIIHD 400 MHz (^{1}H 400 MHz, ^{13}C 100 MHz) and Bruker AVIIIHD 500 MHz (^{1}H 500 MHz, ^{13}C 125 MHz) using tetramethylsilane as the internal standard. Chemical shifts are reported relative to the residual deuterated solvent peaks. Chemical shifts are expressed in parts per million (ppm = δ) values and coupling constants (J) in Hertz (Hz). The terms m, s, d, t and q represent multiplicities of 1H NMR resonances: multiplet, singlet, doublet, triplet and quartet, respectively. For previously unknown compounds, a combination of 2D experiments (COSY, HSQC, HMBC) was often used to complete the assignment of ^{1}H and ^{13}C signals. ^{1}H NMR signals are described by chemical shift δ

(multiplicity, J (Hz), integration). ^{13}C NMR signals are described by chemical shift δ and are singlets unless otherwise specified.

4.5.2 Experimental procedure

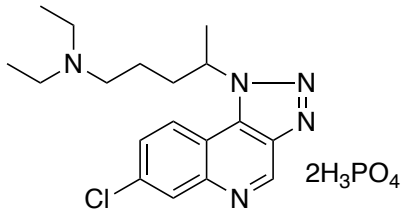

4-(7-chloro-1*H*-[1,2,3]triazolo[4,5-*c*]quinolin-1-yl)-*N*,*N*-diethylpentan-1-amine diphosphate (4.4)

A solution of 7-chloro-*N*4-(5-(diethylamino)pentan-2-yl)quinoline-3,4-diamine (50 mg, 0.14 mmol) in of 3.2 M sulfuric acid (98%), is cooled to 0°C and a 1 mL solution of 2.5 M sodium nitrite is added dropwise. The reaction mixture is stirred at this temperature for 15 minutes. After 15 minutes, 1 mL of 4.5 M sodium azide is added dropwise to the reaction mixture at 0°C. Addition of azide results in visible N_2 gas evolution. The reaction mixture is left to stir for a further 1 hour and the mixture is allowed to warm from 0°C to RT. Once complete, the reaction mixture is treated with saturated Na_2CO_3 solution and the compound is extracted with DCM (3 X 10 mL). The combined organic layers are rinsed with brine and dried over anhydrous $MgSO_4$. The solvent is removed under reduced vacuum to reveal a bright orange oil. The oil was purified by flash chromatography on silica gel with the solvent system: 55% Hex, 40% DCM, 5% NEt_3 to give a bright yellow oil 24 mg, 46% yield.

The free-base is then converted to a phosphate salt with phosphoric acid as follows: To a solution of the free base 4-(7-chloro-1H-[1,2,3]triazolo[4,5-c]quinolin-1-yl)-*N*,*N*-diethylpentan-1-amine (24 mg, 0.069 mmol) in 1 mL of MeOH is added, with cooling, a phosphoric acid solution

made from 0.14 g of 85% phosphoric acid and 3 mL of MeOH. Isopropyl alcohol is then added to separate the salt from the solution as an oil. The oil is triturated with ether and stirred until it solidifies. The mixture was then filtered, the diphosphate washed with ether and quickly placed in a vacuum oven overnight. White powder 26.3 mg, 70 %.

Yield: 26.3 mg, 70%. **^{1}H NMR** (400 MHz, Deuterium Oxide-d_2) δ 9.26 (s, 1H), 8.26 (d, J = 9.0 Hz, 1H), 7.78 (d, J = 2.1 Hz, 1H), 7.69 (dd, J = 8.9, 2.2 Hz, 1H), 5.43 (p, J = 6.6 Hz, 1H), 3.19 – 3.09 (m, 6H), 2.47 – 2.34 (m, 1H), 2.28 – 2.15 (m, 1H), 1.81 (d, J = 6.6 Hz, 3H), 1.79 – 1.63 (m, 2H), 1.22 – 1.18 (m, 6H). **^{13}C NMR** (126 MHz, Deuterium Oxide-d_2) δ 144.70, 142.82, 139.06, 135.94, 133.40, 129.23, 126.81, 123.73, 113.20, 57.99, 50.95, 47.23, 32.16, 19.96, 19.89, 8.07 (d, J = 4.6 Hz). **^{31}P NMR** (162 MHz, Deuterium Oxide-d_2) δ 0.03. **HRMS** (ESI) calcd. for $C_{18}H_{25}ClN_5$ [M+H]: 346.1798, found: 346.1793.

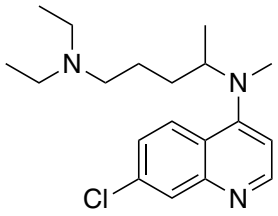

***N*^{4}-(7-chloroquinolin-4-yl)-*N*^{1},*N*^{1}-diethyl-*N*^{4}-methylpentane-1,4-diamine (4.6)**

The mixture of 4,7-dichloroquinoline (500 mg, 2.5 mmol) and *N*^{1},*N*^{1}-diethyl-*N*^{4}-methylpentane-1,4-diamine (652.6 mg, 3.8 mmol, 1.5 equiv.) are placed in a microwave flask with p-toluenesulfonic acid (816 mg, 4.3 mmol, 1.7 equiv.). This mixture was heated at 120^{o}C for 1.5 hours. Once complete, the reaction is let cool to RT. The mixture is poured into ice H_2O, and then 1 M NaOH is added. This is extracted with EtOAc (3 X 100 mL), washed with brine, and the organic layers are then dried over anhydrous $MgSO_4$. The solvent is removed under reduced vacuum to reveal an orange oil. The oil was purified by flash chromatography on silica gel with

the solvent system: 50% Hex, 50% to 100% EtOAc and 5 - 10% NEt_3 to give an orange oil 534.5 mg, 63% yield.

Yield: 534.5mg, 63%. **^{1}H NMR** (500 MHz, Chloroform-*d*) δ 8.60 (d, *J* = 5.2 Hz, 1H), 7.99 (d, *J* = 2.2 Hz, 1H), 7.88 (d, *J* = 9.0 Hz, 1H), 7.35 (dd, *J* = 9.0, 2.2 Hz, 1H), 6.75 (d, *J* = 5.2 Hz, 1H), 3.85 (h, *J* = 6.8 Hz, 1H), 2.85 (s, 3H), 2.43 (qd, *J* = 7.1, 1.6 Hz, 4H), 2.34 – 2.29 (m, 2H), 1.76 – 1.65 (m, 1H), 1.56 – 1.47 (m, 1H), 1.46 – 1.31 (m, 0H), 1.25 (d, *J* = 6.5 Hz, 3H), 0.94 (t, *J* = 7.1 Hz, 6H). **^{13}C NMR** (126 MHz, Chloroform-*d*) δ 157.55, 151.53, 150.78, 134.64, 128.90, 125.98, 125.22, 121.86, 109.02, 58.80, 52.87, 46.91, 32.49, 32.35, 24.64, 17.10, 11.70. **HRMS** (APCI) calcd. for $C_{19}H_{29}ClN_3$ [M+H$^+$]: 334.2045, found: 334.2046.

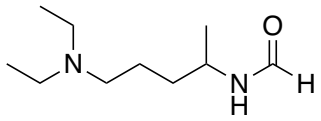

***N*-(5-(diethylamino)pentan-2-yl)formamide (4.9)**

A mixture of 2-Amino-5-diethylaminopentane (5 g, 31.6 mmol) and ethyl formate (7.7 mL, 3 equiv.) is heated at 70°C for 18 hours in a round-bottom flask with molecular sieves. After completion the mixture was cooled to RT and EtOAc was added. The resulting solution was washed with 1 M HCl and extracted with EtOAc (3 X 150 mL). The organic layer was then basified with 1 M NaOH and extracted with EtOAc (3X 200 mL) then rinsed with brine and dried over anhydrous magnesium sulfate. The solvent was evaporated under reduced pressure to get *N*-(5-(diethylamino)pentan-2-yl) formamide product, used without further purification to give an orange oil, 5.689 g, 97% yield.

Yield: 5.689 g, 97%. **Major trans rotamer**: **^{1}H NMR** (500 MHz, Chloroform-*d*) δ 8.10 (s, 1H), 6.55 (s, 1H), 4.08 – 3.97 (m, 1H), 2.53 (dd, *J* = 7.2, 4.7 Hz, 4H), 2.45 – 2.35 (m, 2H), 1.50 (dd, *J*

= 6.2, 3.8 Hz, 4H), 1.15 (d, *J* = 6.6 Hz, 3H), 1.04 – 1.00 (m, 6H). **^{13}C NMR** (126 MHz, Chloroform-*d*) δ 160.68, 53.02, 46.77, 44.01, 34.80, 23.14, 20.84, 11.42. **Minor cis rotamer:** **^{1}H NMR** (500 MHz, Chloroform-*d*) δ 8.07 (d, *J* = 12.0 Hz, 1H), 5.93 (s, 1H), 3.49 (s, 1H), 2.53 (dd, *J* = 7.2, 4.7 Hz, 4H), 2.45 – 2.35 (m, 2H), 1.50 (dd, *J* = 6.2, 3.8 Hz, 4H), 1.21 (d, *J* = 6.6 Hz, 3H), 0.99 (s, 6H). **^{13}C NMR** (126 MHz, Chloroform-*d*) δ 163.78, 52.65, 48.37, 46.86, 36.00, 23.58, 22.79, 11.62. **HRMS** (APCI) calcd. for $C_{10}H_{23}ON_2$ [M+H]: 187.18049, found: 187.18033.

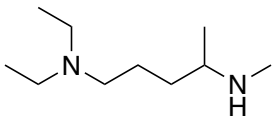

***N*^{1},*N*^{1}-diethyl-*N*^{4}-methylpentane-1,4-diamine (4.10)**

To a suspension of 2 M LiAlH4 in THF, *N*-(5-(diethylamino)pentan-2-yl)formamide (4.5 g, 24.2 mmol), which is dissolved and degassed in anhydrous THF, is added portion-wise under stirring and cooling with an ice bath. The mixture is let stir at 0^{o}C for 30 minutes, and then the reaction mixture is refluxed for 24 hours under nitrogen. After completion 1 M NaOH is added dropwise to hydrolyze any remaining $LiAlH_4$. All precipitates are filtered off and washed with THF. The filtrate is then placed in a separatory funnel and the organic layer separates. The organic layer is then acidified with 1 M HCl and extracted with DCM (3 X 200 mL). The combined organic layers are then basified with sat. NaOH and extracted with DCM (3 X 300 mL). The organic layers are then rinsed with brine and dried over anhydrous $MgSO_4$ and the solvent is removed under reduced pressure to reveal pure *N*^{1},*N*^{1}-diethyl-*N*^{4}-methylpentane-1,4-diamine, which was used without further purification. Orange oil, 2.685 g, 65% yield.

Yield: 2.685 g, 65% yield. **^{1}H NMR** (500 MHz, Chloroform-*d*) δ 2.52 (q, *J* = 7.2 Hz, 4H), 2.40 (d, *J* = 6.5 Hz, 5H), 1.51 – 1.42 (m, 3H), 1.34 – 1.23 (m, 1H), 1.05 (d, *J* = 6.3 Hz, 3H), 1.01 (t, *J*

= 7.2 Hz, 6H). **^{13}C NMR** (126 MHz, Chloroform-*d*) δ 55.07, 53.32, 46.87, 34.91, 33.79, 23.68, 19.79, 11. **HRMS** (APCI) calcd. for $C_{10}H_{25}N_2$ [M+H]: 173.20123, found: 173.20097.

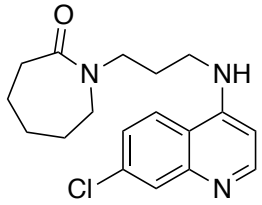

1-(3-((7-chloroquinolin-4-yl)amino)propyl)azepan-2-one

4,7-dichloroquinoline (126 mg, 0.64 mmol), N^1,N^1-diethyl-*N*4-methylpentane-1,4-diamine (100 mg, 0.58 mmol) and DBU (0.43 mL, 2.9 mmol) are placed in a round bottom flask and heated to 125ºC. The mixture was let stir for 18 hours. The brown mixture is then cooled to RT and washed with sat. NaOH and extracted with EtOAc (3 X 100 mL). The combined organic layers are then rinsed with H_2O and dried over anhydrous $MgSO_4$ and the solvent was removed under reduced pressure. The oil was purified by flash chromatography on silica gel with the solvent system: 85%, EtOAc, 10% MeOH and 5% NEt_3 to give a white solid, 173.8 mg, 82% yield.

Yield: 173.8 mg, 82%**.^{1}H NMR** (500 MHz, Chloroform-*d*) δ 8.46 (d, *J* = 5.5 Hz, 1H), 8.00 (d, *J* = 9.0 Hz, 1H), 7.95 (d, *J* = 2.2 Hz, 1H), 7.39 (dd, *J* = 9.0, 2.2 Hz, 1H), 7.02 (s, 1H), 6.39 (d, *J* = 5.6 Hz, 1H), 3.53 – 3.47 (m, 2H), 3.41 – 3.33 (m, 4H), 2.64 – 2.58 (m, 2H), 1.85 – 1.70 (m, 6H), 1.67 (p, *J* = 5.6 Hz, 2H). **^{13}C NMR** (126 MHz, Chloroform-*d*) δ 177.42, 151.23, 150.33, 148.73, 135.16, 127.91, 125.47, 122.25, 117.65, 98.09, 49.88, 45.11, 38.47, 37.17, 29.93, 28.44, 25.63, 23.46. **HRMS** (ESI) calcd. for $C_{18}H_{23}ClN_3O$ [M+H]: 332.1524, found: 332.1520.

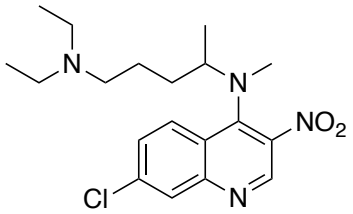

N^4-(7-chloro-3-nitroquinolin-4-yl)-N^1,N^1-diethyl-N^4-methylpentane-1,4-diamine (4.15)

To a solution of 4,7-dichloro-3-nitroquinoline (500 mg, 2.1 mmol) in acetonitrile is added N^1,N^1-diethyl-N^4-methylpentane-1,4-diamine (709 mg, 4.1 mmol, 2 equiv.) and *N*,*N*-diisopropylethylamine (0.54 mL, 1.5 equiv.) which is stirred until it formed a homogenous solution. This mixture is let stir at RT for up to 10 minutes. The reaction mixture is then transferred to an 85°C oil bath and let stir for 30 minutes. Once complete the reaction mixture is evaporated to dryness under reduced pressure. The residue is diluted with EtOAc and H_2O and basified with 1 M NaOH. The resulting solution is extracted with EtOAc (3 X 100 mL). The combined organic layers were then rinsed with brine and dried over anhydrous $MgSO_4$. The solvent is removed under reduced pressure. The crude product is purified by flash silica column chromatography with 85% Hex, 10% EtOAc, 5% NEt_3 to reveal a bright orange solid, 719.7mg, 92%.

Yield: 719.7 mg, 92%. **^{1}H NMR** (500 MHz, Chloroform-*d*) δ 8.93 (s, 1H), 8.06 (d, *J* = 2.2 Hz, 1H), 8.02 (d, *J* = 9.2 Hz, 1H), 7.50 (dd, *J* = 9.1, 2.2 Hz, 1H), 4.03 – 3.95 (m, 1H), 2.85 (s, 3H), 2.51 (d, *J* = 7.3 Hz, 4H), 2.42 (d, *J* = 7.7 Hz, 2H), 1.89 – 1.81 (m, 1H), 1.65 (dq, *J* = 13.5, 8.0 Hz, 1H), 1.47 (q, *J* = 7.8 Hz, 2H), 1.43 (d, *J* = 6.6 Hz, 3H), 1.00 (t, *J* = 7.1 Hz, 6H). **^{13}C NMR** (126 MHz, Chloroform-*d*) δ 151.13, 150.70, 147.90, 137.63, 137.04, 129.68, 127.55, 127.18, 123.82, 60.99, 52.76, 46.94, 33.91, 32.73, 24.46, 18.19, 11.42. **HRMS** (APCI) calcd. for $C_{19}H_{27}ClN_4O_2$ [M-H^+]: 378.1828, found: 378.1822.

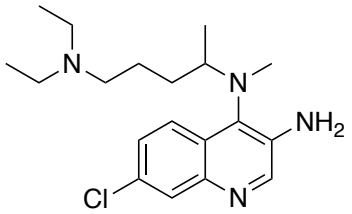

7-chloro-*N*^{4}-(5-(diethylamino)pentan-2-yl)-*N*^{4}-methylquinoline-3,4-diamine (4.16)

N^4-(7-chloro-3-nitroquinolin-4-yl)-*N*^{1},*N*^{1}-diethyl-*N*4-methylpentane-1,4-diamine (500 mg, 1.3 mmol) and stannous chloride (1.49 g, 5 equiv.) are placed in a round bottom flask. EtOH is added and the mixture was let stir at 80^{o}C for 2 hours. Once complete the mixture is let cool to RT. Once cool, the solvent is removed by reduced pressure. The residue is diluted with EtOAc and basified with sat. NaOH and extracted with EtOAc (3 X 50 mL). The combined organic layers are washed with brine and dried over anhydrous $MgSO_4$. The solvent is removed under reduced pressure to reveal a dark orange oil. This was purified by column chromatography with the solvent system: EtOAc (100→90%)/ MeOH (0→10%)/ NEt_3 (5%) to give an orange oil, 313 mg, 68% yield.

Yield: 313 mg, 68%. **^{1}H NMR** (400 MHz, Dimethyl sulfoxide-d_6) δ 9.40 (s, 1H), 8.62 (s, 1H), 7.97 (d, J = 9.2 Hz, 1H), 7.92 (d, J = 2.2 Hz, 1H), 7.53 (dd, J = 9.2, 2.2 Hz, 1H), 3.56 – 3.47 (m, 1H), 3.10 – 2.99 (m, 3H), 2.93 (s, 5H), 1.66 – 1.48 (m, 4H), 1.18 (d, J = 6.5 Hz, 3H), 1.12 (t, J = 7.2 Hz, 6H). **^{13}C NMR** (101 MHz, Dimethyl sulfoxide-d_6) δ 140.47, 139.38, 138.79, 138.67, 130.61, 127.23, 126.25, 125.55, 124.01, 55.24, 50.92, 46.45, 46.30, 35.02, 31.32, 20.25, 17.77, 8.55 (d, J = 1.7 Hz). **HRMS** (ESI) calcd. for $C_{19}H_{30}ClN_4O_2$ [M+H$^-$]: 349.2153, found: 349.2143.

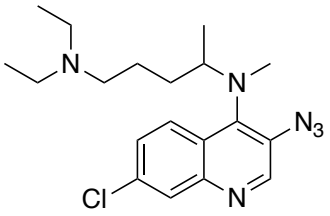

N^4-(3-azido-7-chloroquinolin-4-yl)-N^1,N^1-diethyl-N^4-methylpentane-1,4-diamine (4.17)

7-chloro-N^4-(5-(diethylamino)pentan-2-yl)-N^4-methylquinoline-3,4-diamine (330 mg, 0.95 mmol) is dissolved in a solution of concentrated sulfuric acid 98% and H_2O (3.2 M). The resultant solution is cooled to 0°C; to this, a sodium nitrite solution in H_2O (2.5 M) is added dropwise with stirring. The solution was stirred at this temperature for 5 min. Then a solution of sodium azide in H_2O (4.5 M) is added to it with vigorous stirring. The mixture was stirred for 5 minutes at 0°C. The reaction mixture is then quenched with sat. $NaCO_3$ and extracted with EtOAc (3 X 25 mL). The combined extracts are rinsed with brine and dried over anhydrous $MgSO_4$ and solvent is removed under reduced pressure to reveal a dark orange oil. This oil is purified by column chromatography with the solvent system: 65% EtOAc, 35% Hex, 5% NEt_3 to reveal a dark orange oil, 101 mg, 28%.

Yield: 101 mg, 28%. **^{1}H NMR** (500 MHz, Chloroform-*d*) δ 8.67 (s, 1H), 8.00 (d, *J* = 2.2 Hz, 1H), 7.98 (d, *J* = 9.0 Hz, 1H), 7.42 (dd, *J* = 9.0, 2.2 Hz, 1H), 3.49 (q, *J* = 6.4 Hz, 1H), 2.49 (q, *J* = 7.2 Hz, 4H), 2.38 (t, *J* = 7.3 Hz, 2H), 1.69 – 1.61 (m, 1H), 1.53 – 1.43 (m, 3H), 1.21 (d, *J* = 6.5 Hz, 3H), 0.98 (t, *J* = 7.1 Hz, 6H). **^{13}C NMR** (126 MHz, Chloroform-*d*) δ 147.93, 146.13, 145.08, 134.30, 128.91, 128.14, 127.48, 125.96, 125.91, 58.61, 53.02, 46.94, 35.52, 32.74, 24.11, 17.90, 11.54. **IR** (cm^{-1}) 2966.6, 2933.2, 2110.6, 1559.3, 1451.4, 1381.8, 1319.9, 1073.4, 915.8. **HRMS** (ESI) calcd. for $C_{19}H_{28}ClN_6$ [M+H$^+$]: 375.2072, found: 375.2074.

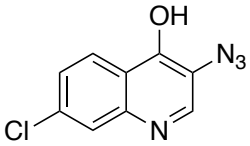

3-azido-7-chloroquinolin-4-ol (4.18)

See procedure for **4.17** and **4.18** was a precipitate that was filtered, washed with H_2O and dried under house vacuum overnight to give a brown solid, 81.1 mg, 39%.

Yield: 81.1 mg, 39%. **^{1}H NMR** (500 MHz, Dimethyl sulfoxide-d_6) δ 12.23 (d, J = 6.2 Hz, 1H), 8.11 (d, J = 8.7 Hz, 1H), 7.95 (d, J = 6.3 Hz, 1H), 7.63 (d, J = 2.0 Hz, 1H), 7.38 (dd, J = 8.7, 2.0 Hz, 1H). **^{13}C NMR** (126 MHz, Dimethyl sulfoxide-d_6) δ 171.72, 139.35, 136.45, 130.19, 127.04, 124.10, 122.37, 120.30, 117.71. **IR** (cm^{-1}) 3075.6, 2124.7, 1627.9, 1558.2, 1512.3, 1460.4, 1350.8, 1188.7, 1075.2, 812.8. **HRMS** (ESI) calcd for $C_9H_5ClN_4O$ [M+Na^+]: 243.0044, found: 243.0043.

4.5.3 X-ray crystallography

Crystals for the ring-opened DBU adduct 1-(3-((7-chloroquinolin-4-yl)amino)propyl)azepan-2-one are grown from DCM and Hex. A large 0.1 mm x 0.1 mm x 0.06 mm prism is mounted on a glass fibre with epoxy resin. Single-crystal X-ray diffraction is then measured at RT with a BRUKER SMART CCD or BRUKER APEX-II CCD diffractometer by using graphite-monochromated $Mo_{K\alpha}$ radiation (λ = 0.71073 Å). The crystal crystallizes in the monoclinic space group $P2_1/c$ with the unit cell parameters a = 10.65(2); b = 16.68(3); c = 10.68(2) Å and α = γ = 90 and β = 116.34(3) ° which corresponds to V = 1700.0(6) Å^3 and Z = 4. SAINT is used for integration of the intensity reflections and scaling and SADABS for absorption correction. A combination of intrinsic phasing and direct methods were used for solving the structure which were subsequently anisotropically refined after all non-hydrogen atoms were located by difference Fourier maps and final solution refinements are solved by full-matrix least-squares method on F^2

of all data, by using SHELXTL software. The hydrogen atoms are placed in calculated positions. The final refinement has R_1 = 0.0340 and S_{gof} = 1.167.

4.5.4 UV-Vis Studies

A 2.4 mg of 3-N_3MeCQ is dissolved in 30 mL of MeOH to make a 213.4 μM stock solution. Then 2.9 mg of 3-N_3MeCQ is dissolved in 1 mL of MeOH and the resulting mixture is diluted with 29 mL of H_2O to make a 257.8 μM stock solution. A 3.8 mg of GlyGlyGly is dissolved in 30 mL deionized H_2O to make a 669.6 μM stock solution. Then 6.5 mg of *N*-Phenylmaleimide was dissolved in 30 mL of MeOH to make a 1,251.2 μM stock solution.

General procedure

A 2 mL blank solution of deionized H_2O or MeOH in a 4 mL quartz cuvette is taken in an Agilent UV-Vis Spectrophotometer for the area 190 nm – 1100 nm. To a different 4 mL quartz cuvette is added 333 μL of the 257.8 μM stock solution and 1,667 μL of deionized H_2O to make a 42.97 μM 3-N_3MeCQ solution. This is thoroughly mixed using a micropipette to make a homogeneous solution. A stir bar is placed in the cuvette and the cuvette is capped and placed in a cuvette holder fitted with a 365 nm penlight and the setup is then covered with aluminum foil. The control spectrum is measured with the light off. The experiment is then started in kinetics mode for a spectrum to be taken every 10 seconds for 300 seconds whilst the light is on and the solution is stirring. When the experiment is finished the resulting solution is transferred into a 2mL Eppendorf tube for mass spectroscopy.

To a different 4 mL quartz cuvette the stock 3-N_3MeCQ solution is diluted with deionized H_2O or MeOH to make the desired concentrated solution. This is thoroughly mixed using a micropipette to make a homogeneous solution. A stir bar is placed in the cuvette and the cuvette is capped and placed in a cuvette holder fitted with a 365 nm penlight and the setup is then covered with aluminum foil. The control spectrum is measured with the light off. The experiment is then started in kinetics mode for a spectrum to be taken every 10 seconds for 300 seconds whilst the light is on and the solution is stirring. When the experiment is finished the resulting solution is transferred into a 2 mL Eppendorf tube for mass spectroscopy.

Insertion experiments

21.49 μM 3-N_3MeCQ and GlyGlyGly in H_2O (1:1)

5,000 μL of the 257.8 μM 3-N_3MeCQ stock solution is further diluted into 30 mL of deionized H_2O to make a 42.97 μM solution, and 1,000 μL of this solution is then transferred into a 4 mL quartz cuvette. 2,000 μL of the 669.6 μM GlyGlyGly stock solution is further diluted into 30 mL of deionized H_2O to make a 44.64 μM and 1,000 μL of this solution is added into the above 4 mL cuvette to give final concentrations of 21.49 μM and 22.32 μM of 3-N_3MeCQ and GlyGlyGly respectively. The kinetics experiment is run as mentioned above.

4.29 μM 3-N_3MeCQ and GlyGlyGly in H_2O (1:9.4)

200 μL of the freshly made 42.97 μM 3-N_3MeCQ solution is transferred into a 4 mL quartz cuvette. To this is added 1,800 μL of the freshly made 44.64 μM GlyGlyGly solution to give final concentrations of 4.29 μM and 40.18 μM of 3-N_3MeCQ and GlyGlyGly, respectively. The kinetics experiment is run as mentioned above.

19.56 μM 3-N_3MeCQ and *N*-Phenylmaleimide in MeOH (1:1)

5,000 μL of the 213.4 μM 3-N_3MeCQ stock solution is further diluted into 30 mL of MeOH to make a 35.57 μM solution and 1,100 μL of this solution is then transferred into a 4 mL quartz cuvette. 1,000 μL of the 1,251.2 μM *N*-Phenylmaleimide stock solution is further diluted into 30 mL of MeOH to make a 41.71 μM solution and 900 μL of this solution is added into the above 4 mL cuvette to give final concentrations of 19.56 μM and 18.78 μM of 3-N_3MeCQ and *N*-Phenylmaleimide respectively. The kinetics experiment is run as mentioned above.

7.11 μM 3-N_3MeCQ and *N*-Phenylmaleimide in MeOH (1:4.7)

400 μL of the freshly made 35.57 μM 3-N_3MeCQ solution is transferred into a 4 mL quartz cuvette. To this is added 1,600 μL of the freshly made 41.71 μM *N*-Phenylmaleimide solution to give final concentrations of 7.11 μM and 33.37 μM of 3-N_3MeCQ and *N*-Phenylmaleimide, respectively. The kinetics experiment is run as mentioned above.

3.56 μM 3-N_3MeCQ and *N*-Phenylmaleimide in MeOH (1:10.6)

200 μL of the freshly made 35.57 μM 3-N_3MeCQ solution is transferred into a 4 mL quartz cuvette. To this is added 1,800 μL of the freshly made 41.71 μM *N*-Phenylmaleimide solution to give final concentrations of 3.56 μM and 37.54 μM of 3-N_3MeCQ and *N*-Phenylmaleimide, respectively. The kinetics experiment is run as mentioned above.

4.5.5 NMR experiments

General procedure

In a 0.5-dram vial is added 3-N_3MeCQ, the electron acceptor and 500 μL of deuterated MeOH. This is thoroughly mixed to make a homogenous solution. This mixture is then transferred into an 8" NMR tube fitted with a stir bar. A 365 nm penlight is positioned 5 cm from the NMR tube. In a dark fume hood with the setup covered in aluminum foil, the solution is let stir exposed to 365 nm for 6 to 9 minutes. Once the time elapses the stir bar is removed and a ^{1}H NMR spectrum is measured.

3-N_3MeCQ and *N*-Phenylmaleimide

5 mg of 3-N_3MeCQ and 2.3 mg of *N*-Phenylmaleimide were used and irradiated for 6 minutes.

N-Phenylmaleimide

2.3 mg of *N*-Phenylmaleimide used and irradiated for 9 minutes.

3-N_3MeCQ and Tetracyanoethylene

5 mg of 3-N_3MeCQ and 2.3 mg of Tetracyanoethylene were used and irradiated for 9 minutes.

4.6 References

(1) Slater, A. F. G. Chloroquine: Mechanism of Drug Action and Resistance in Plasmodium Falciparum. *Pharmacol. Ther.* **1993**, *57* (2–3), 203–235.

(2) Drinkwater, N.; McGowan, S. From Crystal to Compound: Structure-Based Antimalarial Drug Discovery. *Biochem. J.* **2014**, *461* (3), 349–369.

(3) Sullivan, D. J. Quinolines Block Every Step of Malaria Heme Crystal Growth. *Proc. Natl. Acad. Sci.* **2017**, *114* (29), 7483–7485.

(4) Kapishnikov, S.; Staalsø, T.; Yang, Y.; Lee, J.; Pérez-Berná, A. J.; Pereiro, E.; Yang, Y.; Werner, S.; Guttmann, P.; Leiserowitz, L.; Als-Nielsen, J. Mode of Action of Quinoline Antimalarial Drugs in Red Blood Cells Infected by Plasmodium Falciparum Revealed in Vivo. *Proc. Natl. Acad. Sci. U. S. A.* **2019**, *116* (46), 22946–22952.

(5) Bray, P. G.; Park, B.; Asadollaly, E.; Biagini, G.; Jeyadevan, J.; Berry, N.; Ward, S.; O' Neill, P. A Medicinal Chemistry Perspective on 4-Aminoquinoline Antimalarial Drugs. *Curr. Top. Med. Chem.* **2006**, *6* (5), 479–507.

(6) Foley, M.; Deady, L. W.; Ng, K.; Cowman, A. F.; Tilley, L. Photoaffinity Labeling of Chloroquine-Binding Proteins in Plasmodium Falciparum. *J. Biol. Chem.* **1994**, *269* (9), 6955–6961.

(7) Mueller, D. M.; Hudson, R. A.; Lee, C.-P. Azide Photoaffinity Analogs for Acridine Dye Binding Sites. *J. Am. Chem. Soc.* **1981**, *103* (7), 1860–1862.

(8) Desneves, J.; Thorn, G.; Berman, A.; Galatis, D.; La Greca, N.; Sinding, J.; Foley, M.; Deady, L. W.; Cowman, A. F.; Tilley, L. Photoaffinity Labeling of Mefloquine-Binding Proteins in Human Serum, Uninfected Erythrocytes and Plasmodium Falciparum-Infected Erythrocytes. *Mol. Biochem. Parasitol.* **1996**, *82* (2), 181–194.

(9) Lekostaj, J. K.; Natarajan, J. K.; Paguio, M. F.; Wolf, C.; Roepe, P. D. Photoaffinity Labeling of the Plasmodium Falciparum Chloroquine Resistance Transporter with a Novel Perfluorophenylazido Chloroquine †. *Biochemistry* **2008**, *47* (39), 10394–10406.

(10) Edaye, S.; Tazoo, D.; Bohle, D. S.; Georges, E. 3-Iodo-4-Aminoquinoline Derivative Sensitises Resistant Strains of Plasmodium Falciparum to Chloroquine. *Int. J. Antimicrob. Agents* **2016**, *47* (6), 482–485.

(11) Edaye, S.; Tazoo, D.; Bohle, D. S.; Georges, E. 3-Halo Chloroquine Derivatives Overcome Plasmodium Falciparum Chloroquine Resistance Transporter-Mediated Drug Resistance in P. Falciparum. *Antimicrob. Agents Chemother.* **2015**, *59* (12), 7891–7893.

(12) Ribas, X.; Güell, I. Cu(I)/Cu(III) Catalytic Cycle Involved in Ullmann-Type Cross-Coupling Reactions. *Pure Appl. Chem.* **2014**, *86* (3), 345–360.

(13) Andersen, J.; Bolvig, S.; Liang, X. Efficient One-Pot Synthesis of 1-Aryl 1,2,3-Triazoles from Aryl Halides and Terminal Alkynes in the Presence of Sodium Azide. *Synlett* **2005**, *2005* (19), 2941–2947.

(14) Lanke, S. R.; Bhanage, B. M. Copper Bis(2,2,6,6-Tetramethyl-3,5-Heptanedionate)–Catalyzed Coupling of Sodium Azide with Aryl Iodides/Boronic Acids to Aryl Azides or Aryl Amines. *Synth. Commun.* **2014**, *44* (3), 399–407.

(15) Zhu, W.; Ma, D. Synthesis of Aryl Azides and Vinyl Azides via Proline-Promoted CuI-Catalyzed Coupling Reactions. *Chem. Commun.* **2004**, No. 7, 888–889.

(16) Markiewicz, J. T.; Wiest, O.; Helquist, P. Synthesis of Primary Aryl Amines Through a Copper-Assisted Aromatic Substitution Reaction with Sodium Azide. *J. Org. Chem.* **2010**, *75* (14), 4887–4890.

(17) Messaoudi, S.; Brion, J.-D.; Alami, M. An Expeditious Copper-Catalyzed Access to 3-

Aminoquinolinones, 3-Aminocoumarins and Anilines Using Sodium Azide. *Adv. Synth. Catal.* **2010**, *352* (10), 1677–1687.

(18) Goriya, Y.; Ramana, C. V. The [Cu]-Catalyzed SNAR Reactions: Direct Amination of Electron Deficient Aryl Halides with Sodium Azide and the Synthesis of Arylthioethers under Cu(II)–Ascorbate Redox System. *Tetrahedron* **2010**, *66* (38), 7642–7650.

(19) Qin, Z.; Kastrati, I.; Chandrasena, R. E. P.; Liu, H.; Yao, P.; Petukhov, P. A.; Bolton, J. L.; Thatcher, G. R. J. Benzothiophene Selective Estrogen Receptor Modulators with Modulated Oxidative Activity and Receptor Affinity. *J. Med. Chem.* **2007**, *50* (11), 2682–2692.

(20) Gehringer, M.; Forster, M.; Pfaffenrot, E.; Bauer, S. M.; Laufer, S. A. Novel Hinge-Binding Motifs for Janus Kinase 3 Inhibitors: A Comprehensive Structure-Activity Relationship Study on Tofacitinib Bioisosteres. *ChemMedChem* **2014**, *9* (11), 2516–2527.

(21) Kaila, N.; Green, N.; Li, H.-Q.; Hu, Y.; Janz, K.; Gavrin, L. K.; Thomason, J.; Tam, S.; Powell, D.; Cuozzo, J.; Hall, J. P.; Telliez, J.-B.; Hsu, S.; Nickerson-Nutter, C.; Wang, Q.; Lin, L.-L. Identification of a Novel Class of Selective Tpl2 Kinase Inhibitors: 4-Alkylamino-[1,7]Naphthyridine-3-Carbonitriles. *Bioorg. Med. Chem.* **2007**, *15* (19), 6425–6442.

(22) Rahman, M.; Kundu, D.; Hajra, A.; Majee, A. Formylation without Catalyst and Solvent at 80°C. *Tetrahedron Lett.* **2010**, *51* (21), 2896–2899.

(23) Kim, J.-G.; Jang, D. Facile and Highly Efficient N-Formylation of Amines Using a Catalytic Amount of Iodine under Solvent-Free Conditions. *Synlett* **2010**, *2010* (14), 2093–2096.

(24) Shastri, L. A.; Shastri, S. L.; Bathula, C. D.; Basanagouda, M.; Kulkarni, M. V. Mild, Simple, and Efficient Method for N -Formylation of Secondary Amines via Reimer–Tiemann Reaction. *Synth. Commun.* **2011**, *41* (4), 476–484.

(25) Collet, J. W.; Ackermans, K.; Lambregts, J.; Maes, B. U. W.; Orru, R. V. A.; Ruijter, E. Modular Three-Component Synthesis of 4-Aminoquinolines via an Imidoylative Sonogashira/Cyclization Cascade. *J. Org. Chem.* **2018**, *83* (2), 854–861.

(26) Pajkert, R.; Böttcher, T.; Ponomarenko, M.; Bremer, M.; Röschenthaler, G.-V. Synthesis and Characterization of Novel Carbene Complexes of Phosphorus(V) Fluorides with Potential Liquid-Crystalline Properties. *Tetrahedron* **2013**, *69* (42), 8943–8951.

(27) Sánchez-Martín, R.; Campos, J. M.; Conejo-García, A.; Cruz-López, O.; Báñez-Coronel, M.; Rodríguez-González, A.; Gallo, M. A.; Lacal, J. C.; Espinosa, A. Symmetrical Bis-Quinolinium Compounds: New Human Choline Kinase Inhibitors with Antiproliferative Activity against the HT-29 Cell Line. *J. Med. Chem.* **2005**, *48* (9), 3354–3363.

(28) Rodrigues, T.; Guedes, R. C.; dos Santos, D. J. V. A.; Carrasco, M.; Gut, J.; Rosenthal, P. J.; Moreira, R.; Lopes, F. Design, Synthesis and Structure–Activity Relationships of (1H-Pyridin-4-Ylidene)Amines as Potential Antimalarials. *Bioorg. Med. Chem. Lett.* **2009**, *19* (13), 3476–3480.

(29) Natarajan, J. K.; Alumasa, J. N.; Yearick, K.; Ekoue-Kovi, K. A.; Casabianca, L. B.; De Dios, A. C.; Wolf, C.; Roepe, P. D. 4-N-, 4-S-, and 4-O-Chloroquine Analogues: Influence of Side Chain Length and Quinolyl Nitrogen PKa on Activity vs Chloroquine Resistant Malaria. *J. Med. Chem.* **2008**, *51* (12), 3466–3479.

(30) Shi, M.; Shen, Y. A Novel Reaction of 1,8-Diazabicyclo[5.4.0]Undec-7-Ene (DBU) or 1,5-Diazabicyclo[4.3.0]Non-5-Ene (DBN) with Benzyl Halides in the Presence of Water. *Helv. Chim. Acta* **2002**, *85* (5), 1355.

(31) Kraft, A. Branched Non-Covalent Complexes between Carboxylic Acids and Two Tris(Amidines). *J. Chem. Soc. Perkin Trans. 1* **1999**, No. 6, 705–714.

(32) Hyde, A. M.; Calabria, R.; Arvary, R.; Wang, X.; Klapars, A. Investigating the Underappreciated Hydrolytic Instability of 1,8-Diazabicyclo[5.4.0]Undec-7-Ene and Related Unsaturated Nitrogenous Bases. *Org. Process Res. Dev.* **2019**, *23* (9), 1860–1871.

(33) Sather, A. C.; Lee, H. G.; De La Rosa, V. Y.; Yang, Y.; Müller, P.; Buchwald, S. L. A Fluorinated Ligand Enables Room-Temperature and Regioselective Pd-Catalyzed Fluorination of Aryl Triflates and Bromides. *J. Am. Chem. Soc.* **2015**, *137* (41), 13433–13438.

(34) Sinha, M.; Dola, V. R.; Soni, A.; Agarwal, P.; Srivastava, K.; Haq, W.; Puri, S. K.; Katti, S. B. Synthesis of Chiral Chloroquine and Its Analogues as Antimalarial Agents. *Bioorg. Med. Chem.* **2014**, *22* (21), 5950–5960.

(35) Johnson, W. S.; Buell, B. G. A New Synthesis of Chloroquine. *J. Am. Chem. Soc.* **1952**, *74* (18), 4513–4516.

(36) Gorlitzer, K.; Kramer, C.; Meyer, H.; Walter, R. D.; Jomaa, H.; Wiesner, J. Pyrido[3,2-b]Indol-4-Yl-Amine – Synthese Und Prufung Auf Wirksamkeit Gegen Malaria. *Die Pharm. - An Int. J. Pharm. Sci.* **2004**, *59* (4), 243–250.

(37) Liu, Y.; Zhang, Z.; Wu, A.; Yang, X.; Zhu, Y.; Zhao, N. A Novel Process for Antimalarial Drug Pyronaridine Tetraphosphate. *Org. Process Res. Dev.* **2014**, *18* (2), 349–353.

(38) Elslager, E. F.; Gold, E. H.; Tendick, F. H.; Werbel, L. M.; Worth, D. F. Amodiaquine N-Oxides and Other 7-Chloro-4-Aminoquinoline n-Oxides. *J. Heterocycl. Chem.* **1964**, *1* (1), 6–12.

(39) Wang, X.; Pan, W.; Cai, Y.; Xie, X.; Huang, C.; Li, J.; Chen, W.; He, M. Microwave-Assisted Efficient Synthesis of 4-Substituted Amino-2-Methylquinolines Catalyzed by p-Toluenesulfonic Acid. *Heterocycles* **2016**, *92* (10), 1864.

(40) Bayley, H.; Staros, J. V. Photoaffinity Labeling and Related Techniques. In *Azides and Nitrenes*; Elsevier, 1984; pp 433–490.

(41) Vezmar, M.; Georges, E. Direct Binding of Chloroquine to the Multidrug Resistance Protein (MRP). *Biochem. Pharmacol.* **1998**, *56* (6), 733–742.

(42) Baruah, H.; Puthenveetil, S.; Choi, Y.-A.; Shah, S.; Ting, A. Y. An Engineered Aryl Azide Ligase for Site-Specific Mapping of Protein-Protein Interactions through Photo-Cross-Linking. *Angew. Chemie Int. Ed.* **2008**, *47* (37), 7018–7021.

(43) Berman, A.; Shearing, L. N.; Ng, K. F.; Jinsart, W.; Foley, M.; Tilley, L. Photoaffinity Labelling of Plasmodium Falciparum Proteins Involved in Phospholipid Transport. *Mol. Biochem. Parasitol.* **1994**, *67* (2), 235–243.

(44) Wang, J.; Burdzinski, G.; Platz, M. S. Ultrafast Time-Resolved Studies of the Photochemistry of Aryl Azides. In *Nitrenes and Nitrenium Ions*; 2013; pp 1–31.

(45) Vyas, S.; Winter, A. H.; Hadad, C. M. Theory and Computation in the Study of Nitrenes and Their Excited-State Photoprecursors. In *Nitrenes and Nitrenium Ions*; John Wiley & Sons, Inc.: Hoboken, NJ, USA, 2013; pp 33–76.

(46) Bräse, S.; Banert, K. *Organic Azides*; Brse, S., Banert, K., Eds.; John Wiley & Sons, Ltd: Chichester, UK, 2009.

(47) Zott, H.; Heusinger, H. Photolysis of Maleic Anhydride and Maleimides in Solution Studied by Electron Spin Resonance. *Radiat. Phys. Chem.* **1977**, *10* (5–6), 297–302.

(48) Kiselev, V. D.; Kashaeva, H. A.; Potapova, L. N.; Kornilov, D. A.; Latypova, L. I.; Konovalov, A. I. Hydrophobic Acceleration in the Diels—Alder Reaction of 9-Hydroxymethylanthracene with N-Phenylmaleimide. *Russ. Chem. Bull.* **2016**, *65* (9), 2202–2205.

(49) Murata, S.; Abe, S.; Tomioka, H. Photochemical Reactions of Mesityl Azide with Tetracyanoethylene: Competitive Trapping of Singlet Nitrene and Didehydroazepine. *J. Org. Chem.* **1997**, *62* (10), 3055–3061.

Chapter 5

The Determination of Heme and Chloroquine Interactions with *Plasmodium falciparum* Chloroquine Resistance Transporter (PfCRT)

5.1 Preamble

In the previous chapter, the synthesis and utilization of our photoaffinity label was described. This label is expected to cross-link to PfCRT. PfCRT contains several point mutations that have been directly linked to CQ resistance. There is much debate about this protein's function, whether it acts as a transporter or channel and if it is energy coupled.[1] There is also evidence of cross-resistance between different classes of antimalarials, and the mechanism of substrate recognition is also poorly understood.[2] As our photoaffinity label contains minor modifications compared to CQ, this possibly avoids unnecessary interactions with surrounding proteins. PfCRT has been isolated, and its cryo-electron microscopy structure was determined for the first time.[3] Therefore, before embarking on photoaffinity labelling on PfCRT, we wanted to determine the binding interactions and binding affinity of PfCRT with CQ and heme. In collaboration with the Fidock group who provided PfCRT isoform, we carried out fluorescence and UV-Vis studies. These studies were carried out in buffers of pH 7.0 – 8.0, which is within the range of cytosolic pH. The challenge with carrying out this assay is that PfCRT is a transmembrane protein with one side exposed to pH 5.2 and the other at pH 7.4. Therefore we chose to model the cytosolic pH.

5.2 Introduction

CQ, first synthesized in 1934, revolutionized antimalarial therapy. It was viewed as the drug that would eradicate malaria. Unfortunately, in the early 1960s, resistance to CQ was discovered.[4] A tremendous amount of effort has been made in determining the antimalarial mechanism of CQ and the origin of its resistance.[5–9] The structure of hemozoin which is a biomineralization byproduct synthesized by the parasite to detoxify free heme in the DV was solved in 2000.[10] A lysine to

threonine mutation at position 76 (K76T) on the PfCRT is a biomarker for CQ resistance that was also discovered in 2000.[6] PfCRT has been sequenced, and there has been much speculation on the mechanism in which the protein recognizes antimalarial drugs. Moreover, for the first time, a PfCRT isoform of CQ-resistant 7G8 parasites was isolated using single-particle cryo-electron microscopy and antigen-binding technology in 2019.[3] The nanodisc-incorporated PfCRT 7G8 isoform was solved at 3.2 Å.

The isolated PfCRT isoform is a 424 amino acid protein with a molecular weight of 48 kDa. It is a monomeric transmembrane protein that consists of ten transmembrane (TM) helices and two juxtamembrane helices. One is exposed to the parasite cytosol and the other to the DV (**Figure 5.1**). The transmembrane domains form 5 helical pairs, and TM1-4 and 6-9 form a central cavity of around 3,300 Å^3. The K76T mutation is located within the lining of the cavity. The cavity has a net negative charge influenced by three aspartate residues, suggesting positively charged substrates in acidic media.[3]

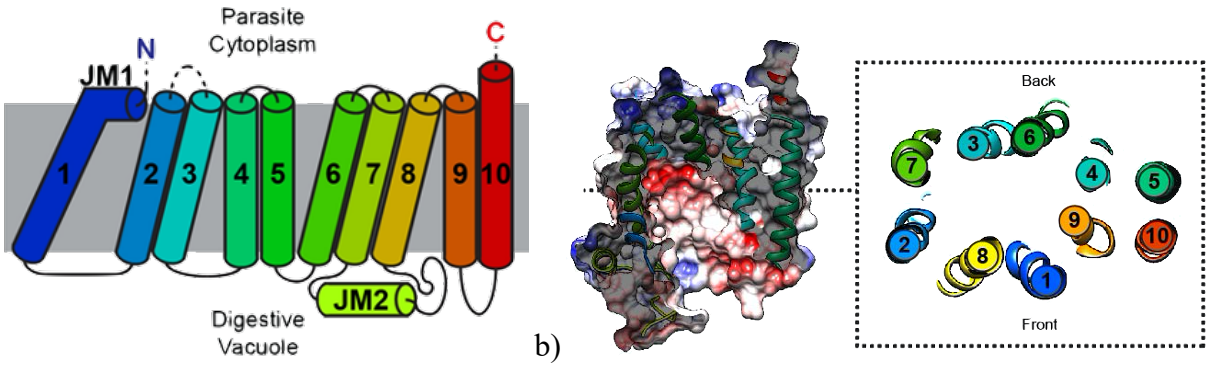

Figure 5.1. Structure of PfCRT 7G8 isoform. A) Topology showing inverted antiparallel TM helices. B) Surface representation of the electrostatic potential of the central cavity with red and blue indicating negative and positive residues, respectively. Figures adapted from Kim *et al.*[3]

In this chapter, fluorescence spectroscopy and ultraviolet-visible spectroscopy were two techniques used to determine interactions between CQ and heme with PfCRT are described. Including two control substrates: empty nanodisc (1D1), which has the same lipid membrane used for PfCRT filled with lipids and unrelated GtrB from an enterobacteria phage enclosed in a different nanodisc (1E3D1). This ensemble will be referred to as membrane proteins and lipid membrane ensemble (MPLME).

5.3 Results and Discussion

In collaboration with Prof. David Fidock's lab, we were generously gifted PfCRT 7G8 isoform, nanodisc and GtrB. It was first believed that the cavity with a volume of 3,300 $Å^3$ was large enough to transport out the CQ - heme complex that forms within the DV. CQ and hemin have approximate volumes of 396 $Å^3$ and 702 $Å^3$, respectively (as estimated from crystallographic results). We began with binding studies of the individual drugs with the ensembles to determine possible recognition of CQ or heme with the transporter protein. To determine the interactions between CQ, heme and PfCRT, we carried out some fluorescence titration assays.

5.3.1 Fluorescence Studies

5.3.1.1 Fluorescence studies with CQ

Fluorescence spectroscopy is a very useful tool in determining protein-drug interactions.[11] It is proposed that CQ is transported out of the DV by PfCRT, which will entail recognition, binding and transport.[2,6] The observed PfCRT fluorescence primarily originates from tryptophan (Trp) 280 and 316, with the empty nanodisc contains 2 Trp residues and GtrB 3 Trp residues. As Trp emission is highly sensitive to its microenvironment, changes in fluorescence are used to determine protein-drug interactions.[12] PfCRT's two Trp residues are located in the juxtamembrane, two and TM eight, exposed to the DV, **Figure 5.1**. Fluorescence quenching and shifts in the emission wavelength typically indicate protein binding or collisional quenching by the drug.

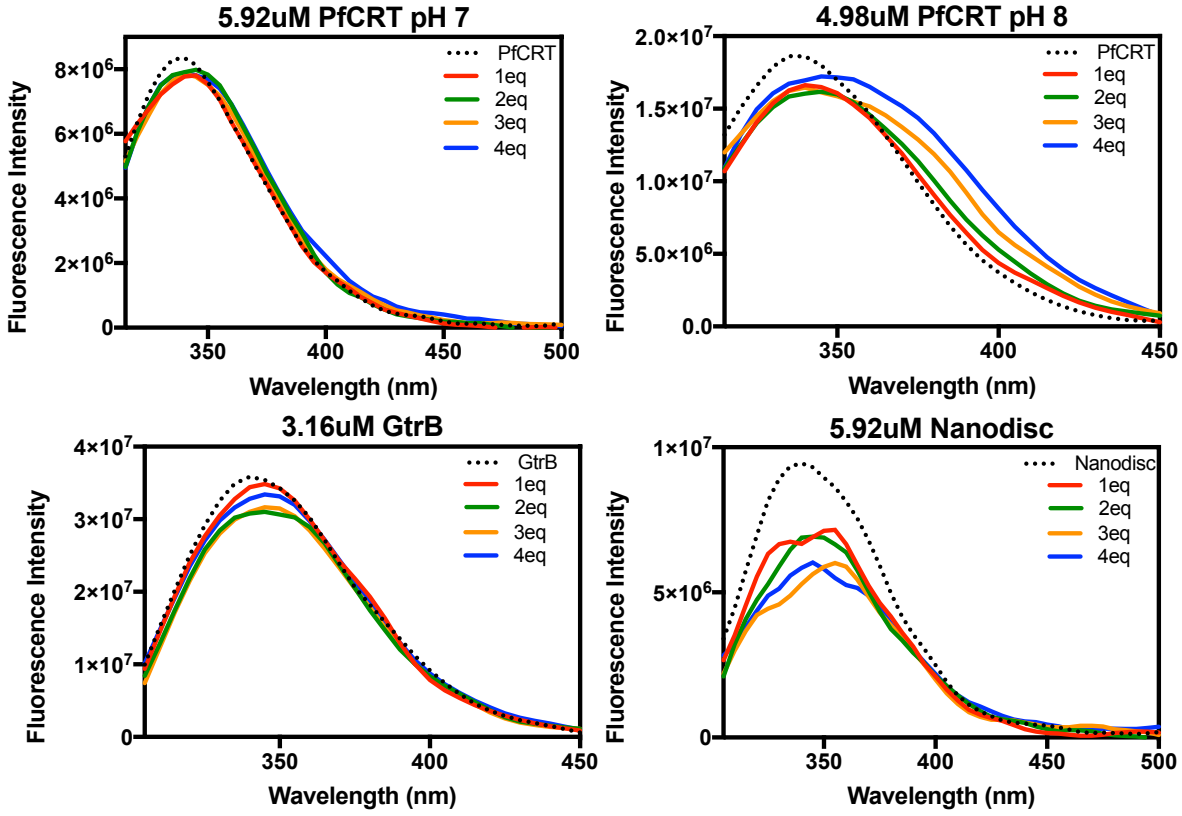

Figure 5.2. Effect of 4 equivalent of CQ on the emission spectrum of PfCRT at pH 7, PfCRT at pH 8, GtrB and nanodisc.

We assayed PfCRT at pH 7 and pH 8, GtrB at pH 7 and nanodisc at pH 7 with $CQ{\cdot}2H_3PO_4$ (in solution as CQH^{2+}). As shown in **Figure 5.2**, increasing amounts of CQ, up to 4 equivalents, causes a slight decrease in emission energy, and this decrease is more pronounced in empty nanodisc. Furthermore, we observe the following shifts in the fluorescence maxima: PfCRT pH 8 10 nm red shift, GtrB 5 nm red shift and nanodisc 5 nm red shift. The fluorescence quenching constant was analyzed using the Stern-Volmer equation[11] (1):

$$\frac{F_0}{F} = 1 + k_q \tau_0 [Q] = 1 + K_{SV}[Q]$$

where F_0 and F are the fluorescence intensities of the protein in the absence and presence of the quencher, respectively, k_q is the bimolecular quenching constant, τ_0 is the protein unquenched lifetime, K_{SV} is the Stern-Volmer quenching constant and $[Q]$ is the concentration of the quencher.

Table 5.1. Stern-Volmer quenching constants for CQ.

PROTEIN	$K_{SV} \times 10^4$ (M^{-1})
PfCRT pH 7	0.14 ± 0.14
PfCRT pH 8	0.06 ± 0.31
GtrB	1.54 ± 0.41
Nanodisc	3.55 ± 0.44

Table 5.1 shows the K_{SV} values of our membrane proteins and lipid membrane ensemble (MPLME) and CQ. The higher the quenching constant, the stronger the association. The data shows that nanodisc has the highest quenching constant. In general, a linear plot suggests the occurrence of either static or dynamic quenching, **Figure 5.3**. Static quenching involves the formation of nonfluorescent complexes between the fluorophore and the quencher that occur in the ground state. Dynamic quenching, which occurs in the excited state, involves the diffusion of the fluorophore during the lifetime of the excited state. The fluorophore then returns to the ground state upon contact without emission of a photon. Both types of quenching mechanisms occur only through space contact between the fluorophore and quencher and do not result in a permanent change to the molecules involved.[11]

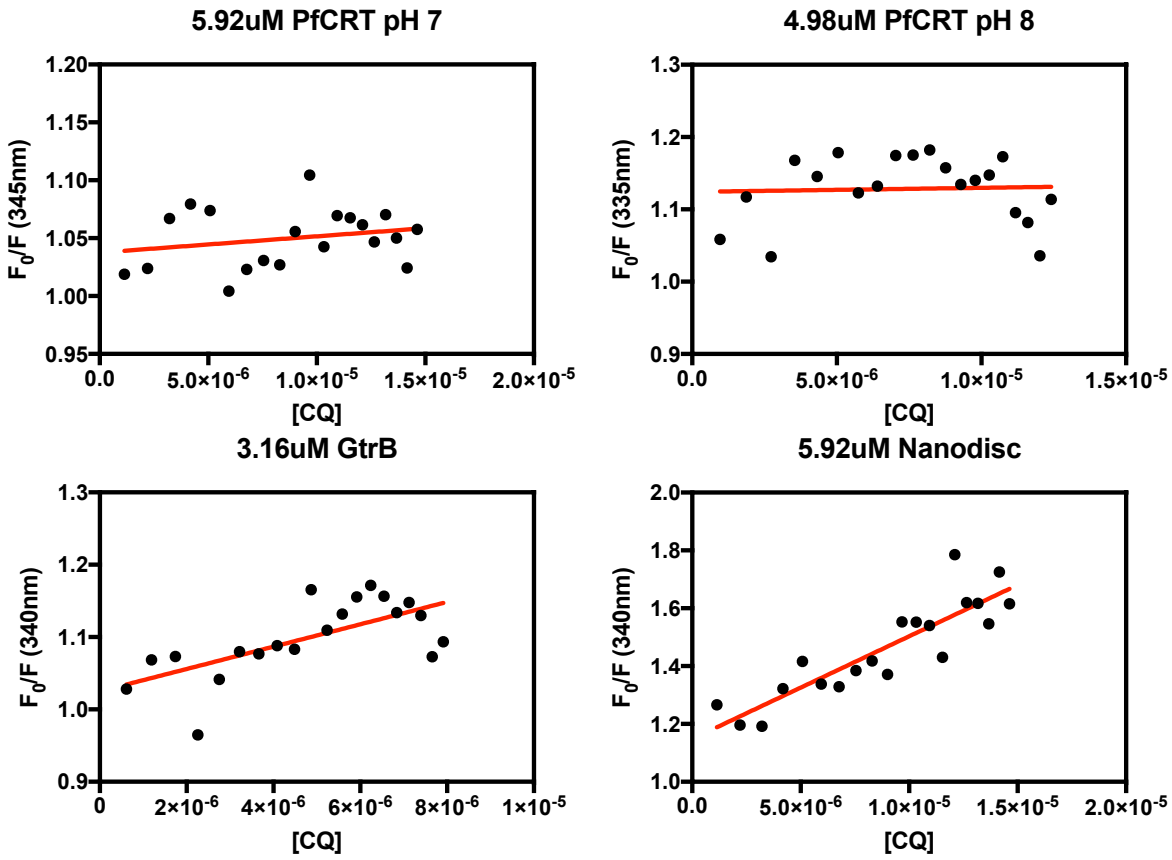

Figure 5.3. Stern-Volmer plots for PfCRT, GtrB and nanodisc quenched with up to 4 equivalents of CQ (each dot represents a 0.2 molar addition).

A factor affecting the specific quenching mechanism is the accessibility of the quencher to the fluorophore. The fraction of accessible fluorophores can be measured using the modified Stern-Volmer, equation (2):

$$\frac{F_0}{F_0 - F} = \frac{1}{\alpha K_a [Q]} + \frac{1}{\alpha}$$

Where F_0 and F are the fluorescence intensities in the presence and absence of the quencher, α is the fraction of accessible fluorophores, K_a is the effective quenching constant and $[Q]$ is the concentration of the quencher.

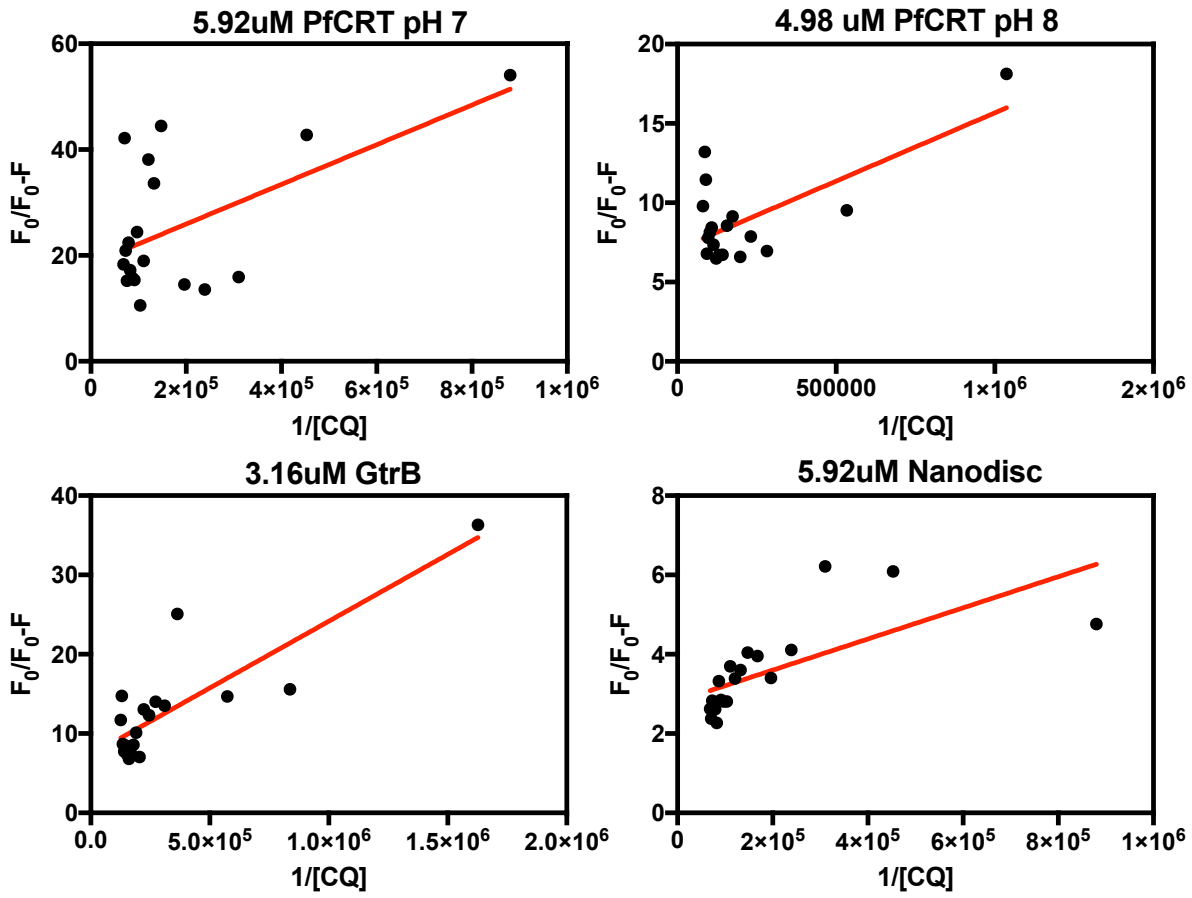

Figure 5.4. Modified Stern-Volmer plots for PfCRT, GtrB and nanodisc quenched with up to 4 equivalents of CQ (each dot represents a 0.2 molar addition).

The modified Stern-Volmer plots, shown in **Figure 5.4**, give an α value of 35% or less. In general, α values less than 100% are a result of fractional accessibility, which is due to the existence of at least two fluorophore populations with one that is accessible and the other is buried or inaccessible.[13] Each of these fluorophores would have varying K_{SV} values and are differently accessible to the quencher. The K_a value, in **Table 5.2**, is the effective quenching constant of accessible fluorophores, this is in accordance with the K_{SV} values in **Table 5.1**. CQ in nanodisc is exposed to the highest fraction of accessible fluorophores as it has the highest K_{SV} value. CQ has little accessibility to the Trp residues found in PfCRT at both pH 7 and 8.

Table 5.2. Modified Stern-Volmer constants for CQ.

PROTEIN	$K_a \times 10^5$ (M^{-1})	α (%)
PfCRT pH 7	4.92 ± 2.58	5.42
PfCRT pH 8	8.21 ± 3.09	14.16
GtrB	4.35 ± 4.79	13.65
Nanodisc	7.17 ± 2.62	35.51

Interestingly, there appears to be a concentration dependant response from the Stern-Volmer plot for PfCRT pH 7 and CQ, **Figure 5.5**. . The data points of 0 - 1 equiv. give K_{SV} of 1.69×10^{-4} M^{-1} and 1 - 4 equiv. of 0.19×10^{-4} M^{-1}. This may be due to conformational change following binding of one equivalent of CQ which reduces the accessibility of fluorophores to additional CQ. Similarly, for PfCRT pH 8 and CQ, data points of 0 – 2 equiv. give K_{SV} of 1.5×10^{-4} M^{-1}; however, 2 – 4 equiv. of -2.2×10^{-4} M^{-1},

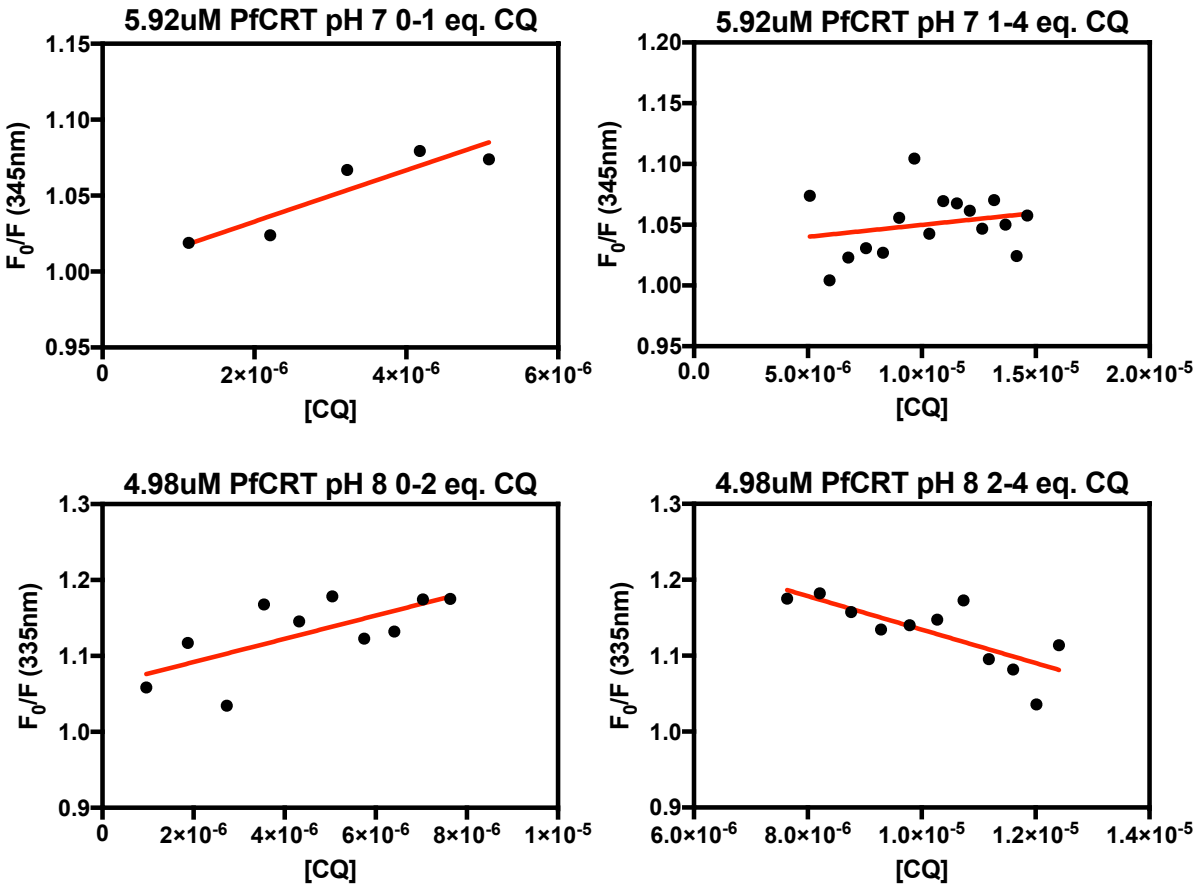

Figure 5.5. Concentration-dependent response of PfCRT to CQ.

To determine the number of binding sites for CQ present on the MPLME, we use the following equation (3)[14]:

$$\log\frac{F_0 - F}{F} = \log K_b \ + n \log [Q]$$

where F_0 and F are fluorescent intensities in the presence and absence of a quencher, K_b is the binding constant, n is the number of binding sites and $[Q]$ is the quencher concentration.

Table 5.3. Binding constant and number of binding sites for CQ with MPLME.

PROTEIN	$\log K_b$	n
PfCRT pH 7	0.06 ± 0.83	0.27 ± 0.16
PfCRT pH 8	0.01 ± 0.87	0.18 ± 0.17
GtrB	1.89 ± 0.58	0.54 ± 0.11
Nanodisc	3.05 ± 0.37	0.67 ± 0.07

Stronger binding interactions give higher $\log K_b$ values, and the values in **Table 5.3**. are in accordance with previous K_{SV} and K_a values. Nanodisc displays the strongest binding interactions with CQ in the ensemble, although with an n value of 0.67, we cannot conclusively say that nanodisc contains a binding site for CQ, **Figure 5.6**. PfCRT at both pH's form weak associations with CQ and does not have a specific CQ binding site. The control, GtrB, forms stronger associations with CQ than PfCRT; however, it does not contain a binding site for CQ.

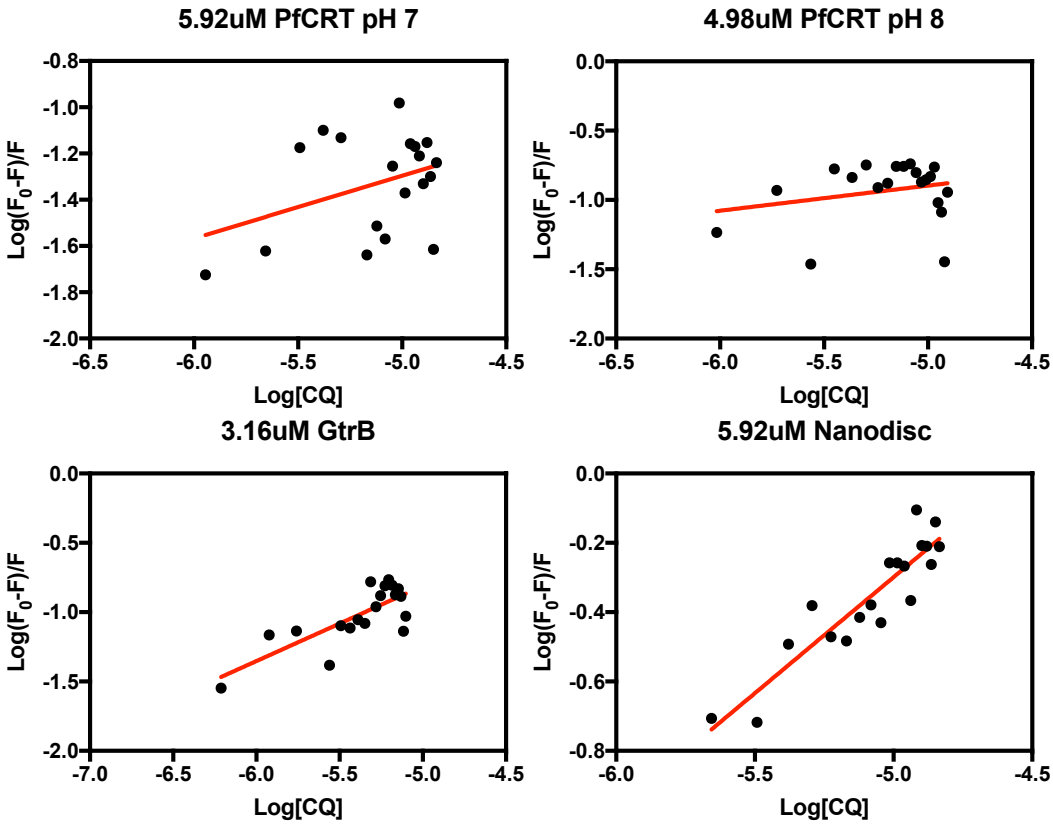

Figure 5.6. Binding plot to determine the number of CQ binding sites and binding constant.

All assays were carried out at 25°C at pH 7, except PfCRT at pH 8. At pH 7, CQ is approximately 65% diprotonated and 35% monoprotonated; however, at pH 8 CQ is approximately 83% monoprotonated and 17% diprotonated. Thus, the results showing a lower binding affinity for CQ at pH 8 than pH 7 are reasonable. Furthermore, it is known that the DV has a pH of approximately 5.2[15], this is the optimal condition for PfCRT activity, therefore it is not surprising that we do not see strong binding interactions or higher fractions of accessible fluorophores at pH 7. Furthermore, this supports the belief that PfCRT is responsible for CQ efflux from the DV, and not its influx as it does not bind CQ at cytosolic pH.[4,16]

5.3.1.2 Fluorescence studies with heme

Heme can form reversible non-covalent binding interactions with proteins and these interactions cause spectral changes that can be measured by UV-Vis and Fluorescence spectroscopy.[13] High-spin Fe^{3+} porphyrins are fluorescence quenchers due to their low-lying excited states and paramagnetism allowing for multiple relaxation pathways.[17] Therefore, any observed fluorescence quenching between heme and proteins results from non-covalent complex formation.

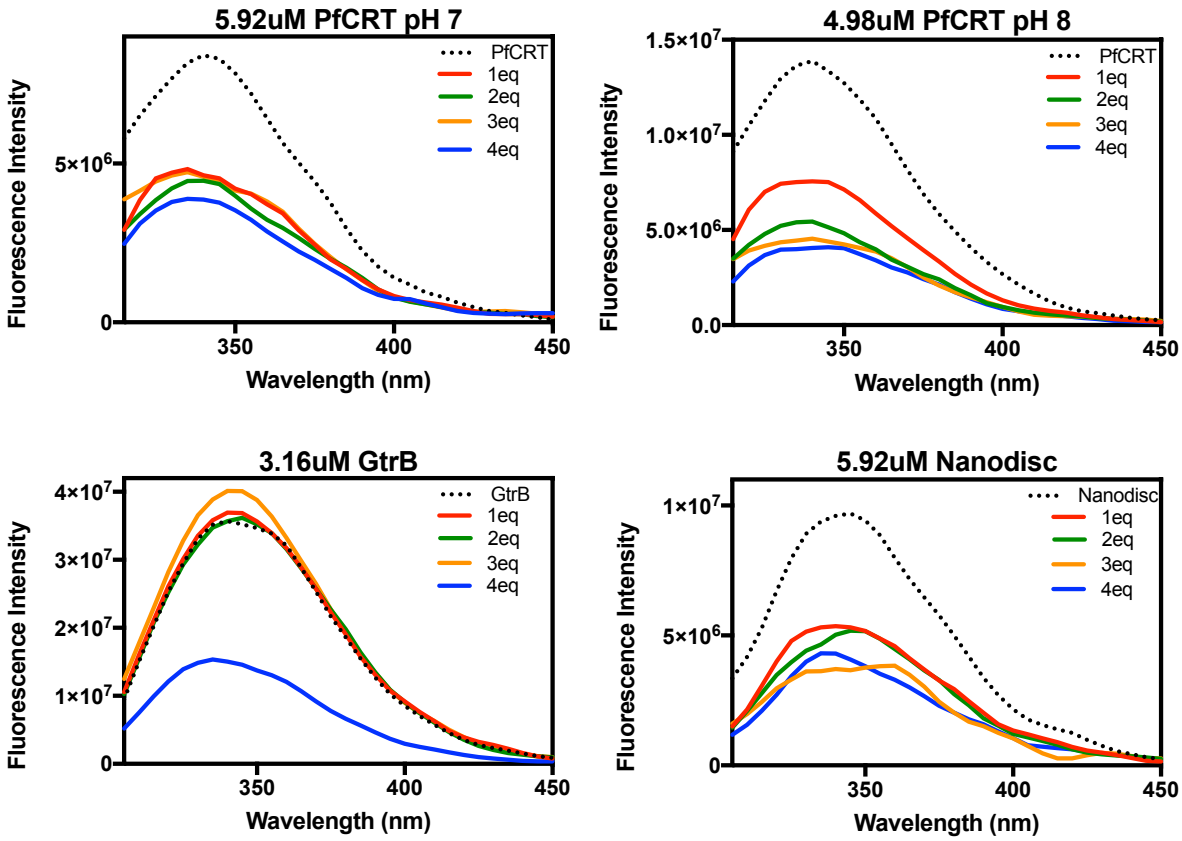

Figure 5.7. Effect of heme on fluorescence spectrum of PfCRT at pH 7 and 8, GtrB and nanodisc.

As shown in **Figure 5.7** in PfCRT and nanodisc, increasing amounts of hemin cause a decrease in fluorescence intensity. However, in the case of GtrB a decrease in fluorescence is only observed

when at least 4 equiv. of hemin is added. To determine the fluorescence quenching constant for heme, we used the Stern-Volmer equation (1) as noted above.

Table 5.4. Stern-Volmer quenching constants with heme.

PROTEIN	$K_{SV} \times 10^4$ (M^{-1})
PfCRT pH 7	3.03 ± 1.00
PfCRT pH 8	17.98 ± 1.08
GtrB	-
Nanodisc	9.15 ± 0.86

The K_{SV} values, in **Table 5.4**, show a strong quenching constant of heme in PfCRT at pH 8 and to a lesser extent in nanodisc as can be seen in **Figure 5.8**. we get a negative slope when heme is added to GtrB, this is attributed to the inaccessibility of heme to GtrB fluorophores. In this experiment, we can see the effect of pH and protein conformation with heme association. There is an order of magnitude difference in the Stern-Volmer constant with the pH is lowered by one unit.

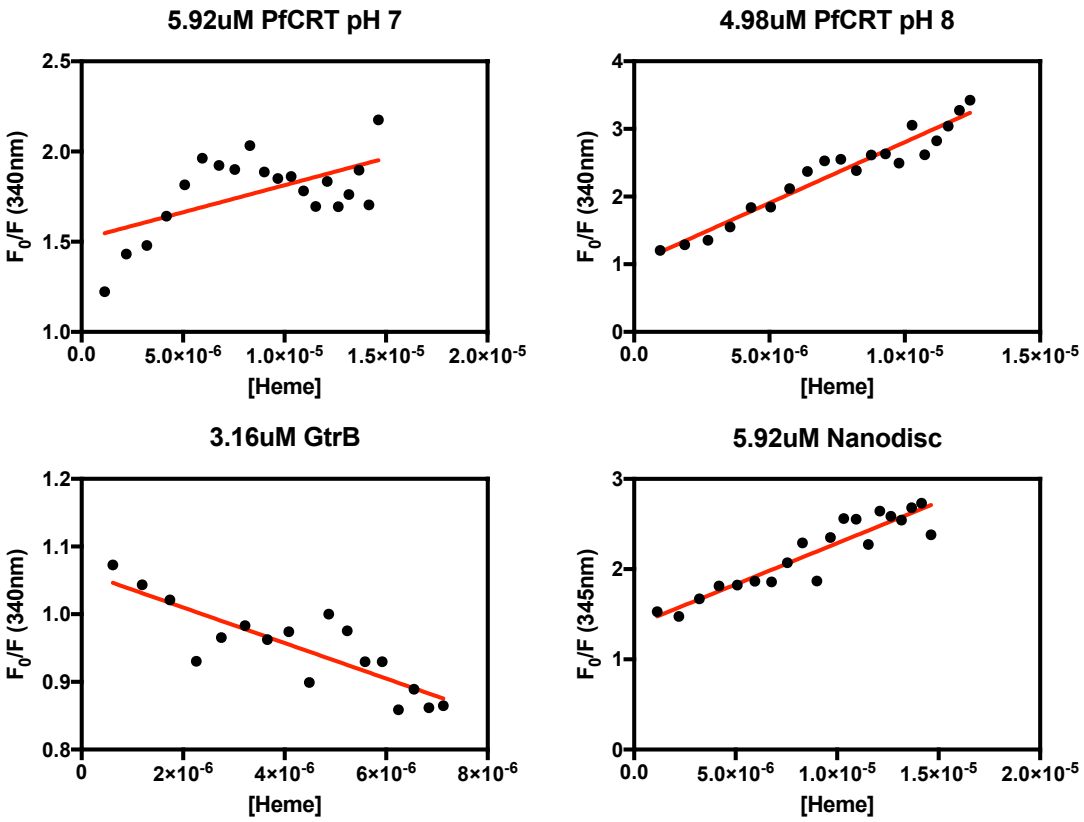

Figure 5.8. Stern-Volmer plot for PfCRT, GtrB and nanodisc quenched with up to 4 equivalents of Heme (each dot represents a 0.2 molar addition).

To determine the fraction of accessible fluorophores, we used the modified Stern-Volmer equation (2), the results are displayed in **Table 5.5** and **Figure 5.9**. The fraction of accessible fluorophores is greater for PfCRT at pH 8 than pH 7. Whereas in the case of GtrB there are no accessible fluorophores for heme to interact with. This is in agreement with the null K_{SV} value in **Table 5.4**.

Table 5.5. Modified Stern-Volmer constants for Heme.

PROTEIN	$K_a \times 10^5$ (M^{-1})	α (%)
PfCRT pH 7	4.45 ± 2.59	56.82
PfCRT pH 8	2.18 ± 3.05	89.85
GtrB	-	-
Nanodisc	8.47 ± 2.59	61.05

Lastly, to determine whether the proteins contain binding sites for heme, we used equation (3), the plots are shown in **Figure 5.10** and values are shown in **Figure 5.6**.

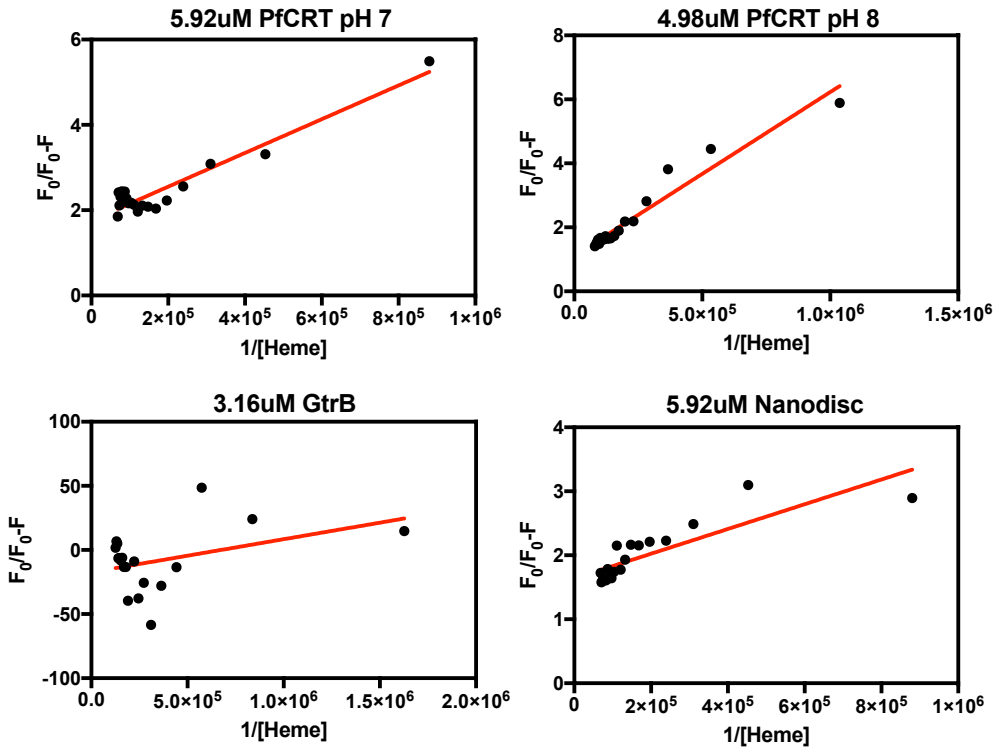

Figure 5.9. Modified Stern-Volmer plots for PfCRT, GtrB and nanodisc quenched with up to 4 equivalents of heme (each dot represents a 0.2 molar addition).

GtrB does not contain any binding sites for heme, and we get a negative slope and intercept values for the Stern-Volmer quenching constants; thus, we can say that heme is not a substrate for GtrB.

PfCRT at pH 8 contains one binding site for heme, this is in accordance with the 90% accessibility of fluorophores and strong Stern-Volmer quenching constant.

Table 5.6. Binding constants and number of binding sites for heme with MPLME.

PROTEIN	$\log K_b$	n
PfCRT pH 7	2.08 ± 0.39	0.43 ± 0.08
PfCRT pH 8	5.34 ± 0.25	1.02 ± 0.05
GtrB	-	-
Nanodisc	2.81 ± 0.26	0.54 ± 0.05

The difference of one pH unit has a 1,000 - fold impact as at pH 7 PfCRT does not contain any binding sites for heme. Consequently, heme has access to a lesser percentage of the fluorophore resulting in a low quenching constant. Finally, nanodisc does not contain any binding sites for heme, which is also in accordance with previous results. The same nanodisc is incorporated onto PfCRT to keep it membrane-bound; thus, these results indicate that at pH 8 heme is truly binding to the protein not the membrane and that there is a significant conformational change to the protein at lower pH as heme no longer binds.

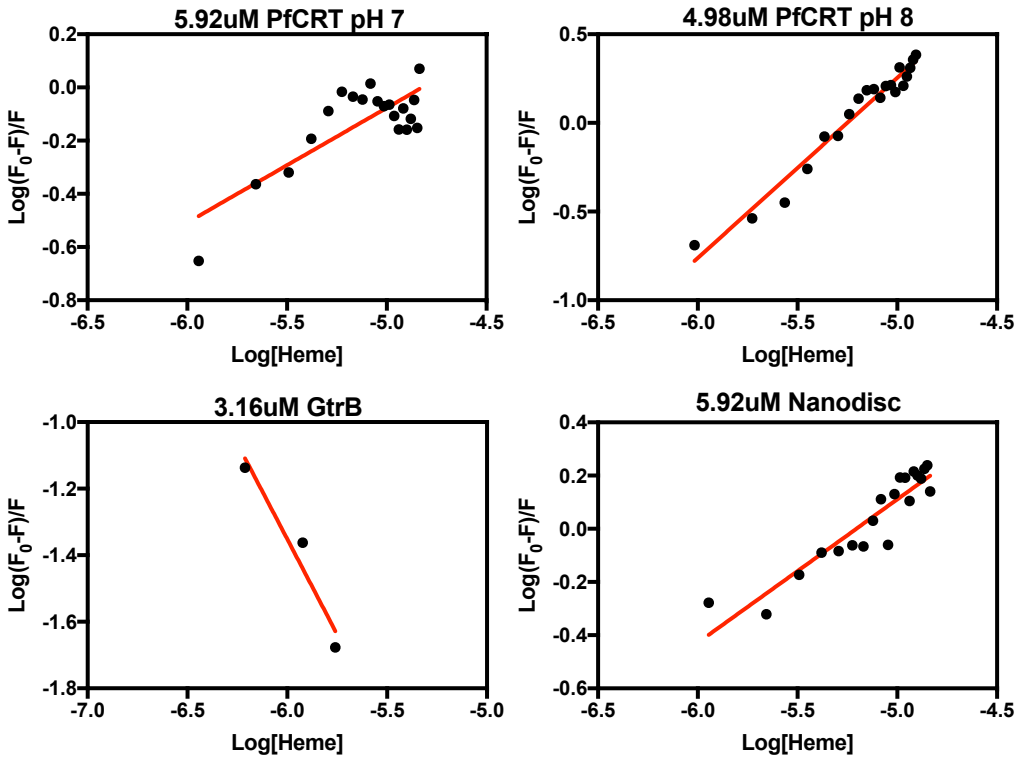

Figure 5.10. Binding plot to determine the number of heme binding sites and binding constant.

As mentioned above, it is important to remember that heme is possibly removed out of the DV by PfCRT at pH 5.2. Secondly, the two PfCRT Trp residues are located on the DV portion of the membrane; thus, at physiological pH results may differ. It may be the case that PfCRT indeed contains at least one binding site for CQ and heme at physiological pH. Nonetheless, we were able to demonstrate that PfCRT binds heme at pH 8.

The PfCRT central cavity has a volume of approximately 3,300 $Å^3$, heme and CQ molecules have approximate volumes of 702 $Å^3$ and 396 $Å^3$, respectively. Furthermore, the cavity has a max diameter of 25 Å, with the max diameters for heme and CQ being approximately 14 Å and 8 Å, respectively. Hence, it is possible that the resistance protein is capable of effluxing both heme and CQ as individual drugs and efflux the heme:CQ complex.

5.3.2 UV-Vis Studies

5.3.2.1 UV-Vis Studies with heme

The heme Soret, Q-bands and charge transfer bands can be identified by UV-Vis spectroscopy and are used to determine changes to heme oxidation state and spin state. We can use the observed changes of these bands to determine whether heme is involved in any binding interactions, especially those with direct iron-protein interactions.

All heme solutions were made in a 40% DMSO/ aqueous mixture, in this solution, heme is in its monomeric form.[18] As shown in **Figure 5.11**, for GtrB, there is no observed shift of the Soret band when two molar equivalents of heme are added. Heme added to the empty nanodisc causes a small 2 nm hypochromic shift (blue shift) from 412 nm to 410 nm and a greater 6 nm blue shift for the Q band. When heme is added to PfCRT, we observe the greatest change, an 8 nm blue shift, from 403 nm to 395 nm with no change to the Q band. Changes to the Soret peak which are associated with $\pi \rightarrow \pi^*$ transition suggesting the occurrence of heme binding interactions.[19]

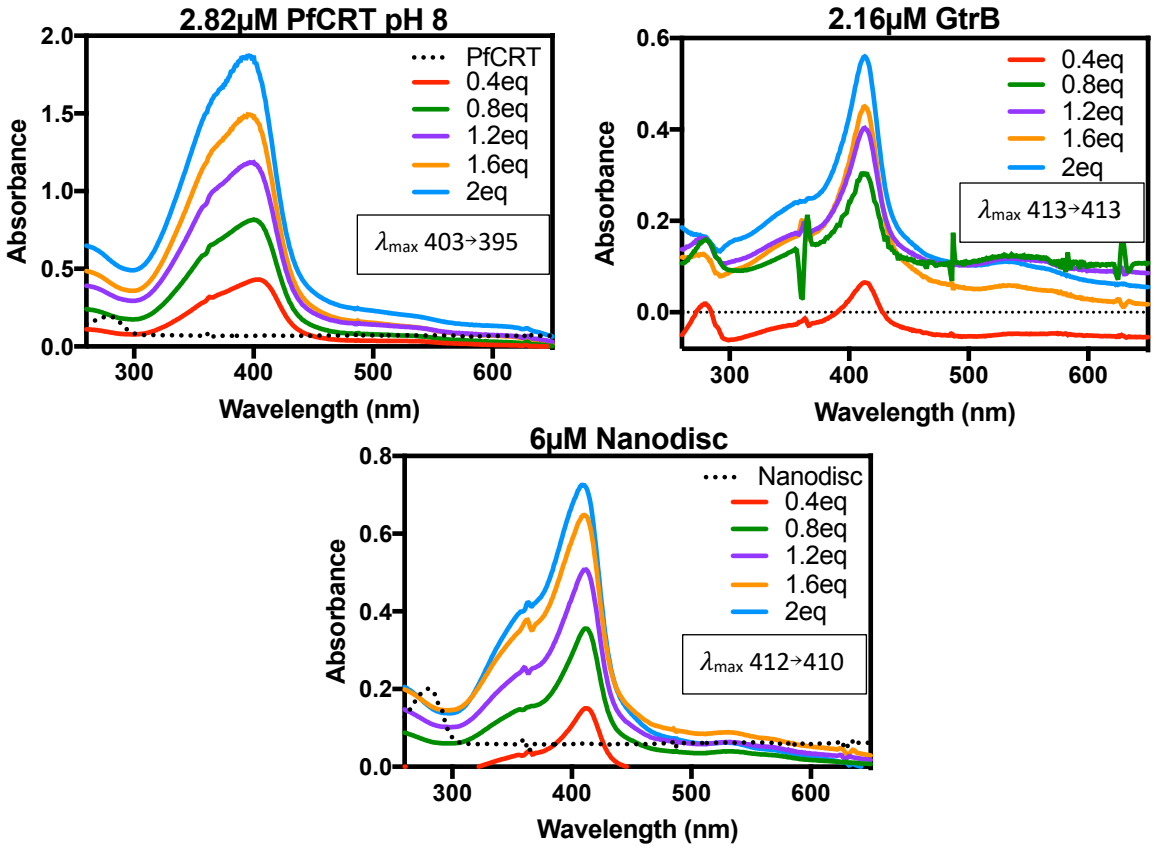

Figure 5.11. Changes to MPLME with up to 2 molar addition of heme.

The control protein GtrB does not bind with heme as there is no measured shift in the Soret peak. This was confirmed with fluorescence assays which showed that GtrB has no binding sites for heme (**Table 5.6**). In the case of lipid nanodisc, we observe a small 2 nm shift when two molar equivalents of heme are added, which we attribute to weak associations of heme with the membrane. Fluorescence studies showed that heme has a $\log K_b$ value of 2.81, which is stronger than with GtrB but less than with PfCRT at pH 8. When heme is added to PfCRT at pH 8 we see the greatest shift of 8 nm, indicating greater binding interactions between PfCRT - Heme than with nanodisc and GtrB. Furthermore, these interactions are independent of the nanodisc, which gave a

2 nm shift. These results are in accordance with fluorescent studies, which show that PfCRT at pH 8 contains one binding site for heme; furthermore, heme has access to 90% of its Trp fluorophores.

5.4 Conclusion

CQ resistance was first discovered in the 1960s, and there has been sustained research into determining the mechanism(s) of resistance and how to reverse and/or prevent it. A central protein involved in CQ resistance has for the first time been isolated, this breakthrough will allow for a better understanding of the resistance mechanism. In collaboration with the Fidock group, we worked with samples of the PfCRT 7G8 isoform and were able to carry out fluorescence and UV-Vis studies to determine binding of CQ and heme to the protein (an empty nanodisc membrane in which PfCRT is embedded in and an unrelated control protein GtrB) at cytosolic pH.

Fluorescence studies with GtrB show that it does not bind CQ or heme. We also determined that CQ and heme have little to no access to fluorophores located on the protein. Empty nanodisc does not bind CQ or heme, indicating that these drugs do not get embedded within these membranes. Additionally, heme has access to a greater fraction of fluorophores than CQ, which highlights the different interactions between the drugs and the protein. Lastly, PfCRT interactions are pH-dependent. At pH 7 PfCRT does not bind CQ or heme, this is in accordance with previous reports that state PfCRT effluxes CQ from the DV into the cytosol, it does not transport CQ into the DV. Therefore, binding interactions possibly occur in vacuolar pH.

We also carried out UV-Vis experiments of heme with GtrB, nanodisc and PfCRT at pH 8. We used the change in the Soret peak as an indication of non-covalent binding interactions. There were

no observed changes in the Soret peak with GtrB and a 2 nm blue shift with nanodisc. We observed an 8 nm blue shift of the Soret peak in PfCRT. This 8 nm shift indicates significant interactions between heme and PfCRT.

The results of our fluorescence and UV-Vis studies demonstrate that PfCRT at pH 8, contains one binding site for heme and at lower pH does not bind heme. At pH 7 and 8, PfCRT does not form significant binding interactions with CQ. This supports the belief that PfCRT transports CQ from the DV into the cytosol. Future work would involve performing fluorescence assays at vacuolar pH to determine binding interactions in an acidic environment.

5.5 Experimental

5.5.1 General information

All solvents and reagents were obtained commercially and used without further purification unless noted. The UV-Vis spectra were measured on Agilent 8453. The fluorescence measurements are performed on a Molecular Devices SpectraMax i3x, equipped with a black bottom 96 well plate obtained from Corning.

The PfCRT 7G8 isoform, nanodisc (MSP1D1 + POPG) and GtrB (encapsulated in MSP1E3D1) gifted from Prof. David Fidock's group at Columbia University. PfCRT at pH 7, nanodisc and GtrB were provided in a buffer solution containing 20 mM HEPES and 150 mM NaCl. PfCRT at pH 8 was provided in a buffer solution containing 20 mM TRIS pH 8 and 150 mM NaCl. CQ and hemin solutions were made in the appropriate buffers.

All solutions are freshly prepared and deionized H_2O is used in the preparation of all buffer solutions. All data analysis is performed using Prism 7.0a (GraphPad Software). Cole Parmer Microcomputer pH-Vision Model 05669-20 pH Meter used with Sigma-Aldrich micro pH combination electrode, glass body, which is calibrated with standard buffer solutions before use.

1.3 mg of hemin is dissolved in 2 mL 100% DMSO to make a 1 mM stock solution. 10.3 mg of chloroquine diphosphate is dissolved in 10 mL of buffer to make a 2 mM stock solution. A vortex mixer was used to ensure complete dissolution.

5.5.2 Fluorescence Spectroscopy Procedure

The emission spectra are then measured at 25.0^{o}C and are recorded in a wavelength range of 305-500 nm for nanodisc and GtrB following excitation at 280 nm. The emission spectra for PfCRT

are recorded with a wavelength range of 315-500 nm following excitation at 290 nm. The excitation and emission bandwidths are 5 nm. The initial volume of all proteins in the 96 well plates is 100 μL. Titrations are done manually using micropipettes.

PfCRT pH 7 and nanodisc experiments: 39 μL of hemin stock solution is diluted into 1 mL 40% DMSO, 60% buffer mixture to make a 39 μM 40% hemin solution. 39 μL of CQ stock is then diluted into 2 mL of buffer to make a 39 μM solution. PfCRT is used undiluted as a 5.92 μM HEPES solution. 19 μL of 31.8 μM Nanodisc is diluted into 81 μL buffer to make a 5.92 μM solution.

PfCRT pH 8 experiments: 66.2 μL of hemin stock solution is diluted into 2 mL 40% DMSO, 60% buffer mixture to make a 33.1 μM 40% hemin solution. 82.7 μL of CQ stock is then diluted into 5 mL of buffer to make a 33.1 μM solution. PfCRT is used undiluted as a 4.98 μM TRIS solution.

GtrB experiments: 21.1 μL of hemin stock solution is diluted into 1 mL 40% DMSO, 60% buffer mixture to make a 21.1 μM 40% hemin solution. 52.8 μL of CQ stock is then diluted into 5 mL of buffer to make a 21.1 μM solution. GtrB is used undiluted as a 3.16 μM HEPES solution.

Once prepared the solutions are kept on ice in a polystyrene cooler box. CQ or hemin is then titrated in 3 μL increments which correspond to 0.2 molar equivalents addition. Once four equiv. of the drug are added subsequent additions are in 15 μL increments until 7 molar equivalents are added. The equilibrium time between each addition is 10 minutes. During titration the solution is stirred and kept at a constant temperature of 25^{o}C. The total volume of drug added is 150 μL.

5.5.3 Ultraviolet-Visible Spectroscopy Procedure

At RT, the spectrophotometer is equipped with a 1 cm quartz cuvette of 4 mL capacity. All spectra are recorded against the appropriate blank buffer solution in the range of 260-800 nm.

Nanodisc: 76 µL of 39.5 µM nanodisc in HEPES pH 7.5 buffer is diluted in 1 mL buffer to make a 6 µM solution. 400 µL of hemin stock solution is diluted into 1 mL 40% DMSO, 60% buffer mixture to make a 400 µM 40% hemin solution.

PfCRT: 100 µL of 14.1 µM PfCRT is diluted to 500 µL TRIS pH 8 buffer to make a 2.82 µM solution. 188 µL of hemin stock solution is diluted into 1 mL 40% DMSO, 60% buffer mixture to make a 188 µM 40% hemin solution.

GtrB: 340 µL of 3.18 µM GtrB is diluted into 500 µL HEPES pH 7.5 buffer to make a 2.16 µM solution. 144 µL of hemin stock solution is diluted into 1 mL 40% DMSO, 60% buffer mixture to make a 144 µM 40% hemin solution.

Heme is titrated in 3 µL increments which correspond to 0.4 molar equivalents addition. Heme is added until 2 molar equiv. are reached, with an equilibrium time of 10 minutes between additions.

5.6 References

(1) Sanchez, C. P.; Stein, W. D.; Lanzer, M. Is PfCRT a Channel or a Carrier? Two Competing Models Explaining Chloroquine Resistance in Plasmodium Falciparum. *Trends Parasitol.* **2007**, *23* (7), 332–339.

(2) Johnson, D. J.; Fidock, D. A.; Mungthin, M.; Lakshmanan, V.; Sidhu, A. B. S.; Bray, P. G.; Ward, S. A. Evidence for a Central Role for PfCRT in Conferring Plasmodium Falciparum Resistance to Diverse Antimalarial Agents. *Mol. Cell* **2004**, *15* (6), 867–877.

(3) Kim, J.; Tan, Y. Z.; Wicht, K. J.; Erramilli, S. K.; Dhingra, S. K.; Okombo, J.; Vendome, J.; Hagenah, L. M.; Giacometti, S. I.; Warren, A. L.; Nosol, K.; Roepe, P. D.; Potter, C. S.; Carragher, B.; Kossiakoff, A. A.; Quick, M.; Fidock, D. A.; Mancia, F. Structure and Drug Resistance of the Plasmodium Falciparum Transporter PfCRT. *Nature* **2019**, *576* (7786), 315–320.

(4) Ecker, A.; Lehane, A. M.; Clain, J.; Fidock, D. A. PfCRT and Its Role in Antimalarial Drug Resistance. *Trends Parasitol.* **2012**, *28* (11), 504–514.

(5) Chinappi, M.; Via, A.; Marcatili, P.; Tramontano, A. On the Mechanism of Chloroquine Resistance in Plasmodium Falciparum. *PLoS One* **2010**, *5* (11), e14064.

(6) David A. Fidock; Nomura, T.; Talley, A. K.; Cooper, R. A.; Dzekunov, S. M.; Ferdig, M. T.; Ursos, L. M. B.; Sidhu, A. bir S.; Naudé, B.; Deitsch, K. W.; Su, X.; Wootton, J. C.; Roepe, P. D.; Wellems, T. E. Mutations in the P. Falciparum Digestive Vacuole Transmembrane Protein PfCRT and Evidence for Their Role in Chloroquine Resistance. *Mol. Cell* **2000**, *6* (4), 861–871.

(7) Djimdé, A.; Doumbo, O. K.; Cortese, J. F.; Kayentao, K.; Doumbo, S.; Diourté, Y.; Coulibaly, D.; Dicko, A.; Su, X.; Nomura, T.; Fidock, D. A.; Wellems, T. E.; Plowe, C. V.

A Molecular Marker for Chloroquine-Resistant Falciparum Malaria. *N. Engl. J. Med.* **2001**, *344* (4), 257–263.

(8) Price, R. N.; Cassar, C.; Brockman, A.; Duraisingh, M.; Van Vugt, M.; White, N. J.; Nosten, F.; Krishna, S. The Pfmdr1 Gene Is Associated with a Multidrug-Resistant Phenotype in Plasmodium Falciparum from the Western Border of Thailand. *Antimicrob. Agents Chemother.* **1999**, *43* (12), 2943–2949.

(9) Duraisingh, M. T.; Cowman, A. F. Contribution of the Pfmdr1 Gene to Antimalarial Drug-Resistance. *Acta Trop.* **2005**, *94* (3), 181–190.

(10) Pagola, S.; Stephens, P. W.; Bohle, D. S.; Kosar, A. D.; Madsen, S. K. The Structure of Malaria Pigment β-Haematin. *Nature* **2000**, *404* (6775), 307–310.

(11) Lakowicz, J. R. *Principles of Fluorescence Spectroscopy*; Lakowicz, J. R., Ed.; Springer US: Boston, MA, 2006.

(12) Marković, O. S.; Cvijetić, I. N.; Zlatović, M. V.; Opsenica, I. M.; Konstantinović, J. M.; Terzić Jovanović, N. V.; Šolaja, B. A.; Verbić, T. Human Serum Albumin Binding of Certain Antimalarials. *Spectrochim. Acta - Part A Mol. Biomol. Spectrosc.* **2018**, *192*, 128–139.

(13) Makarska-Bialokoz, M. Interactions of Hemin with Bovine Serum Albumin and Human Hemoglobin: A Fluorescence Quenching Study. *Spectrochim. Acta - Part A Mol. Biomol. Spectrosc.* **2018**, *193*, 23–32.

(14) Tunç, S.; Duman, O.; Bozoğlan, B. K. Studies on the Interactions of Chloroquine Diphosphate and Phenelzine Sulfate Drugs with Human Serum Albumin and Human Hemoglobin Proteins by Spectroscopic Techniques. *J. Lumin.* **2013**, *140*, 87–94.

(15) Kuhn, Y.; Rohrbach, P.; Lanzer, M. Quantitative PH Measurements in Plasmodium

Falciparum-Infected Erythrocytes Using PHluorin. *Cell. Microbiol.* **2007**, *9* (4), 1004–1013.

(16) Valderramos, S. G.; Fidock, D. A. Transporters Involved in Resistance to Antimalarial Drugs. *Trends Pharmacol. Sci.* **2006**, *27* (11), 594–601.

(17) Dodd, E. L.; Bohle, D. S. Orienting the Heterocyclic Periphery: A Structural Model for Chloroquine's Antimalarial Activity. *Chem. Commun.* **2014**, *50* (89), 13765–13768.

(18) Egan, T. J.; Mavuso, W. W.; Ross, D. C.; Marques, H. M. Thermodynamic Factors Controlling the Interaction of Quinoline Antimalarial Drugs with Ferriprotoporphyrin IX. *J. Inorg. Biochem.* **1997**, *68* (2), 137–145.

(19) Dayer, M.; Moosavi-Movahedi, A.; Dayer, M. Band Assignment in Hemoglobin Porphyrin Ring Spectrum: Using Four-Orbital Model of Gouterman. *Protein Pept. Lett.* **2010**, *17* (4), 473–479.

Chapter 6

Conclusions and Future Work

6.1 Conclusion

When I started my Ph.D., the main objective was to synthesize a chloroquine photoaffinity label with the simple addition of an azide at the 3-position. In pursuit of the azide, the discovery of undesired products led to the creation of projects that make the body of my thesis. This is a testament to not dismissing side/byproduct formation. As chemists, we must truly get in the flask to understand why and what reactions are occurring to the best of our ability. In that sense, is there truly such a thing as a failed reaction?

In my first chapter, I described the optimization of 3-NH_2CQ synthesis. This project was born out of the formation of the 3-NH_2CQ rather than 3-N_3CQ. To optimize amine formation, large amounts of the precursor 3-BrCQ were required. However, the known synthetic route for 3-BrCQ at the time did not allow large-scale synthesis. Therefore, 3-BrCQ synthesis was optimized using microwave-assisted synthesis and excess amounts of a brominating agent. We were able to scale the reaction to gram scale and obtain a 64% yield. With large amounts of my precursor, we were able to carry out a series of experiments with varying copper catalysts, ligands, solvents, reducing agents, and nitrogen sources. A moderate yield of 55% with the optimized reaction conditions was reached.

The formation of 3-NH_2CQ opened up the possibility of derivatization, which paved the way for chapter 2. A quick search of the literature for 4-aminoquinolines reveals compounds that only contain a 7-chloro substituent on the quinoline ring. Fortunately, previous work done in our lab showed that 3-ICQ, when used in combination with CQ, resensitizes the parasite to CQ. Therefore, we decided to exploit the newly formed 3-NH2CQ to synthesize a library of 3-substituted CQ

derivatives. These derivatives would then be tested for any synergistic effects they may have in combination therapy. Derivatives were synthesized with varying electronic and hydrophobic effects, with guidance from the Craig Plot and consideration of Lipinski's Rule of 5. Various benzamides were synthesized, and we determined that para - chloro substituent showed the best antiplasmodial activity. In CQS 3D7 strains, it was 3 – fold more effective, and in CQR Dd2 strains it was 1.8 – fold less effective than CQ. The equivalent para – chloro sulfonamide and Schiff base were less active than the chlorobenzamido derivative.

The precursor for the desired photoaffinity label was 3-NH_2CQ. However, as explained in chapter 4, we were unable to synthesize the photoaffinity label with only one modification at the 3-position. Doing so leads to the creation of a triazole product. To prevent cyclization, we blocked the reactivity of the 4-amine by installing a methyl to form a tertiary amine. A methyl was chosen due to its small size and lack of reactivity. This minor modification then allowed the synthesis of the desired photoaffinity label. Preliminary experiments to test the reactivity of the aryl azide were carried out.

The final chapter is a result of a collaboration that arose after an oral conference presentation. Prof. Fidock was interested in the potential of the photoaffinity label and disclosed that they had, for the first time, resolved the cryo-EM structure of *Plasmodium falciparum* Chloroquine Resistant Transporter (PfCRT) isoform. We obtained samples of the isoform and were able to carry out binding studies. We determined that there was no evidence of CQ binding to PfCRT at pH 7 and 8. We also determined that heme binds to PfCRT at pH 8. As mentioned in chapter 5, binding is very dependent on pH; therefore, at lower pH, CQ might bind to PfCRT.

6.2 Future Work

Regarding the 3-substituted CQ library, future steps involve isobolographic analysis to determine whether interactions between the derivatives and CQ are synergistic, additive, or antagonistic. Results from such experiments can give more detailed S.A.R. data about the derivatives and their targets. The 3-NH_2CQ can be further derivatized to expand the library and synthesize different families of antimalarial compounds. As the synthetic route for 3-N_3CQ has been developed. It can be used as a precursor to a family of triazole derivatives for click chemistry, thus further expanding the library of compounds.

The photoaffinity label has been synthesized and can be irradiated with UV light of 365 nm. The synthetic route developed can be used for various 4-aminoquinolines, thus allowing adequate labelling of many antimalarial drug candidates. More studies need to be carried out to determine the best conditions required for C-H, C-N, and C-C insertion and the optimal stoichiometry that will produce the highest conversion and yield. Future work involves using the label with proteins of interest to determine the insertion of the PAL. Such studies will have a significant impact on our understanding of CQ's biological pathway. Furthermore, once successfully incorporated into the target protein, one can carry out protein digestion for mass spectroscopy. This will allow for the identification of the insertion product along the protein sequence.

We have demonstrated that PfCRT binds heme at pH 8 and does not bind CQ at pH 7 and 8. The next area of interest is determining the binding mechanism (static or dynamic) by carrying out temperature-dependent fluorescence assays. Static quenching is a result of complex formation between the quencher and the fluorophore in the ground state. Dynamic quenching is a result of

interactions between the quencher and fluorophore in the excited state. Quenching emission is temperature-dependent; therefore, temperature-dependent assays can give valuable information on the mechanism of interaction between the quencher and fluorophore. Lastly, it would be of great interest to determine the binding behaviour of PfCRT towards CQ and heme at lower pH such as pH 5.2.

Appendix

Chapter 3

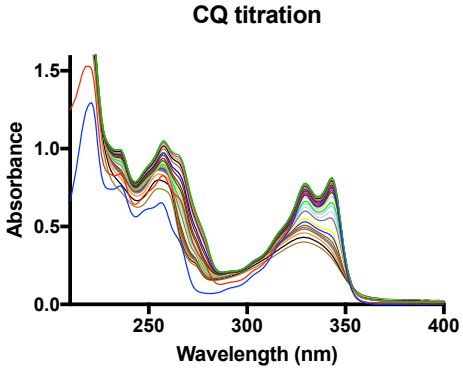
CQ titration
Absorbance
Wavelength (nm)
1.5
1.0
0.5
0.0
250
300
350
400

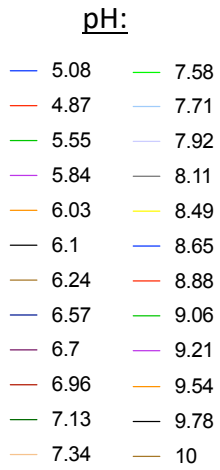
pH:
5.08
4.87
5.55
5.84
6.03
6.1
6.24
6.57
6.7
6.96
7.13
7.34
7.58
7.71
7.92
8.11
8.49
8.65
8.88
9.06
9.21
9.54
9.78
10

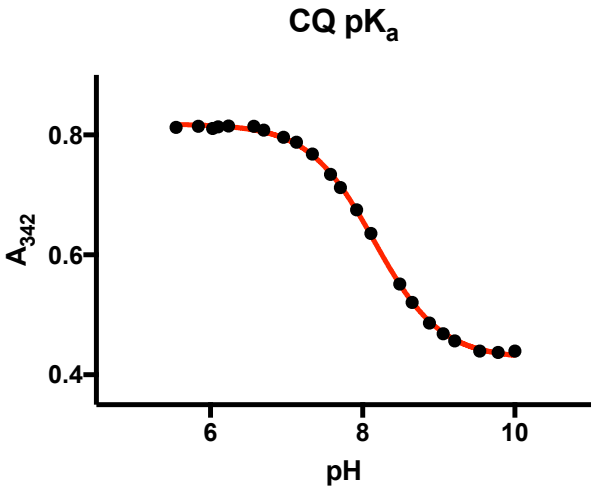
CQ pK$_a$
A$_{342}$
pH
0.8
0.6
0.4
6
8
10

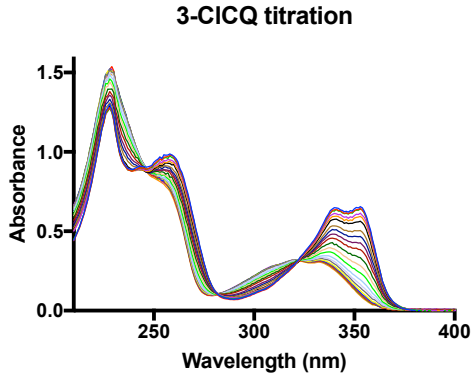
3-ClCQ titration
Absorbance
Wavelength (nm)
1.5
1.0
0.5
0.0
250
300
350
400

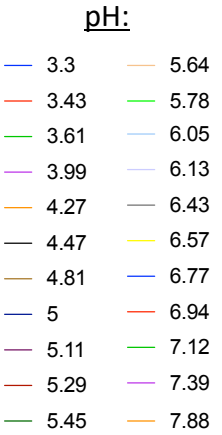
pH:
3.3
3.43
3.61
3.99
4.27
4.47
4.81
5
5.11
5.29
5.45
5.64
5.78
6.05
6.13
6.43
6.57
6.77
6.94
7.12
7.39
7.88

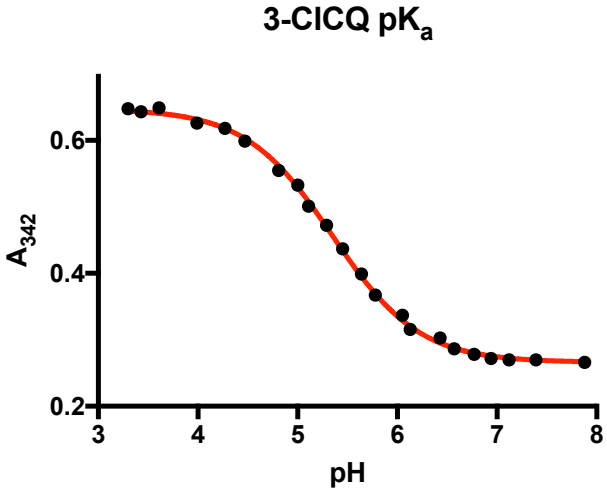
3-ClCQ pK$_a$
A$_{342}$
pH
0.6
0.4
0.2
3
4
5
6
7
8

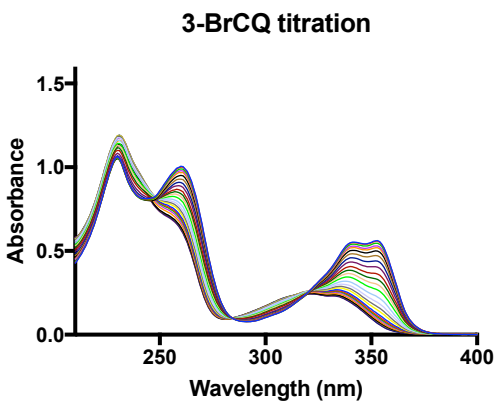

pH:

3.42	5.69
3.57	5.85
3.77	6
4.13	6.12
4.23	6.27
4.39	6.39
4.62	6.48
4.81	6.61
4.98	6.72
5.17	6.89
5.26	7.08
5.41	7.58
5.53	8.14

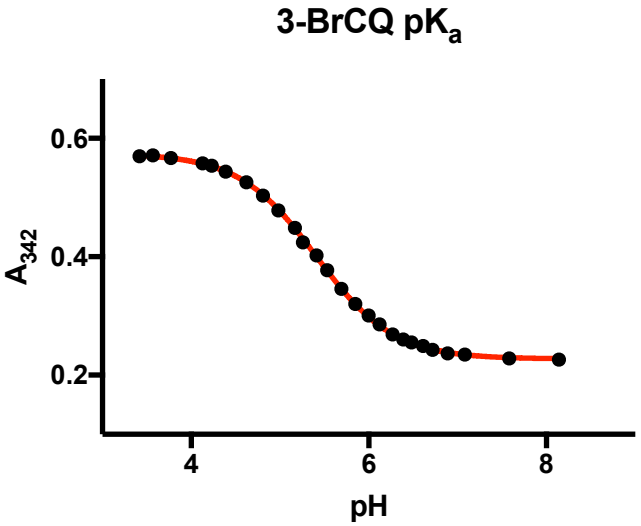

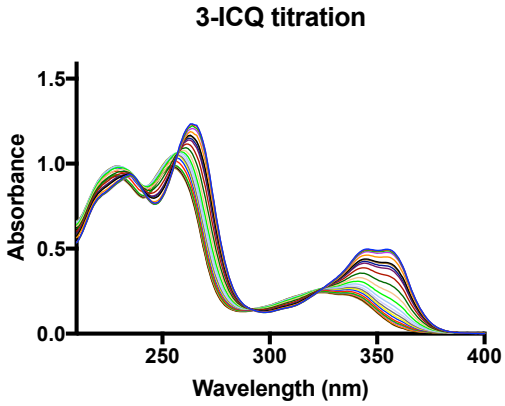

pH:

3.39	5.8
3.53	5.94
3.73	6.09
3.97	6.23
4.42	6.34
4.77	6.44
4.83	6.59
4.95	6.69
5.02	6.92
5.21	7.14
5.43	7.52
5.61	8.04

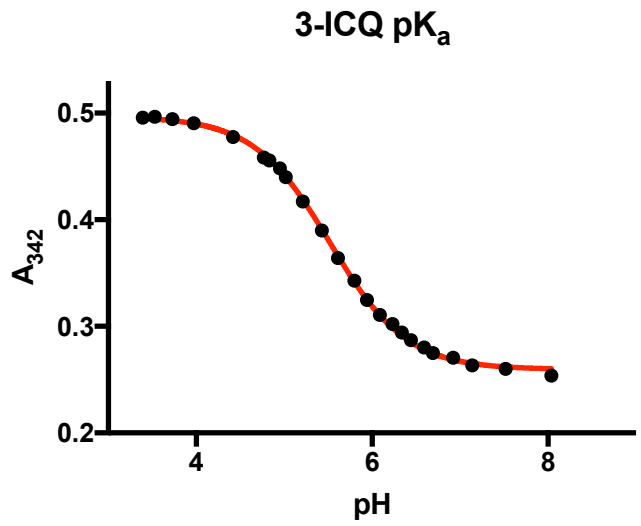

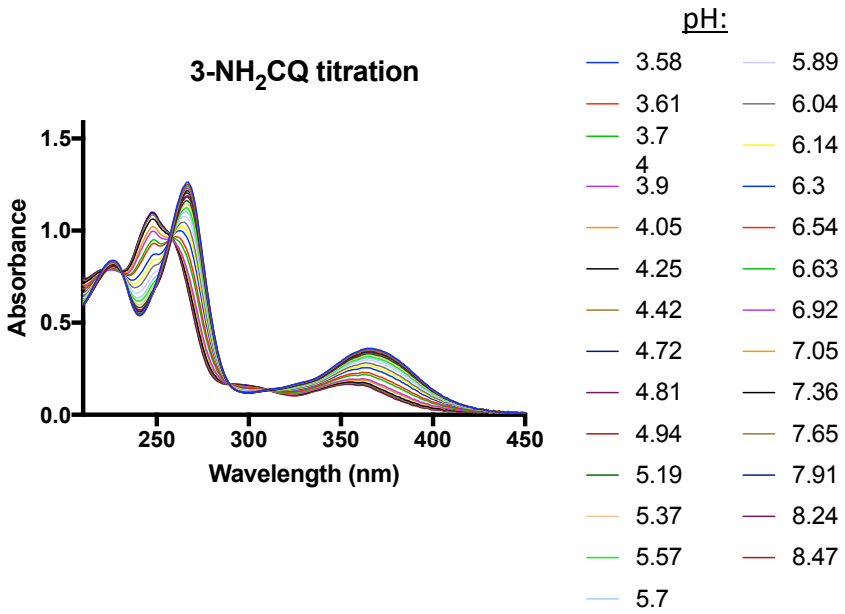
3-NH2CQ titration
Absorbance
1.5
1.0
0.5
0.0
250
300
350
400
450
Wavelength (nm)
pH:
3.58
3.61
3.7
4
3.9
4.05
4.25
4.42
4.72
4.81
4.94
5.19
5.37
5.57
5.7
5.89
6.04
6.14
6.3
6.54
6.63
6.92
7.05
7.36
7.65
7.91
8.24
8.47

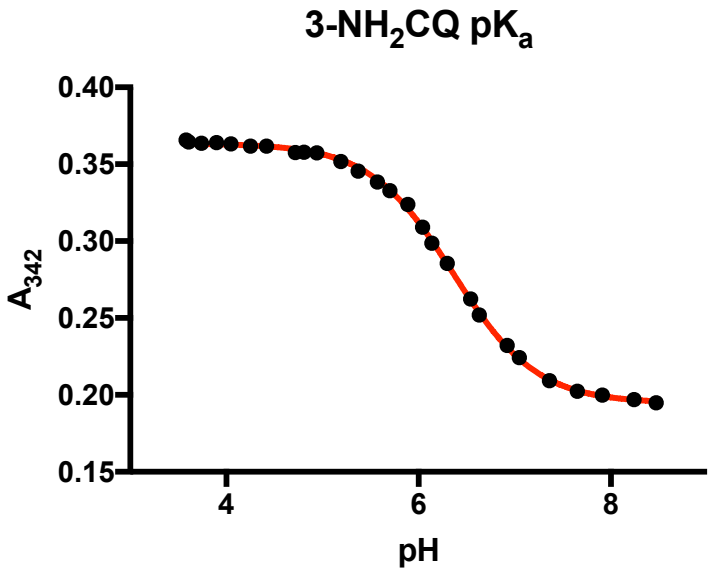
3-NH2CQ pKa
A342
0.40
0.35
0.30
0.25
0.20
0.15
4
6
8
pH

Chapter 5

Fluorescence Studies with chloroquine

Linear equation for Stern-Volmer plot:

$$\frac{F_0}{F} = 1 + k_q \tau_0 [Q] = 1 + K_{SV}[Q]$$

PROTEIN	EQUATION	K_{SV} X 10^4 (M^{-1})	R^2
PfCRT pH 7	Y = 1405*X + 1.038	0.14 ± 0.14	0.0536
PfCRT pH 8	Y = 558.9*X + 1.124	0.056 ± 0.31	0.001812
GtrB	Y = 15442*X + 1.025	1.54 ± 0.41	0.4437
Nanodisc	Y = 35486*X + 1.148	3.55 ± 0.44	0.7811

Linear equation for modified Stern-Volmer plot:

$$\frac{F_0}{F_0 - F} = \frac{1}{\alpha K_a [Q]} + \frac{1}{\alpha}$$

PROTEIN	EQUATION	K_a X 10^5 (M^{-1})	α (%)	R^2
PfCRT pH 7	Y = 3.748e-005*X + 18.44	4.92 ± 2.58	5.42	0.3195
PfCRT pH 8	Y = 8.604e-006*X + 7.064	8.21 ± 3.09	14.16	0.468
GtrB	Y = 1.684e-005*X + 7.324	4.35 ± 4.79	13.65	0.7143
Nanodisc	Y = 3.925e-006*X + 2.816	7.17 ± 2.62	35.51	0.4535

Linear equations to determine the number of binding sites:

$$\log \frac{F_0 - F}{F} = \log K_b + n \log [Q]$$

PROTEIN	EQUATION	$\log K_b$	n	R^2
PfCRT pH 7	Y = 0.2715*X + 0.06151	0.06 ± 0.83	0.27 ± 0.16	0.1424
PfCRT pH 8	Y = 0.1811*X + 0.009318	0.009 ± 0.87	0.18 ± 0.17	0.06101
GtrB	Y = 0.5416*X + 1.897	1.89 ± 0.58	0.54 ± 0.11	0.5993
Nanodisc	Y = 0.6693*X + 3.047	3.05 ± 0.37	0.67 ± 0.07	0.8366

Concentration-dependent Stern-Volmer plot, with CQ.

PROTEIN	EQUATION	K_{SV} X 10^4 (M^{-1})	R^2
PfCRT pH 7 0-1 eq	Y = 16892*X + 0.9991	1.69 ± 0.44	0.8333
PfCRT pH 7 1-4 eq	Y = 1967*X + 1.03	0.19 ± 0.21	0.05661
PfCRT pH 8 0-2 eq	Y = 15324*X + 1.061	1.53 ± 0.57	0.4715
PfCRT pH 8 2-4 eq	Y = -22032*X + 1.355	-2.2 ± 0.61	0.5949

Fluorescence Studies with heme

Linear equation for Stern-Volmer plot:

$$\frac{F_0}{F} = 1 + k_q \tau_0 [Q] = 1 + K_{SV}[Q]$$

PROTEIN	EQUATION	K_{SV} X 10^4 (M^{-1})	R^2
PfCRT pH 7	Y = 30034*X + 1.513	3.03 ± 1.0	0.3324
PfCRT pH 8	Y = 179807*X + 1.006	17.98 ± 1.08	0.9386
GtrB	Y = -26259*X + 1.063	-	0.7085
Nanodisc	Y = 91473*X + 1.373	9.15 ± 0.86	0.8622

Linear equation for modified Stern-Volmer plot:

$$\frac{F_0}{F_0 - F} = \frac{1}{\alpha K_a [Q]} + \frac{1}{\alpha}$$

PROTEIN	EQUATION	K_a X 10^5 (M^{-1})	α (%)	R^2
PfCRT pH 7	Y = 3.956e-006*X + 1.76	4.45 ± 2.59	56.82	0.9076
PfCRT pH 8	Y = 5.116e-006*X + 1.113	2.18 ± 3.05	89.85	0.9414
GtrB	Y = 2.575e-005*X - 17.34	-	-	0.1494
Nanodisc	Y = 1.933e-006*X + 1.638	8.47 ± 2.59	61.05	0.7061

Linear equations to determine the number of binding sites:

$$\log \frac{F_0 - F}{F} = \log K_b + n \log [Q]$$

PROTEIN	EQUATION	$\log K_b$	n	R^2
PfCRT pH 7	Y = 0.4313*X + 2.08	2.08 ± 0.39	0.43 ± 0.08	0.6413
PfCRT pH 8	Y = 1.016*X + 5.336	5.34 ± 0.25	1.02 ± 0.05	0.9618
GtrB	Y = -1.147*X - 8.234	-	-	0.9376
Nanodisc	Y = 0.539*X + 2.805	2.81 ± 0.26	0.54 ± 0.05	0.8589

NMR Spectra

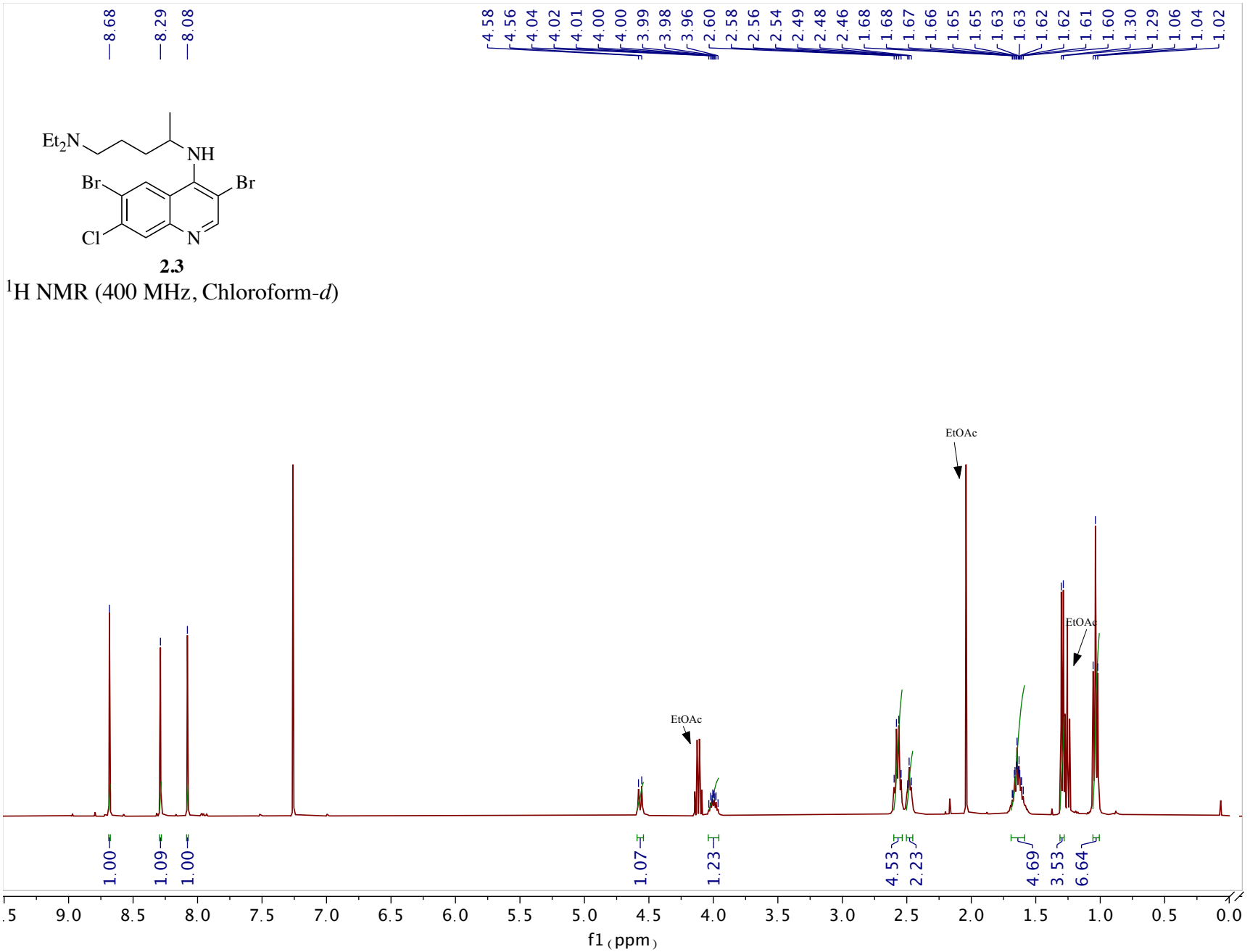

2.3

^{1}H NMR (400 MHz, Chloroform-*d*)

^{13}C NMR (201 MHz, Chloroform-*d*)

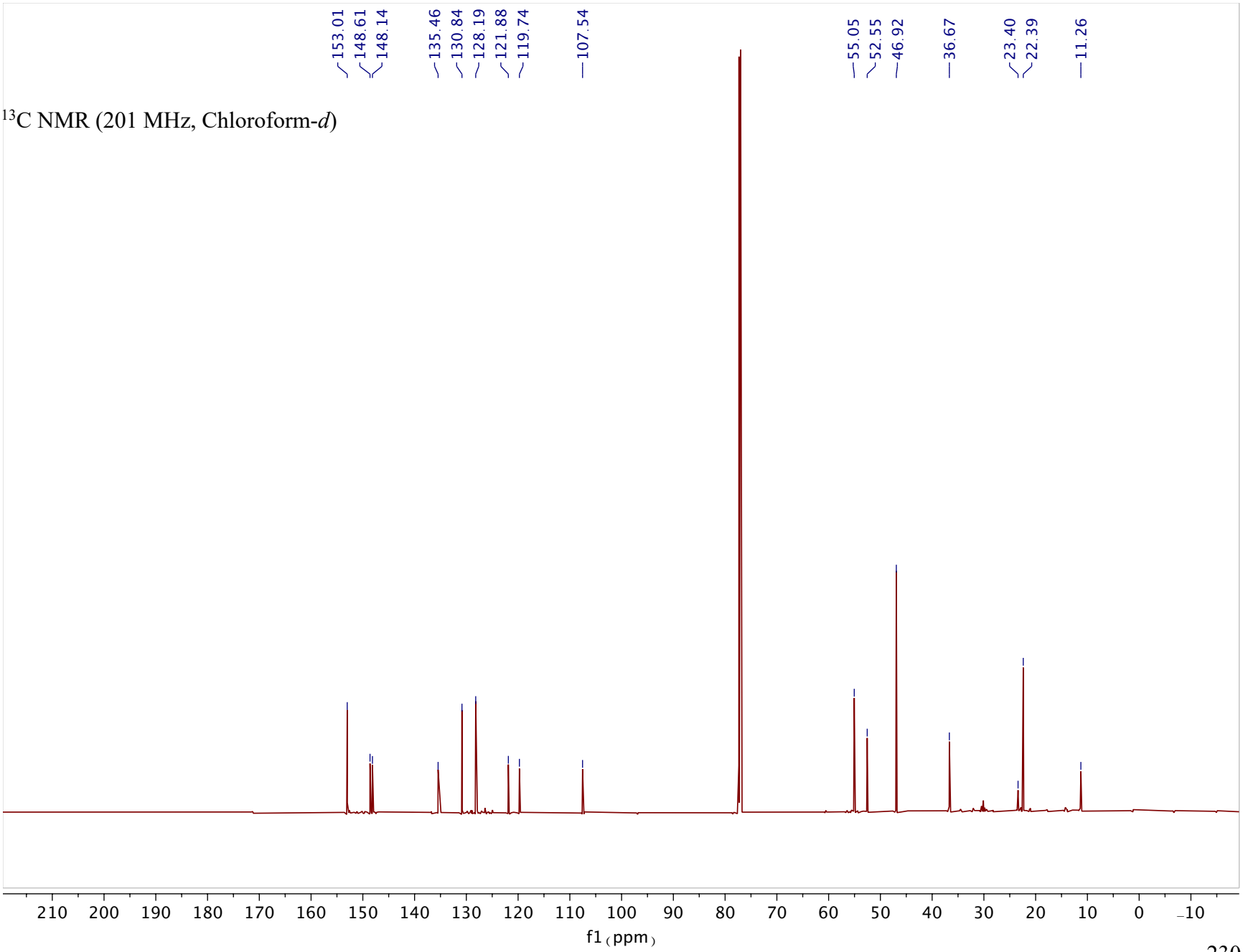

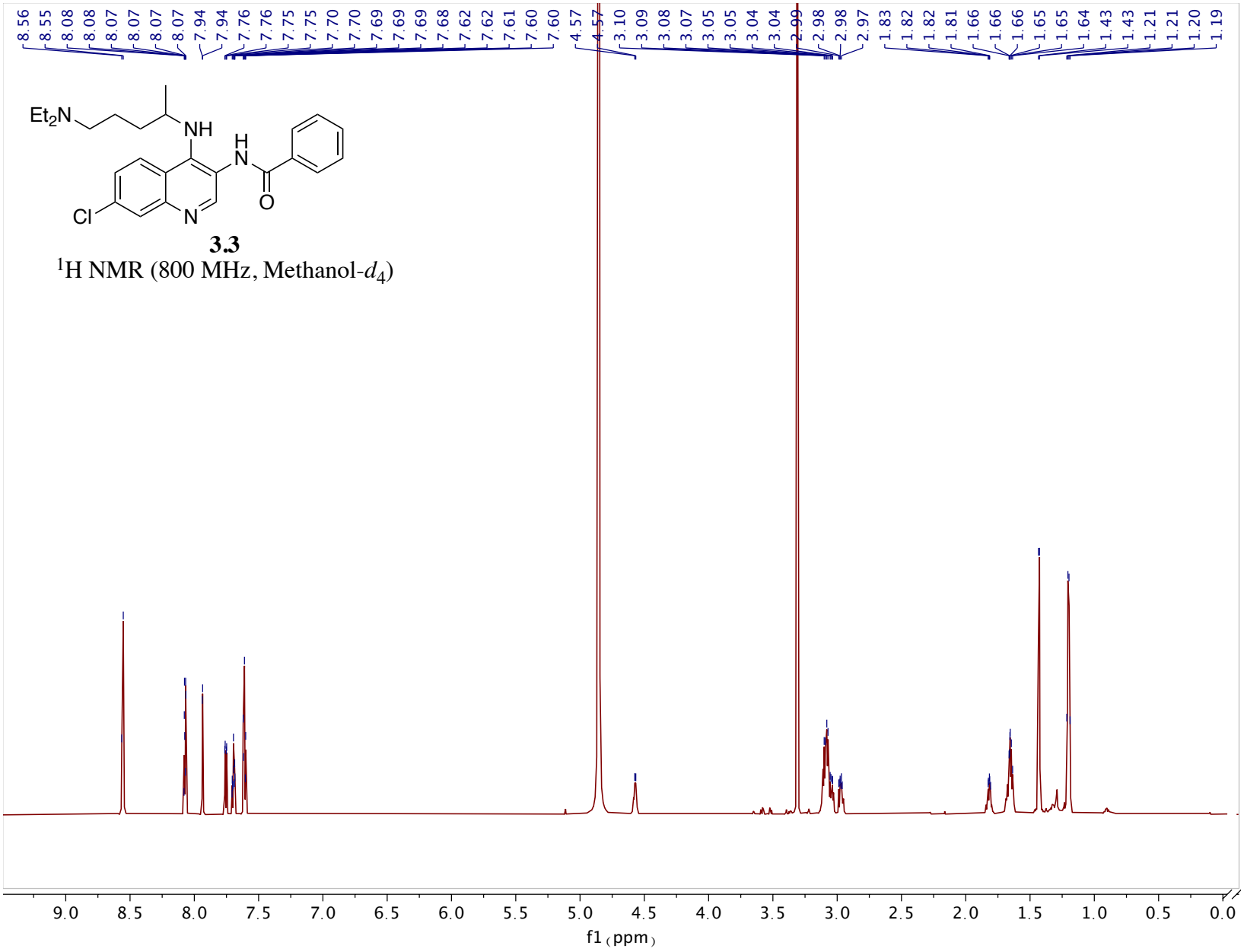

3.3

^{1}H NMR (800 MHz, Methanol-d_4)

^{13}C NMR (201 MHz, Methanol-d_4)

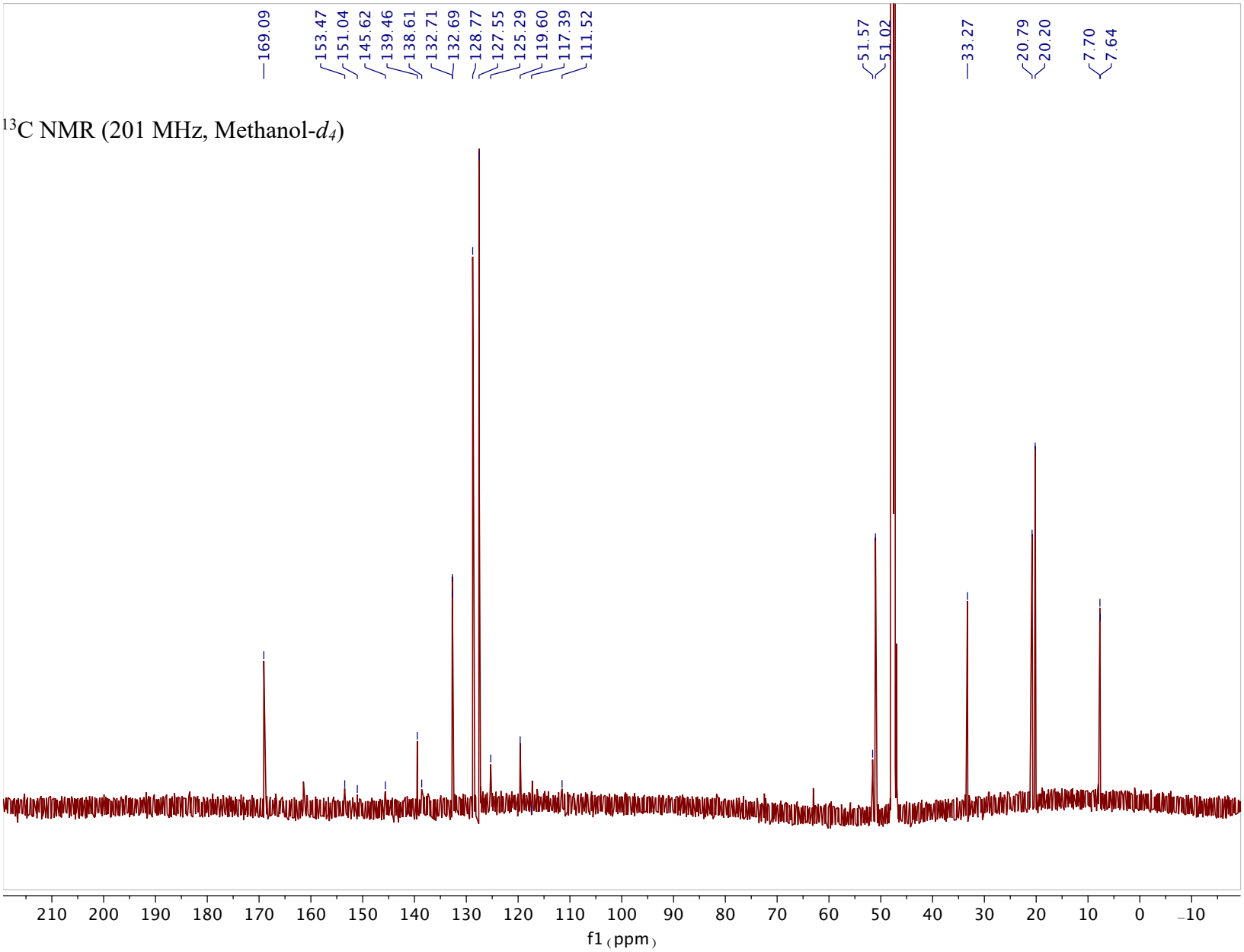

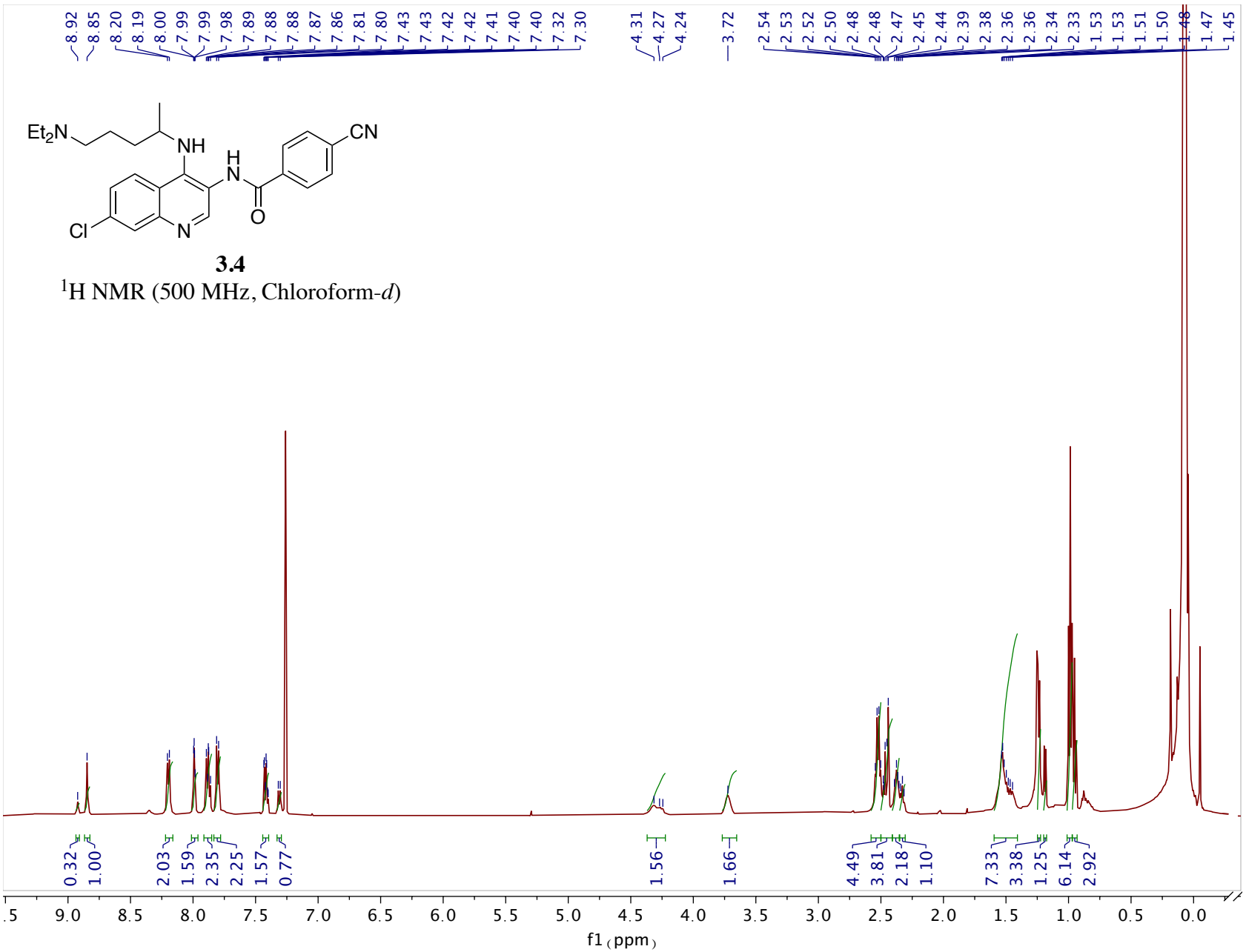

3.4

^{1}H NMR (500 MHz, Chloroform-*d*)

^{13}C NMR (126 MHz, Chloroform-*d*)

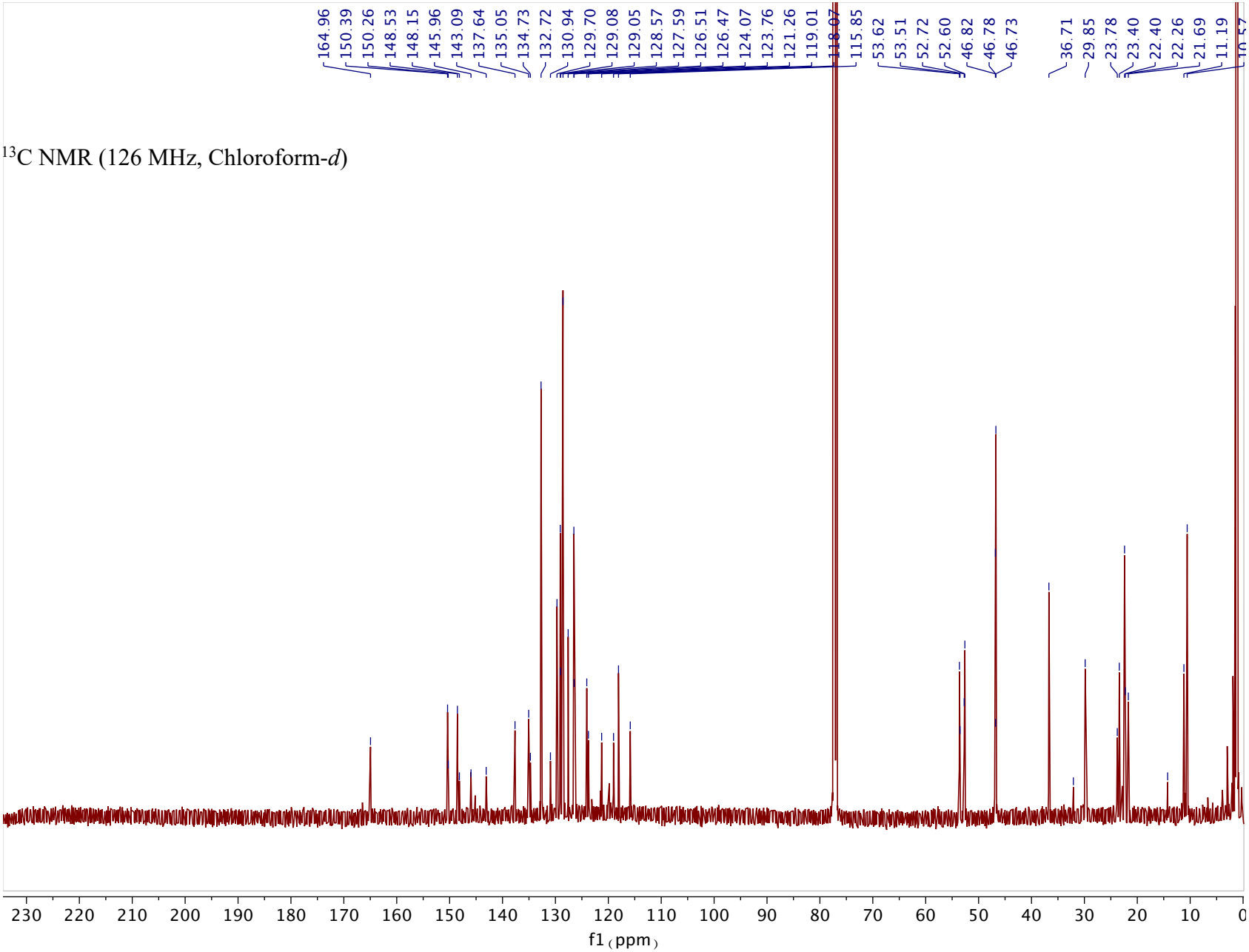

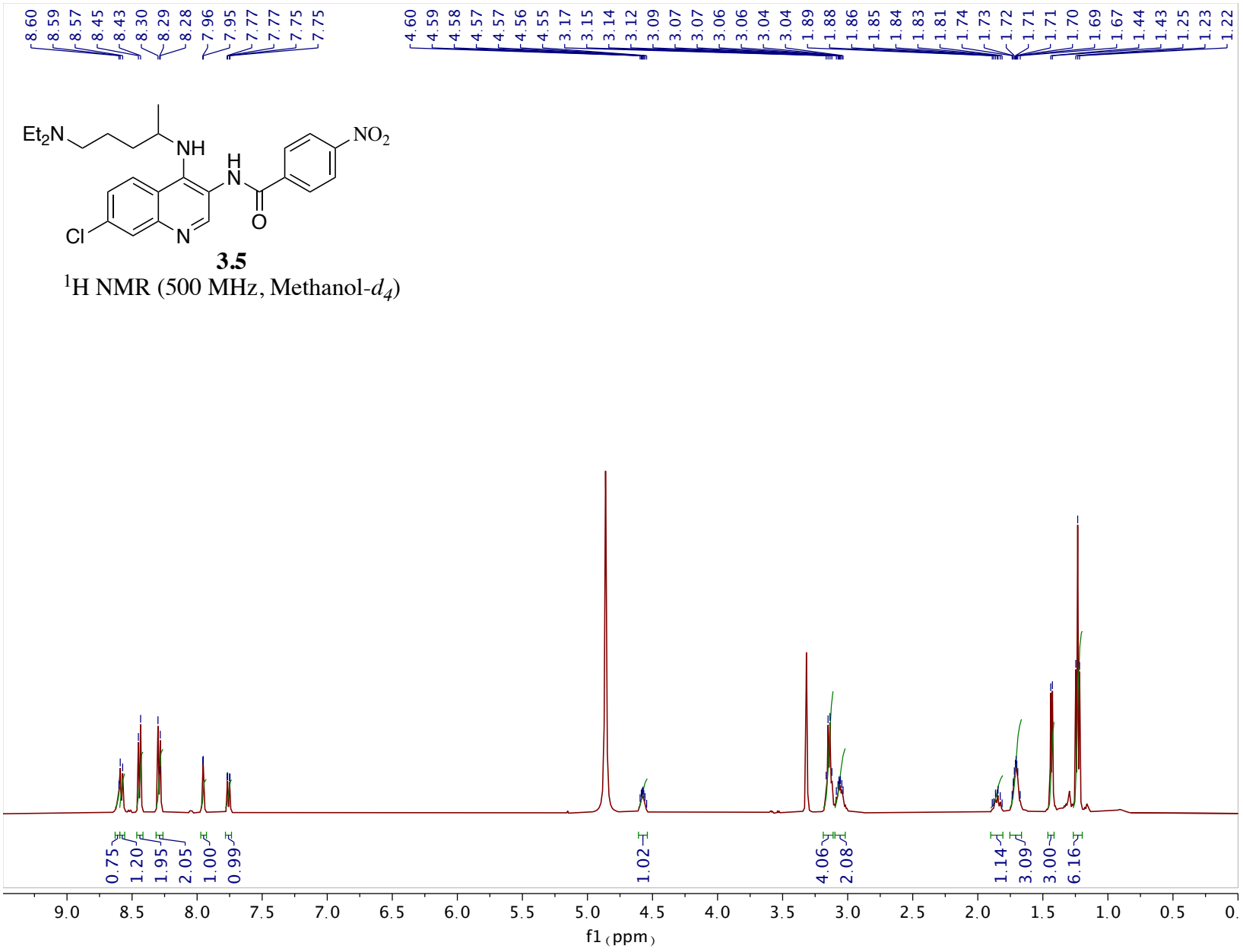

3.5

^{1}H NMR (500 MHz, Methanol-d_4)

^{13}C NMR (126 MHz, Methanol-d_4)

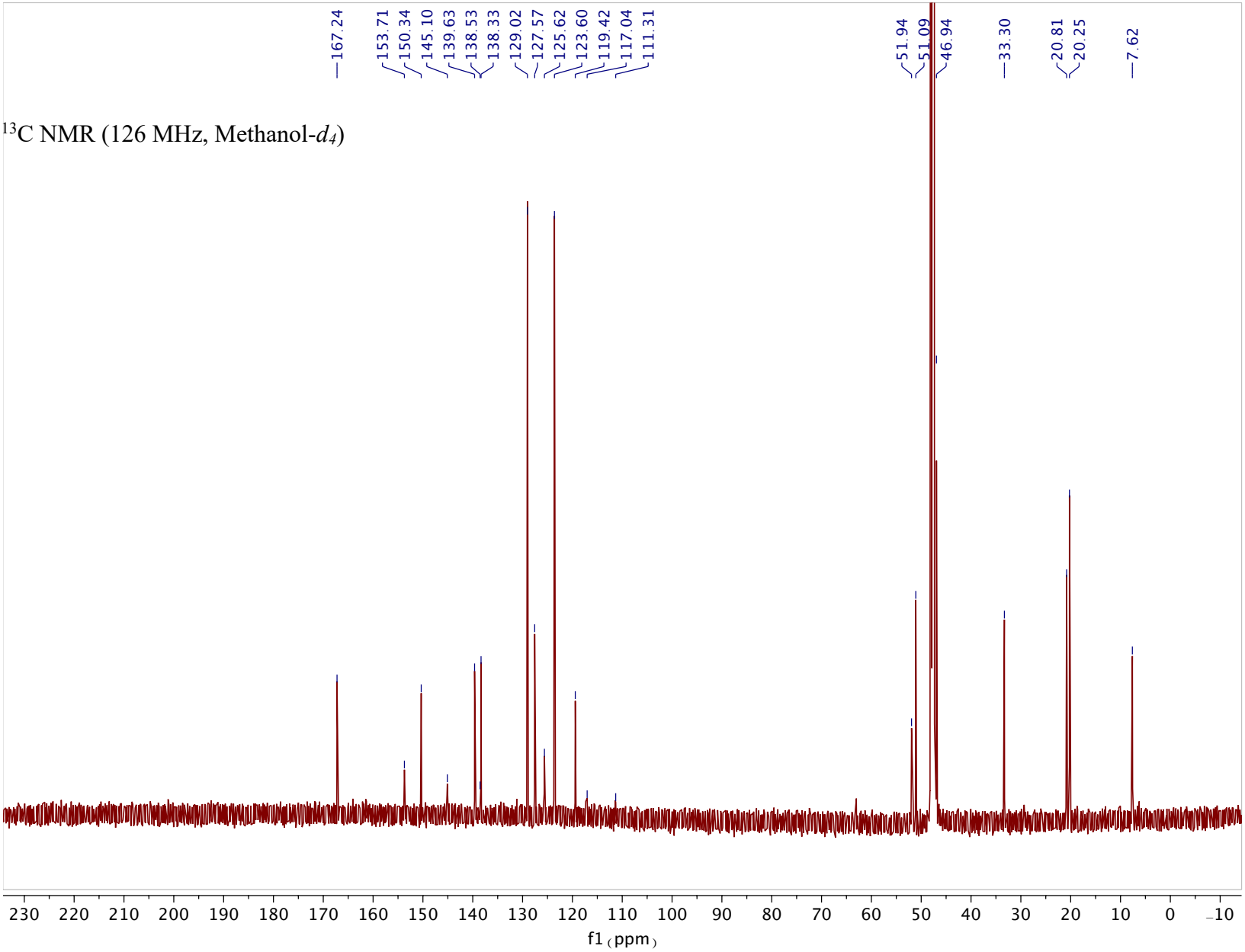

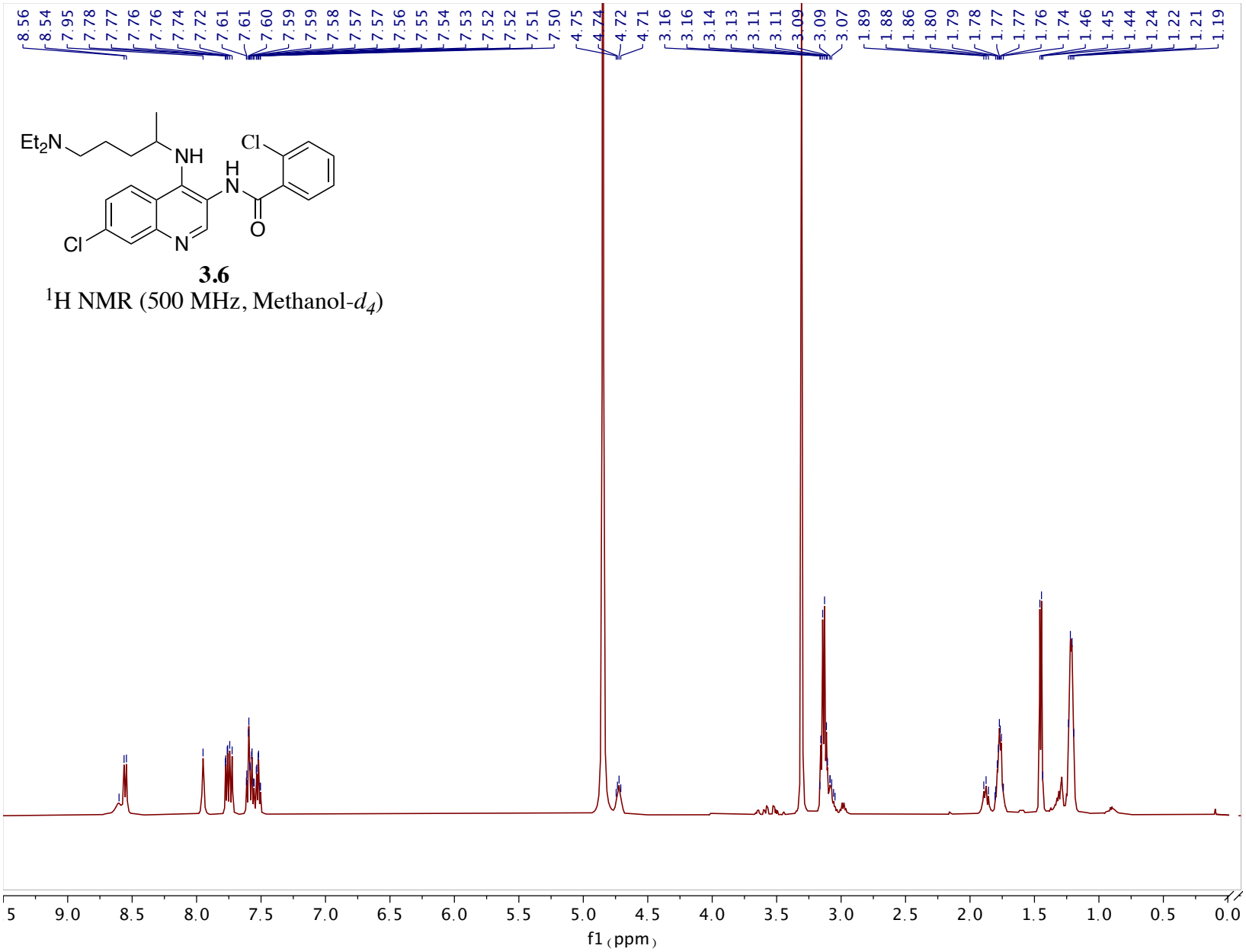

3.6

^{1}H NMR (500 MHz, Methanol-d_4)

^{13}C NMR (126 MHz, Methanol-d_4)

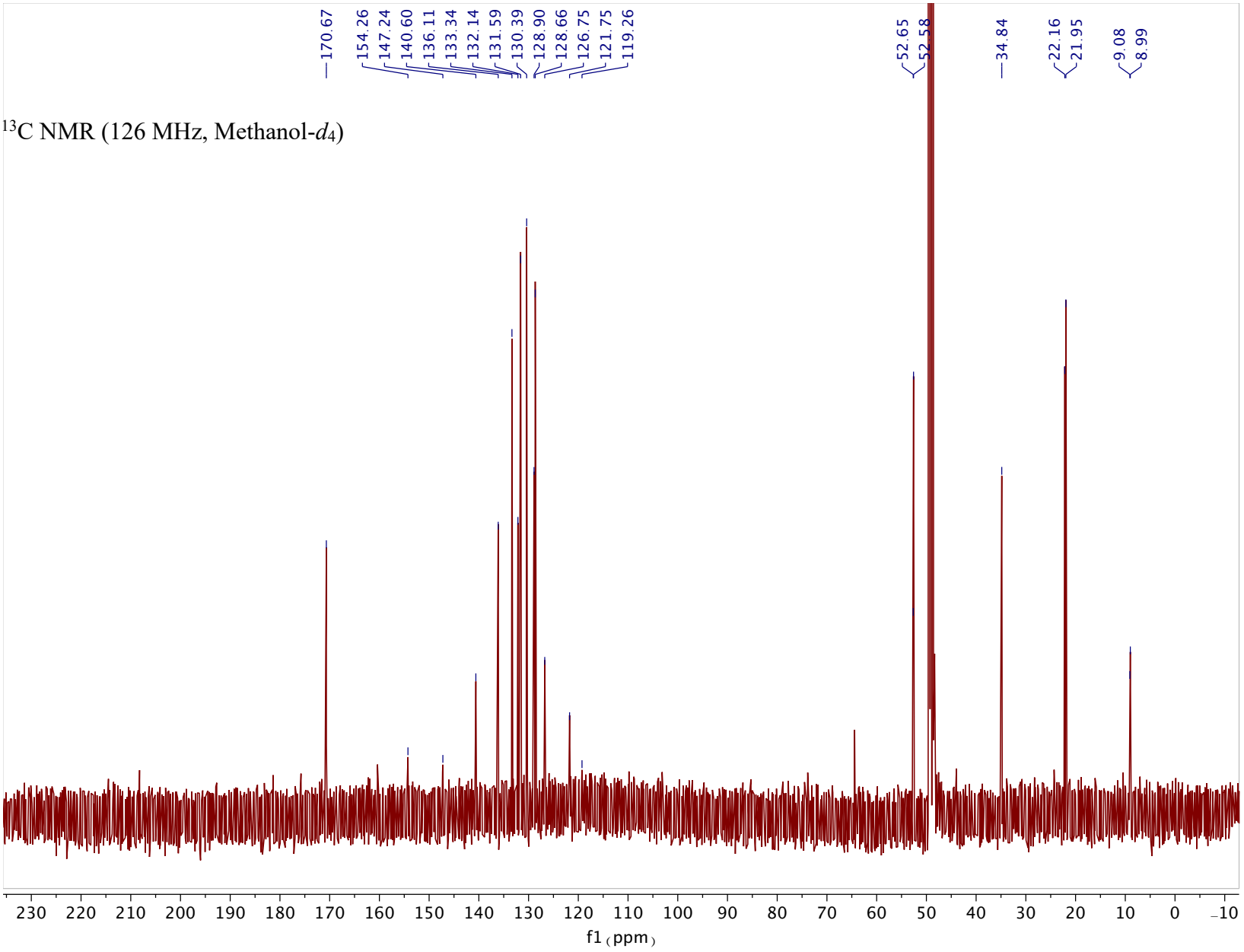

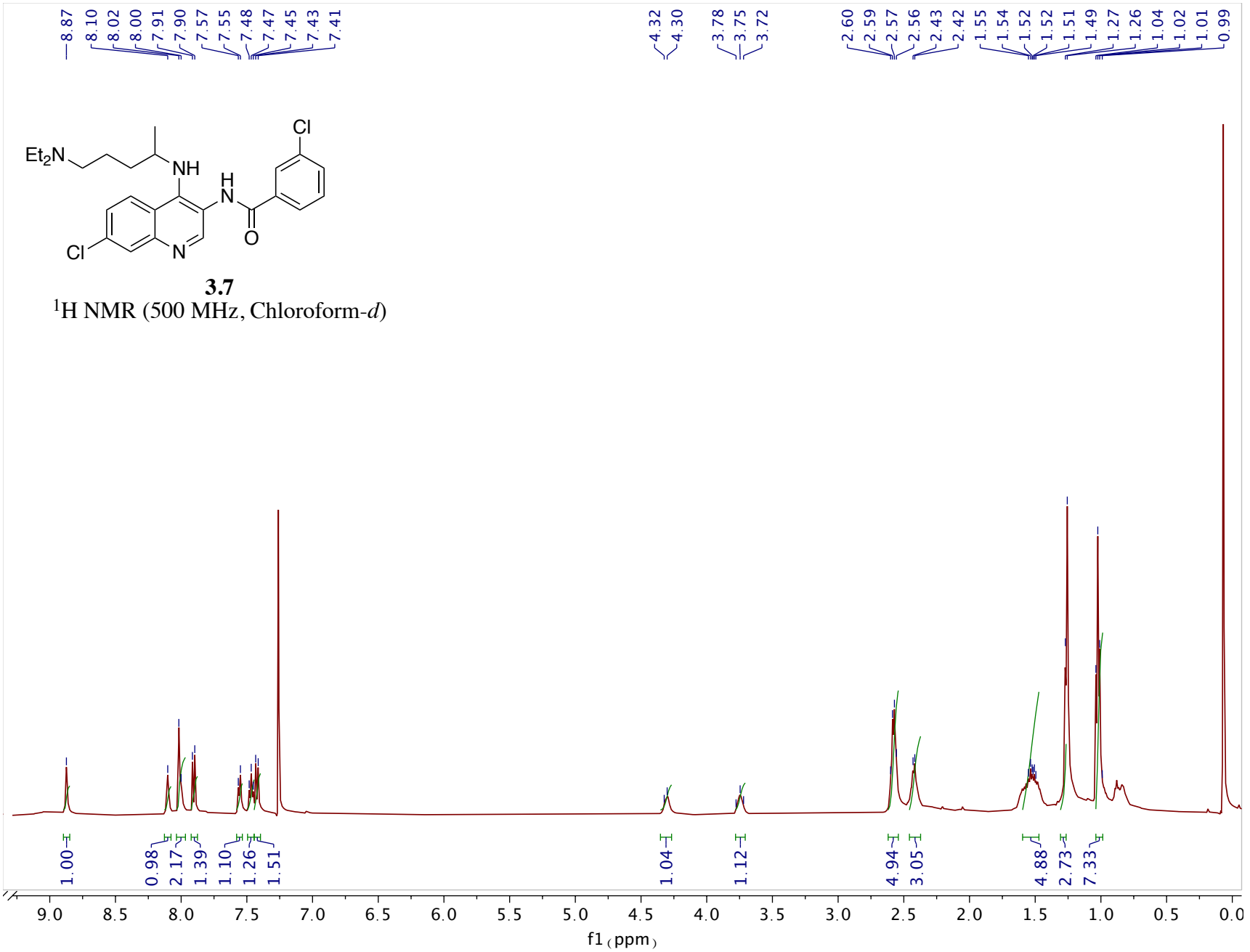

3.7

^{1}H NMR (500 MHz, Chloroform-*d*)

^{13}C NMR (126 MHz, Chloroform-*d*)

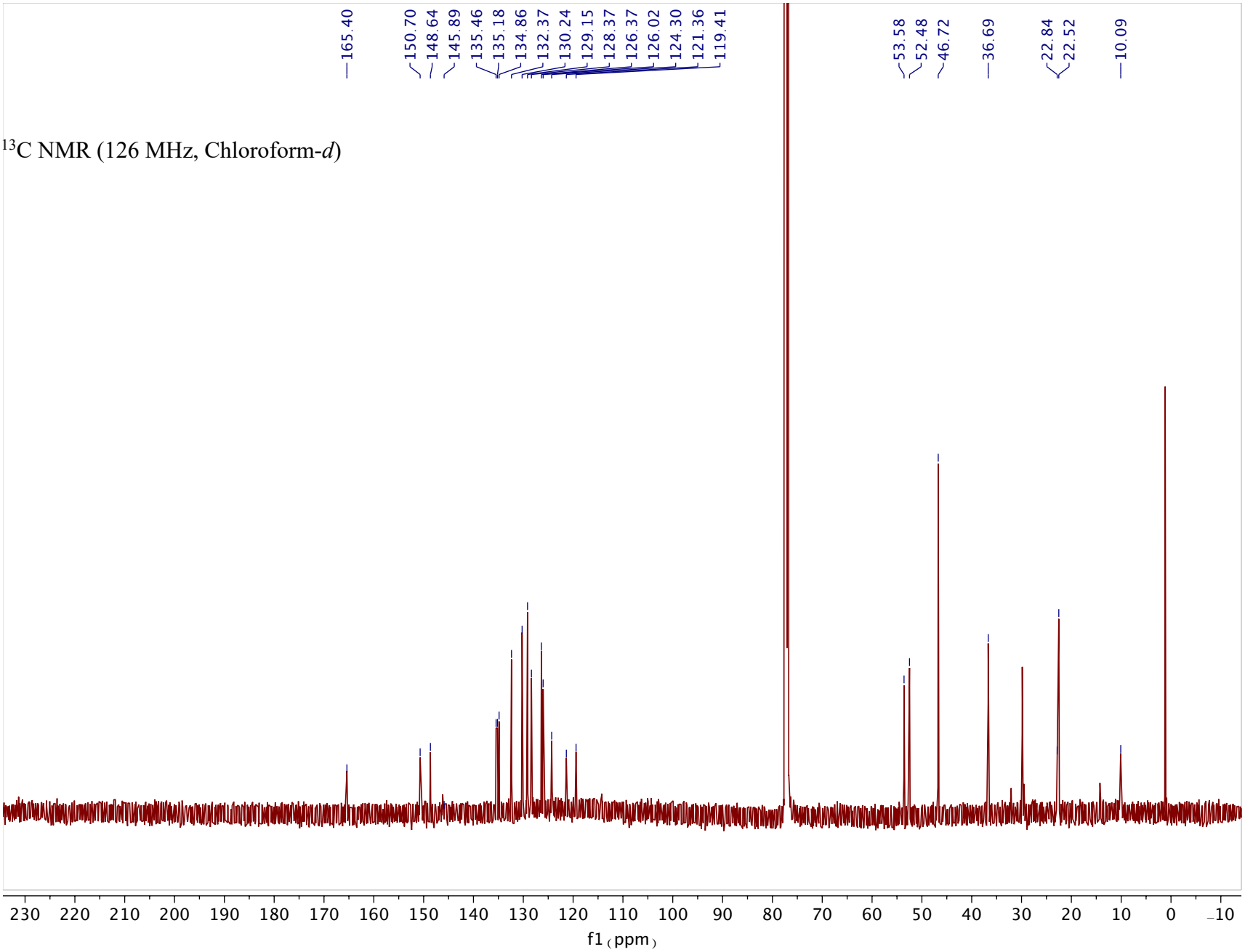

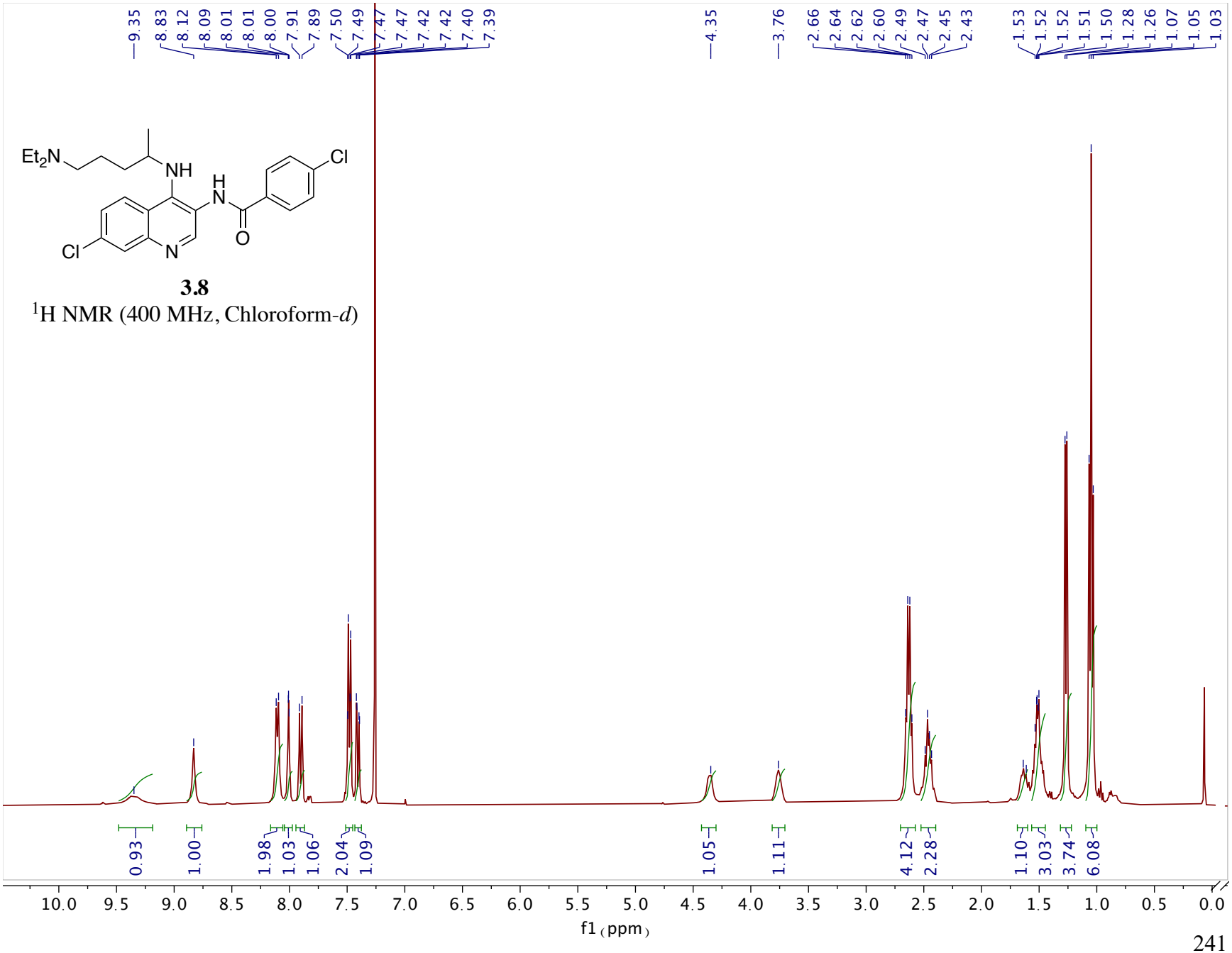

3.8

^{1}H NMR (400 MHz, Chloroform-*d*)

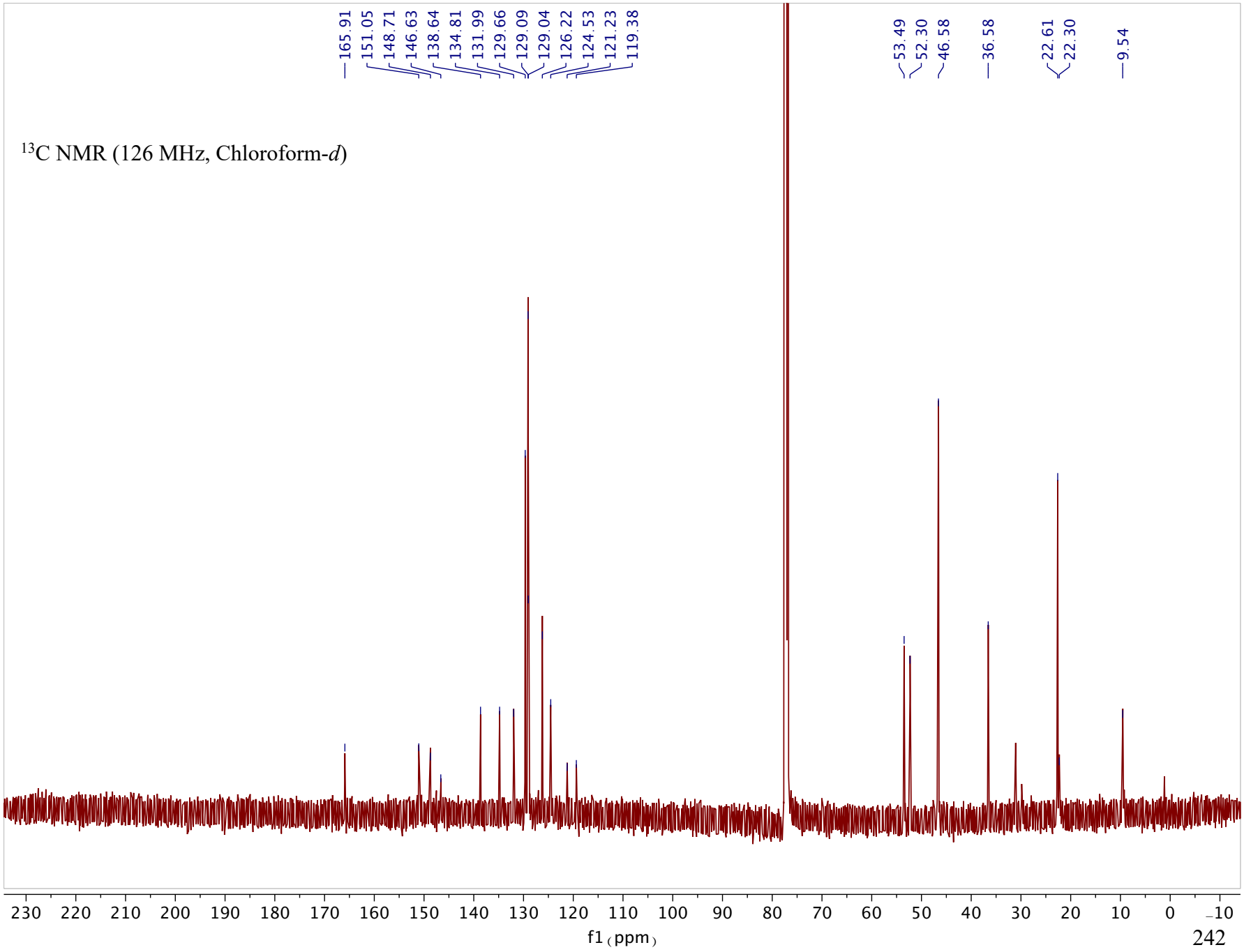
165.91
151.05
148.71
146.63
138.64
134.81
131.99
129.66
129.09
129.04
126.22
124.53
121.23
119.38
53.49
52.30
46.58
36.58
22.61
22.30
9.54
13C NMR (126 MHz, Chloroform-d)
230 220 210 200 190 180 170 160 150 140 130 120 110 100 90 80 70 60 50 40 30 20 10 0 -10
f1 (ppm)

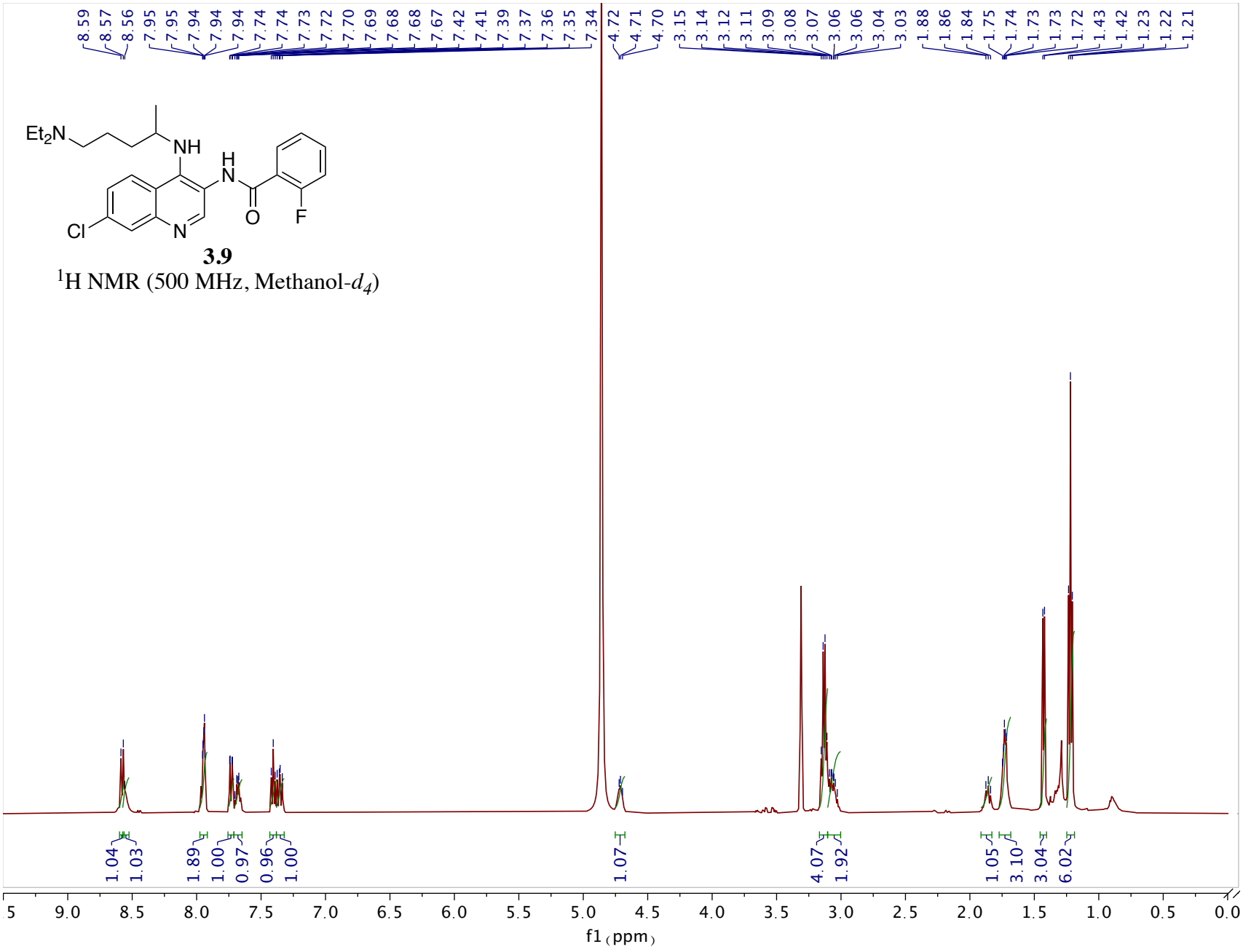

3.9

^{1}H NMR (500 MHz, Methanol-d_4)

^{13}C NMR (126 MHz, Methanol-d_4)

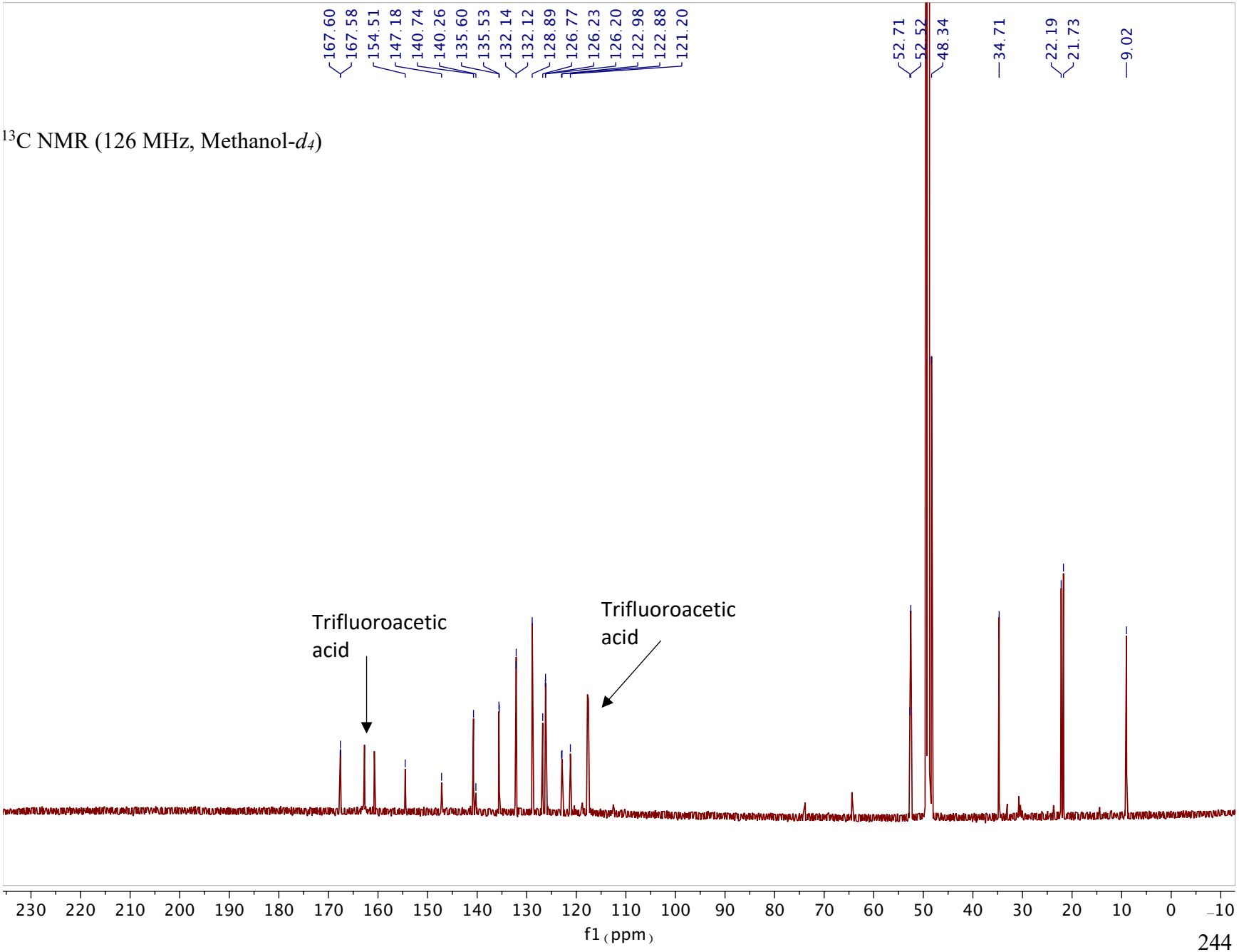

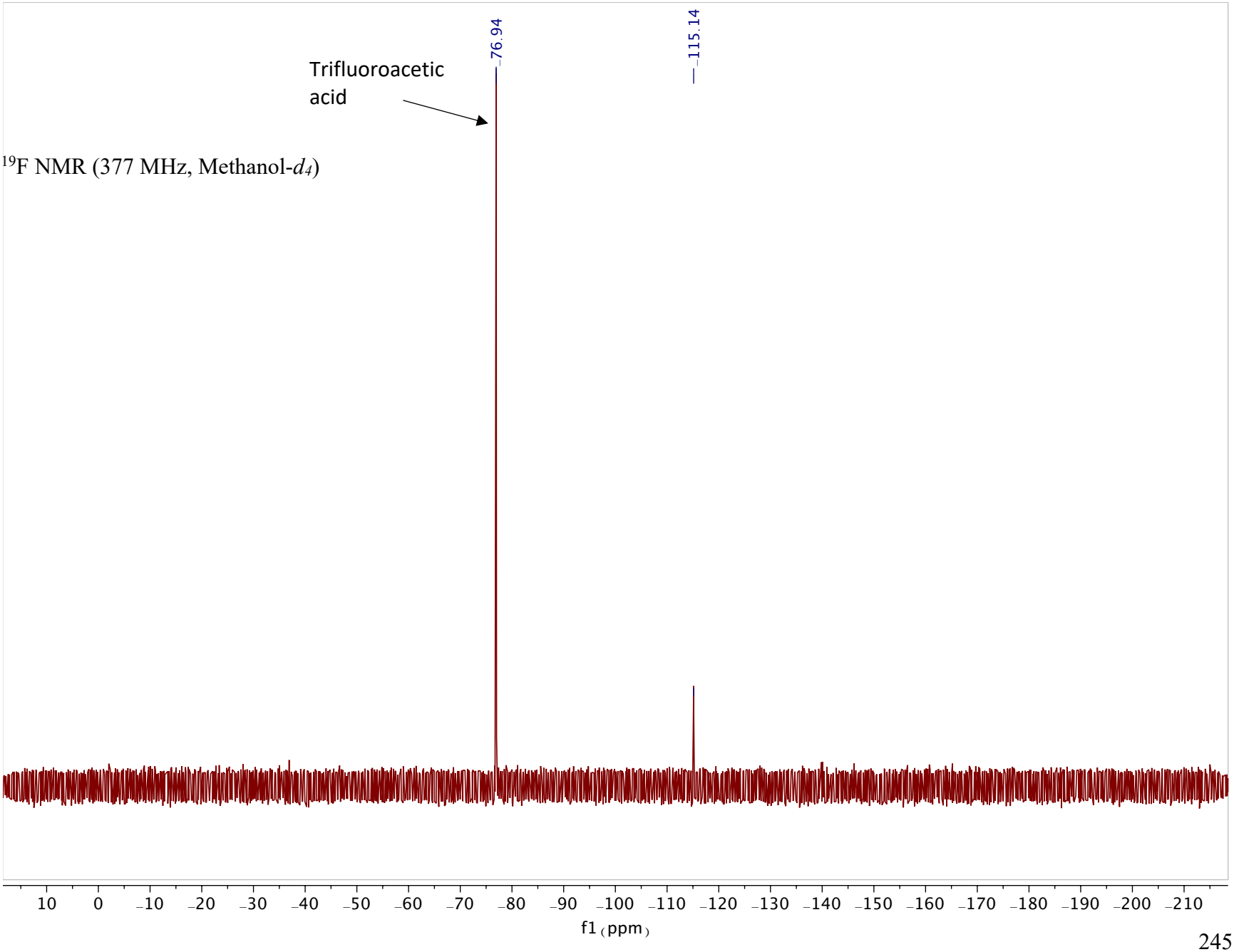

^{19}F NMR (377 MHz, Methanol-d_4)

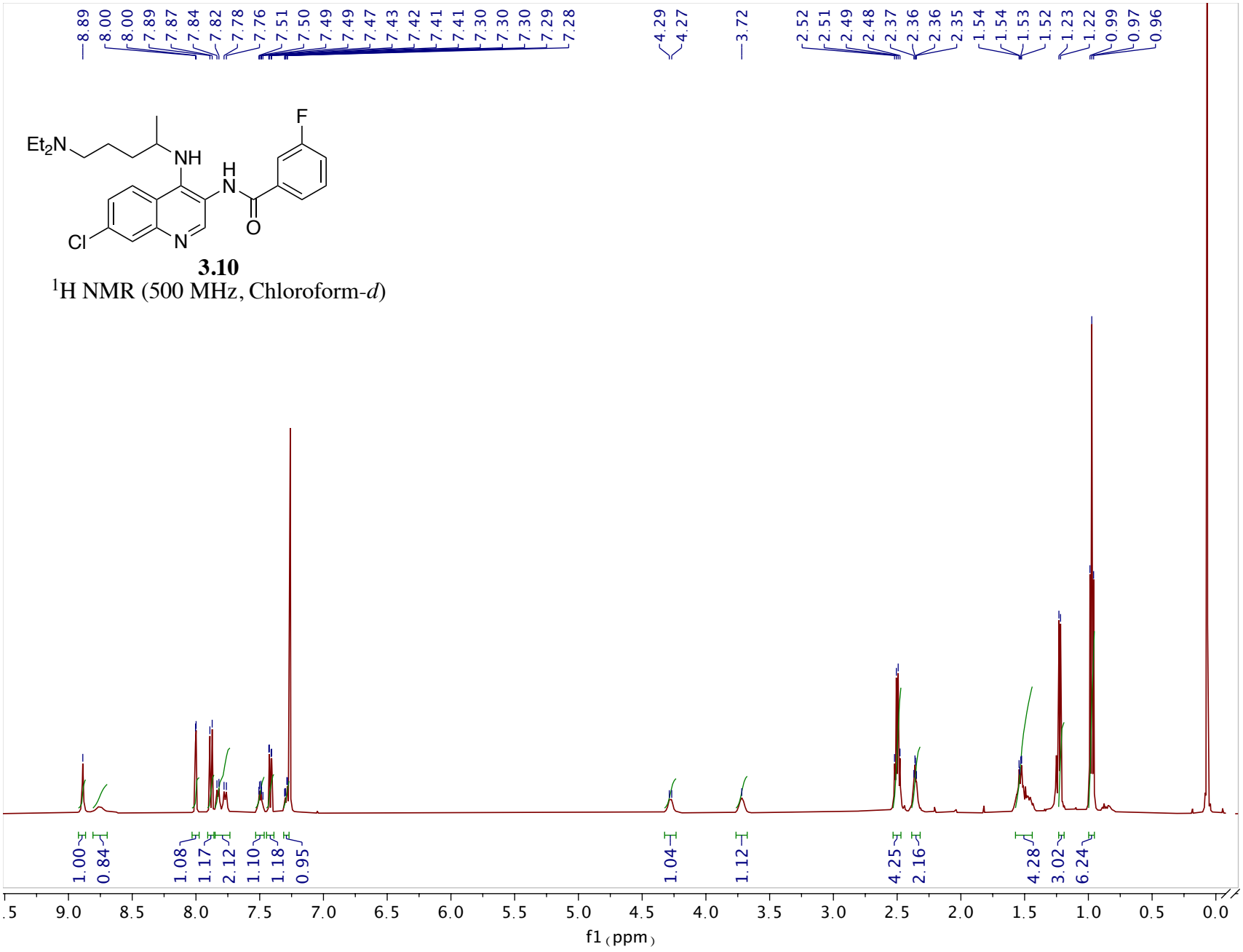

3.10

^{1}H NMR (500 MHz, Chloroform-*d*)

^{13}C NMR (126 MHz, Chloroform-*d*)

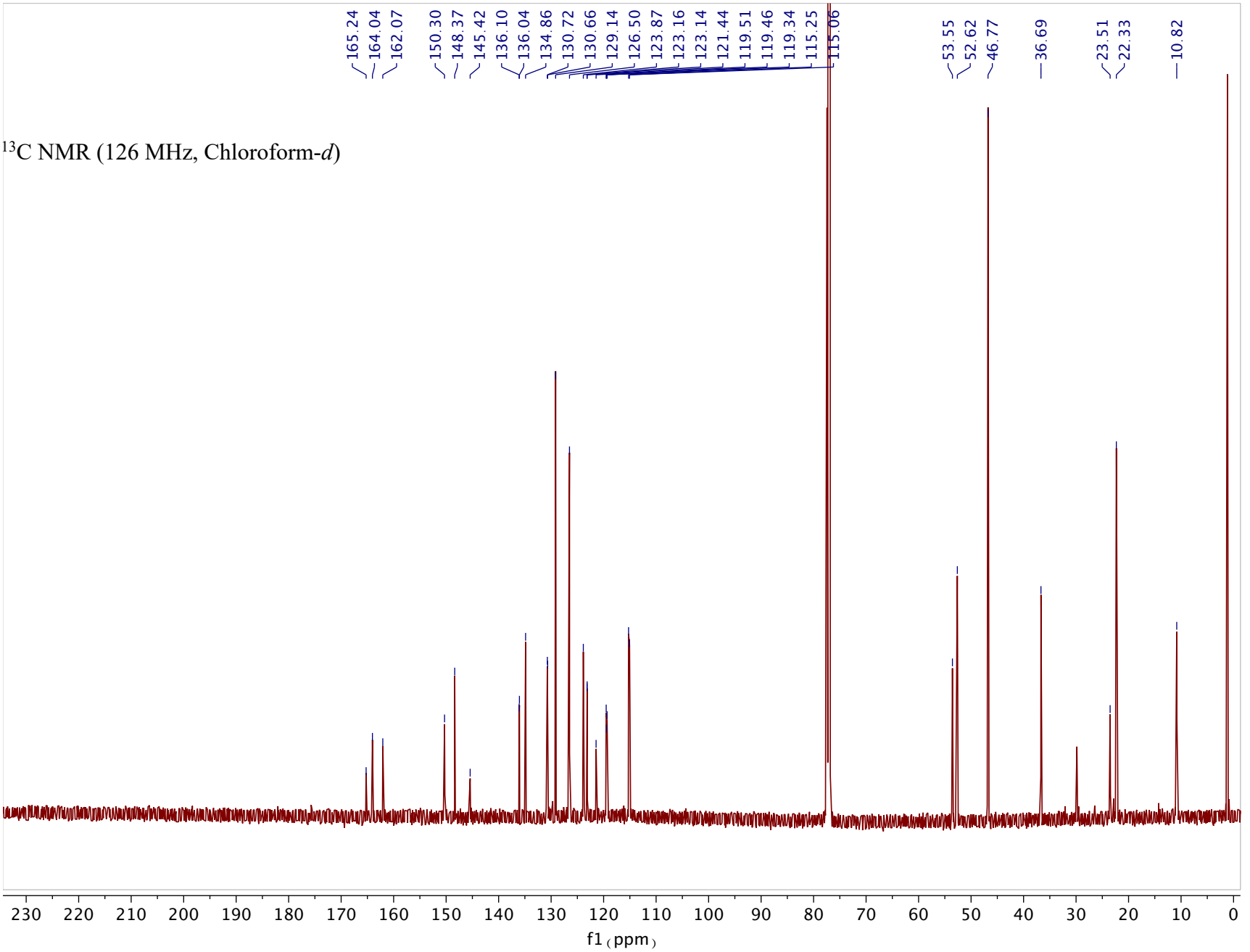

^{19}F NMR (377 MHz, Chloroform-*d*)

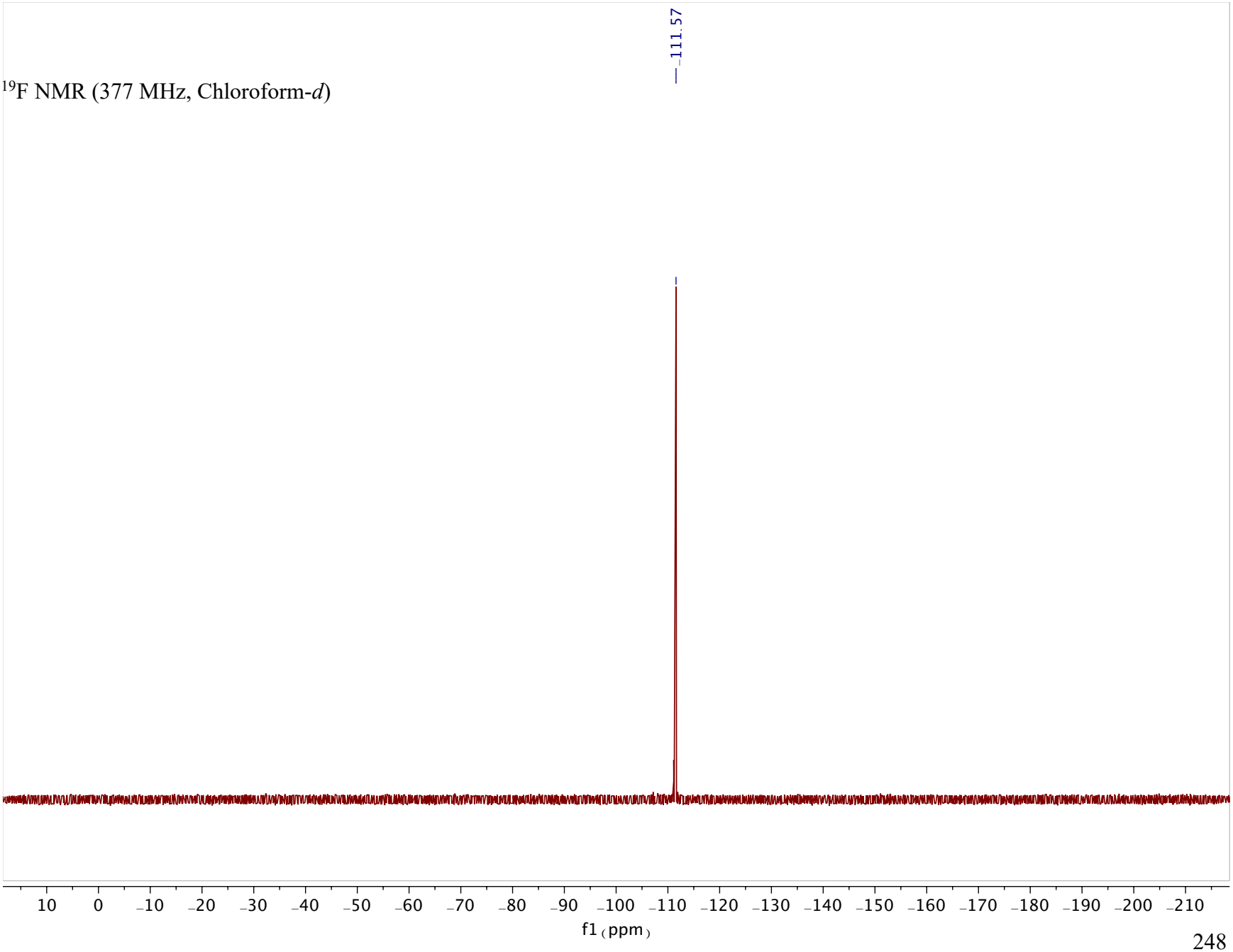

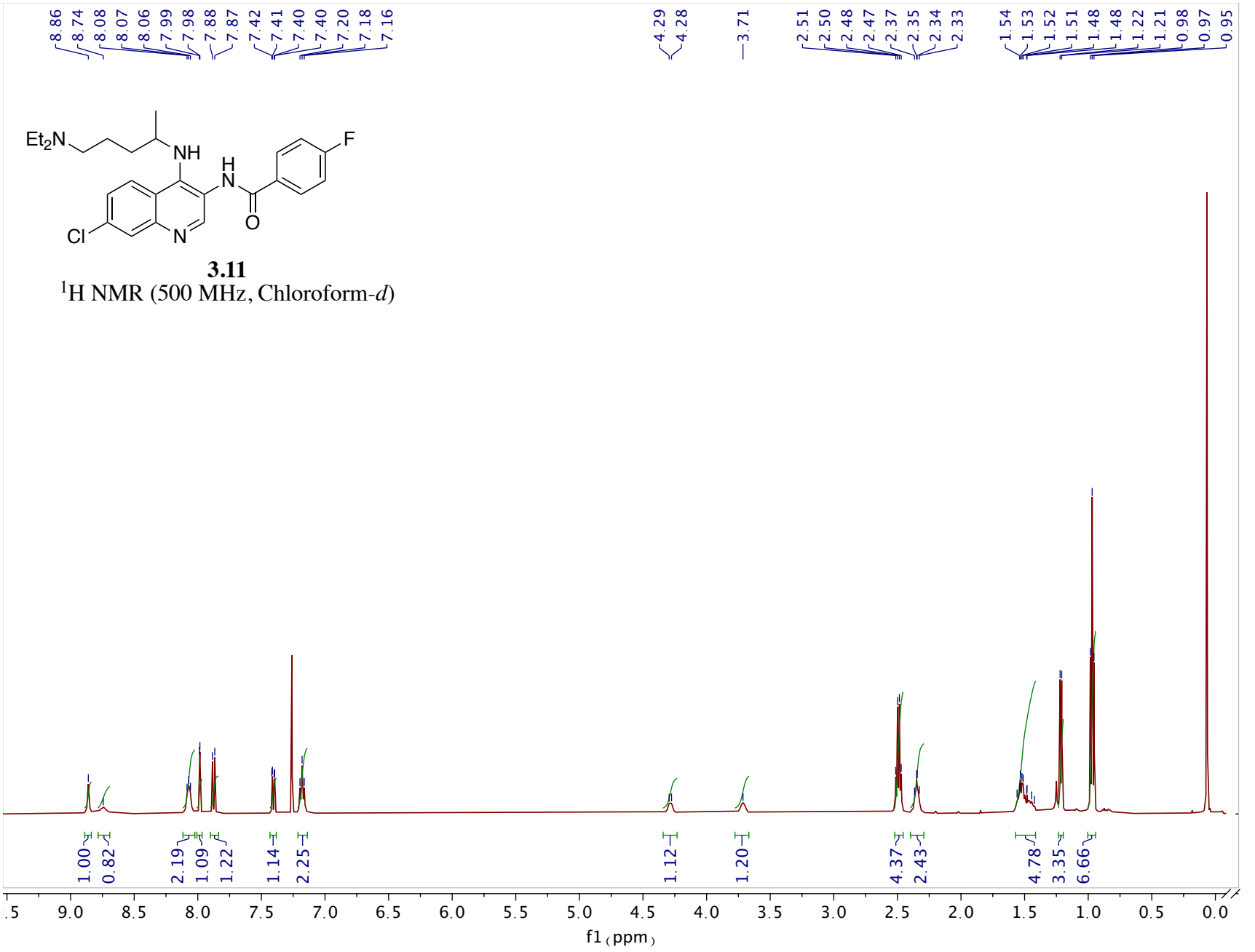

3.11

^{1}H NMR (500 MHz, Chloroform-*d*)

^{13}C NMR (126 MHz, Chloroform-*d*)

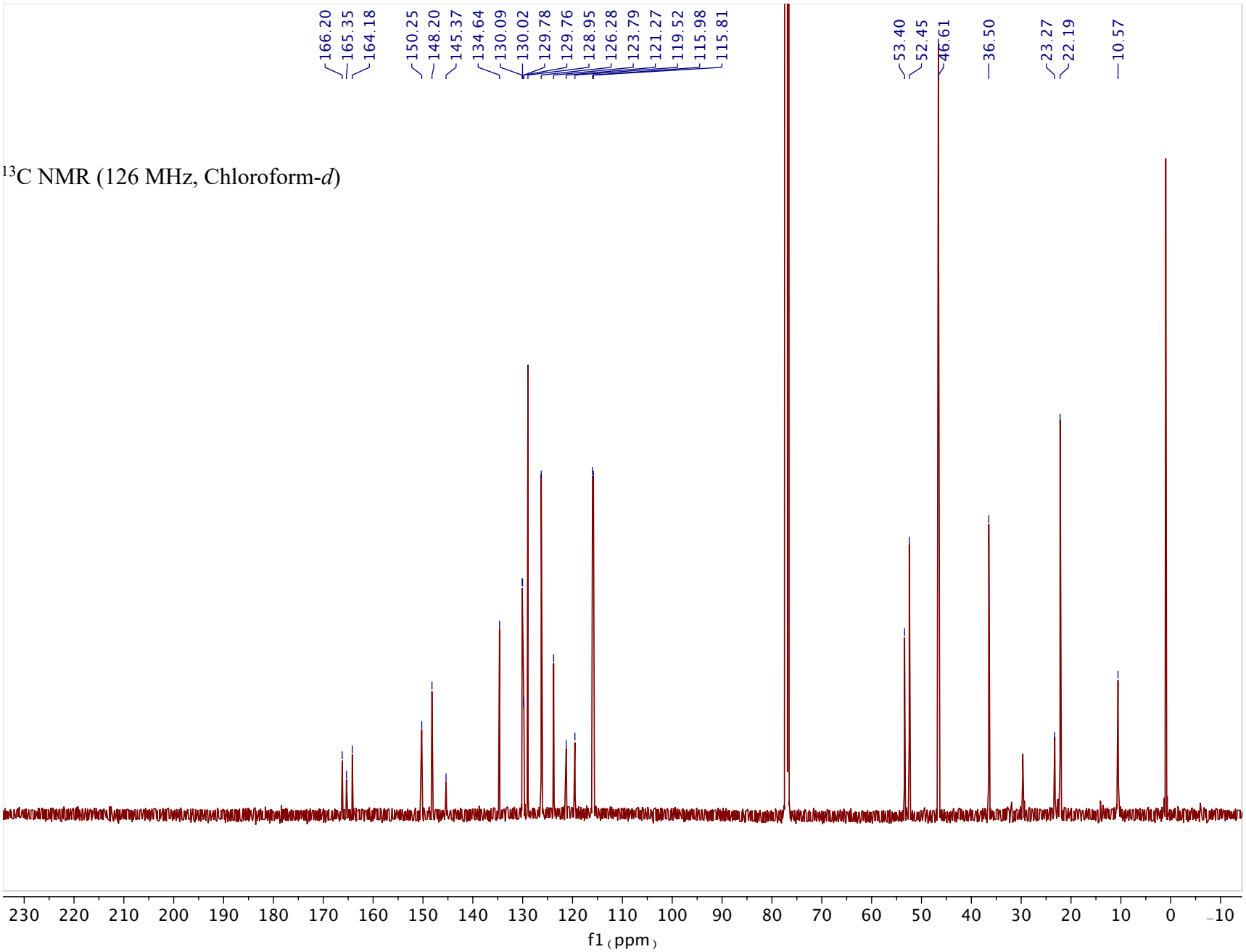

^{19}F NMR (377 MHz, Chloroform-*d*)

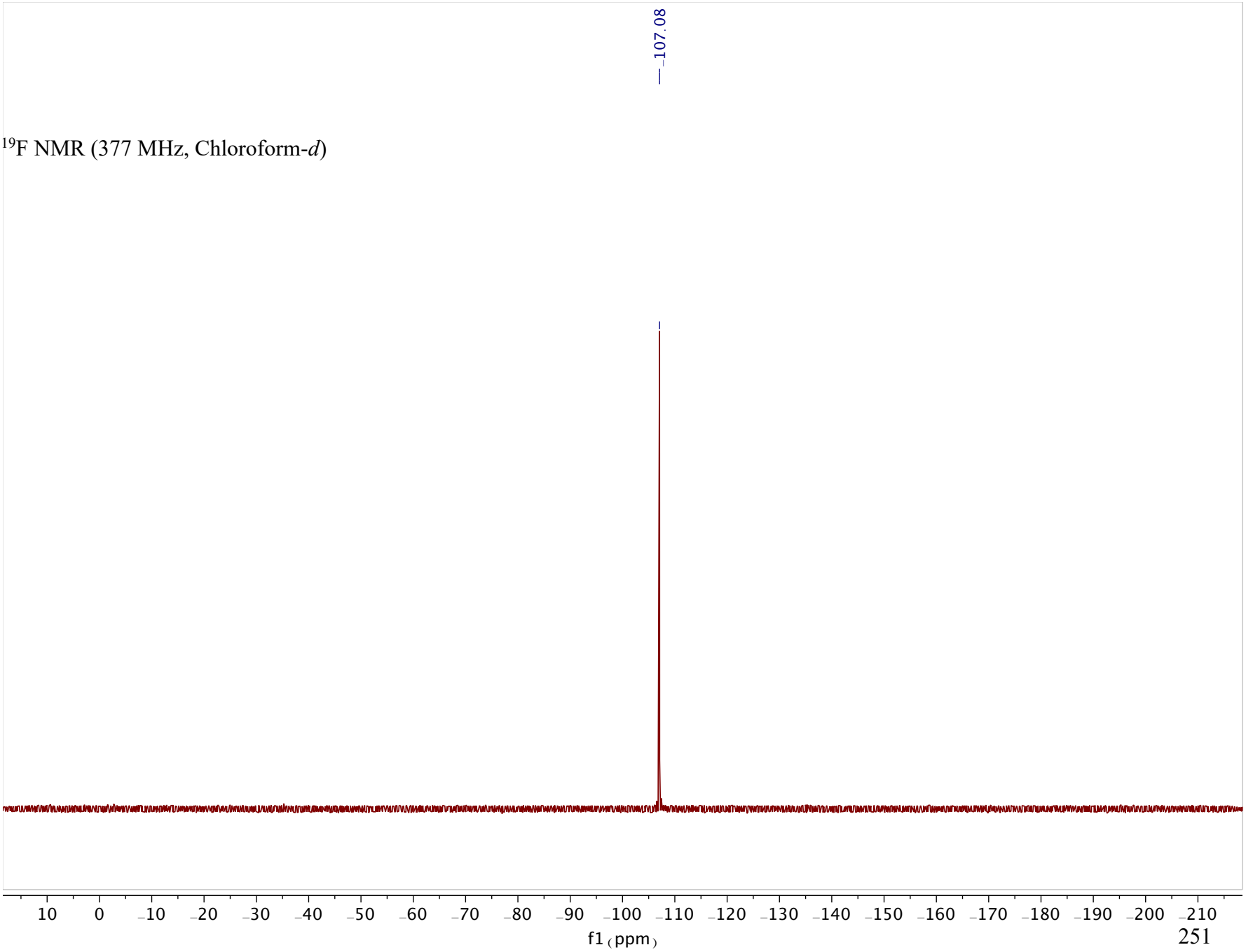

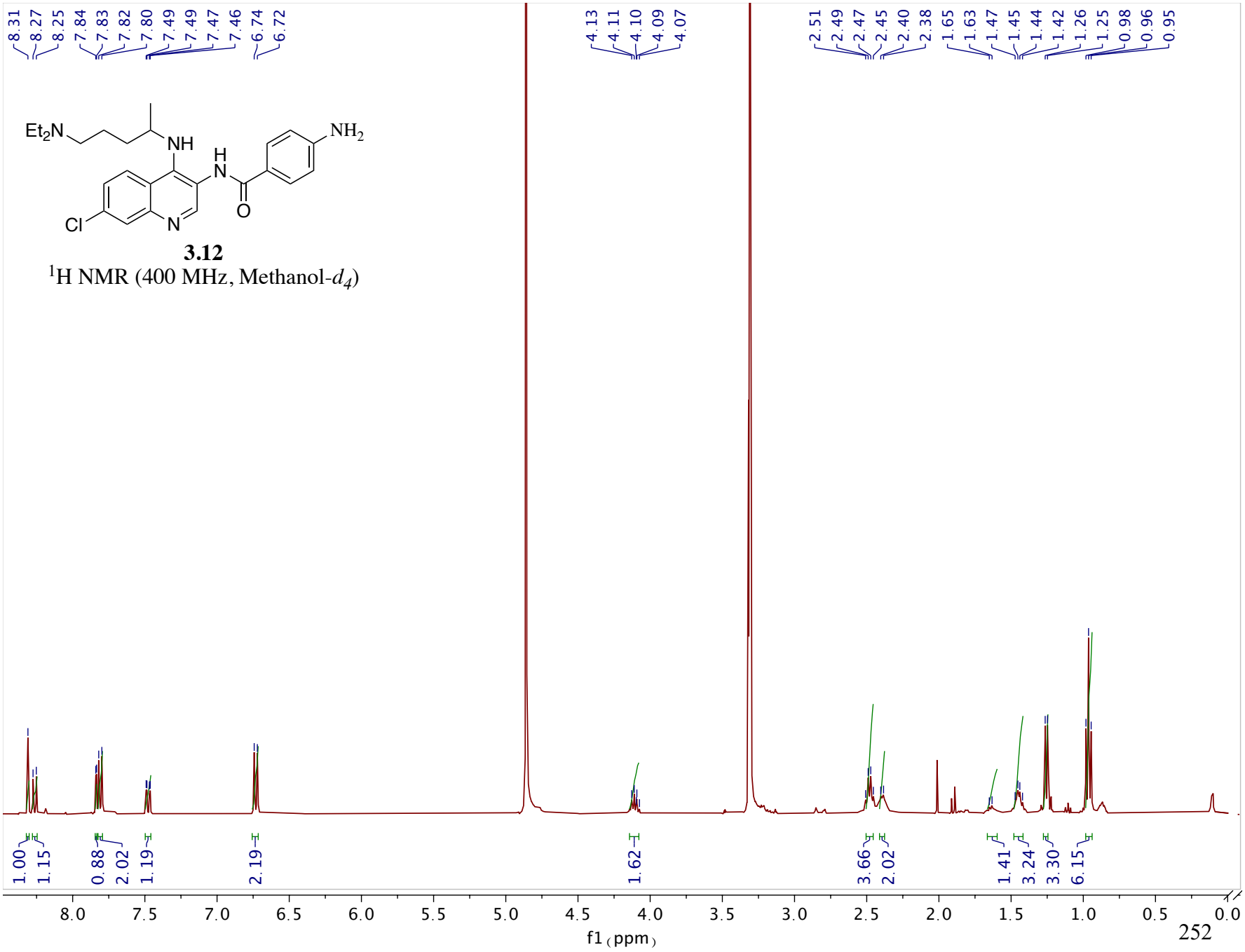

3.12

^{1}H NMR (400 MHz, Methanol-d_4)

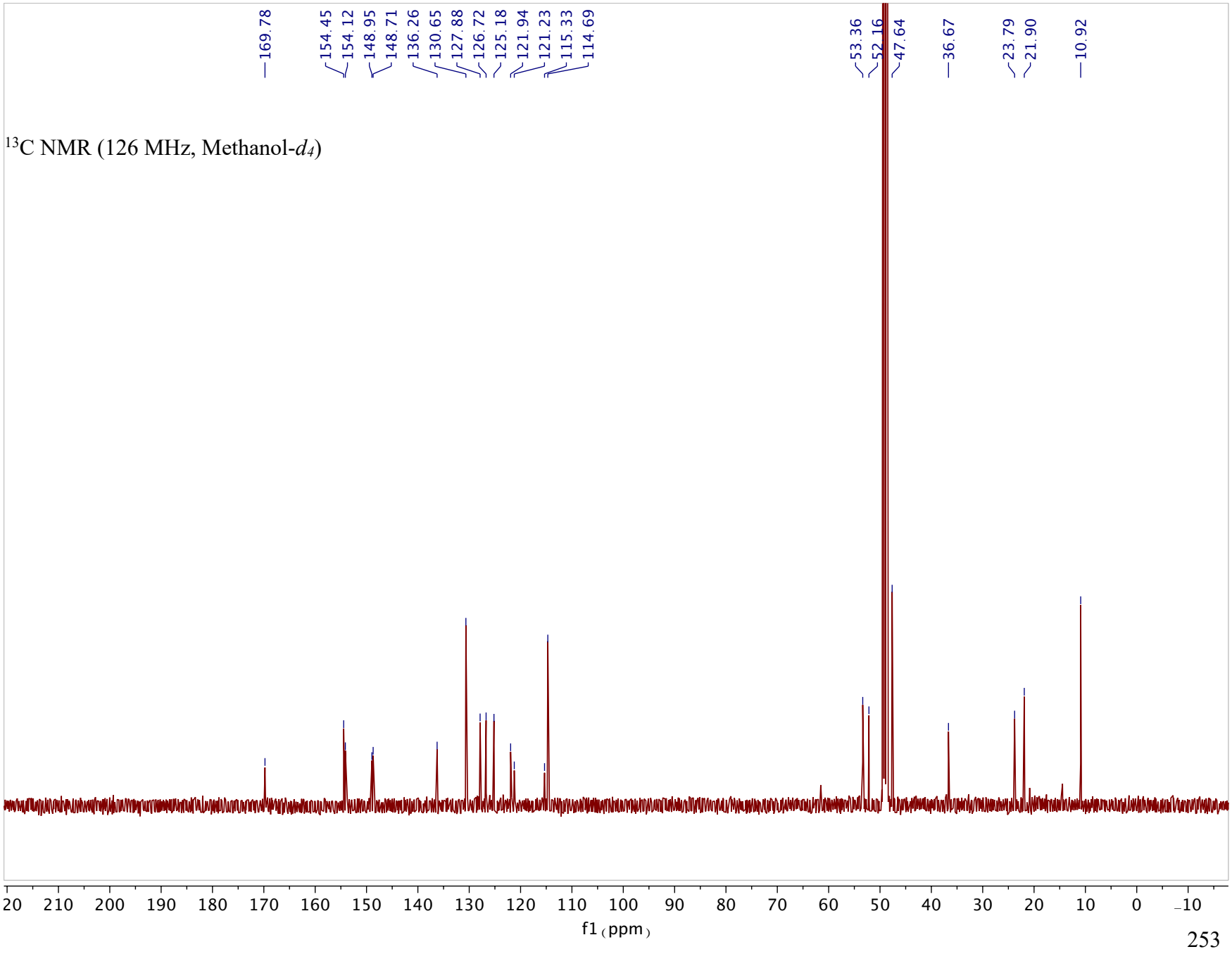

^{13}C NMR (126 MHz, Methanol-d_4)

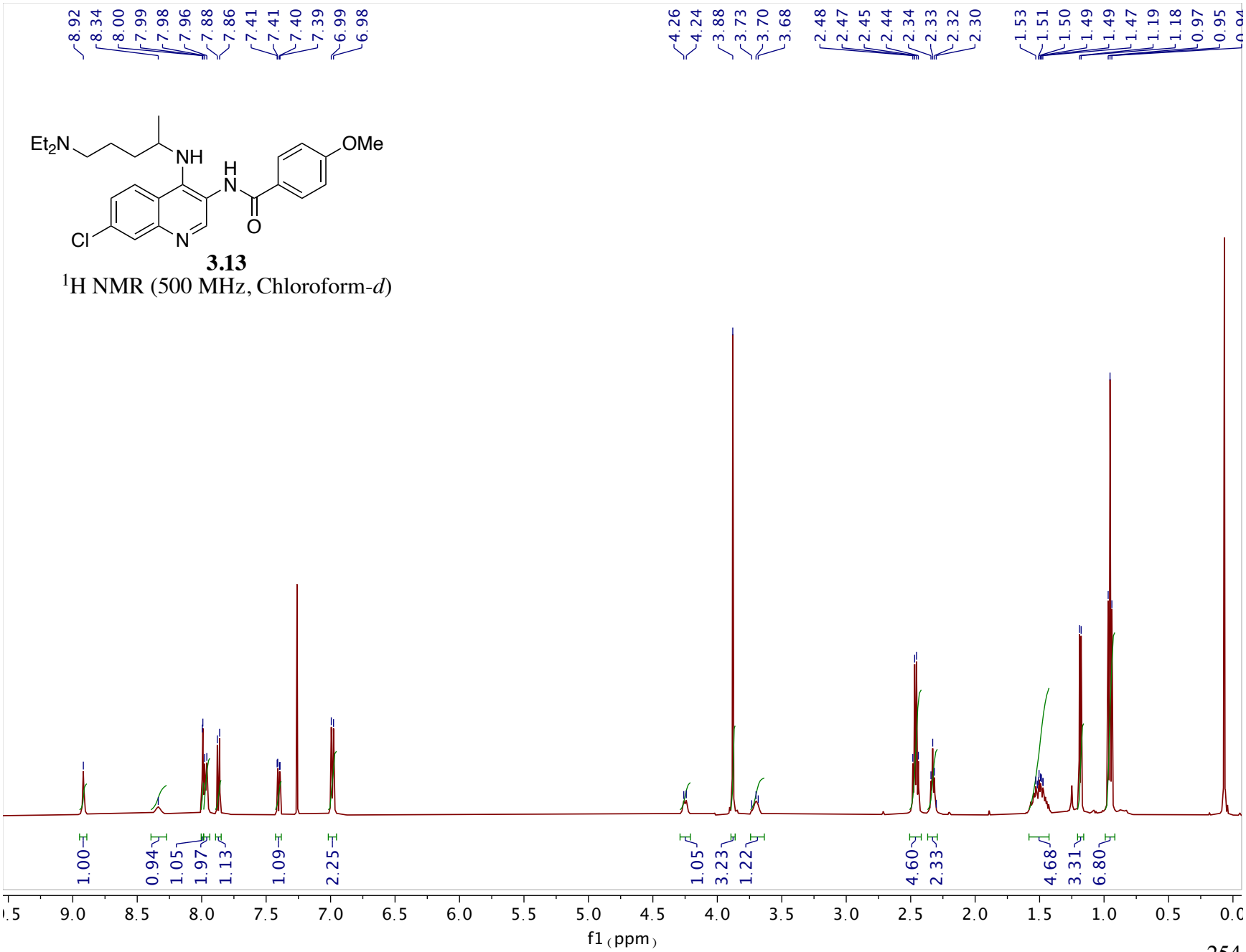

3.13

^{1}H NMR (500 MHz, Chloroform-*d*)

^{13}C NMR (126 MHz, Chloroform-*d*)

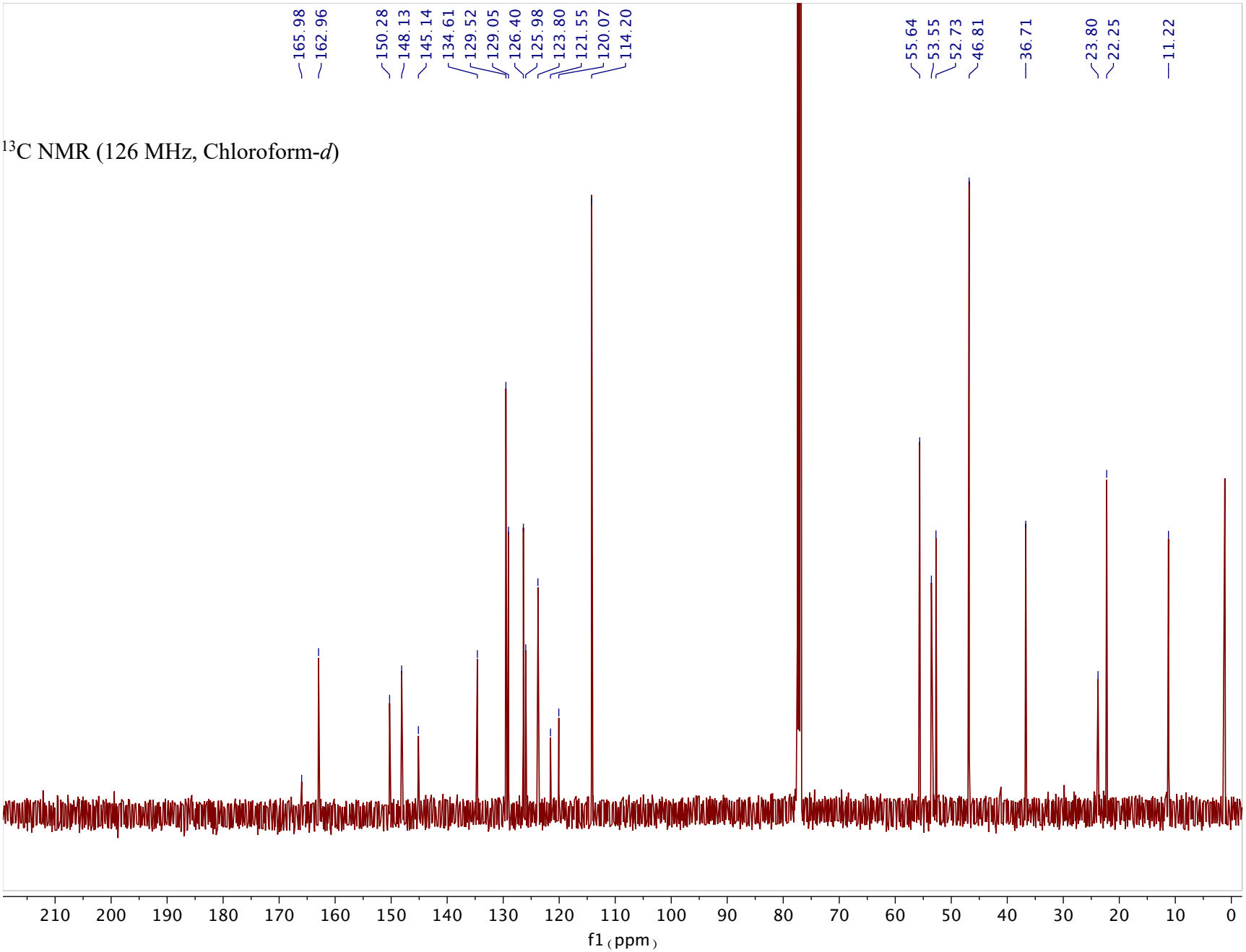

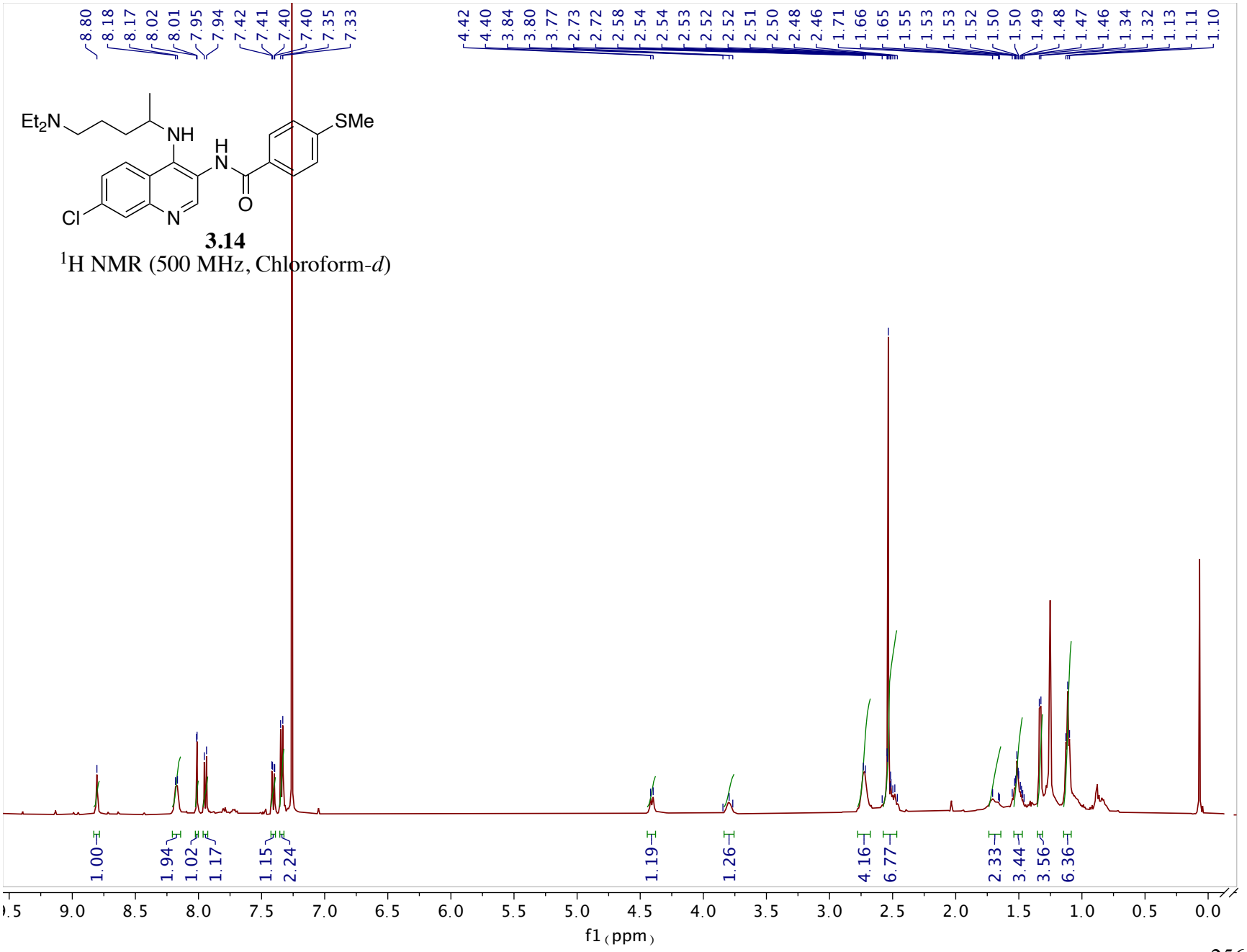

3.14

^{1}H NMR (500 MHz, Chloroform-*d*)

^{13}C NMR (126 MHz, Chloroform-*d*)

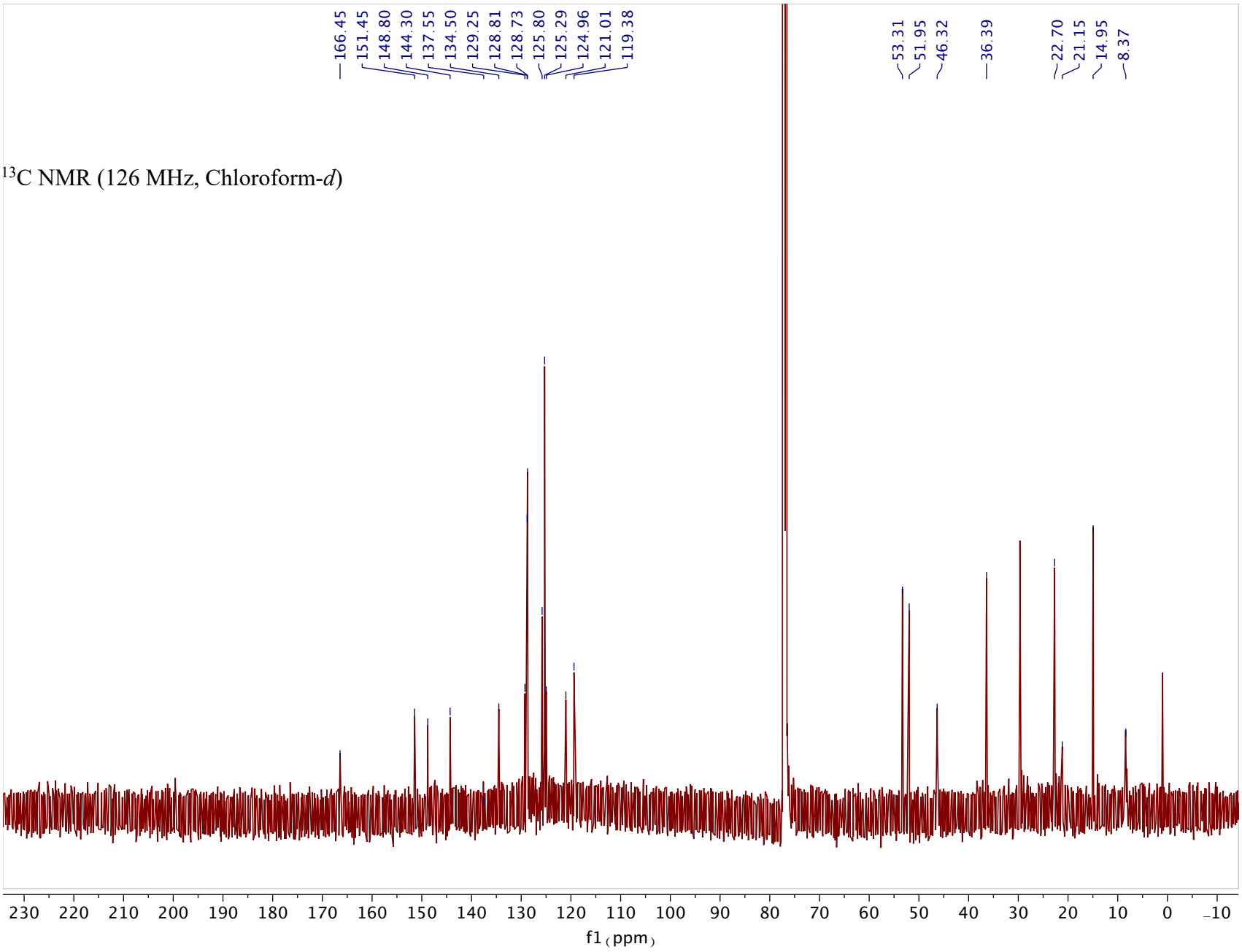

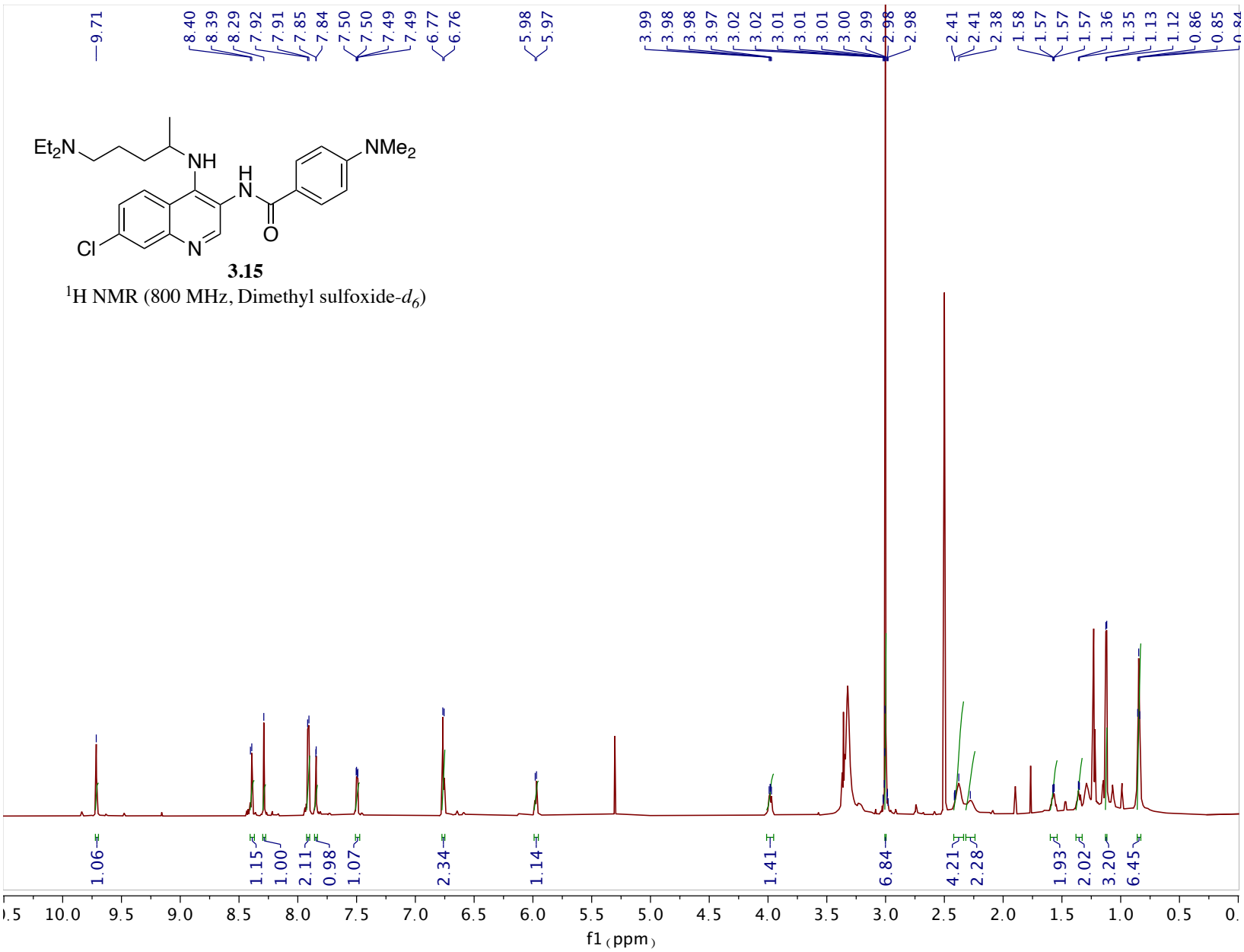

3.15

^{1}H NMR (800 MHz, Dimethyl sulfoxide-d_6)

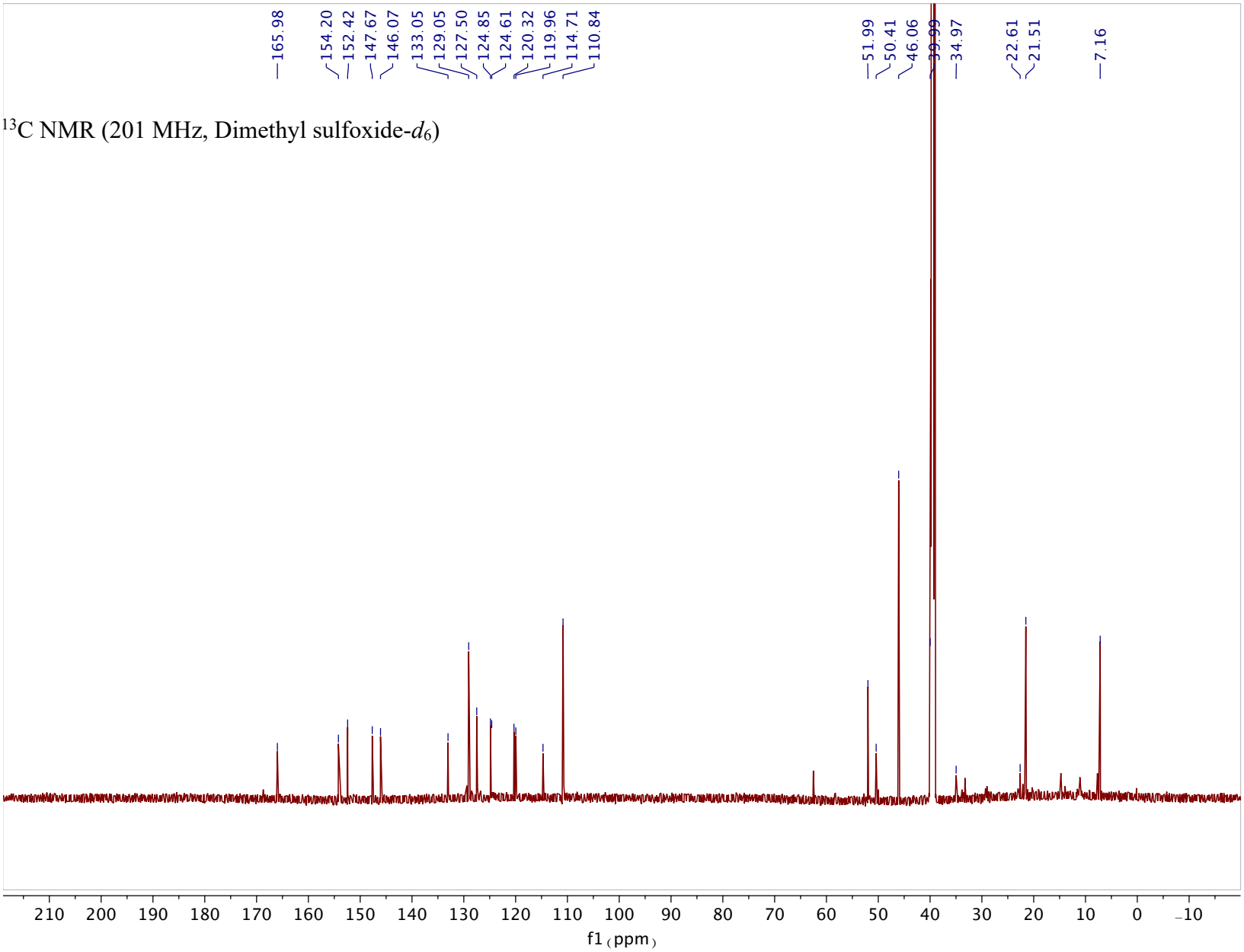

^{13}C NMR (201 MHz, Dimethyl sulfoxide-d_6)

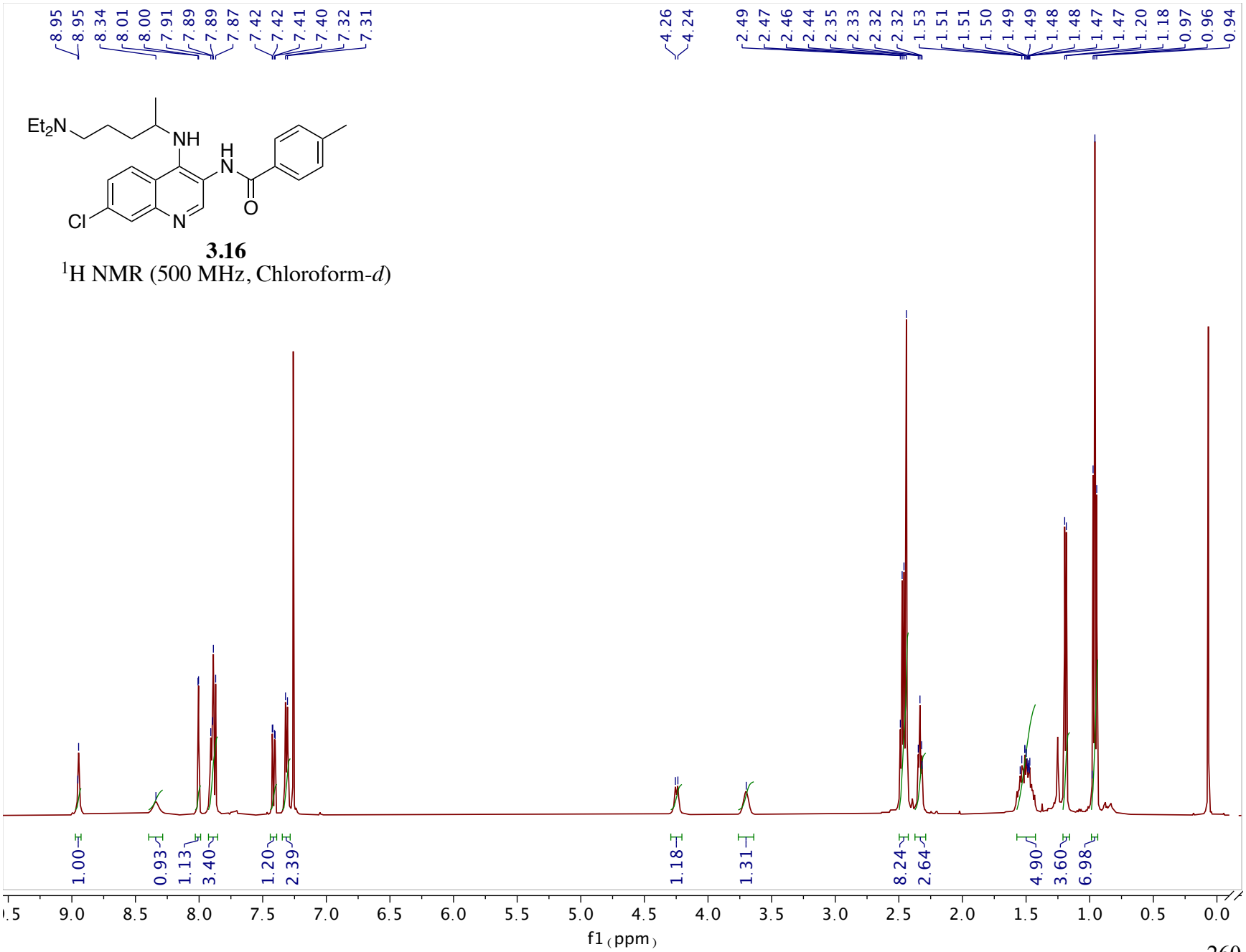

3.16

^{1}H NMR (500 MHz, Chloroform-*d*)

^{13}C NMR (126 MHz, Chloroform-*d*)

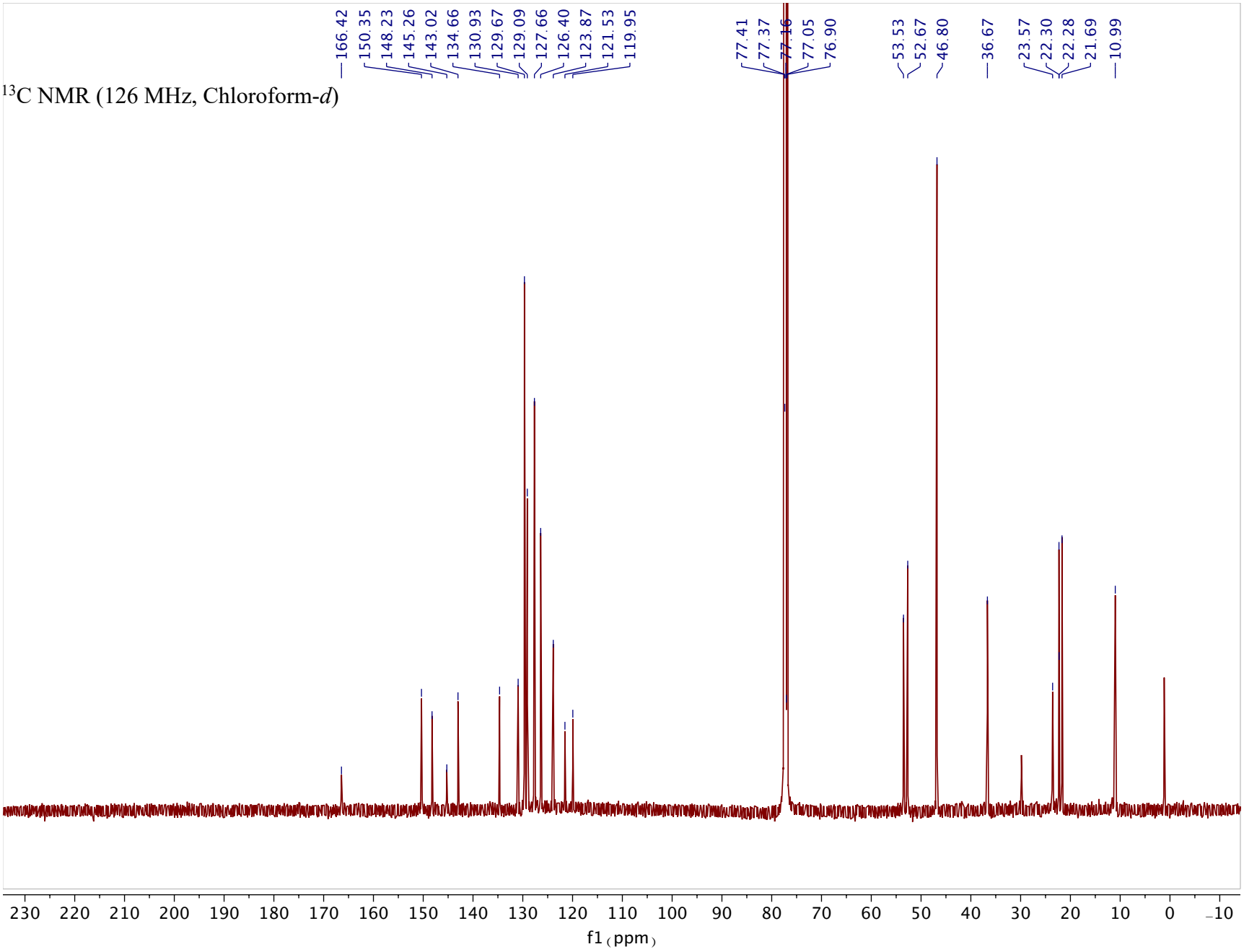

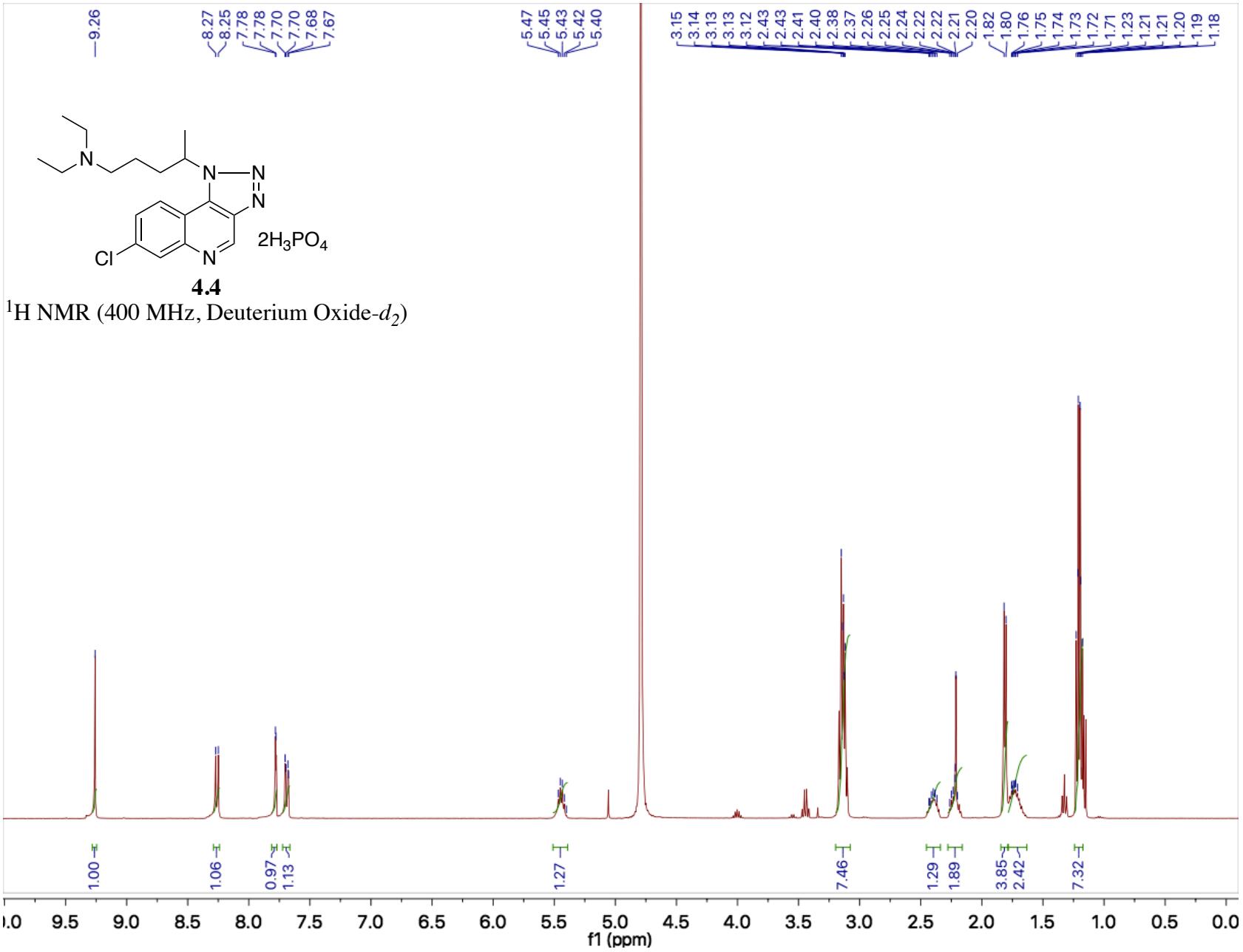

4.4

^{1}H NMR (400 MHz, Deuterium Oxide-d_2)

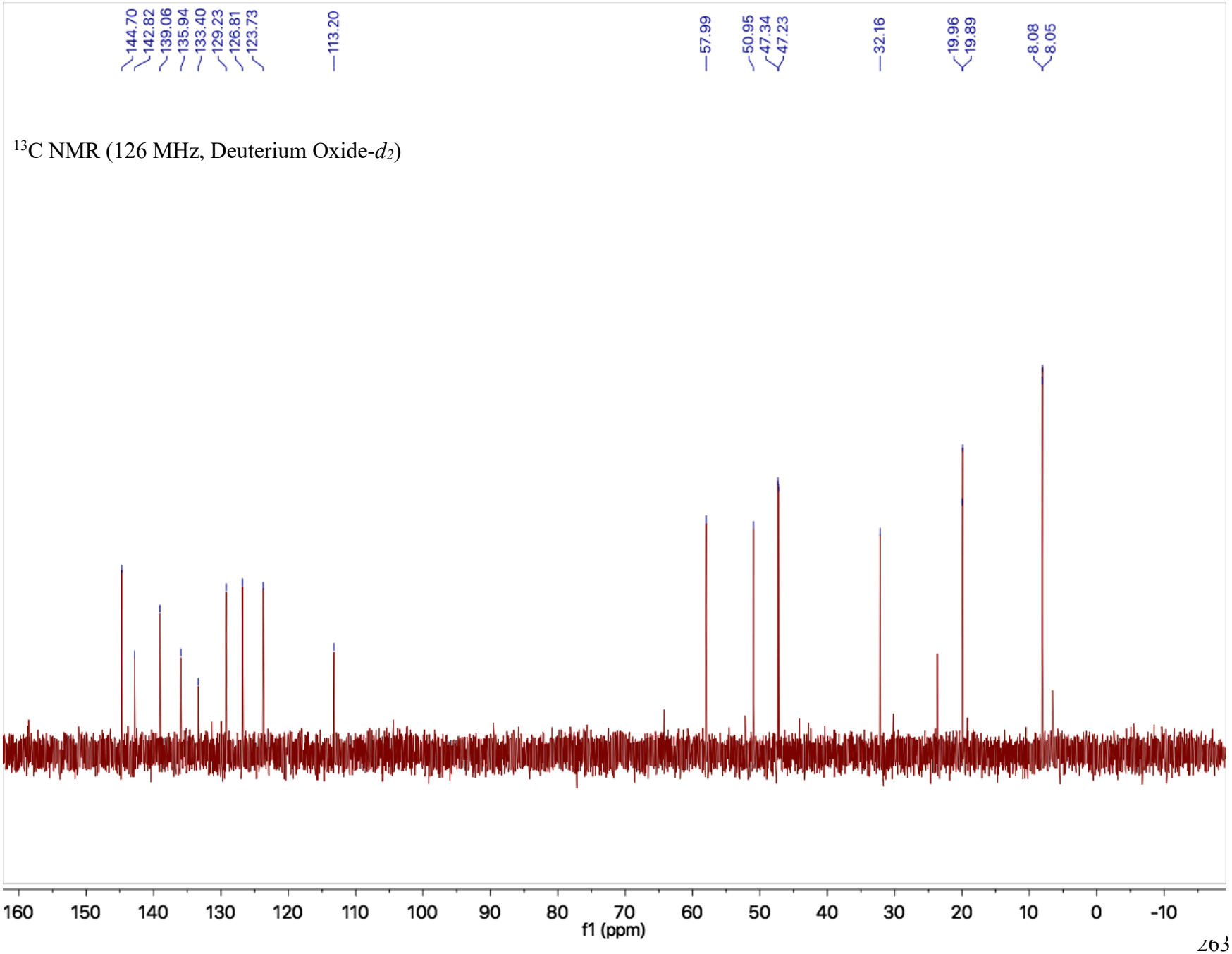

^{13}C NMR (126 MHz, Deuterium Oxide-d_2)

^{31}P NMR (162 MHz, Deuterium Oxide-d_2)

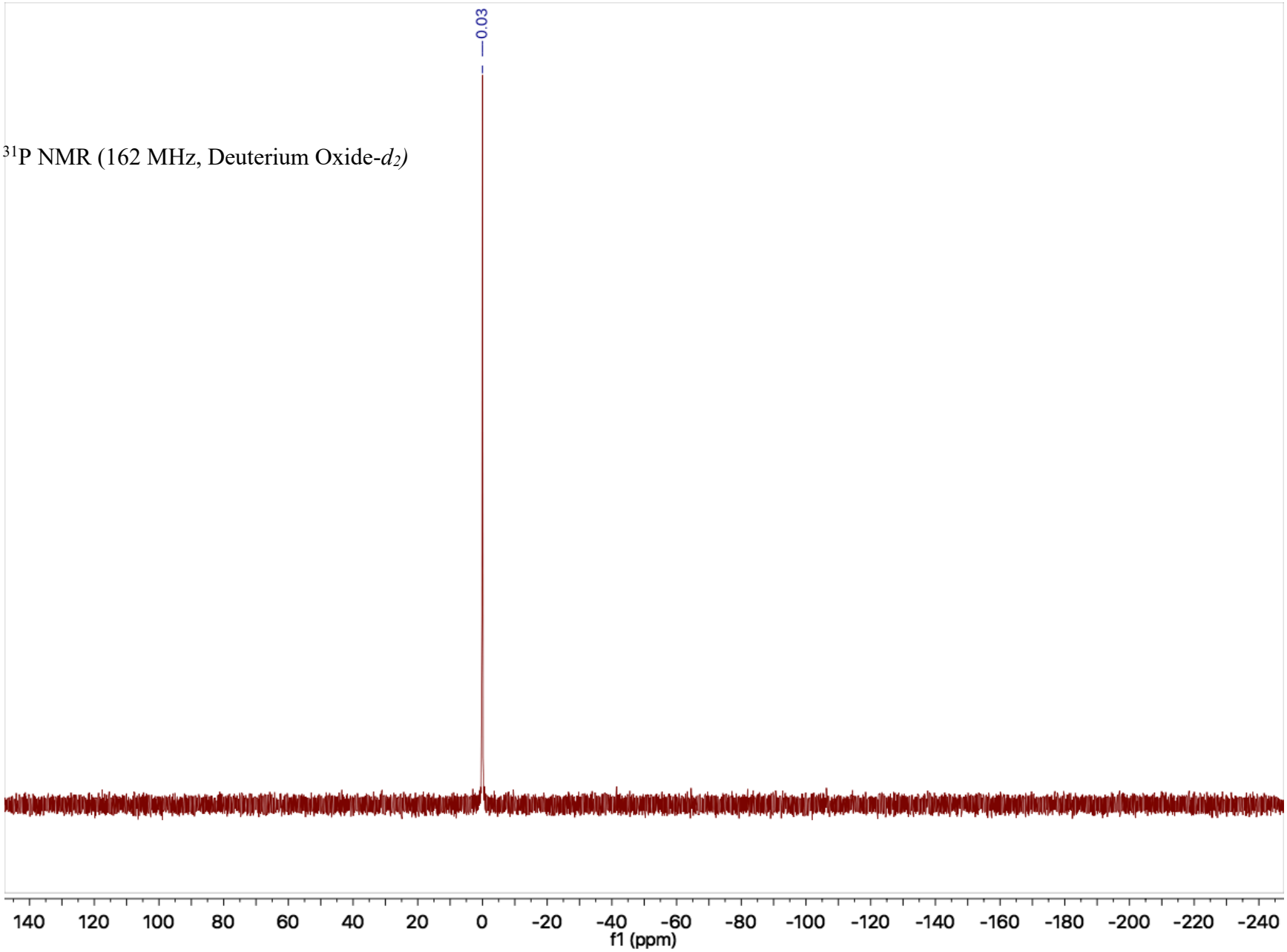

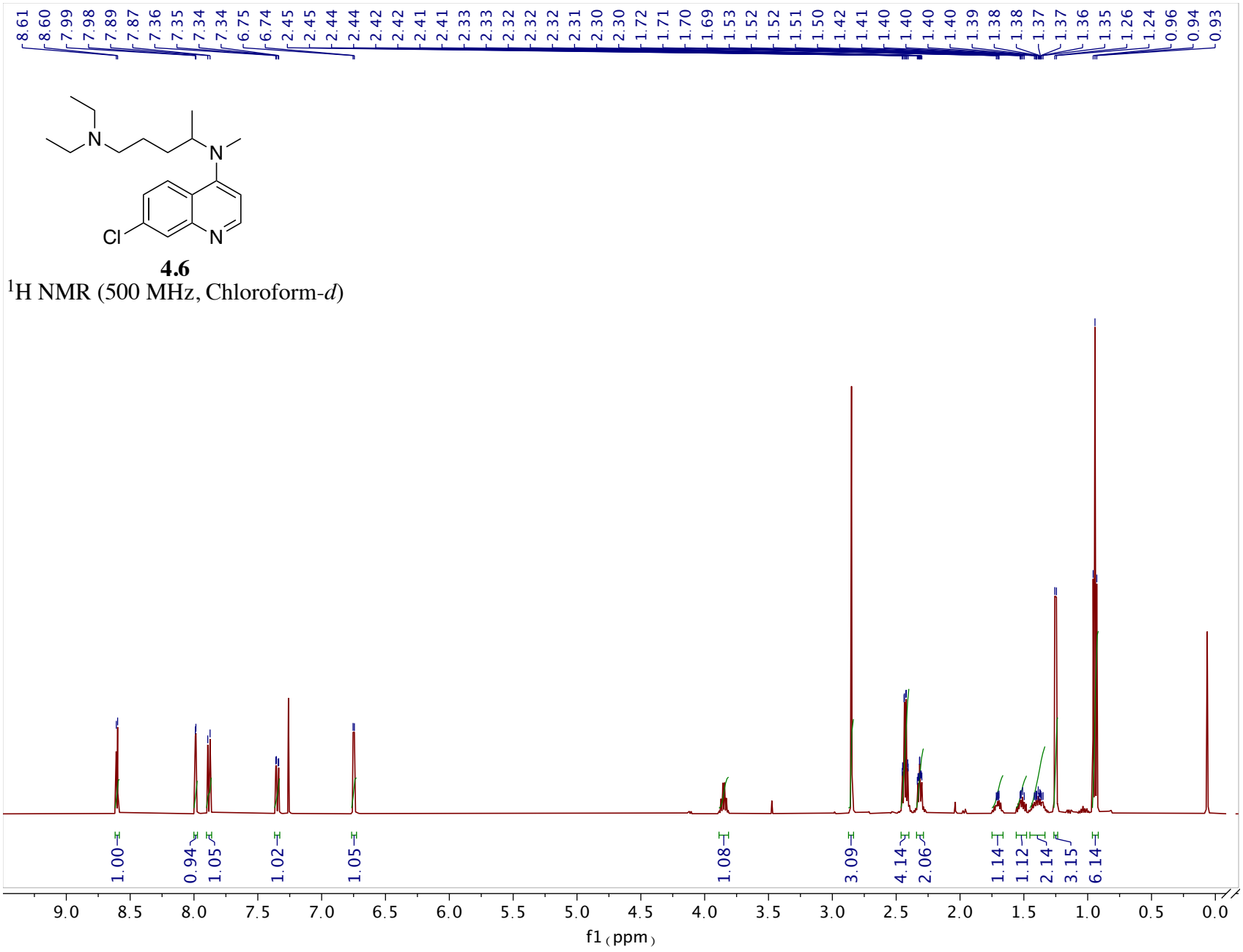

4.6

^{1}H NMR (500 MHz, Chloroform-*d*)

^{13}C NMR (126 MHz, Chloroform-*d*)

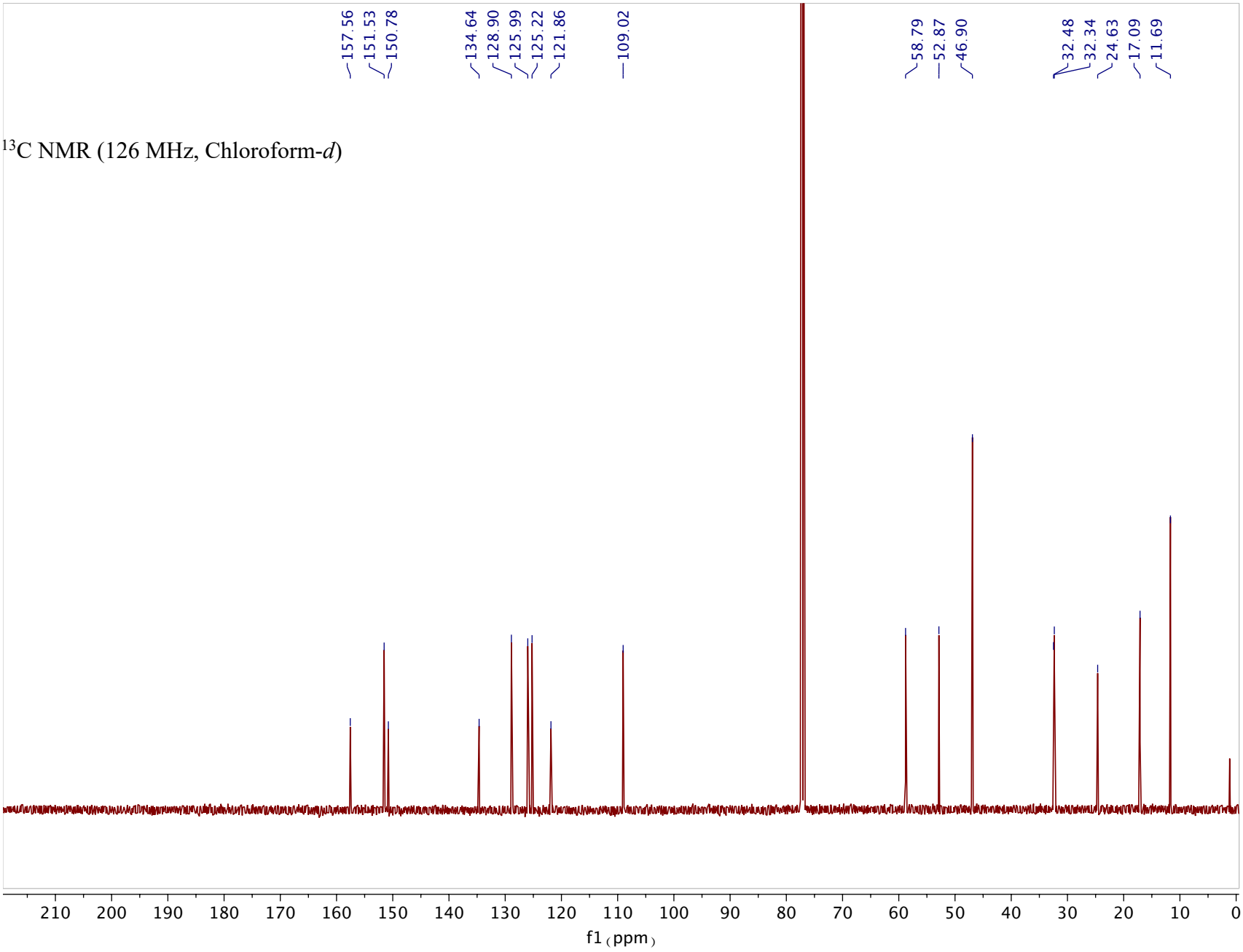

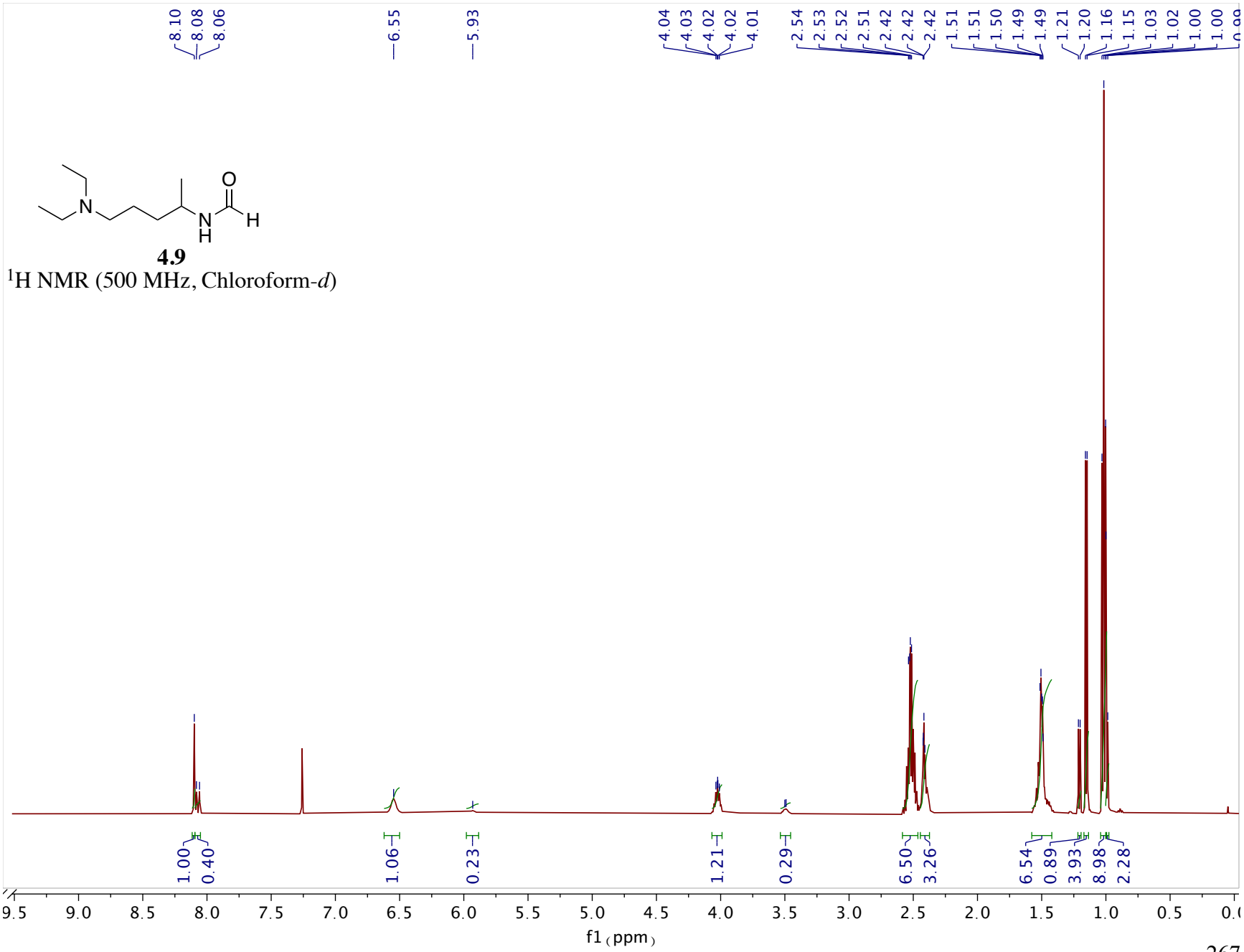

4.9

^{1}H NMR (500 MHz, Chloroform-*d*)

^{13}C NMR (126 MHz, Chloroform-*d*)

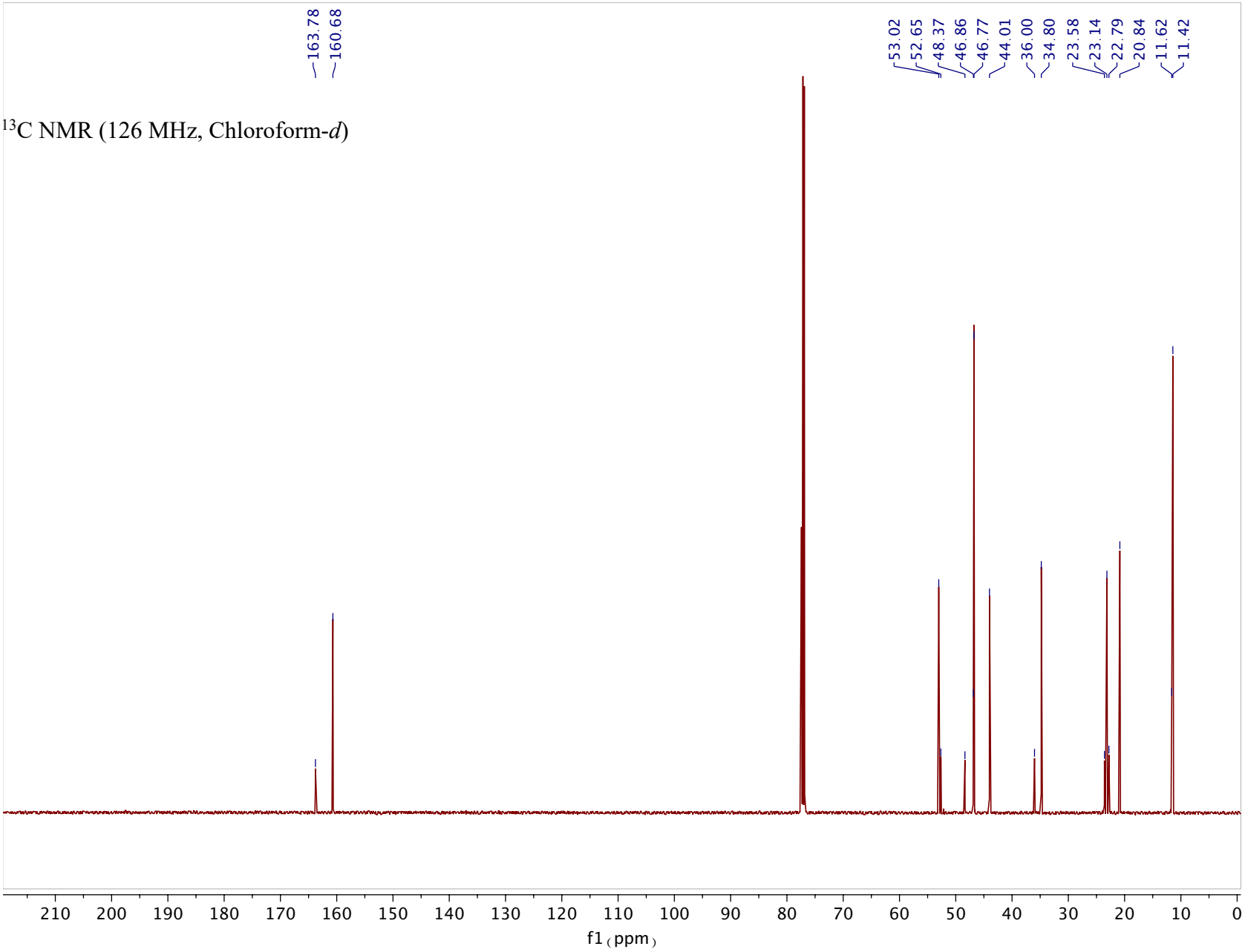

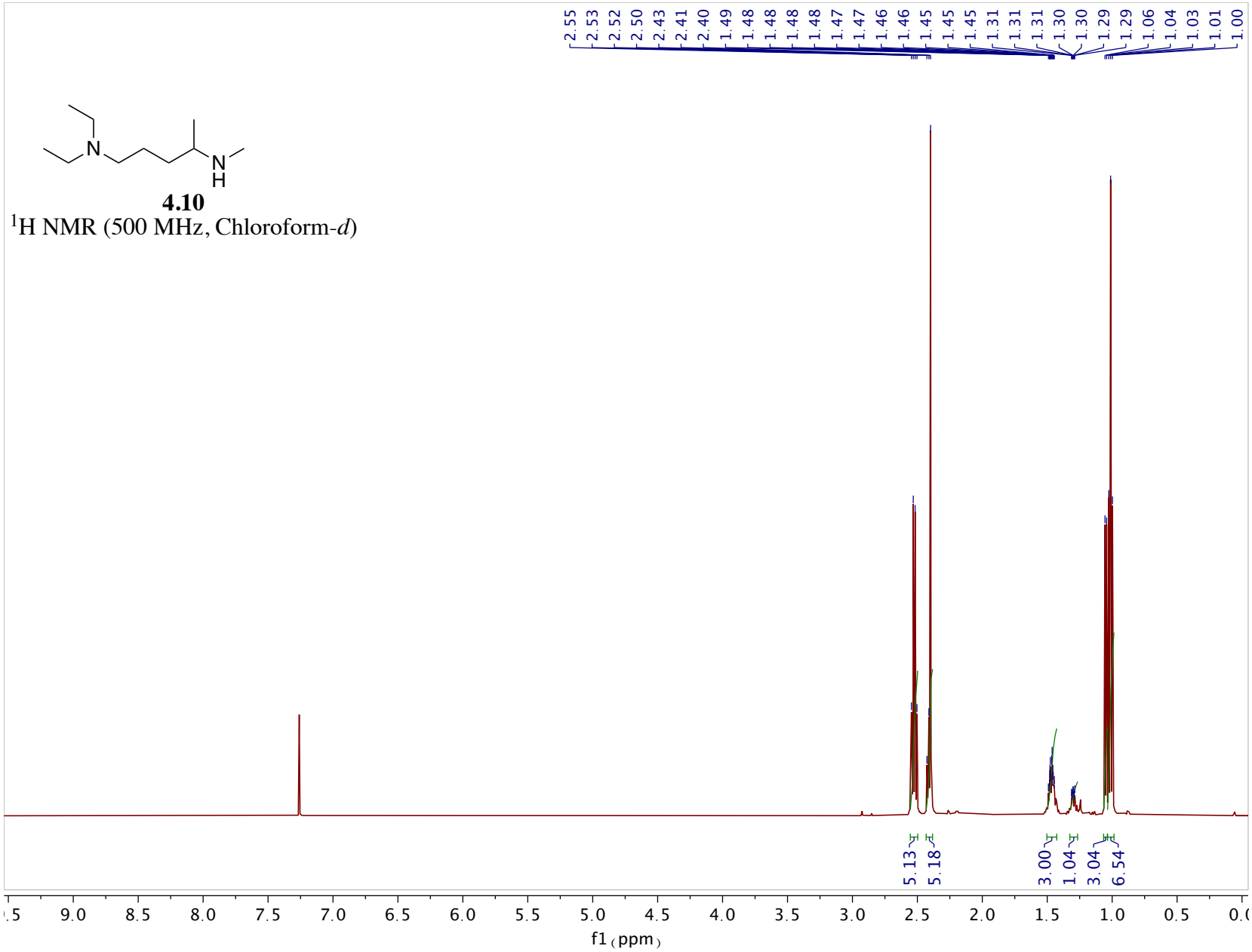

4.10

^{1}H NMR (500 MHz, Chloroform-*d*)

^{13}C NMR (126 MHz, Chloroform-*d*)

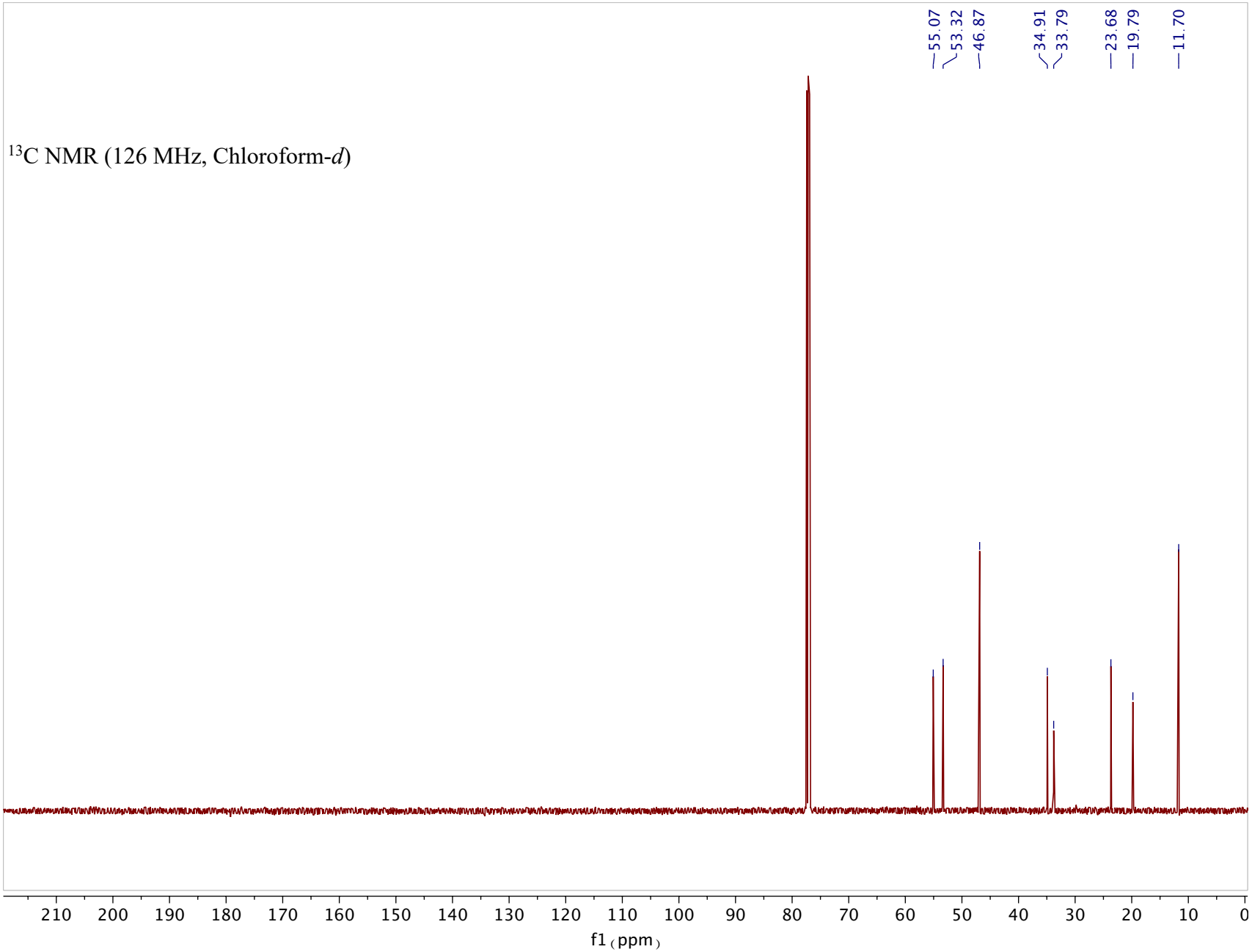

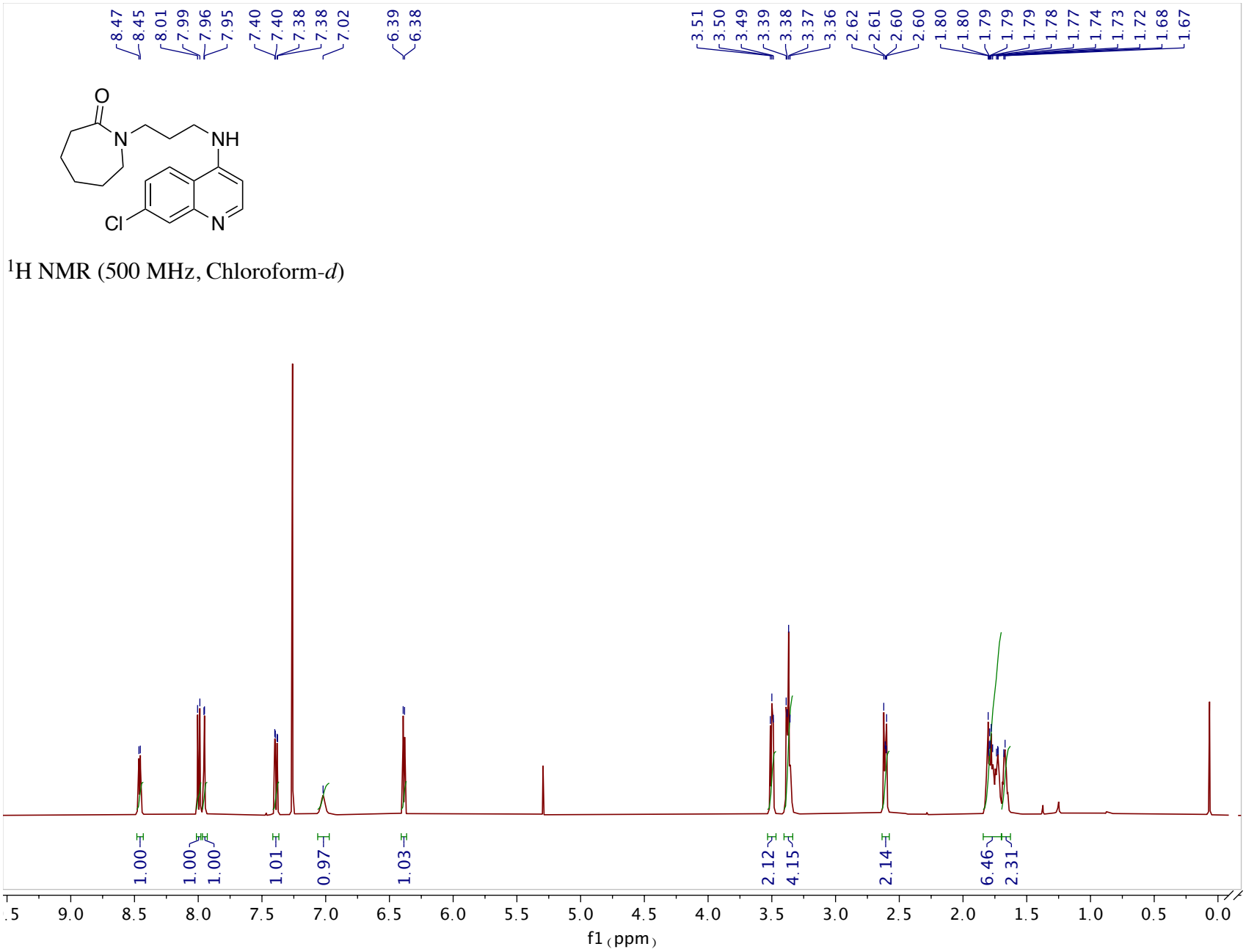

^{1}H NMR (500 MHz, Chloroform-*d*)

^{13}C NMR (126 MHz, Chloroform-*d*)

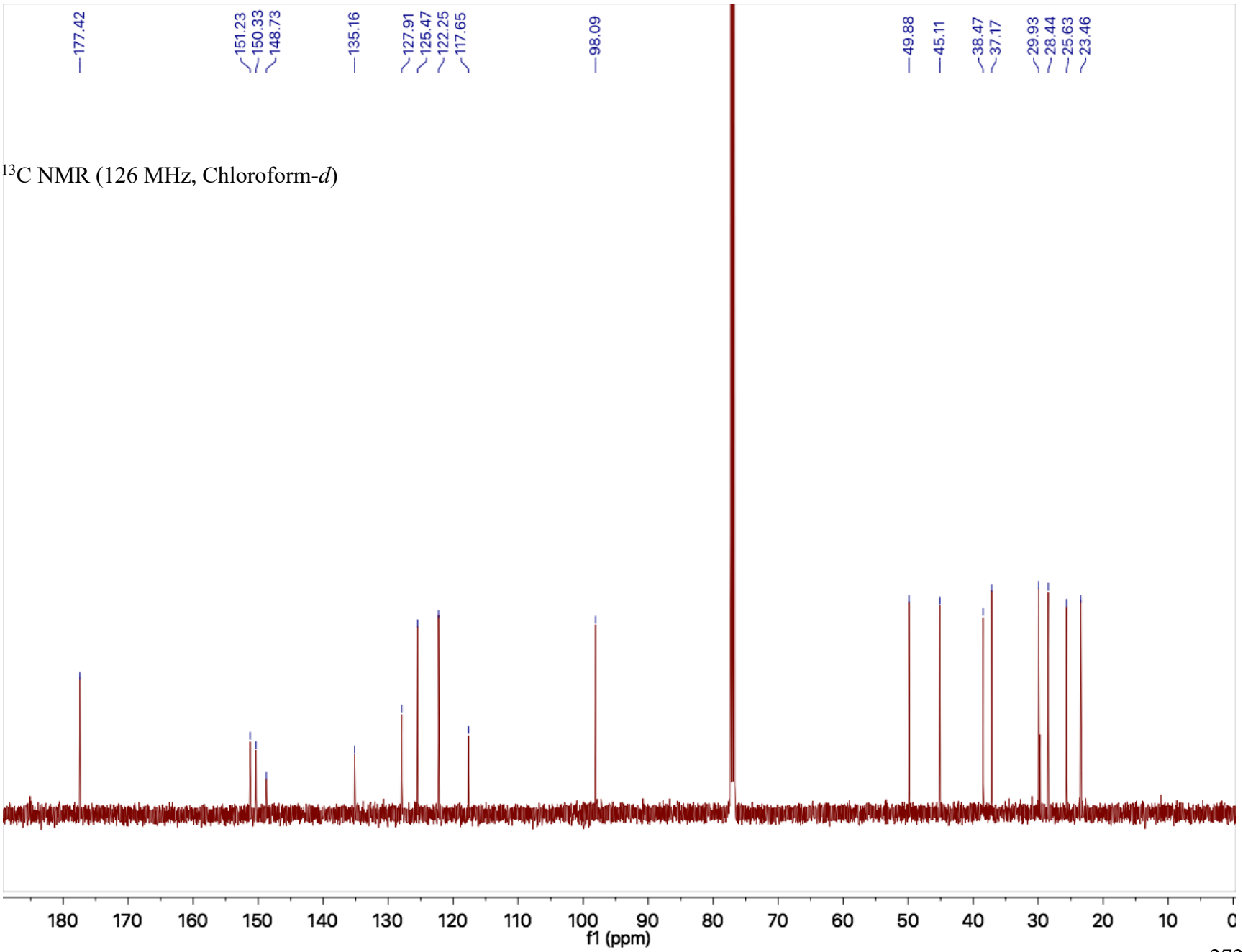

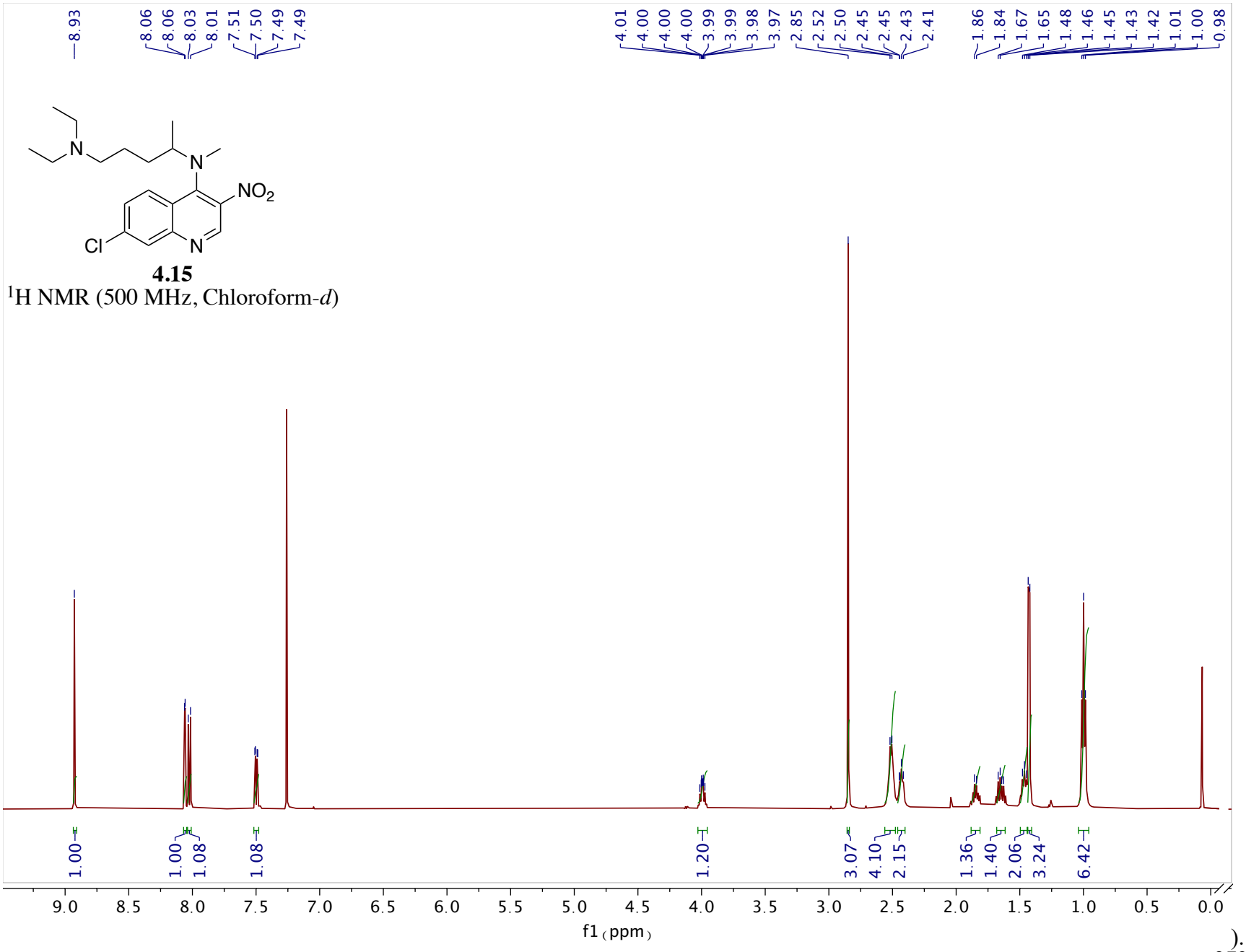

4.15

^{1}H NMR (500 MHz, Chloroform-*d*)

).

^{13}C NMR (126 MHz, Chloroform-*d*)

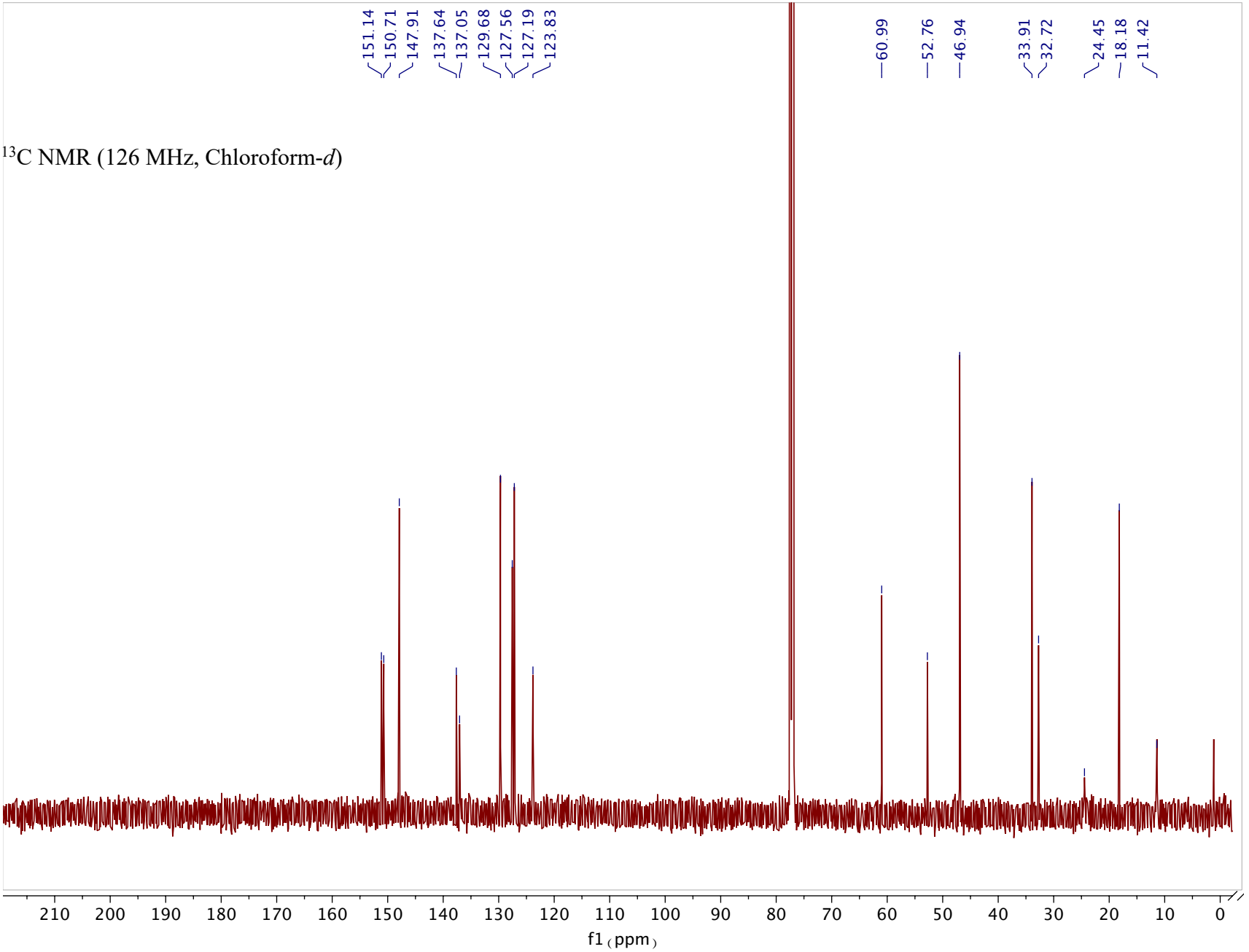

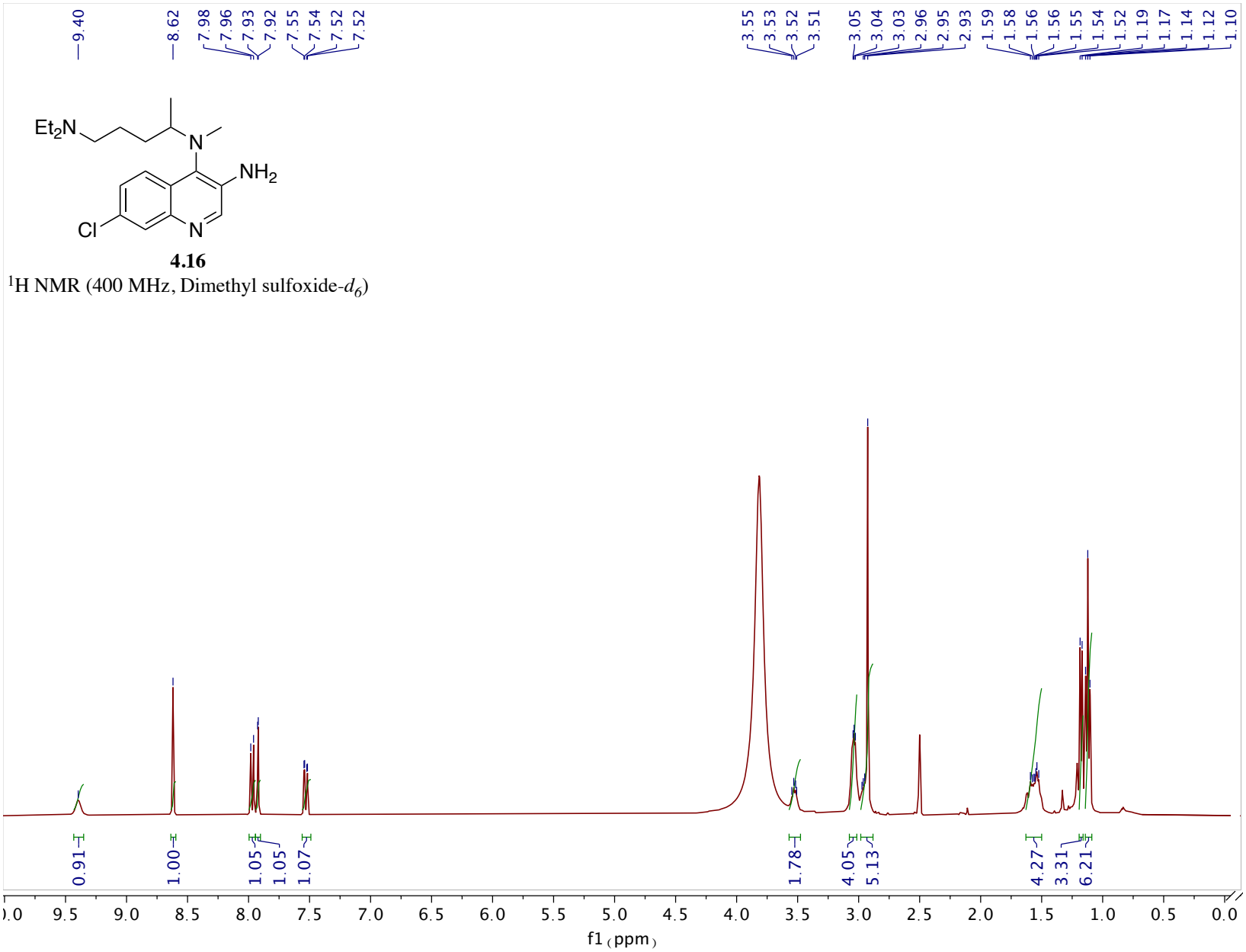

4.16

^{1}H NMR (400 MHz, Dimethyl sulfoxide-d_6)

^{13}C NMR (101 MHz, Dimethyl sulfoxide-d_6)

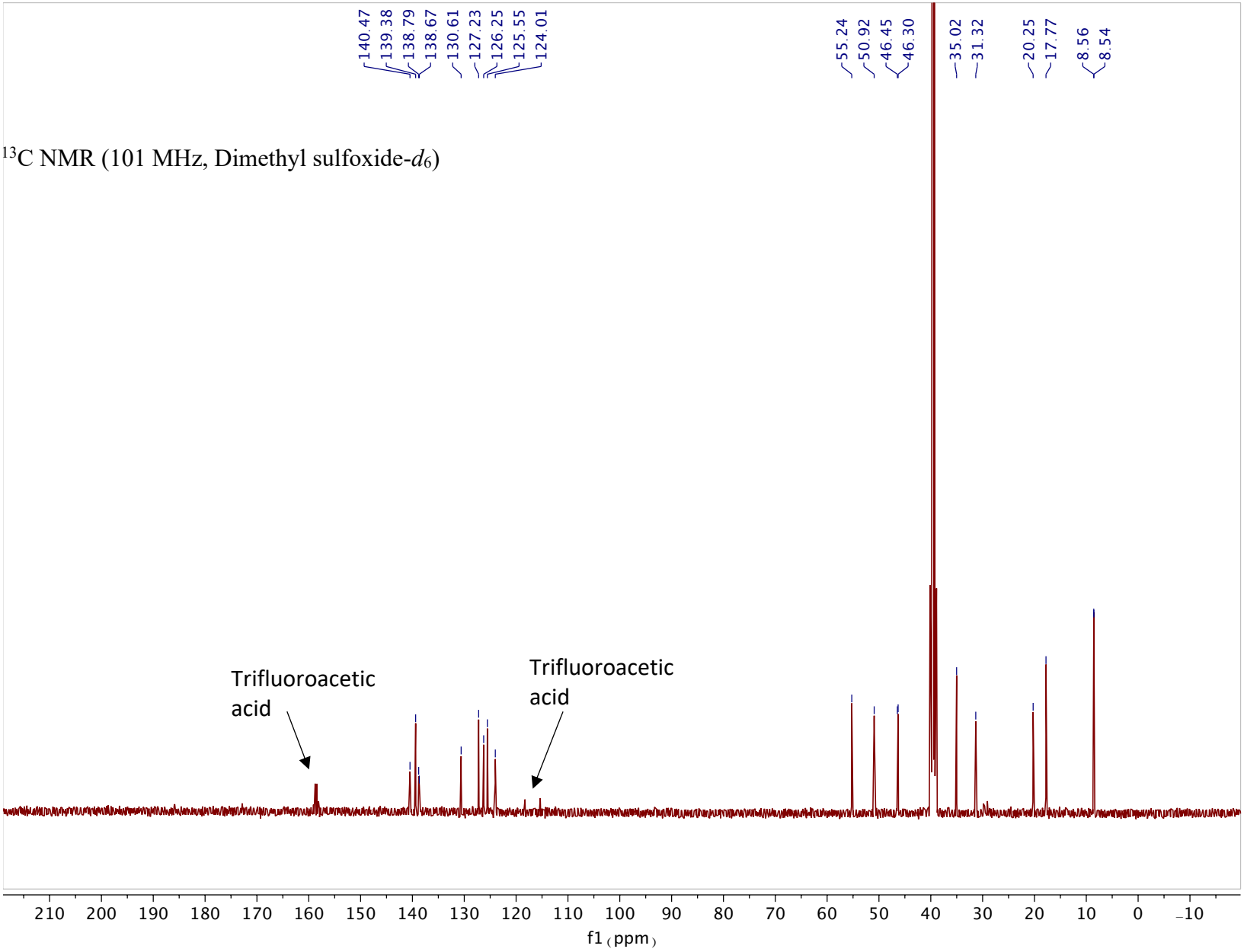

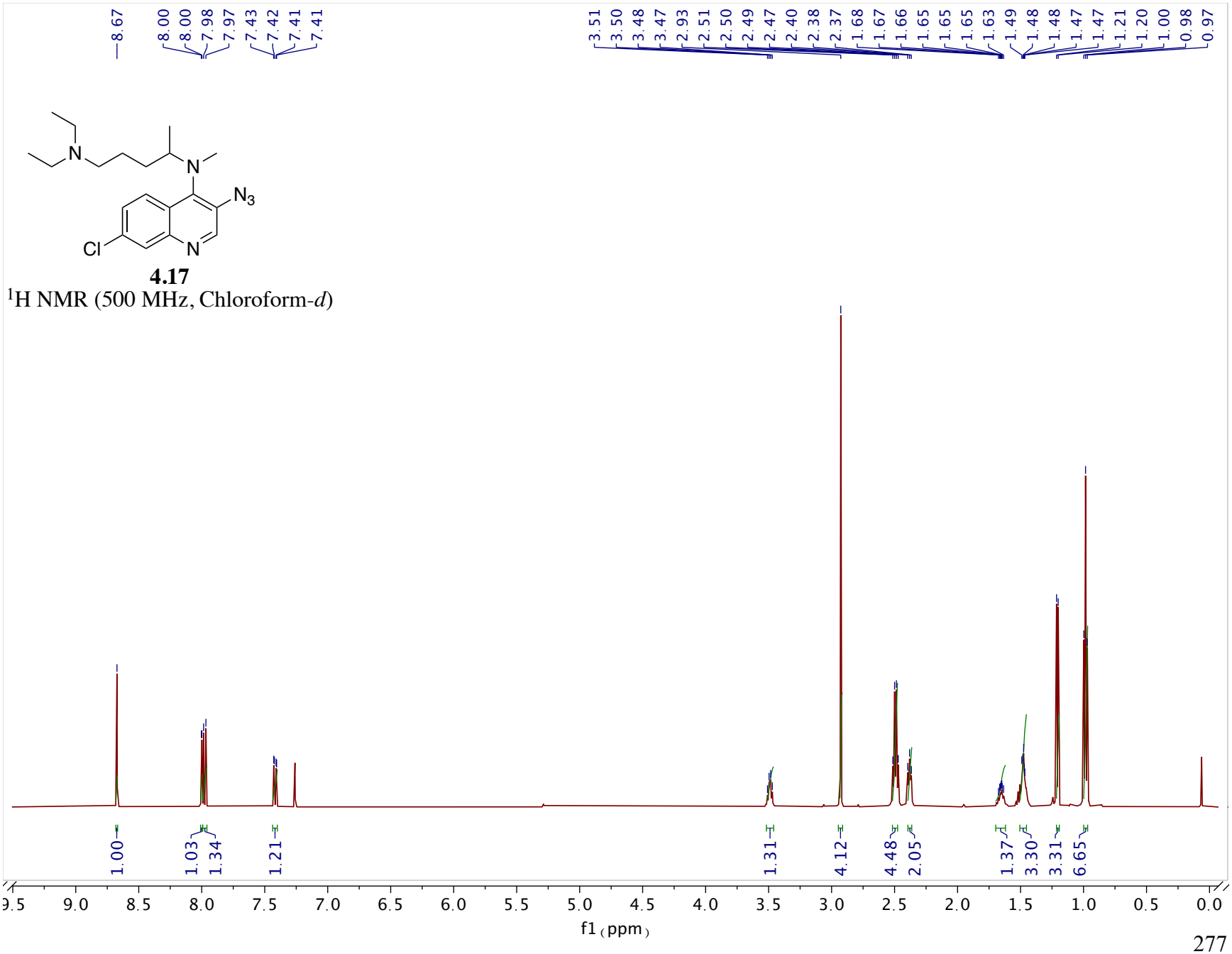

4.17

^{1}H NMR (500 MHz, Chloroform-*d*)

^{13}C NMR (126 MHz, Chloroform-*d*)

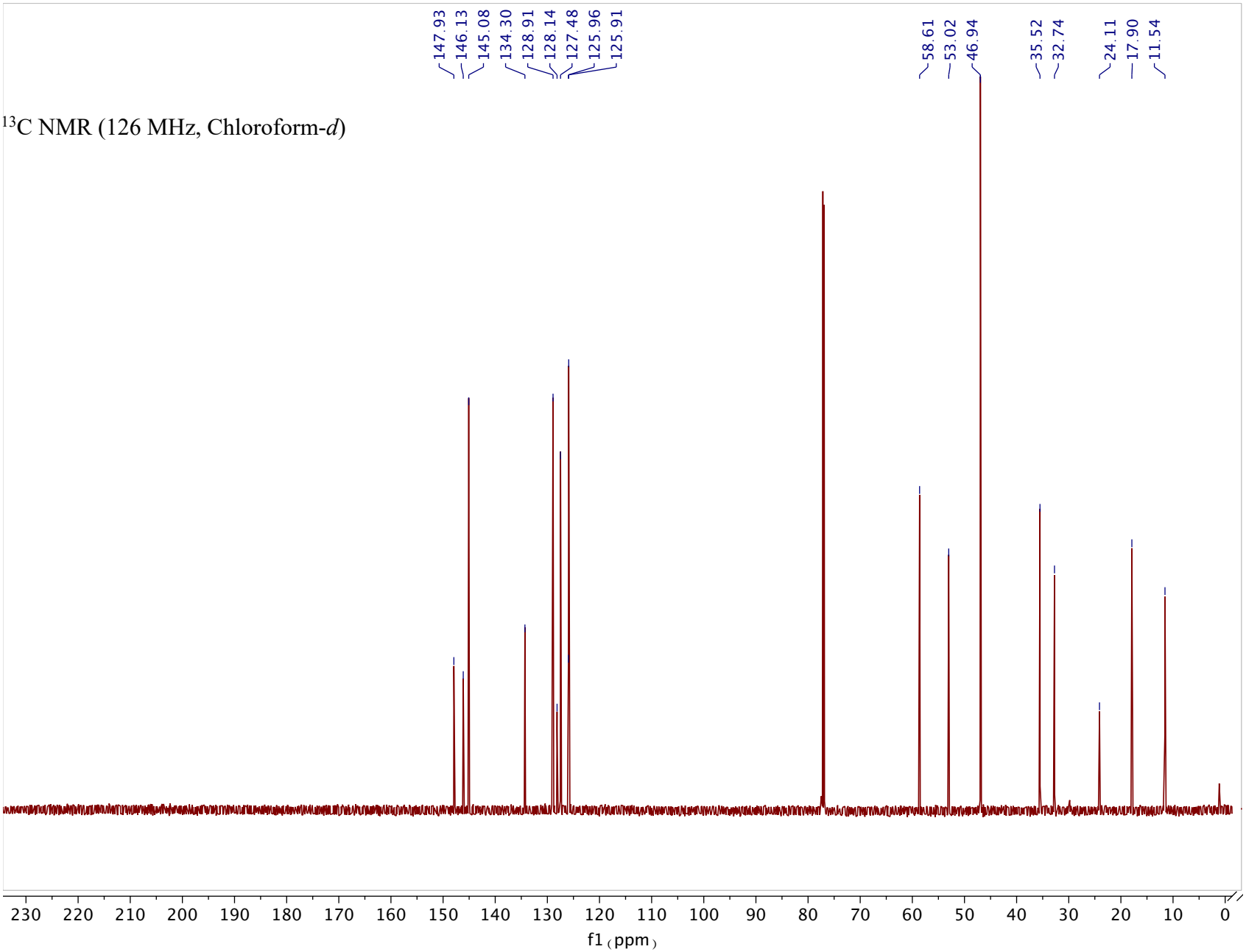

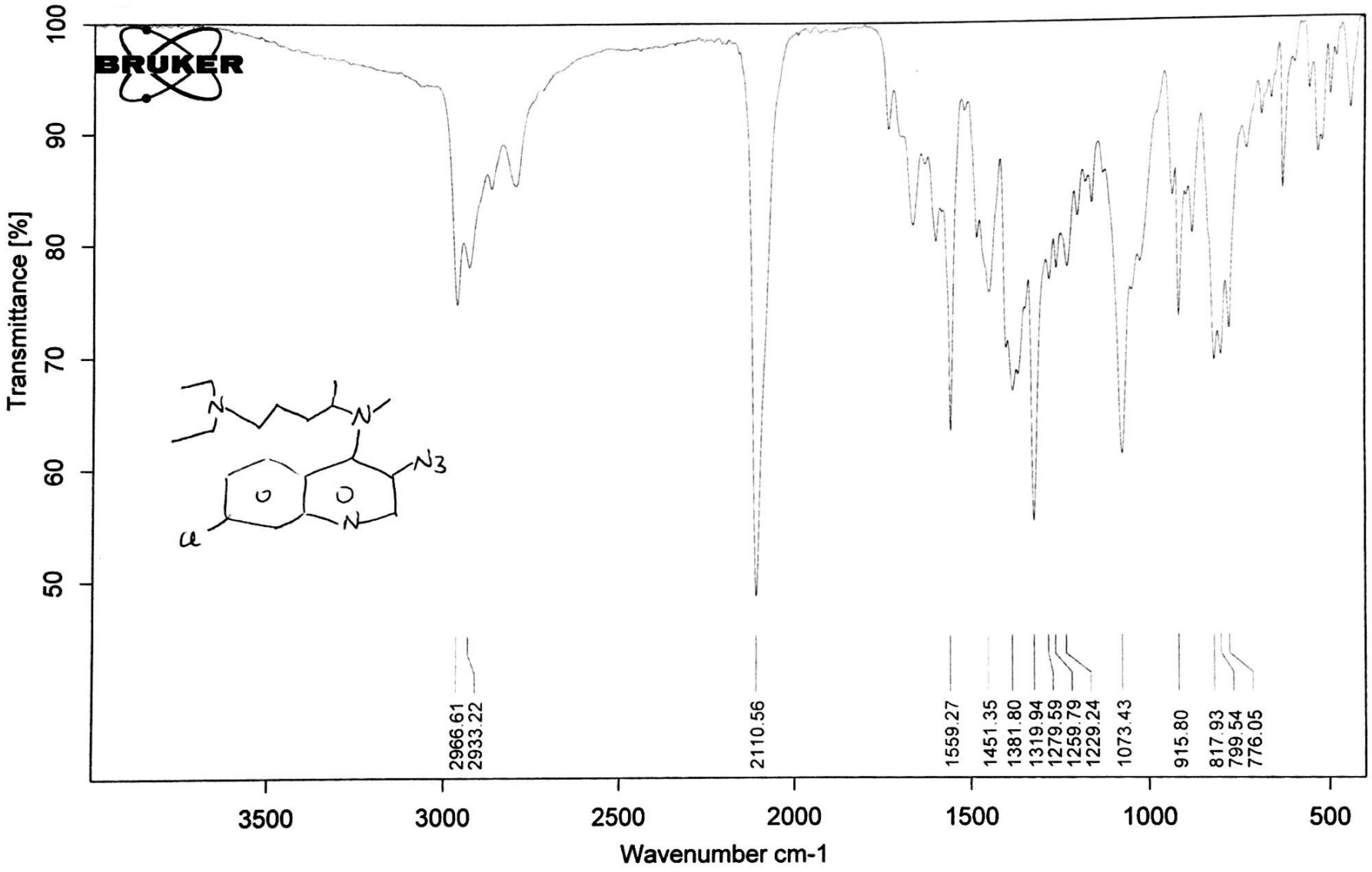
BRUKER
Transmittance [%]
100
90
80
70
60
50
3500
3000
2500
2000
1500
1000
500
Wavenumber cm-1
2966.61
2933.22
2110.56
1559.27
1451.35
1381.80
1319.94
1279.59
1259.79
1229.24
1073.43
915.80
817.93
799.54
776.05

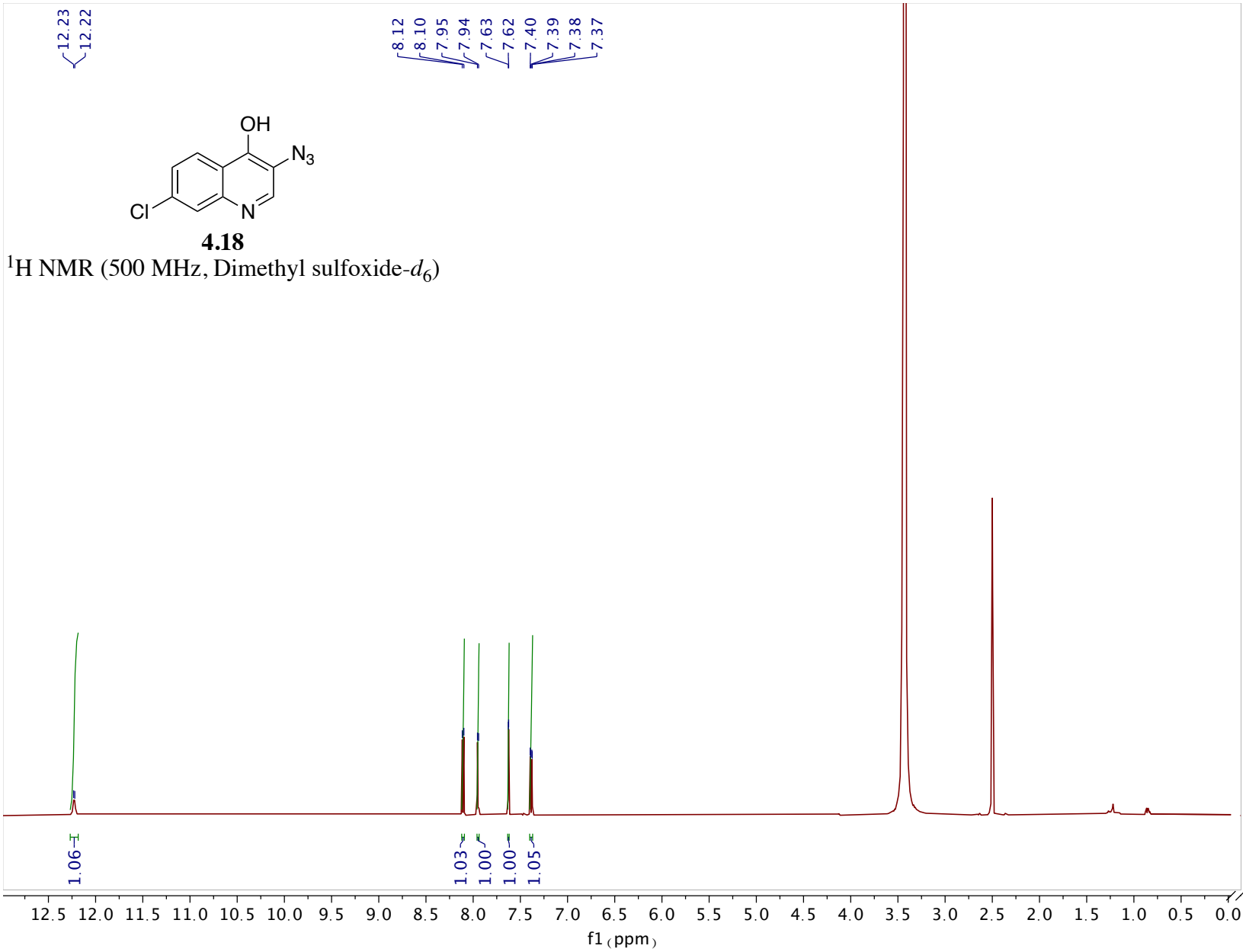

4.18

^{1}H NMR (500 MHz, Dimethyl sulfoxide-d_6)

^{13}C NMR (126 MHz, Dimethyl sulfoxide-d_6)

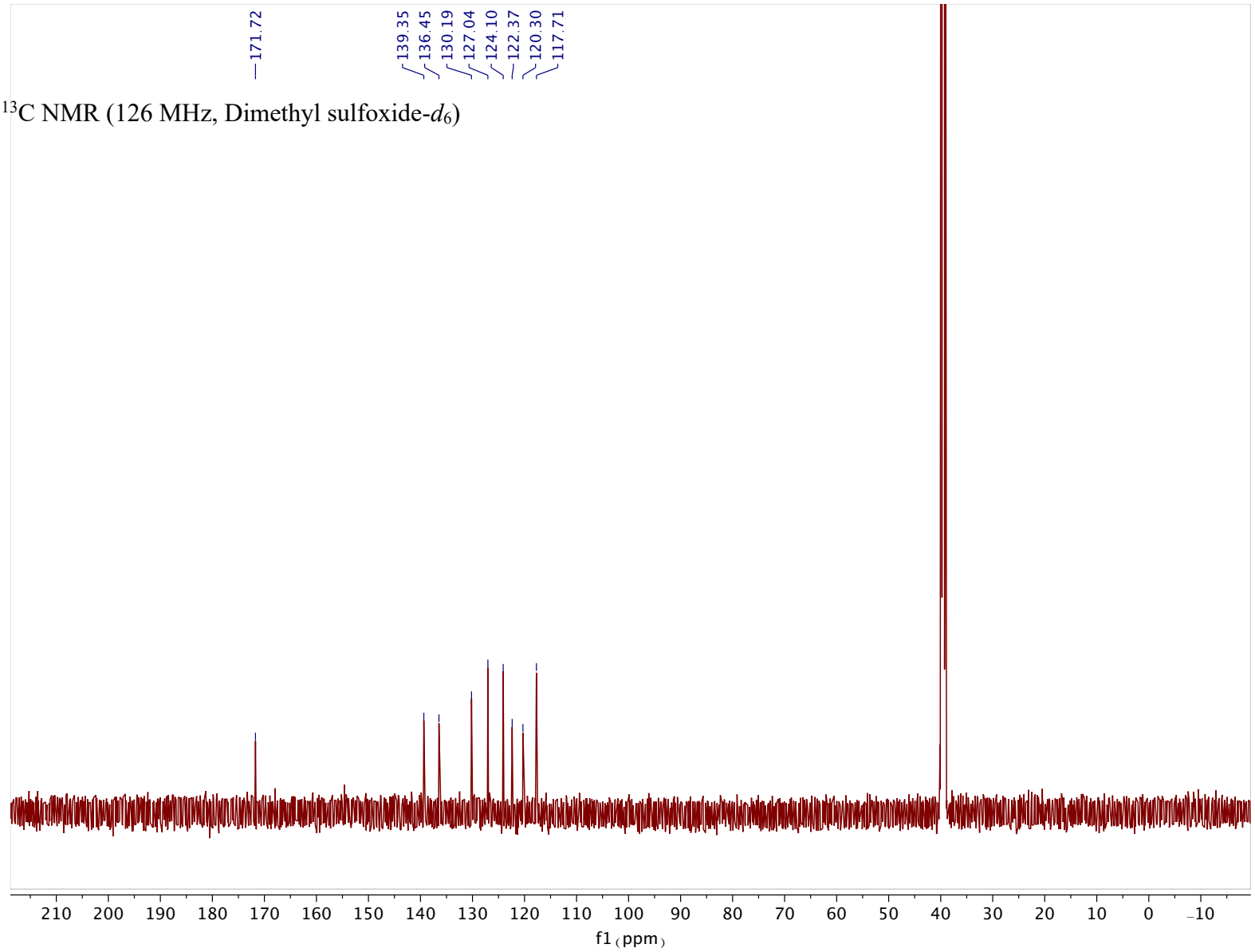

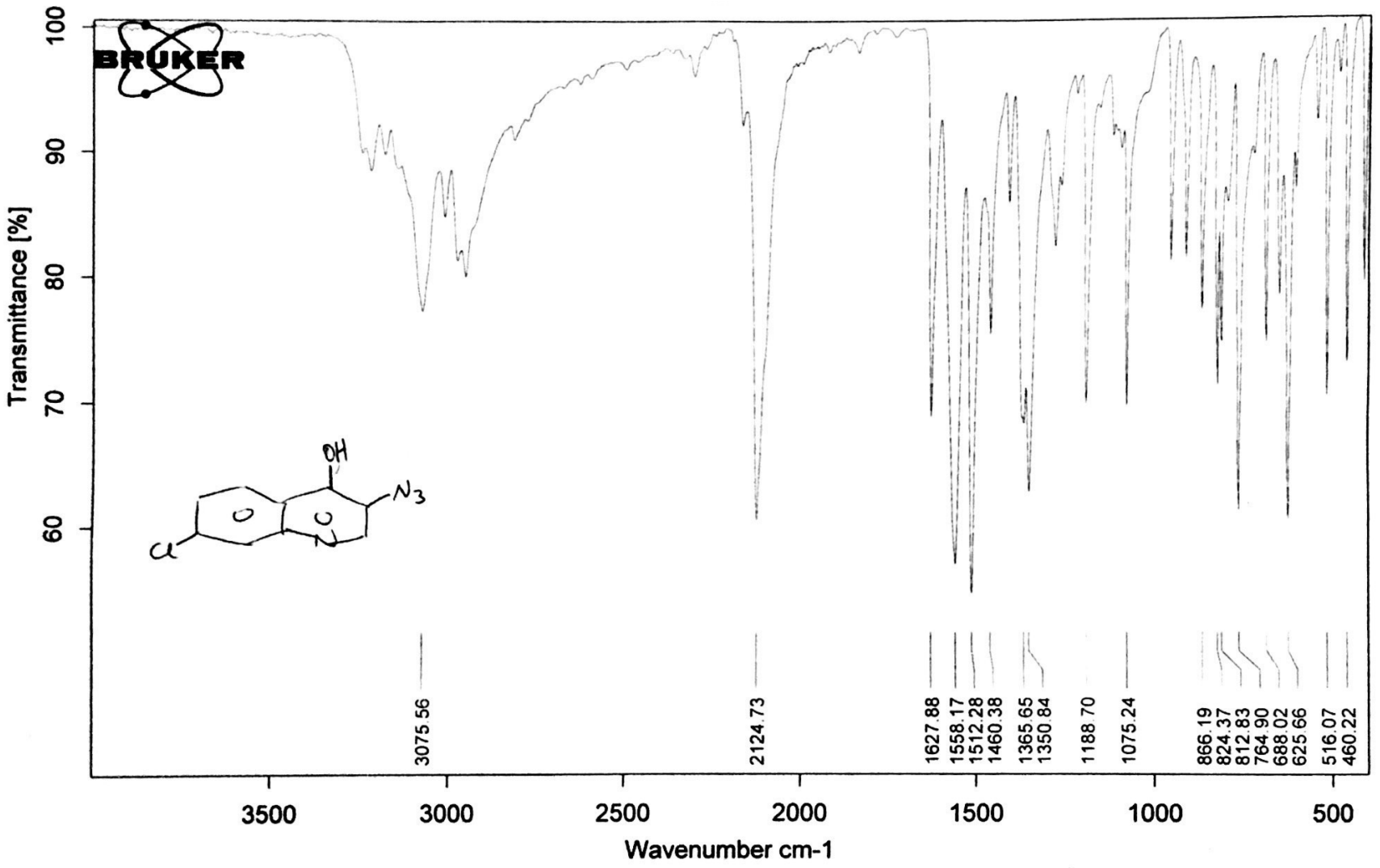
BRUKER
Transmittance [%]
100
90
80
70
60
3500
3000
2500
2000
1500
1000
500
Wavenumber cm-1
3075.56
2124.73
1627.88
1558.17
1512.28
1460.38
1365.65
1350.84
1188.70
1075.24
866.19
824.37
812.83
764.90
688.02
625.66
516.07
460.22
OH
N_3
O
C
N
Cl